WATER-BASED PROCESSING STRATEGY FOR CELLULOSE NANOCRYSTAL/POLYMER NANOCOMPOSITES

A Dissertation
Presented to
The Academic Faculty

by

Caitlin Meree

In Partial Fulfillment
of the Requirements for the Degree
Doctorate of Philosophy in Materials Science and Engineering in the
School of Materials Science and Engineering

Georgia Institute of Technology
May 2015

WATER-BASED PROCESSING STRATEGY FOR CELLULOSE NANOCRYSTAL/POLYMER NANOCOMPOSITES

Approved by:

Dr. Meisha Shofner, Advisor
School of Materials Science and Engineering
Georgia Institute of Technology

Dr. Norman Marsolan
School of Chemical and Biomolecular Engineering
Georgia Institute of Technology

Dr. David Bucknall
School of Materials Science and Engineering
Georgia Institute of Technology

Dr. Donggang Yao
School of Materials Science and Engineering
Georgia Institute of Technology

Dr. Anselm Griffin
School of Materials Science and Engineering
Georgia Institute of Technology

Date Approved: March 27, 2015

To my parents and brother:
For giving me the courage and strength to follow what I love
And to Conrad:
For believing in me even when I didn't

ACKNOWLEDGEMENTS

I would like to thank my advisor, Dr. Meisha Shofner, for giving me guidance and support throughout this research project and teaching me how to think critically and objectively about complex engineering and science challenges. I would like thank Dr. Shofner for being supportive and giving me the opportunity to work in her lab and learn so much. Without her guidance, I wouldn't be the engineer I have become.

I would also like to thank my committee members, Dr. David Bucknall, Dr. Dongang Yao, Dr. Anselm Griffin, and Dr. Norman Marsolan. Thank you for being a part of my committee and giving me critique and guidance on my research. Your input has been critical in the completion of my doctorate. Thank you for all your time and effort.

I would like to thank my research group members, both past and present including Dr. Michelle Kincer, Dr. Ji Hoon Lee, Dr. Stephanie Lin, Bradley Johnson, Prateek Verma, Matt Orr, Natalie Girouard, and Emily Fitzharris. Your help, input, support, and friendship helped to give me the strength to complete this work. I would like to thank my undergraduate students, Emily Fitzharris and Christine Smith for their hard work and dedication. Their help and effort was invaluable to the completion of this research.

I would like to thank Huibin Cho and Dr. An-Ting Chien for all their help and training with x-ray diffraction. I would also like to thank Nathan Evans for his help and support on the micro-tensile testing machine. I would like to thank Natalie Girouard for her help and training on the centrifuge, zeta potential measurements, and FTIR. I would like to thank Dr. Yao for allowing me to use his rheometer.

Finally, I would like to thank Dr. Michelle Kincer for her mentorship during my undergraduate research. Without her, I would have never had the desire or courage to pursue a Ph.D. Watching her and learning from her gave me the courage to continue in my education.

I would like to thank my funding source, the Renewable Bioproducts Institute for awarding a Paper Science and Engineering Fellowship as well as support for the purchase of some of the materials and supplies used in this work. I thoroughly enjoyed being a Paper Science Fellow and learning from leaders in the bioproducts field. The technical conferences provided by RBI were a blast and a great networking opportunity, and I loved the math jokes. I would also like to thank the USFS Forest Products Laboratory for providing some of the CNCs used in this work.

Lastly but certainly not least, I would like to thank my family and friends, specifically, my mom, dad, and brother. Without your supports, trips to Atlanta, and consistent love I could have never completed this research or my Ph.D. I love each of you so much. I would like to thank my friends, specifically Kathryn Folkner, Tristan Rice, Kristina Self, Ashley Nelson, Catherine Kearns, and Megan Diebold. Thank you for giving me laughter, late night wine talks, love, and support. You guys are awesome. Finally, I'd like to thank Conrad Lawson for believing in me when I didn't, loving me when I couldn't, and being the person who somehow made it all better when I thought it was completely broken. Thank you for showing me how to let go and enjoy every little bit of life. I love you and I couldn't have done this without you.

TABLE OF CONTENTS

LIST OF TABLES

LIST OF FIGURES

LIST OF SYMBOLS

A_c	Area of the crystalline peak
A_m	Area of the amorphous peak
A_{mCNC}	Area of the CNC amorphous peak
A_{mPVA}	Area of the PVA amorphous peak
b	Orientation parameter for the mechanically percolated network
β	Radius ratio of the batch mixing blades
d	Spacing between perfectly dispersed CNCs
d_x	Spacing between perfectly dispersed CNCs in the x direction
E	Halpin-Tsai predicted modulus
E'	Storage modulus
E''	Loss modulus
E_c	Composite modulus
E_f	Fiber modulus
E_f^{disp}	Modulus of the dispersed CNC network
E_f^{agg}	Modulus of the aggregated CNC network
E_l	Longitudinal modulus
E_m	Polymer matrix modulus
E_t	Transverse modulus
g	Gear ratio
γ	Strain
$\dot{\gamma}$	Shear rate

Γ	Batch mixer torque
G'	Shear storage modulus
G''	Shear loss modulus
ΔH_f	Change in heat flow
K	Yield stress fitting parameter
L	Length of the mixing blades
l/d	Aspect ratio
λ	Percolation model fitting parameter
m	Power law consistency index for steady shear
m'	Power law consistency index for storage modulus
m^*	Power law consistency index for complex viscosity
η	Steady shear viscosity
η^*	Complex viscosity
n	Power law exponent for steady shear
n'	Power law exponent for storage modulus
n^*	Power law exponent for complex viscosity
n_l	Halpin-Tsai longitudinal fitting parameter correlating stiffness
n_t	Halpin-Tsai transverse fitting parameter correlating stiffness
N	Mixer speed in RPM
R_e	External radius of the mixing blades
R_i	Internal radius of the mixing blades
S'	Percent swell
S^n	Normalized percent swell
S_c	Control percent swell

T_g	Glass transition temperature
T_m	Melting temperature
τ_0	Yield stress
τ	Stress
V_c	Percolation threshold
V_f	Volume fraction
w_f	Final weight
w_i	Initial weight
W_{rc}	Percent water recovery
ω	Angular frequency
X_c	PVA crystallinity

LIST OF ABBREVIATIONS

31K	31,000 to 50,000 g/mol
85K	85,000 to 125,000 g/mol
146K	146,000 to 186,000 g/mol
BC	Bacterial Cellulose
CMC	Cellulose Microcrystal
CMF	Cellulose Microfiber
CNC	Cellulose Nanocrystal
CNF	Cellulose Nanofibers
DSC	Differential Scanning Calorimetry
DMA	Dynamic Mechanical Analysis
DMF	Dimethylformamide
DMSO	Dimethyl Sulfoxide
FT-IR	Fourier Transform Infrared Spectroscopy
MTT	Micro-tensile Testing
NMP	N-Methyl-2-pyrrolidone
PAA	Poly(acrylic acid)
PDI	Polydispersity Index
PEO	Poly(ethylene oxide)
PEG	Poly(ethylene glycol)
PHB	Poly(hydroxybutyrate)
PHBV	poly(3-hydroxybutyrate-co-3-hydroxyvalerate)
PLA	Poly (lactic acid)

PP-g-MA	Polypropylene-graft-maleic anhydride
PVA	Poly(vinyl alcohol)
PVAc	Poly(vinyl acetate)
PVC	Poly(vinyl chloride)
RDFD	Redispersed Freeze-Dried
SCB	Sugarcane Bagasse
gel – sol	gel - solution
TGA	Thermogravimetric Analysis
WF	Wood fibers
XRD	X-Ray Diffraction

SUMMARY

The objective of this research is to develop a water-based processing method for incorporating large filler loadings into nanocomposite systems. Specifically, cellulose nanocrystal/poly(vinyl alcohol) (CNC/PVA) nanocomposite aqueous suspensions and films were processed and characterized at CNC loadings up to 67 wt.% with respect to polymer concentration. Both aqueous suspended and freeze-dried CNCs were studied with this method. Two methods for incorporating the CNCs were investigated: solution processing and batch mixing of aqueous suspensions. The materials produced by these methods were characterized using rheology of aqueous suspensions and a method for understanding the morphology of these aqueous suspension through rheological characterization was developed. The CNC/PVA suspensions were dried and the structure of the film studied using x-ray diffraction, Fourier transform infrared spectroscopy, and differential scanning calorimetry. With regard to characterization of polymer structure by these methods, PVA crystallinity was seen to increase with increasing CNC loading. Finally, dynamic mechanical analysis and micro-tensile testing were conducted on consolidated films and CNCs were seen to increase modulus, yield stress but decrease strain at failure. Biodegradation studies were also conducted and CNCs were seen to increase the biodegradation characteristics of PVA. While the general trends in experimental data were the same, differences in properties between systems made with solution processing and batch mixing were observed, attributed to differences in the CNC dispersion. Overall, results indicated that this methodology is feasible for the industrially scalable production of highly loaded nanocomposites.

CHAPTER 1

INTRODUCTION

The objective of this research is to develop a water-based processing method for polymer nanocomposites containing cellulose nanocrystals (CNCs) and poly(vinyl alcohol) (PVA) using traditional shear processing. This research tested the hypothesis that a conventional polymer processing method can be used with robust nanocomposite suspensions to produce nanocomposites with high filler loadings and avoid thermal degradation of the components. Ultimately, a scalable, more sustainable route to process highly-loaded CNC nanocomposites with improved mechanical performance was sought. The efficacy of the method was assessed through optical microscopy, rheological, structural, mechanical, thermal, and biodegradation characterization techniques. Through this research, an increased understanding in the processing – structure – property relationships of CNC/polymer nanocomposite was achieved.

The motivation to pursue this research is related to the limited thermal stability of some renewable and/or biodegradable polymers and fillers. Specifically, the composite systems applicable for this research are those in which the melting temperature and the degradation temperature of the polymer matrix are in such proximity that melt processing leads to degradation before final forming or those which contain fillers that are not thermally robust. Common polymeric materials that display these characteristics are renewable biopolymer systems such as silk, collagen, soy, cotton, and starch-based polymers and synthetic biodegradable polymer systems such as PVA.[1] Renewable and biodegradable cellulosic materials are also thermally sensitive, with degradation

temperatures around 200 °C and 300 °C,[2–4] and the thermal degradation temperature of CNCs has been found to be related to its surface chemistry.[2] The limited thermal stability of these composite components therefore leads the development of alternative processing methods. In this work, a water-based processing method using melt processing equipment is sought and thought to be advantageous in the advancement of these renewable or biodegradable systems.

It is crucial to further the development of renewable materials to decrease the amount of waste in landfills, the dependence on slowly depleting petroleum supplies, energy requirements, and the environmental footprint of the manufacturing industry.[5–9] It is estimated that about 80% of the current polymer market is composed of nonrenewable, petroleum based polymers leading to much opportunity for improvements in sustainability and environmental stewardship.[5] A definition of biodegradable polymers from Malinconic *et al.*[5] states biodegradable polymers are those "materials obtained by nature or by synthetic route which are designed and engineered for one time use and easily degradable, maybe by living organisms." In order to qualify as a fully renewable and biodegradable composite, the matrix and the filler must both be produced from renewable resources. The polymer used in this work, PVA, is a suitable model for renewable polymers. Though it is not derived from renewable resources, it displays similar characteristics to polymers produced from renewable resources such as biodegradability, and PVA is not processed by melt techniques easily.[10–12] Additionally, PVA is water-soluble allowing for inherent compatibility with CNCs. Therefore, this nanocomposite system is expected to be a good system for testing the processing method and translating this work to fully renewable composite systems.

In addition to developing a processing method, the presented research addresses the challenge in the nanocomposite field to manipulate renewable and biodegradable resources into mechanically robust nanocomposites, particularly at high filler loadings. Through utilizing the current properties of some of these materials, such as water solubility and biodegradability, nanocomposites with high mechanical performance and usability can be formulated for packaging, biomedical use, and fuel cell membranes or tailored to possess the necessary thermo-mechanical properties for other applications.

This dissertation is organized in the following manner. In Chapter 2, background information discussing PVA, CNCs, and cellulose/polymer nanocomposite systems is presented. The synthesis and properties of PVA and CNCs are outlined. The processing, rheology, structure, and mechanical properties of cellulose/polymer nanocomposite systems are also presented. In Chapter 3, the methods and procedures used to develop the water-based processing strategy and characterize the CNC/PVA systems are described. In Chapter 4, the processing strategies used to produce the CNC/PVA nanocomposite systems are described. Optical microscopy is also characterized to better understand the morphology of the suspensions. In Chapter 5, aqueous suspended CNC and freeze dried CNC rheology are discussed. A method for understanding the morphology of CNC/PVA suspensions through rheological characterization is presented. In Chapter 6, the structure of the CNC/PVA systems is analyzed and discussed through x-ray diffraction (XRD), Fourier transform infrared spectroscopy (FT-IR), and differential scanning calorimetry (DSC). The crystallinity and molecular mobility are presented. In Chapter 7, the mechanical properties are shown via dynamic mechanical analysis (DMA) and microtensile testing (MTT) to understand the dynamic and static mechanical behavior of

the CNC/PVA systems. In Chapter 8, the biodegradation, water recoverability, and scalability of the CNC/PVA systems are described and presented. The feasibility for industrial implementation is discussed. In Chapter 9, the processing-structure-property relationships are discussed and summarized in the conclusion. Potential future studies are outlined.

CHAPTER 2

BACKGROUND

In this chapter, the background information necessary to gain increased understanding of the presented research is discussed. First, information about the materials used, PVA and CNCs, and the current knowledge of their structure and properties as determined from literature will be presented. The chapter also presents an analysis of the literature available on cellulose/PVA composites in terms of their rheological, structural, mechanical, and biodegradation properties.

2.1 Poly(vinyl alcohol)

PVA is a synthetically-derived, flexible, water-soluble, biodegradable, and non-toxic polymer[13–16] as well as the most widely produced synthetically derived water-soluble polymer.[17] PVA is used in a variety of industries including the medical, packaging, and food industry as well as paper manufacturing.[10,13,18,19] PVA is frequently used as a membrane due to its /barrier properties against oxygen and aromatic compounds as well as its resistance to many solvents and oils.[20] It is also commonly used for biomedical applications such as tissue mimicking, cell culturing, and vascular implants.[19]

2.1.1 Synthesis and Structure

PVA contains a hydrocarbon backbone and hydroxyl group branches, shown in Figure 2.1. The native PVA main chain is usually over 90% hydrolysis, but the degree of hydrolysis varies due to the synthesis of the polymer.[21]

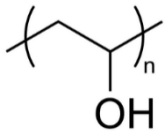

Figure 2.1: Structure of PVA

The synthesis of PVA is different for typical polymer systems in that there is no direct polymerization path available due to the instability of the vinyl alcohol monomer, a form of acetaldehyde.[22,23] PVA is produced via hydrolysis or ester interchange of polyvinyl esters in alkaline or acid environments. The synthesis schemes for PVA can be found in Figure 2.2. PVA can be synthesized through the cleavage of polyvinyl acetate (PVAc) by bases using the stirrer method or the masticator method. In the stirrer method, a low viscosity solution of PVAc mixed in an alcohol-water with catalyst (alkali hydroxide) solution is agitated, and PVA is produced. It is difficult to produce a medium grade hydrolysis (between 86 and 90% hydrolyzed) via the stirrer method due to the processing conditions. The mastication method uses batch or continuous shear processing with PVAc to distribute catalyst in an ester exchange process using methanol or absolute alcohol. The mastication method allows for control of the degree of hydrolysis. PVA can also be synthesized from PVAc via acidolysis via ester interchange in an absolute

alcohol, hydrolyzation in alcohol-water system, or hydrolysis in aqueous solution and subsequent removal of produced acetic acid.[23]

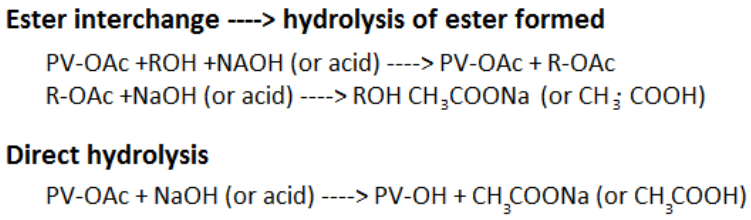

Figure 2.2: PVA synthesis schemes

In the solid state, PVA tends to form a monoclinic crystal structure with five main crystal peaks with Miller indices shown in Table 2.1.[24] The crystallinity index of these crystal peaks increases with plasticizing agents such as water as the water molecules increase chain mobility, shown through the shift in reflection from 4.5 Å in the dry state to 3.9 Å in wet films. This shift indicated that more perfectly layered three dimensional structure was formed. The addition of water molecules to the PVA breaks apart the hydrogen bonds formed between the hydroxyl groups of the polymer chains, increasing chain mobility as well as the order of the system, increasing the longitudinal dimension of the crystalline regions from 50 to 60 Å.[25] With the incorporation of water, the intensity of the peaks at 101 and $10\bar{1}$ are reversed due to the direction of the hydroxyl groups.[24,26] Increasing the degree of hydrolysis has also been seen to increase the crystallinity of PVA due to increased hydrogen bonding.[27]

Table 2.1: Miller indices for main PVA crystal peaks measured with CuKα

2θ (degrees)	Miller Indices
11.5	100
19.5	$10\bar{1}$
20.1	101
23.0	200
40.5	111, $1\bar{1}1$, 210 $2\bar{1}0$

2.1.2 PVA Solutions

Physical gelation in polymer solutions occurs via the formation of thermally reversible junctions between the polymer molecules.[28] The physical gelation of PVA has been studied to understand the behavior needed to conduct aqueous extrusion and produce PVA fibers.[29,30] PVA solutions have also been studied for their application as membranes and in biomedical and pharmaceutical applications due to their biocompatibility, elasticity, and permeability.[31–34] During PVA gelation, crystallite formation occurs in which at least two polymer molecules align next to one another and hydrogen bond together over a few molecular segments. This crystallite formation is very similar to the crystal structure in the solid state of PVA.[22] The formation of these crystallites will increase with time, increasing the viscosity of the solution in a process known as aging. Aging of PVA also occurs as the polymer chain entanglement is increased through diffusion in the gel.[22] The degree of hydrolysis plays a role in the viscoelastic properties of PVA solutions. Increasing the degree of hydrolysis strongly

increases the storage modulus (G') in PVA gel systems due to increased hydrogen bonding.[21] The degree of hydrolysis also affects the degree of swelling, in that the larger the degree of hydrolysis, the lower the degree of swell.[35]

In addition to the degree of hydrolysis, the tacticity of PVA affects gel formation. While isotactic PVA can be dissolved even in cold water, syndiotactic PVA is barely water soluble.[21] In the crystal structure, PVA chains form a planar zigzag confirmation, similar to polyethythene.[36] These planar zigzag confirmations will order themselves depending on the amount of syndiotacticity. Syndiotactic PVA solutions tend to have increased crystallinity compared to atactic and isotactic due to a larger affinity for water in syndiotactic solutions.[13] The gelation behavior is also dependent on the stereography of the PVA. While isotactic and atactic PVA sequences form intramolecular hydrogen bonds, syndiotactic sequences form intermolecular junctions. In the case of isotactic and atactic PVA, intramolecular hydrogen bonds do play a significant role in the gelation and aggregation properties, causing isotactic PVA to form weaker gel systems. In contrast, the intermolecular junctions formed in syndiotactic PVA are responsible for the aggregation and gelation behavior giving stronger gel systems.

2.1.3 Thermal and Mechanical Properties

One reason that PVA is relevant to this research is because its melting temperature is very close to its degradation temperature leading to rapid polymer degradation and extremely sensitive temperature control requirements. PVA degrades

between 220 and 250 °C depending on the degree of hydrolysis. Increasing the degree of hydrolysis increases the available processing temperature range, therefore increasing the degradation temperature due to increased bonding.[17] During PVA thermal degradation, bound water is released from the matrix in turn increasing the discharge of volatile compounds such as acetic acid. As these compounds are released, polyene is formed resulting in discoloration and PVA degradation.[10] With increased demand for more environmentally compatible products, much research is being done with regards to melt processing PVA.[37,38] In these studies, the plasticizers apart from water are employed to increase the gap between the melting and degradation temperature allowing for PVA to be traditionally melt processed. In the presented work, the processing of CNC/PVA nanocomposite systems without the use of plasticizers besides water will be studied.

Atactic, syndiotactic and isotactic PVA films have been seen to have crystallinities no larger than 40% with a melting range of about 220 to 250 °C, with syndiotactic PVA melting in the lower range and atactic PVA melting in the higher temperature range.[22,39] This large melting range is attributed to the loss of water leading to degradation as well as the increase and formation of cold-formed crystallites.[22] PVA will begin to degrade in this melting region, making it difficult to study the crystallization kinetics via traditional DSC as well as process using traditional melt processing equipment. PVA is sensitive to humidity and water absorption and will become more flexible in more humid environments and more brittle when dry.[40] PVA has a tensile modulus between 2-4 GPa and a tensile strength between 60 -100 MPa depending on molecular weight, crystallinity, and tacticity.[17,41,42]

2.2 Cellulose Nanocrystals

2.2.1 Synthesis and Structure

There are two main forms of cellulose nanomaterials: Cellulose nanofibers (CNFs) and CNCs. CNFs are produced from wood or plant fibers via chemical treatment and very fine fibrillation to give them sizes on the nanoscale. They are 0.5 to 2 μm long and 4 to 20 nm wide with square cross sections. CNCs, the type of cellulosic nanomaterial used in this work, are nanofillers derived from cellulose fibers found in wood, hemp, cotton, and linen.[43] They are rod-like particles with lengths of 0.05 to 0.5 μm and 3 to 5 nm in width. The structure of cellulose can be found in Figure 2.3. By extracting CNCs from these renewable cellulose sources, CNCs have the potential to act as novel renewable reinforcing fillers in polymer systems. The precursor material for CNCs, cellulose, is composed of linearly attached ringed glucose molecules aligned in a ribbon like structure. The repeat unit of cellulose is composed of anhydroglucose rings covalently bonded with oxygen, as shown in Figure 2.3.[44,45] These cellulose chains hydrogen bond to one another to form fibrils.[44] While hydrogen bonding within the cellulose chains causes agglomeration in some systems, hydrogen bonding also stabilizes fibril conformation giving cellulose fibrils high axial strength. Within the cellulose fibrils, there are regions exhibiting amorphous and crystalline behavior. Through the extraction of these crystalline regions via acid hydrolysis at the nanoscale, CNCs are formed. During this acid hydrolysis, the amorphous regions of the cellulose fibrils are hydrolyzed leaving only the CNCs.[44] Figure 2.4 displays the relationship between trees and CNCs. CNCs' mechanical properties,[46] found in Table 2.2, and biocompataiblity[43,46]

enable them to be viable substitutes for traditional nonrenewable nanomaterials. For example, CNCs are expected to have a higher axial elastic modulus than Kevlar and exposed –OH groups on their surface. These exposed hydroxyl groups allow for CNC surface functionalization, therefore giving opportunity for potential increase in component interaction, dispersion, as well as self-assembly.[45] Wood based CNCs, those implemented in the presented research, have aspect ratios of about 20 and low densities of about 1.5 g/cm^3 allowing for improved mechanical performance and lighter overall weight application.[20]

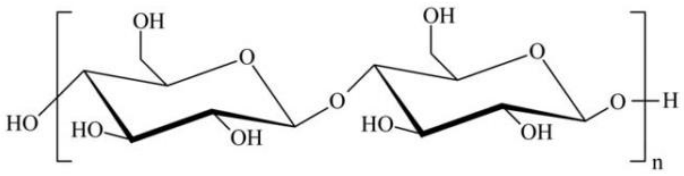

Figure 2.3: Structure of Cellulose

Table 2.2: Mechanical properties of wood based CNCs

Mechanical Property	Value
Tensile Modulus (GPa)[4]	2 – 16
Percent Crystallinity [4,45]	80 – 92
Elastic Modulus (GPa)[45]	18 – 50

While CNCs may possess a variety of crystal structures depending on the source and method of production, wood based CNCs are categorized with cellulose I and/or II crystal structure.[45] Cellulose I is typically found in nature while cellulose II is formed

from cellulose I via swelling of cellulose I in sodium hydroxide aqueous solutions or regeneration.[4] There are two allomorphs of cellulose I: triclinic (Iα) and monoclinic (Iβ) crystal structures. The Iα structure tends to be dominant in cellulose produced from algae and bacteria while the Iβ is the primary cellulose structure produced from plants and tunicates. As the cellulose discussed in this research is derived from wood, the Iβ structure will be predominant with Miller indices of 200, 110, and $1\bar{1}0$ at $2\theta = 22.5°$, 16°, and 15° respectively and the cellulose II peak of 100 at $2\theta = 19.8°$ with respect to CuKα.[45]

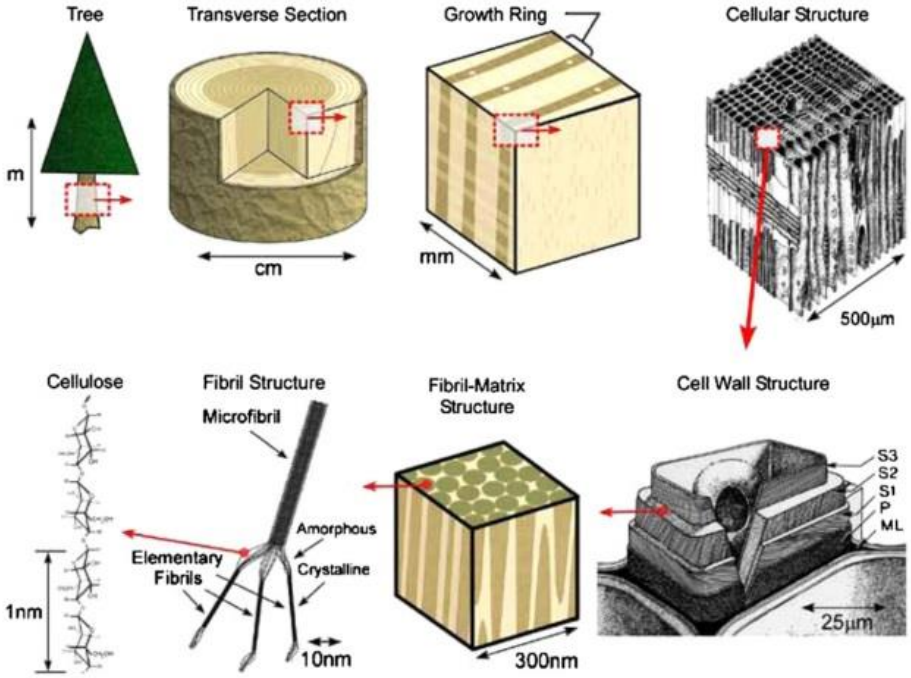

Figure 2.4: Schematic of the transformation process from tree to CNC where ML is the middle lamellae between tracheids, P is the primary cell wall, and S1, S2, and S3 are the cell wall layers.[43]

2.2.2. Properties

In order to maximize the reinforcing potential of CNCs in a PVA matrix, effective interaction must be achieved between the CNCs and the solvent. There are five different mechanisms for cellulose/solvent and cellulose/cellulose bonding: inter and intra molecular bonding between the cellulose hydroxyl groups, hydrogen bonding between the cellulose hydroxyl groups and solvent, hydrogen bonding between the solvent molecules, and electrostatic interaction between the solvent molecules. These all must be considered to develop a water-based processing method for CNC/PVA nanocomposites. Cai and Zang[47] have shown that the strength of hydrogen bonding in cellulosic gels is highly dependent on temperature. From this study it was seen that as temperature was increased from 0 °C to 55 °C in an aqueous NaOH/urea solution, hydrogen bonding characteristics were decreased between the cellulose particles and the solvents (free water, NaOH hydrates, and urea hydrates) while inter and intra molecular bonding character between the cellulose chains was increased. This phenomenon was attributed to a strong self-association tendency of cellulose particles to one another, leading to agglomeration and CNC polymer chain entanglement. This study also showed cellulose gelation in NaOH/urea aqueous solution is highly dependent on concentration as well as molecular weight of the cellulose providing insight into the processing behavior of CNC/PVA solutions and the need to successfully couple concentration and molecular weight of the proposed components.[47] Due to the agglomeration of the CNCs at high temperatures, it will be necessary to induce increased shear forces to maintain dispersion while also balancing mechanical and thermal degradation during processing. In another study conducted by Dorris and Gray,[48] stable thixotropic CNC gels were formulated

through the control of time, temperature, and agitation in a suspension of CNCs produced via acid hydrolysis in glycerol. In this study, gelation was observed at concentrations as low as 3 wt.% CNC.[48] These data are supported by Cai and Zhang[47] who also saw that temperature induced gelation did not occur below 3 wt.% CNC.[47] As the presented research proposes CNC concentration of over 50 wt.% with respect to PVA, gelation should readily occur increasing viscosity and processing capability.

2.3 Cellulose/Polymer Nanocomposites

2.3.1 Nanocomposites

There has been increased interest in nanocomposites in recent years due to their thermal, mechanical, and electrical properties. The increase in mechanical properties is due to the differences in the role of stress transfer at the nanoscale, increased surface area, and increased bonding interaction while changes in thermal and electrical properties can be attributed to increased component interaction at the surface of the nanomaterials and the inherent properties of the nanomaterials such as electrical and thermal conductivity. Van der Waals forces and electrostatic forces play a larger role when dealing with nanocomposites in increasing the dipole interaction. Quantum mechanics must also be taken into account as electron hopping influences the thermal and electrical properties of the nanocomposite. The effect of Brownian motion must also be taken into account when dealing with nanomaterials as the length scales are much closer to that of the constantly moving atoms, giving rise to increased random motion inside the

nanocomposite systems.[49] These forces come together to affect the thermal, mechanical, and electrical properties of nanocomposites.

2.3.2 Processing of Cellulose/Polymer Nanocomposite Systems

Processing strategy of nanocomposite systems affects dispersion, polymer/polymer, polymer/filler, and filler/filler actions, and mechanical properties, therefore; it is important to understand the effect of processing strategy on nanocomposite morphology. Cellulose/polymer nanocomposite systems are generally processed through the formulation of a polymer solution or suspension and a cellulose suspension and then mixed.[4] Cellulose nanomaterials pose a distinct processing challenge as they have a high affinity for self-association due to the interaction of their hydroxyl groups on the surface of the molecules. These hydroxyl groups are beneficial as they allow the cellulose to form percolating networks, but they also can cause aggregates in suspension leading to loss of the nanoscale size and reinforcement capabilities. Simultaneously, the smaller the cellulose nanomaterial size, the more aggregation is seen due to increased surface area.[4]

Film casting and evaporation have been studied as methods for incorporating cellulose nanomaterials into polymer systems. For example, a latex system has been studied using tunicin CNCs and poly(S-co-BuA) in which aqueous polymer dispersions with spherical particles on the order of 150 nm were constructed at 50 wt.% solids loading. It was found that formulating a suspension of nanocrystals and polymer particles allowed for the preservation of the CNC dispersion at the individual fiber level. These

CNC/latex solutions were film cast, and the water was allowed to evaporate out at room temperature.[50] In another study done on CNC/latex systems, it was noticed that during the evaporation stage, as the solids content increased, the polymer acted as a binding agent or impenetrable domain due to increasing viscosity, restricting the cellulose nanomaterials from aggregating. It was also seen that latex polymer size influenced the dispersion of the final nanocomposite system as the nanomaterials were held into place by the polymer chains.[51] Freeze dried CNC/latex systems were also studied with CNC derived from wheat straw. From this study, it was found that the nanomaterials were less homogeneous and a gradient of nanomaterial concentration was seen between the upper and lower sides of the nanocomposite film. This gradient of concentration was attributed to settling during the evaporation step of the casting procedure in which the nanomaterials randomly orient themselves on the bottom face of the film and decrease in concentration toward the top face.[52,53] Finally, Dubief *et al*.[51] noticed latex polymer size played a role in the mechanical properties. The larger the polymer size, the higher the mechanical properties due to increased space available for the nanomaterials to interact with one another.

Apart from latex systems, water soluble polymers have also been studied for their processing-property effects. Water soluble polymers contain functional groups, such as hydroxyl groups, that give them an affinity for water. This extent of hydration mainly relies on the number, frequency, and location of the hydroxyl groups and the interaction of the hydrogen bonding and ionic bonding sites to water. The stability of water soluble polymer solutions therefore originates not only from the availability of polar bonding sites but also on the competition between the polymer-water and water-water interaction and hydrophobic interaction from the apolar components of the polymer.[4] To make a

composite film from a water-soluble polymer and cellulose nanomaterials, the polymer can be suspended in the water and mixed with an aqueous solution of cellulose nanomaterials. This cellulose/polymer suspension can then be cast into a film and formed as desired after the water evaporates. Dissolution is important for cellulose/polymer processing as it allows for increased homogeneity of the polymer at the molecular level. The homogeneity of the nanocomposite suspension will depend on the temperature, polymer concentration, and molecular weight and will need to be optimized to produce the highest level of dispersion. Stirring is generally employed to formulate the cellulose/polymer solutions although mixing speed must be taken into account. If the stirring speed is too great, chain scission and aggregation of the polymer chains can occur decreasing the polydispersity index due to chain scission and the resulting mechanical properties.[4] For example, in a study conducted by Bossard *et al.*,[54] chain scission of poly(ethylene oxide) (PEO) in aqueous solution occurred with increasing molecular weight and concentration due to hydrodynamic forces from stirring and the additional stresses placed on the polymer chains during aggregation leading to chain scission.

A variety of water soluble polymers have been used in the processing of cellulose nanomaterial/polymer nanocomposite systems. Reinforced starch,[55–57] silk fibroin, PEO,[58–61] PVA,[17,42,62–66] hydroxypropyl cellulose,[67] carboxymethyl cellulose, soy protein isolate, phenol-formaldehyde resin, and hydroxyethyl cellulose[68] have all been used as hydrophilic polymer matrices for cellulose nanomaterial incorporation. Starch is one of the most commonly used polymers due to its abundance, sustainability, and favorable interaction with cellulose nanomaterials. Plasticizers are generally used when starch is employed in order to decrease the brittleness of the matrix. PVA has also been used as a

matrix for cellulose nanomaterials.[66,69–75] In a study conducted by Paralikar *et al.*,[64] PVA was crosslinked with poly(acrylic acid) (PAA) in conjunction with heat treatment. In this study, the PAA carboxyl groups plus the hydroxyl group on the PVA and CNCs formed ester linkages and hydrogen bonding giving the resulting CNC/PVA nanocomposite good chemical resistance, mechanical response, toughness, and flexibility.

Non-aqueous polymer dispersions can also be formed by dispersing the polymer in an organic medium and coating or functionalizing the cellulose nanomaterials with compatible groups in an effort to reduce the surface energy and stabilize the particles. This can be done through a variety of methods including solvent mixture, solvent exchange, in-situ polymerization, surfactant usage, and surface chemical modification.[4] For example, stable suspensions of acid hydrolyzed cellulose functionalized with negatively charged sulfate ions during the acid hydrolysis process were seen to be stable in polar solutions due to the high dielectric constant of the liquid and the wettability of the cellulose.[76] These sulfate functionalized cellulose nanomaterial solutions could then be freeze dried and dispersed in a non-aqueous polar media such as dimethylformamide (DMF),[76] dimethyl sulfoxide (DMSO), N-methyl pyrrolidine, and formic acid and m-cresol.[77] Solvent mixture and solvent exchange can be conducted on cellulose nanomaterials. In solvent mixing, an aqueous solution of cellulose nanomaterials is mixed with a solvent compatible with water. For example, homogeneous nanocomposite films based on $LiClO_4$-doped ethylene oxide epichlorohydrin copolymer and tunicin nanocrystals were prepared by solution casting tetrahydrofuran/water mixtures and compression molded.[78] An all cellulose film was formed from CNCs and cellulosic matrix regenerated from NaOH-urea solvent system of cellulose II using solvent mixing

due to the temperature dependent solubility of each of the components.[79] Solvent exchange was used to suspend cellulose in solution for further chemical modification and for mixing the suspension with polymer solution. Solvent exchange has been used to produce films with aqueous solutions of cotton derived CNCs in which the water was exchanged with n-methyl-2-pyrrolidone (NMP) and polysulfone.[80] Slow solvent exchange was also used to exchange water with acetone and then with DMF to prepare cellulose/epoxy nanocomposite films.[81] In-situ polymerization, in which the polymer nanocomposite is impregnated with monomer and the monomer is polymerized, has also been used to formulate cellulose/polymer nanocomposites. In in-situ polymerization, the monomer serves as dispersant for the nanomaterials as well as a matrix precursor. This technique has been used to make films of cellulose microcrystals (CMC) derived CNCs and polyfurfuryl alcohol without solvents or surfactant in which the polymerization of the furfuryl alcohol was catalyzed by the sulfate groups from the CNC surface. Finally, surfactants have been used to lower the surface tension of the liquid used to suspend the CNCs, interfacial tension between two liquids, or interfacial tension between a liquid and a solid in order to make non-aqueous CNC nanocomposite suspensions. For example, cotton and tunicin CNCs were coated with phosphoric ester of polyoxyethyene(9)nonylphenylether and stable suspensions in toluene and cyclohexane or chloroform were produced. From these suspensions, the excess surfactant could be removed by centrifuging or freeze drying the material and then redispersing the nanomaterial in a polar solvent.[82,83]

Apart from solution processing, melt compounding such as mixing, extrusion, hot pressing, or injection molding can also be used to make cellulose/polymer nanocomposite

systems. These techniques are not traditionally employed due to thermal stability of the cellulose nanocomposite systems and polymer incompatibility as many polymers are hydrophobic causing phase separation of the components. The thermal stability of the CNCs must also be taken into account as the sulfate groups that stabilize the CNC in suspension also decrease the thermal stability, giving a limited processing window.[4] To add cellulose nanomaterials into a polymer matrix, the components must be compatibilized using one of the previously discussed techniques and potentially subsequently dried for incorporation into the polymer. If the polymer matrix is polar, no compatibilization is necessary while if the polymer is apolar, solvent enhancement or functionalization must occur.[4] This drying can occur through oven-drying, air-drying, freeze-drying, supercritical drying, or spray-drying.[84] When freeze-drying and air-drying were compared, it was seen that the crystal structure and crystallinity was maintained through both freeze and air-drying but that the thermal stability varied depending on drying technique. For example, when comparing the amount of char produces through different drying methods in the TGA, there was a larger amount of char after air-drying compared to freeze-drying due to the regular packing of the air dried CNCs.[85]

Melt processing without compatibilization has been conducted on starch and PEO polymer with cellulose nanomaterials. Starch reinforced CNC monofilaments and films were produced via extrusion and seen to have an improvement in tensile strength due to shear alignment of the filler.[86] High molecular weight PEO reinforced with CNCs was produced via extrusion in which the components were freeze dried after an aqueous mixture was formed and melted in an extruder under nitrogen. From this study, the CNCs were extracted from the PEO in order to gain understanding of the effects of extrusion on

CNCs. It was seen that extrusion decreased the length and cross section of the CNCs from 200 nm to 120 nm and 7 nm to 5 nm respectively.[87]

Melt compounding with compatibilization was conducted using solvent exchange. A study was conducted by Suryanegora *et al*.[88] in which a cellulose microfibril (CMF) water dispersion was mixed with acetone and poly(lactic acid) (PLA) was added under stirring. The liquid was evaporated, and the solids were mixed in a roller mixer and crushed. The CMF/PLA mixture was then injection molded and increased stiffness was seen at CMF loading of 10 wt.% with no change in crystallinity.[88,89] Bondeson and Oksman[90] used PVA as a compatibilized to promote CNC dispersion in PLA. The PVA was fed into the extruder via dry mixing of the CNCs with PLA prior to extrusion and direct suspension pumping. In this study, phase separation occurred between the PVA and the PLA with PVA as the discontinuous phase and PLA as the continuous phase. The CNCs were found mostly in the PVA phase due to the increased hydrophilicity of the PVA compared to PLA. This phase separation lead to poor mechanical performance of the system.

Besides solution processing and melt compounding, a few other techniques have been studied to incorporate cellulose nanomaterials into polymer matrices such as filtration and impregnation, fiber electrospinning and spinning, and the formation of multilayer films. In the filtration and impregnation processes, an aqueous solution of cellulose nanomaterials is filtered out to get a continuous film or mat of cellulose and this film is immersed in a polymer solution under vacuum to promote wetting.[4] Studies have been conducted on the processing of cellulose nanocomposite films using transparent

thermosetting resins such as pheno formaldehyde, epoxy, acrylic, and melamine formaldehyde.[91–93] In the electrospinning process, polymer fibers are produced. Electrospinning presents some processing challenges such as control and correction between operational conditions, difficult morphology control due to variation in voltage, distance between spinning tip and collector, and polymer material properties such as conductivity, viscosity, density, surface tension, and flow rate.[4] Bacterial cellulose (BC)/PEO nanocomposites were electrospun and gave diameters less than 1 μm with globally well embedded and aligned CNCs despite partial CNC aggregation.[94] CNC/PVA nanofiber mats were made through electrospinning giving fibers on the nanoscale in diameter with enhanced mechanical properties.[95] Cotton CNC/PVA fibers were gel spun using methanol and dried. The fibers produced had draw ratios of 20 to 38 with high orientation and mechanical properties. The Young's modulus of these fibers was found to be 56 GPa with 30 wt.% CNCs.[69] Finally, multilayer films were made through layer by layer assemblies in which thin films with oppositely charged layers were deposited atop one another. This technique is desirable as it gives uniformly thick films on the nanoscale and does not require sophisticated hardware.[4] In a study conducted by Podsiadlo *et al.*,[96] cotton CNC multilayer composites with a polycation of poly(diallyl dimethylamonium chloride) were produced with high uniformity due to the dense nanocrystal packing achieved.

The processing of cellulose/polymer nanocomposite systems has been extensively studied. Through these studies, dispersion control was seen to be a challenge. While solution processing of components suspended in suspension tended to give the best dispersion properties due to the homogeneous dispersion of the components before

adding them together. Melt processing is a desirable processing technique as it is both industrially and economically viable as well as allows for greener processing.[4] Currently cellulose challenges that should be addressed are controlling/limiting the thermal degradation of the cellulose during processing and application, increasing polymer-cellulose compatibility, and increasing the understanding of dispersion attained.

2.3.3 Rheology of Cellulose Suspensions and Cellulose/PVA Nanocomposites

Cellulose nanomaterials have high surface area and high density of surface hydroxyl groups influencing the interactions present in the liquid and solid states. Understanding the liquid state interaction through rheological characterization is important for understanding nanocomposite processing. For example, CMF suspensions at 2 wt.% in suspension formed a gel-like structure during suspension homogenization as the viscosity of the suspensions increased with particle interaction.[4] This transition to a gel was attributed to the increasing length to diameter ratio of the suspended nanomaterials as they were dispersed in the suspension. If the solids loading of the CMF was increased to too large of a value, the viscosity became too high and processing became difficult. Studies conducted on CMF suspensions showed that a gel was formed at 2 wt.% CMF in suspension as well as showed shear thinning in response to shear.[97,98] It was also seen that the gels exhibited thixotropic viscosity and increased gel stability when stored or subjected to freeze/thaw cycles. CMF suspensions were also studied by Lowys *et al*.[99] using both cone and plate and parallel plate rheology for steady shear and dynamic viscoelastic measurements respectively. From these studies, it was found that

viscosity increased with increasing CMF loading and that a critical concentration was present in which the suspension became a physically crosslinked gel structure due to CMF entanglements. From this study it was also found that ultrasonic dispersion was more effective at suspending the CMF in suspension compared to mechanical stirring. It was also seen that there was no variation in G' with temperature from 25 to 60 °C. The effect of CMF concentration, temperature, ionic strength, and pH was studied on CMF suspensions at concentrations of 0.5 and 1 wt.% in suspension from either re-suspended freeze dried CMFs or fresh CMF suspensions. While no damage was seen after freeze drying the samples, freeze dried CMF suspensions had G' values three times smaller than fresh CMF suspensions most likely due to aggregation. While altering the pH level and temperature showed no appreciable reinforcement of the system, increasing ionic strength showed increased viscoelastic properties due to increased interaction of the CMFs.[100]

Rod-like CNCs were also studied for their behavior in suspension and it was seen that colloidal systems were formed.[4] Suspension stability was seen to be dependent on CNC dimension, polydispersity, and surface charge. In a study conducted by Araki *et al.*,[101] it was seen that sulfuric acid hydrolyzed nanocrystals gave more stable CNC suspensions compared to hydrochloric acid functionalized nanocrystals due to the negative charge of the sulfuric acid functional group. As discussed, CNCs were formed from acid hydrolysis of cellulose particles to remove the amorphous regions of the cellulose leaving the rod-like crystal regions. During this acid hydrolysis with sulfuric acid, negatively charged sulfate ester groups were formed on the surface of the CNC, forming an electric double layer giving rise to repulsion between the nanocrystals. This repulsion influenced the interaction of the cellulose nanomaterials on the polymer matrix

utilized, the solution used to suspend the solids, and the CNCs themselves.[4] While the sulfate groups help to stabilize the suspension, they also decrease the degradation temperature and increase the amount of char produced after degradation.[3] In order to reduce the amount of thermal degradation present, low concentration of sulfate groups and sulfate to cellulose ratios should be achieved as well as the shortest hydrolysis times that are effective in isolating the CNCs.[4]

In order to get an idea of the dispersion state of CNC suspensions, polarized light is often used to understand CNC orientation and if any ordered structures are present. CNCs have two refractive indices allowing them to have uniaxial anisotropy and are good candidates for polarized light characterization due to their birefringence. When the polarized beam is applied to the CNC suspension, the light refracted is plane polarized showing the birefringent character of CNC suspensions.[4] The birefringent characteristic of CNCs was first seen in 1959 by Marchessault *et al*.[102] In their study, tunicin nanocrystal suspensions at 0.5 wt.% were observed in either water or DMF and electrostatic repulsions was observed due to the negative charges of the functional groups on the CNCs.

In addition, some CNC particles have liquid crystal properties. Liquid crystals are an intermediate state of matter in which both liquid characteristics and solid crystal characteristics are present.[103] Liquid crystals are usually rigid molecules that flow like a fluid but have some kind of particle alignment and are formed by anisotropic molecules or rigid rod-like particles.[104] Liquid crystals can have either nematic or smectic orientation. In the nematic state, the liquid crystals have no positional order but the

particles usually point in the same direction. In the smectic state, one or more degrees of orientation order compared to the pneumatic state are seen but the particles align themselves in planes losing positional order. The smectic state has more solid like characteristics than the nematic state due to their increased order.[4] Some CNC solutions have been seen to form lyotropic liquid crystals. When viewed under a polarized light microscope, texture is seen, due to the rod-like structure of the CNCs.[102] In a study using cotton derived CNCs, phase separation was observed with an isotropic phase in the top part of the solution and a chiral nematic liquid crystal phase in the bottom part of the solution. This phase separation was seen due to differing of textures in each section. Nanocrystals were seen to be ordered within the individual domain.[102] While liquid crystal behavior has been seen for some CNC systems, in the presented research, this behavior was not noticed.

CNC suspensions have been studied with rheology. CNC solutions experience shear thinning even in dilute concentration with shear thinning character increasing with increasing CNC loading, in other words, there is a concentration dependence of the system at low shear rates and a concentration independence of the system at high shear rates.[4] The aspect ratio of CNCs has been found to play a key role in the rheological properties and shear thinning characteristics of CNC suspension. CNCs with larger aspect ratios (lengths around 280 nm) were found to be more susceptible to shear induced orientation than CNCs with lower aspect ratios (around 180 nm), where these lower aspect ratio CNC systems were found to relax much more quickly.[105] CNCs in a 1 wt.% aqueous solution of high molecular weight PEO were studied and it was seen that the viscosity of the suspension decreased when CNCs were added and then increased with a

minimum viscosity found at concentration of 6 wt.% CNC. This decrease and then increase in viscosity with CNC addition was attributed to the strong interactions that were formed between the oxygen bonds on the PEO and the hydroxyl groups of the CNCs. This strong affinity acted like a thermal buffer for the CNCs, allowing them to be melt processed in low density polyethylene with minimal thermal degradation.[106]

The rheological properties of CNC/PVA systems have been briefly studied.[107] Chang *et al.*[107] studied the linear viscoelastic response of powdered cellulose/PVA composites subjected to freeze and thaw cycles in 75/25, 50/50, and 25/75 weight per weight ratios and found that these systems had weak frequency dependence and were highly elastic. In this research, both chemically and physically cross-linked gels were studied. It was seen that the chemically cross-linked systems had a high degree of swelling while the physically cross-linked systems showed higher G' indicating highly developed inter and intra-molecular bonding due to the compaction of the chains during freezing and thawing. It is hypothesized components of this gelation behavior can be used in the development of a shear processing method and then transferred to generate dried nanocomposite systems highly concentrated with CNCs.

2.3.4 Thermal Properties and Crystalline Structure of Cellulose/Polymer Nanocomposites

The thermal properties of nanocellulose/polymer systems have been studied using differential scanning calorimetry (DSC) for their glass transition temperature (T_g), melting temperature (T_m), degradation temperature, and crystallization behavior. As

cellulose is a hydrophilic system, there is always some water present in the form of free water, freeze-bonded water, or bounded water. Free water behaves as normal water during cooling and melting and can be removed through drying the system. Freeze-bonded water will allow for supercooling effects on the system and bonded water will not freeze but will change the physical and chemical properties of the system. CNCs do not show any thermal transitions using DSC before their degradation temperature (no T_g or T_m). Cellulose will degrade around 220 °C but will start to turn a yellowish brown color at 180 °C due to the loss of chemical stability.[4] Cellulose experiences thermal degradation in multiple steps. The first step involves the depolymerization of the cellulose chain producing alkali-soluble products.[108] This depolymerization occurs after the cellulose polymer has absorbed enough energy to cleave the glycosidic bonds and produce glucose. When temperatures above 200 °C are reached, volatiles from the cellulose are produced. Cellulose can also be degraded via transglycosylation, oxidation, decarboxylation, and dehydration and degradation is accelerated if water, acid, or oxygen is present in the system.[4]

CNCs have reduced thermal stability due to the acid hydrolysis step used in the formulation of the nanocrystals, especially the presence of sulfate groups after the hydrolysis step when sulfuric acid is used. The degradation of CNCs hydrolyzed with sulfuric acid was studied by Roman and Winter.[3] In this study, they described CNC degradation in two steps, the first occurring at low temperatures and the second occurring at high temperatures. At low temperatures, the less ordered regions of the CNCs were degraded due to the high concentration of sulfate groups available in these regions. At high temperatures, the crystalline regions of the CNCs were degraded as the sulfate

groups were less available and at lower concentrations in these regions. If the CNCs were very highly sulfonated, an extra degradation step was seen as the sulfonated ends of the CNC crystalline regions degraded.[3]

The thermal degradation of CNC systems can be controlled or decreased through a variety of chemical modifications. Wang *et al.*[2] neutralized sulfuric acid hydrolyzed nanocrystals through the use of NaOH. Similar neutralization was conducted by Habibi *et al.*[109] and an increase in degradation temperature of 50 °C was seen. Thermal stability of CNCs was also seen through the use of surfactants[110] or PEO molecules.[106] By absorbing PEO into the surface of the nanomaterial, the degradation temperature was shifted to higher temperatures with a lower temperature range in which degradation occurred and was only improved through the increase in PEO molecular weight. This increase in thermal stability was attributed to the protection of the CNC by the absorbed PEO.[106] For similar reasons, polymer grafting also increase the thermal stability of CNCs.[4,111] Thermal degradation of CNC/PVA systems can be controlled through monitoring the extent of hydrolysis of PVA. For example, the degree of hydrolysis controls distinct characteristics of synthesized PVA such as gelation, mechanical, and rheological behavior and can vary from 70% to 99%.[10] It is also known that partially hydrolyzed PVA are more susceptible to thermal degradation than fully hydrolyzed PVA due to the vinyl acetate groups.[12]

The T_g of polymer systems filled with nanocellulose particles has been studied. From these experiments it was seen that many cellulose nanomaterial/polymer systems do not experience a change in T_g at loadings below 30 wt.% cellulose.[59–61] Other cellulose

nanomaterial/polymer systems, mainly starch systems, saw a decrease or increase in T_g with CNC incorporation. For example, in a study conducted on glycerol plasticized starch-based composites filled with tunicin nanocrystals, the T_g decreased at low CNC loadings below about 3 wt.% CNC and increased at higher loadings above 6 wt.% CNC. These increasing and decreasing trends of T_g were attributed to the phase separation of the glycerol and start in the neat material, with each polymer phase exhibiting its own T_g. The fluctuation in T_g with CNC loading was attributed to the interaction of the hydroxyl groups on both the cellulose and starch surfaces, the partitioning of water and glycerol inside the starch matrix, and restriction of the starch chain mobility next to the CNCs coated with starch crystallites.[112] In systems containing PVAc reinforced with CNCs, it was seen that the CNCs prevented PVAc from being as plasticized by water compared to neat PVAc systems due to the CNCs restricting polymer chain mobility. Decreased T_g values were seen with increasing water content in nanocomposites compared to the neat polymer matrix. When the moisture content was kept constant and the T_g values were compared with CNC loading, T_g increased for the nanocomposite with increasing CNC concentration. This T_g increase was attributed to the limited ability of the sample to take up water due to a continuous CNC network inside the system.[113] CNCs were studied inside different copolymers of PVAc and PVA with varying degrees of hydrolysis and hydrophilicity to see the effect of hydrolysis and hydration state on CNC/PVAc or PVA nanocomposite systems. The samples were conditioned at different degrees of hydration. It was seen that mobility was decreased (strongest interaction present) in the dry CNC/PVAc or PVA samples for fully hydrolyzed polymer samples compared to partially

hydrolyzed polymers. The T_g increased significantly with CNC addition in wet samples regardless of the degree of hydrolysis.[17]

The degree of crystallinity has also been studied on cellulose nanomaterial/polymer systems. In most cases, adding cellulose nanomaterials into the system increases the degree of crystallinity of the polymer due to nucleation of crystal structures at the cellulose nanomaterial surface but the extent of crystallinity increase varied. Polymer crystallinity is strongly influenced by the processing technique, thermal history, shape, surface area, and rigidity of the nanofiller used. Various factors were seen to limit crystal growth. For example, nanocomposites using polymers such as PVA and PEO with high affinity for cellulose were seen to have restricted mobility when then polymer chains were in contact with the nanocrystal surface limiting crystal growth into the matrix.[17,60,114,115] Also, if the viscosity of the polymer melt was very high and a dense cellulosic network was formed, the activation energy necessary for the diffusion of polymer chains was increased giving smaller and fewer crystals.[60,115]

2.3.5 Mechanical Properties of Cellulose/Polymer Nanocomposites

Studies have been conducted on cellulose/PVA and nanocellulose/PVA systems using cellulose microfibers (MFs), wood fiber (WF),[116,117] CMC,[66,116] CNFs,[118] CMF,[42] fibrous cellulose powder,[107] BC,[119,120] and CNCs.[17,20,46,69,71,95] CNCs are beneficial as structural fillers in these systems as they are have higher aspect ratios than CMFs and MFs and are on the length scales of PVA chains opposed to CMFs, MFs, and BCs. CNCs

also have charged surfaces increasing stress transfer. MFs and CMFs have large amorphous regions opposed to the highly crystalline CNCs, therefore increasing the reinforcing potential of CNCs in the semi-crystalline PVA matrix.[46] From these studies, it was seen that the incorporation of 10 wt.% CNCs derived from okra into PVA increased the modulus from 1.3 GPa in the neat PVA to 1.9 GPa.[70] CNCs derived from corncobs were added into PVA at 9 wt.% and the ultimate tensile strength was increased by 140.2%.[121] When CNC/PVA solutions were gel spun and their mechanical properties characterized, a decrease in tensile strain from 9.4% to 3.8% was seen due to the increased crystallinity of the system with increased CNC loading.[69] Copolymers of PVA and PVAc were also studied for their compatibility with CNCs by Roohani *et al*.[17] In this study, the degree of hydrolysis was varied to see the effect of hydrolysis on the hydrophilicity of the system and the degree of interaction between the polymer and the CNCs. From these studies, it was seen that increasing the degree of hydrolysis increased the tensile modulus due to increased filler/matrix interaction as hydrogen bonding increased. It was also seen from this study that as the water content of the system increased, the reinforcement of the matrix decreased due to plasticization of the matrix and strong water-cellulose interactions that disrupt inter-cellulose connections.

Nanocellulose materials such as CMF and CNCs have been investigated to determine their effectiveness in the improvement of mechanical performance in polymer systems due to their high aspect ratios, mechanical strength and stiffness.[4] In a study conducted by Iwatake *et al*.,[122] CMFs were incorporated into PLA. In this study, Young's modulus was increased by 40% and tensile strength was increased by 25%. Starch based systems filled with nanocellulose have also been studied. CMF/starch systems were

prepared with up to 50 wt.% starch and the tensile modulus was seen to increase from 2 GPa in the neat starch state to 7 GPa with 50 wt.% CMF incorporation.[56,123] The reinforcing potential of CNCs was investigated by Favier *et al*.[50] in 1995 in a matrix of styrene and butyl acrylate (poly(S-co-BuA). From this study, the solid state storage modulus (*E′)* above the T_g was increased by two orders of magnitude through the incorporation of 6 wt.% CNCs.

In order to better understand the reinforcing potential of cellulose nanomaterials on a polymer system, mechanical models have been developed for CNCs and CMFs. CNCs were seen to be easier to model than CMFs due to their more predictable geometry.[4] The mechanical behavior of any multi-component system depends on the component morphology, volume fraction, interfacial properties, and the properties of each component. The mean field and percolation approach have both been used to model cellulose nanomaterials systems.[4] To better understand the reinforcing potential of CNCs, a mean field approach developed by Halpin-Kardos,[124] also known as the "upper bound" of mean field approaches, has been used to predict the elastic shear modulus of short-fiber composites in semicrystalline polymer matrices. This model is only applicable at temperatures much higher or much lower than the T_g, In this model, composite orientation is assumed to be divided into four layers with CNC orientation at 0°, 45°, 90°, and -45° in each layer. As the number of equally oriented plies in the composite increase, the mechanical properties become isotropic. This model incorporates the mechanical properties of the polymer and the filler, the anisotropy of the filler, and the size, shape, and volume fraction of the filler but does not account for the interactions of the individual fibers with one another.[124] This model has been used on CNC/polymer nanocomposites

composed of poly(S-co-BuA)[50,52,125] and PVC,[126] and it was seen that the predicted high temperature modulus did not describe the experimental findings as the glassy modulus was overestimated and the rubbery modulus was underestimated using DMA.[52,126] However, when applied to the glassy modulus of tensile data, the model seemed to be a good indicator of mechanical properties.[125]

An additional model, the percolation approach, has been used to predict the mechanical behavior of CNC nanocomposite systems at which filler loading was large enough to have filler-filler connections and interactions. The percolation threshold is the volume fraction between the connected and disconnected filler states.[127] This threshold can be altered through the orientation,[128] particle interactions, or aspect ratio[129]of the filler.[4] Through the use of the percolation model, it has been seen that a rigid network of CNCs was the reason behind the high reinforcing potential of these fillers, especially at high temperatures. The percolation approach consists of three steps. The first is the determination of the percolation volume fraction, in which the aspect ratio is taken into account and divided by a factor of 0.5 to 0.7.[4,130–132] Once the percolation threshold is determined, the stiffness of the percolating filler network is determined. This stiffness depends on the cellulose origin, cellulose preparation technique, and the inter-particle interaction associated with the cellulose-cellulose bonding. Measurements on the modulus of a CNC range from 500 MPa to 15 GPa[133] compared to 17 GPa for a sheet of CNCs prepared from bacterial cellulose[134] and 10 GPa for cotton cellulose.[135] Finally, the third step in determining the percolation behavior of nanocomposite systems involves correlating the matrix behavior, percolating phase, and non-percolating filler phase in a total description of the nanocomposite behavior. Factors effecting the percolation

behavior of the nanocomposite include the crystallinity of the matrix, processing technique chosen, and any other component that could hinder or help the percolating network.[4]

Processing technique will also affect the mechanical properties. Casting followed by evaporation, hot pressing, and shear mixing have all been studied for cellulose nanomaterial/polymer systems. These three processing strategies were compared by Hajji *et al.*[125] in which an aqueous suspension of nanomaterial and latex were mixed and the effect of processing on film formation using casting and evaporation, freeze-drying and hot pressing, and freeze-drying, hot pressing, and extrusion was studied. CNC content from 0 to 6 wt.% was studied and the effect of processing was compared using tensile tests in both the rubbery and glassy regime. From these studies, it was seen that extrusion provided the least amount of CNC reinforcement while casting and evaporation gave the best reinforcement properties due to breaking and orienting of the CNCs during freeze-drying and extrusion resulting in stress concentrators in the matrix and decreasing reinforcing capability.

Material compatibility also plays a role in mechanical reinforcement of cellulose nanomaterial/polymer systems. For example, polar matrices are compatible with cellulose giving increased stress transfer. For example, CNC/PEO nanocomposite systems were studied using DMA to determine the reinforcement capability of CNCs on PEO. From these studies, no change in crystallinity was seen in the matrix with CNC loading. Therefore, the reinforcement of the nanocomposite system was attributed to the incorporation of the CNCs. In these composites, reinforcement was also seen above the

melting point of the system due to the CNCs ability to limit the flow of the polymer chains as a CNC percolating network was formed.[60]

When examining the relaxation of cellulose nanomaterial/polymer systems in DMA, the magnitude of the relaxation peak (tan δ or loss modulus) decreased with increasing nanomaterial loading. This was attributed to the decrease in the amount of polymer matrix material present. In other words, as the amount of mobile polymer chains decrease, the ability of the system to have a relaxation event decreases. In some cases, the relaxation might increase with increasing cellulose nanomaterial content potentially due to particle-particle slippage or friction, particle-polymer motion at the filler interface, and changes in the properties of the polymer due to adsorption into the filler particle.[4]

2.3.6 Biodegradation of Cellulose/Polymer Nanocomposites

Research has been done specifically on cellulose material filled polymer composites and their biodegradation characteristics to formulate renewable and sustainable nanocomposite systems. For example, PLA, a biodegradable thermoplastic polyester produced from corn,[136] and starch nanocomposite systems have been created as biodegradable systems with improved mechanical properties.[137] Studies have been conducted examining PVA as a synthetically derived biodegradable polymer due to its hydrophilic character.[10] Cellulose filled polymer systems have also been studied to exploit the high stiffness, high yield, and high aspect ratio of cellulose nanomaterials.[136] Although much study has been done to increase the understanding of biodegradable

polymer systems, some challenges still remain. For example, biodegradable systems tend to be brittle, have low thermal stability, and poor barrier properties.[138] Some examples of cellulosic filled polymer systems with biodegradation characteristics include PLA, PHB,[139] and starch based polymer matrices.

The biodegradation of PVA based materials has also been studied.[10] PVA will experience ultimate biodegradation in the presence of *Fusarium lini*, a phytopathogenic fungus produced from CO_2 and water due to extracellular attach by dehydratse.[140] PVA is biodegradable with an increased ability to biodegrade at lower degrees of hydrolysis. When subjected to soil burial tests, the average molecular weight of PVA was seen to increase with the PDI was seen to decrease. This was attributed to the leakage of the low molecular weight fractions from the PVA combined with the preferential bacterial assimilation on low molecular weight PVA chains.[141]In the fully hydrolyzed state, there was a limited ability for PVA to biodegrade in soil with only 10% weight loss over 2 years.[142,143] When lignocellulosic or biodegradable plant based materials are added into PVA, the biodegradation characteristics are increased. For example, the biodegradation properties of starch/PVA systems increased with increasing starch content.[10] Little work has been done on the specific understanding of cellulose/PVA biodegradation, especially in soil. The presented research hopes to increase the understanding on the effects of adding CNCs into PVA and these nanocomposites biodegradation characteristics.

CHAPTER 3

MATERIALS AND METHODS

This Chapter describes the materials and experimental methods used in this research. Nanocomposite samples for this research were composed of PVA or CNCs (either aqueous suspended or freeze-dried). Neat PVA samples were also produced and characterized for comparison. These samples underwent optical and rheological characterization as solutions or suspensions and microstructural and mechanical characterization as dried films produced from these solutions or suspensions. Processing operations to incorporate CNCs included solution processing, batch mixing with a torque rheometer, and redispersing of freeze-dried CNCs. Dried films were cast after these processing operations. Sample microstructure was characterized via optical microscopy, FT-IR spectroscopy, and XRD. Mechanical properties of the films were determined through DSC, DMA and MTT. Biodegradation and water recovery studies were also conducted to determine the sustainability and scalability of the samples and processing method, respectively. The results obtained from these experiments are presented in subsequent Chapters.

3.1 Materials

3.1.1 Poly(vinyl alcohol)

PVA polymers with three different molecular weights were used in this research to understand the effect of polymer molecular weight on component interaction, processing, and properties. PVA polymers purchased from Sigma Aldrich with weight

average molecular weights represented by a range of 31,000–50,000 g/mol (99+% hydrolyzed), 85,000-125,000 g/mol (98-99%% hydrolyzed), and 146,000-186,000 g/mol (99+% hydrolyzed) were used as received. These molecular weights will be references as 31K, 85K, and 146K respectively. Figure 3.1 shows an image of 146K neat PVA as received.

Figure 3.1: 146K Neat PVA pellets as received

3.1.2 Cellulose Nanocrystals

Two types of CNCs were used in this research: aqueous suspended and freeze-dried shown in Figure 3.2. Both types were produced by acid hydrolysis of southern yellow pine by dissolving the pulp with sulfuric acid. The aqueous suspended CNCs were provided by the USFS Forest Products Laboratory and received in aqueous suspension. The suspension had a 5.5 wt.% solids loading. The freeze-dried CNCs were purchased from the University of Maine Process Development Center. Similar wood-derived CNCs have been reported to have lengths of 100-140 nm and diameters of 6-10 nm.[1–3]

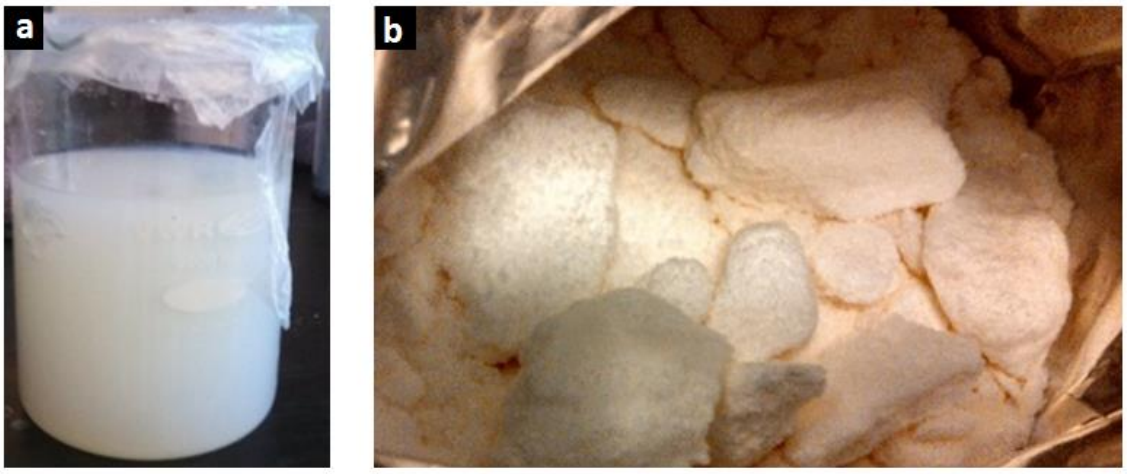

Figure 3.2: CNCs used in this research. a) Aqueous suspended CNCs b) Freeze-dried CNCs.

The zeta potential and size determined through light scattering of the aqueous suspended and freeze-dried CNCs were examined to determine any structural differences. 0.1 wt.% CNC solutions of freeze-dried CNCs and aqueous suspended CNCs were made and tested. Three tests were conducted and averaged. The standard deviation was calculated. The size was given as the z-average. The data from these measurements can be found in Table 3.1. From these data, it was seen that the charge on the CNC regardless of freeze-dried or aqueous suspended was comparable. The aqueous suspended CNC systems showed one peak at 160 nm while the freeze-dried CNCs showed multiple peaks at 40 nm, 340 nm and 3400 nm. The 40 nm peak was small and corresponded to impurities during processing such as dust from the fume hood during the 24 hour redispersion processes. The 340 nm and 3400 nm peaks corresponded to the more dispersed and aggregated freeze-dried CNCs, respectively.

Table 3.1: Zeta potential and size of aqueous suspended and freeze-dried CNCs.

	Aqueous suspended CNCs	**Freeze-dried CNCs**
Zeta potential (mV)	-45.2 ± 1.5	-41.9 ± 0.3
Size (nm)	160.5 ± 0.9	340.4 ± 4.1 or 3400 ± 500

3.1.3 Sample Nomenclature

Throughout the text of the presented research, the samples are named by an abbreviation of the molecular weight used, followed by "neat" if the sample is pure PVA and the percent solids loading if in solutions. For example, the sample name referencing the lowest molecular weight neat PVA solution used at 10 wt.% solids would be 31K neat 10 wt.%. With the addition of CNCs, the nomenclature will change slightly. If referring to the same sample in the dry state, the nomenclature would simply be 31K neat.

With the addition of CNCs, the nomenclature will change. The state of the CNCs will be defined as either aqueous suspended CNCs or freeze-dried CNCs. When referring to the concentration of a specific solution, the amount of CNC with respect to PVA will be used. For example, the sample referring to the highest molecular weight PVA polymer range used at 20 wt.% CNC with respect to PVA in solution will be named 146K 20 wt.% CNC w.r.t. PVA in solution. For the same sample in the dry state, the nomenclature will change to 146K 20 wt.% CNC w.r.t. PVA. The percent solids will be indicated when for sample which are not 15 wt.% solids. Solution processed will be used to describe those samples solution processed, shear mixed samples will be defined as either 40 RPM shear mixed or 91 RPM shear mixed depending on the procedure used in the mixer, and redispersed freeze-dried samples will be referred to as RDFD.

3.2 Methods

3.2.1 Solution Processing

Neat PVA solutions and some CNC/PVA suspensions were prepared using a solution processing protocol in this work. Neat PVA solutions were prepared by heating deionized water to boiling using a hot plate and adding PVA in quantities to produce solutions with solids loadings of 5, 10, and 15 wt.%. The solution temperature was monitored with a thermocouple during the preparation. The PVA solutions were then stirred in a covered beaker for 1 hour using a Talboy overhead mixer model 134-1 at 1900 RPM with a 2 in diameter stainless steel propeller blade. Nanocomposite suspensions were prepared by adding the desired amount of CNCs to the previously prepared PVA solutions at a temperature of 100 °C (boiling). The CNCs were incorporated by stirring with the same overhead mixer at 1900 RPM for 90 minutes. During stirring, the nanocomposite suspensions were left uncovered to allow excess water to evaporate to obtain a final overall solids loading of 15 wt.% in the case of the aqueous suspended CNC systems and the redispersed freeze-dried CNC systems. After sample preparation, the CNC/PVA samples were further treated using a centrifuge at a rotational speed of 3000 RPM for 5 to 30 minutes to remove any visible bubbles present after mixing depending on sample viscosity. Samples were made with all three PVA polymers in the aqueous suspended CNC systems while only 146K molecular weight PVA was used for the freeze-dried systems.

The solids loadings of the neat PVA solutions and nanocomposite suspensions were confirmed using thermogravimetric analysis (TGA) with a TA Instruments Q5000IR TGA. Experiments were conducted in a nitrogen environment at a gas flow

rate of 20 mL/min. A nominal sample mass of 20 mg was tested by heating the samples from room temperature to 120 °C at 10 °C/min followed by an isothermal step at 120 °C for 20 minutes. The solids loading was calculated using the sample weight remaining at the end of the isothermal step. One test was run for each sample.

Freeze-dried CNCs were redispersed in water by adding 5.5 wt.% CNCs into deionized water at 25 °C and stirring the solution with the Talboy overhead mixing unit at 1900 RPM for 24 hours. The solution was covered through the mixing process. 5.5 w.t% CNCs was the loading chosen for the weight percent of the redispersed CNC system to mimic the 5.5 wt.% aqueous suspended CNC solutions.

3.2.2 Shear Mixing

Shear mixing studies were conducted using a Brabender Inteli-Torque Plasti-Corder® Torque Rheometer with a 60 mL internal mixer attachment and roller blades. The shear mixing procedure consisted of preparing a neat PVA solution and adding in the appropriate amount of freeze-dried CNC powder to achieve the desired loading. The freeze-dried CNCs were added into neat PVA solutions in a fume hood to wet the CNCs in which the PVA solution was prepared 2 hours prior. The PVA solution had cooled to room temperature at the time the CNCs were added. The freeze-dried CNCs were incorporated by brief manual stirring. Aqueous suspended CNC/PVA suspensions were mixed at 40 RPM and 80 RPM for 10 minutes while freeze-dried CNC/PVA mixture was placed in the internal mixer using a mixing speed of 40 RPM or 91 RPM for 10 minutes. Different speeds were used for aqueous suspended and freeze-dried CNCs as the aqueous suspended systems were initially tested and the parameters where altered after aqueous

suspension characterization for the freeze-dried systems. After mixing, the CNC/PVA suspensions were removed from the mixing bowl with a spatula, transferred to 10 mL syringes, and centrifuged at 3000 RPM until bubbles were removed. The amount of centrifuging time needed depended on the viscosity of the solution and the CNC loading. Generally, the time needed for this step varied between 5 and 30 minutes. Rheological characterization of suspensions, as described in a subsequent section, occurred the next day. Due to the quantity of material needed to fill the internal mixer, only one test was run for each mixing speed/sample combination.

3.2.3 Rheology

Rheological experiments were performed using a TA Instruments AR2000EX rheometer with a 25 mm parallel plate fixture at 25 °C and a Thermo Mars II parallel plate rheometer, (Thermo Fisher Scientific, Inc., Waltham, MA), with 21mm diameter parallel steel plates at 25 °C. Rheological samples were loaded using a syringe, the gap was lowered to 1000 μm, and the samples were trimmed. After sample loading, a thin coating of silicone oil (Acros Organics) with a viscosity of 150 mPa·s was applied to the exposed sample surface using a pipette to reduce water evaporation during testing. Steady shear and small amplitude oscillatory shear tests were performed in order to determine the viscosity of the solutions so that appropriate molecular weights and solids loadings of PVA could be chosen for shear mixing. Steady shear tests were performed using a shear rate range of 0.1 to 1000 s^{-1} following a pre-shear step at 1 s^{-1} which lasted for 30 seconds. The pre-shear step was determined through steady shear viscosity testing. Steady shear data was collected from 0.1 to 1000 s^{-1} and the lowest shear rate required to

eliminate start-up error due to processing induced orientation effects was determined through leveling out of the viscosity data with shear rate, highlighted in the box in Figure 3.3. A pre-shear time was determined by recommendation of the rheometer manufacturer TA Instruments. These tests were conducted at times points of 1 day, 3 days, and 5 days after sample preparation to determine if any changes in solution structure due to aging were occurring. Steady shear viscosity data were collected and plotted as a function of shear rate to determine which solutions had a high enough viscosity within an acceptable shear range for the mixer. Small amplitude oscillatory shear tests were performed using a frequency range of 0.1 to 100 rad/s at a strain of 1% following a 30 second pre-shear step at 1 s^{-1}. This strain was in the linear viscoelastic region as determined from strain sweep measurements at 100 rad/s. Each test was also conducted at time points of 1 day, 3 day, and 5 day after sample preparation to determine the effect of aging on dynamic behavior. Storage modulus (G'), loss modulus (G''), strain (γ), and stress (τ) data were collected as a function of angular frequency.

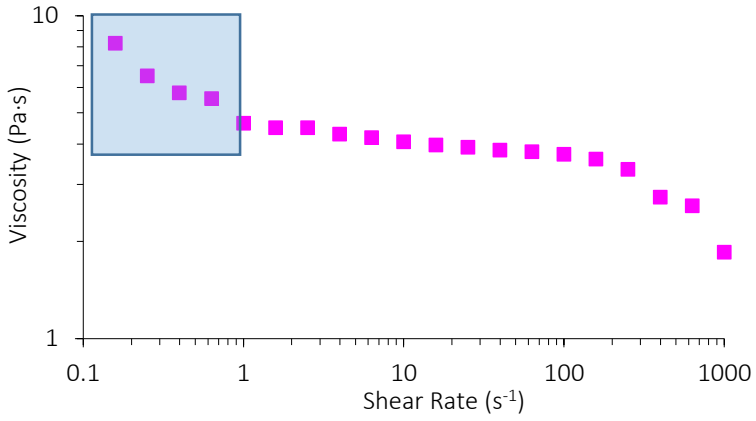

Figure 3.3: Determination of pre-shear for neat PVA and CNC/PVA samples. Pre-shear determined as minimum shear rate necessary to eliminate processing induced orientation shown through the leveling out of the viscosity in the blue box.

Both steady shear and small amplitude oscillatory shear tests were conducted on neat polymer solutions while only small angle oscillatory shear tests were conducted on nanocomposite suspensions. All tests were repeated three times with new samples at each sample concentration. Results are reported as average values with error bars indicating the standard deviation. Rheological data were excluded from analysis if the measurements were below the torque sensor measurement capability or if shear rates were so large that material breakage was observed during testing.

3.2.4 Film Formation

Neat PVA and CNC/PVA films were formed through solution casting of the solution processed material or shear mixed material. Each film was allowed to air dry for 2 weeks prior to any testing. Films formed from solution processed materials were made from solutions and suspensions with 7 wt.% solids loading in order to allow for easier casting of the films. Films formed after shear mixing and centrifuging were manually cast using a doctor blade. All films were cast onto a polystyrene substrate. Films used for DSC, DMA, dry MTT, and biodegradation were dried for 30 minutes in an oven at 110 °C immediately before testing and will be called "dry" samples. Films used for XRD, FT-IR, and wet MTT studies were not dried in an oven and contained approximately 3% bound water. These samples will be called "wet" samples through the presented work.

3.2.5 Optical Microscopy

Polarized light microscopy was conducted to examine the morphology of each sample to determine the effect of processing on sample morphology. Solutions were deposited onto glass slides using a syringe, covered using a glass slide cover, and observed using an Olympus BX51 optical microscope and a 530 nm red wave plate. Five images for each sample were taken using an objective lens magnification of 20x for all samples. Images were analyzed quantitatively using ImageJ, a public domain image analysis software provided by the National Institute of Health. Both fractal dimension and particle size were calculated using functions provided by the software. The data presented are the average of the five images with standard deviation calculated based on those five images.

3.2.7 Fourier Transform Infrared Spectroscopy (FT-IR)

FT-IR spectroscopy was conducted to study the potential differences in structure of freeze-dried and aqueous suspended CNCs. FT-IR spectroscopy was also conducted to monitor the structural changes in the aqueous suspended biodegradation samples with time. FT-IR spectroscopy was performed with a Bruker Hyperion FT-IR with a platinum ATR accessory and KBr as the reference material. The spectra were collected over a wavenumber range of 4000 cm^{-1} to 370 cm^{-1}. The spectra were collected over 64 scans with a resolution of 4 cm^{-1}. Each sample spectra was collected once, and information about peak intensity, location, and area were collected.

3.2.6 X-Ray Diffraction (XRD)

XRD testing was performed to determine the crystal structure and the crystallinity of the PVA in the neat and nanocomposite samples. XRD patterns were obtained with a Rigaku Micromax-002 (operated at 45 kV, 0.65 mA, λ = 1.5418 Å) using a Rigaku R-axis IV++ detection system and CuKα. Each sample was collected once for 1800 s. The diffraction patterns were analyzed using MDI Jade (version 9.0) software as a function of 2θ to index each crystal peak as well as determine crystallinity by calculating the area of the amorphous PVA peak via deconvolution and integration of the raw data. The amorphous peak was constructed with a skew of 0.2 for ease of calculation. PVA crystallinity (X_c) was calculated using the diffraction pattern between 15° to 30°. After the peak areas were known, PVA crystallinity was calculated for each sample using equation 3.1 where A_c is the area of the crystalline peaks and A_m is the area of the PVA contribution to the amorphous peak:

$$X_C = \left(\frac{A_C}{A_c + A_m}\right) \times 100 \qquad (3.1)$$

In order to calculate the percent crystallinity of the PVA in the CNC/PVA nanocomposite systems, the percent amorphous content contributed by the CNCs to the nanocomposite systems was taken out of the area of the amorphous curve, shown by the following equation:

$$A_{m_{PVA}} = A_m - A_m V_{f_{CNC}} A_{m_{CNC}} \qquad (3.2)$$

where $A_{m_{PVA}}$ is the amorphous contribution of the PVA, A_m is the amorphous contribution of the nanocomposite, $V_{f_{CNC}}$ is the volume fraction of the CNCs, $A_{m_{CNC}}$ is the amorphous fraction contribution of the CNCs (0.08 for the aqueous suspended CNCs and 0.04 for the freeze-dried CNCs).

3.2.8 Differential Scanning Calorimetry (DSC)

DSC was done to determine the T_g of the neat PVA and CNC/PVA samples. DSC was conducted using a TA instruments Q200 DSC. Samples with a nominal mass of 5 mg were prepared and sealed in aluminum hermetic pans. Neat PVA and nanocomposite samples were cooled at 10 °C/min to 0 °C, held isothermally for 1 minute, and then heated at 10 °C/min to 250 °C, held isothermally for 1 minute, and then cooled at 10 °C/min to room temperature. Three samples of each composition were tested. T_g data are presented as the average of these three tests with error bars indicating the calculated standard deviation. PVA and CNCs tended to degrade using DSC methods as the instrument was not capable of heating at fast enough heating rates to isolate the melting and degradation temperature of the material, therefore, no second cycle was run. Sample degradation of the sample was confirmed by opening up the DSC sample pan after testing and observing the sample.

3.2.9 Dynamic Mechanical Analysis (DMA)

DMA testing was conducted to determine the storage modulus (E') of the films as a function of temperature as well as the T_g. E' was then used to estimate the CNC concentration associated with mechanical percolation as well as understand the interaction of the CNCs in the PVA through mechanical modeling of the data. DMA testing was performed with a Mettler Toledo DMA861. All testing was done in tension with a sample length of 9 mm, width of 3 mm, and thickness of 0.3 ± 0.5 mm. Testing was conducted at a frequency of 1 Hz with a displacement of 0.05% strain, and data were collected over a temperature range of 30 °C to 120 °C, heating at rate of 2 °C/min. Three samples of each concentration were tested, and the data shown are the average of those three tests. Error bars shown represent the standard deviation.

3.2.10 Micro-tensile Tensile Testing (MTT)

MTT was conducted to determine the tensile strength and strain to failure of the neat and nanocomposite systems according to ASTM standard D1708-13. Load and extension were recorded as a function of time, and the stress and strain were then calculated. Both wet and dry samples were tested as defined in the film formation section. MTT was performed using an Insight MTS tensile testing apparatus with a 100 N load cell and a testing rate of 10 mm/min for wet samples and a 2000 N load cell and a testing rate of 1 mm/min for dry samples. All samples were tested to failure. Samples were all prepared to be 0.15 ± .05 mm in thickness. Each concentration was tested with different 5

samples, and the average value is presented. Error bars shown represent the standard deviation.

3.2.11 Biodegradation

Biodegradation studies were conducted on the neat and nanocomposite samples. Samples were buried in soil collected from Decatur, GA and stored at ambient room temperature and constant relative huminidy as determined through oven drying of a small portion of the soil. At time points of 0, 6, 13, 22, 28, 34, 40, 43, 47, 56, 65, 71, 83, 92, and 100 days over the 100 day period, 30 mg of each sample was collected from the vial, the excess dirt was removed via washing in deionized water, and samples were dried at 110 °C for 60 minutes. Samples taken at time point 0 days were considered the control samples. Changes to the samples were characterized through swell testing, TGA, and FT-IR spectroscopy. The percent swell was measured in order to understand structural changes such as stretching or scission of the polymer backbone. TGA was used to see if the onset of degradation temperature was changing with biodegradation as this would indicate a deterioration in chemical structure, decreasing the onset degradation temperature indicating an increase in degradation . FT-IR spectroscopy was conducted to see if changes to the chemical structure occurred or microbial growth as shown by sharpening of disappearance of the chemical peaks or amide I and II formation respectively. Swell testing was conducted on samples from each time point. TGA and FT-IR spectroscopy were conducted on samples at time points of 0 days, 13 days, and 100 days. Swell testing was conducted by weighing out 5 mg of each sample and placing

the sample in deionized water for 24 hours. After 24 hours, the samples were removed and blotted with tissue wiper to remove surface water. The weight of the sample before and after swell testing was recorded and normalized percent swell (S^n) was calculated through the use of equations 3.3 and 3.4. Equation 3.3 shows the calculation of percent swell (S') where w_i is the initial weight after removal from the soil and w_f is the final weight after 24 hours of swell testing while 3.4 shows the normalization of 3.3 where S_c is the control sample percent swell.

$$S' = \left(\frac{w_i - w_f}{w_i}\right) \times 100 \qquad (3.3)$$

$$S^n = \frac{S}{S_c} \times 100 \qquad (3.4)$$

Swell tests were conducted on three samples at each concentration. The data shown were the average of these three tests while error bars are representative of the standard deviation calculated. TGA testing took place in a TA Instruments Q500 IR TGA with nitrogen purge gas at a flow rate of 20 mL/min. Samples were heated from 30 to 400 °C at rate of 10 °C/min. Sample weight loss was recorded as a function of temperature and from these measurements, the onset degradation temperature was calculated. TGA was run once on each sample. FT-IR spectroscopy was conducted using the same procedure as defined in section 3.5 and the peak positions and intensities were analyzed.

3.2.12 Water Recovery

Water recovery was important to the sustainability goals of the presented research. Water recovery was tested to determine if water could be recovered during drying and then reused throughout the processing method. The ability to recover water from the PVA solutions and nanocomposite samples was determined via dehydration in a vacuum oven. Samples at about 7 wt.% solids were put into a vacuum oven to mimic the formation of the solution processed solution cast samples discussed in Section 3.2.4 with a liquid nitrogen cooled solvent trap for one hour at either 30 or 70 °C. The amount of water recovered was determined by measuring the weight of the samples before and after dehydration. The percent water recovery (W_{rc}) was calculated using equation 3.5 where w_i is the initial weight of the sample and w_f is the final weight of the sample. One test was run on each sample/dehydration procedure combination.

$$W_{rc} = \left(\frac{w_i - w_f}{w_i}\right) \times 100 \qquad (3.5)$$

CHAPTER 4

PROCESSING METHODS

Materials processing played a large role in controlling the morphological and microstructural properties of the CNC/PVA systems discussed in this research. In order to understand the effect of processing on the CNC/PVA systems, both solution processing and shear processing using a batch mixer were conducted. Solution processing was anticipated to produce systems with relatively good dispersion and properties. Shear processing was conducted to understand and compare the efficacy of a more scalable processing technique to solution processing. The research was carried out in two phases: process modeling and process implementation. Process modeling was conducted on aqueous suspended CNC/PVA systems at various PVA molecular weights to understand component interactions. Process implementation was done on freeze-dried CNC/PVA systems at one molecular weight and the effect of various processing methods was assessed.

4.1 Introduction

As industries move toward more environmentally sustainable and safety conscious practices, the use of less-toxic solvents, such as water, are being studied extensively to better understand their processing needs.[146–148] Water is not only renewable and has the potential to be recovered during processing, but it also dictates that lower processing temperatures be used, saving energy.[149] In order to achieve effective water-based processing methods, a few criteria must be met:[150]

- component stability
- appropriate viscosity
- sufficient strength of the dried material

These criteria were considered during the process modeling and process implementation phases later discussed in this Chapter.

4.1.1 Solution Processing

Traditionally, PVA and PVA nanocomposites are prepared via solution processing in a solvent followed by a forming step (i.e. fiber spinning, casting, molding, etc.).[69,116,151] In the solution processing method, PVA is generally added to a solvent, water in this case, and then heated until the PVA is completely dissolved in the solvent. After the PVA has been incorporated into the solvent, nanoparticles are added to the solution and again stirred until the filler is distributed throughout the polymer matrix. From this nanocomposite suspension, suspension characterization is conducted or solid forming occurs and the system is characterized.

4.1.2 Shear processing

Shear processing methods for more environmentally friendly polymers such as PVA water-based systems have received significant attention recently as the push to move away from petroleum based plastic increases.[152–155] Work has also been done on

water-based processing of polypropylene,[147] nylon,[156] and polyamide/clay[148,149] nanocomposites. These studies used extrusion to process the clay/polymer systems. For the polyamide systems, water was seen to increase clay dispersion giving intercalated and partially exfoliated nanocomposites. In the study conducted by Touchaleaume *et al.*,[149] unmodified montmorillonite was dispersed inside a compatibilized polypropylene-graft-maleic anhydride (PP-g-MA) and through the use water-based extrusion, mechanical and thermal properties were achieved close to those of modified montmorillonite. Water was also seen to increase dispersion in the polypropylene/clay nanocomposites as it allowed for an aqueous suspension of clay to be formed as well as increased the interaction capability between the PP-g-MA and clay through hydrogen bonding.[147]

In an effort to take advantage of material compatibility due to the hydrophilic components of PVA and water-dispersible bio-based fillers such as CNCs, work has begun in the characterization and processing of these systems.[46,73,151] As stated in Chapter 2, working with PVA as the polymer matrix poses a problem in that the melting and degradation temperatures are very close to one another, making melt processing difficult. To overcome this challenge, studies have been conducted on the melt processing of CNC/PVA nanocomposites using water as an initial plasticizer followed by the addition of formamide to prevent evaporation during processing as well as co-plasticize PVA to increase the melt-degradation temperature window.[153,155] Polyol plasticizers,[157] and amide containing compounds[38,158] have also been used to increase this melt processing window for PVA. In all of these methods, water was used as an initial plasticizing agent followed by additional chemical plasticizing agents. Polymer processing with CNCs used as the filler also presents a problem in that most polymer melting temperatures are near or

above the degradation temperature of CNCs, and CNCs tend to agglomerate when not previously dispersed in an aqueous medium.[90,159,160] It is the goal of the presented research to develop a method in which no additional plasticizing agents are necessary for shear processing of PVA nanocomposites.

4.2. Methodology

The processing experimental setup for this research consisted of two steps: process modeling and process implementation. A diagram of the processing experimental setup can be found in Figure 4.1. In the process modeling step, neat PVA solutions and aqueous suspended CNC/PVA suspensions were produced via solution processing. Aqueous suspended CNCs were used in the process modeling step as they were expected to give the best dispersion properties due to their pre-dispersed state. After the aqueous suspended CNC/PVA systems were processed, rheological, microstructural, and mechanical characterization were conducted.

Once the solution processed aqueous suspended CNC/PVA systems were characterized, the research progressed into the processes implementation stage. In this stage, freeze-dried CNC/PVA suspensions were formed via solution processing and shear processing. In this stage, solutions were either prepared via solution processing and then characterized rheologically or prepared via shear mixing and then characterized rheologically. In the process implementation stage, only one molecular weight PVA (146K) was used for study. This molecular weight was chosen based on the results

obtained during the process modeling stage. The following processing strategies were examined in the process implementation stage:

1. Solution processing
2. Redispersing of freeze-dried CNCs in deionized water followed by solution processing (RDFD)
3. Shear processing at 40 RPM
4. Shear processing at 91 RPM

A mixing speed of 40 RPM was chosen because it was in the middle range of the shear rates tested during rheological characterization and provided a good starting point to understand the effect of RPM on nanocomposite morphology. 91 RPM was chosen as it was the largest shear rate tested displaying stable nanocomposite viscosity. As CNC aggregation was seen in the 40 RPM shear mixed samples, it was thought that increasing the mixing speed to 91 RPM would decrease the amount of CNC aggregation by breaking up CNC aggregates. Rheological, mechanical, and microstructural characterization followed these processing steps to assess the differences in processing-structure-property relationships between composites produced during the two stages and with the two different types of CNCs (aqueous suspension and freeze-dried). The steps for the processing methodologies used for both the process implementation stage and the process modeling stage can be found in Figure 4.2. These steps are discussed in more detail in this Chapter.

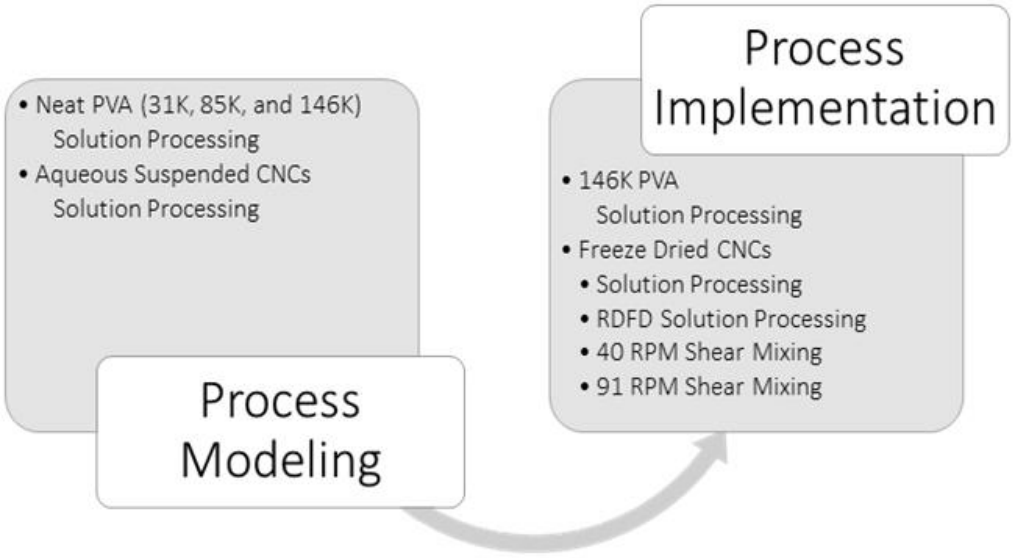

Figure 4.1: Schematic of the process methodology used in this research

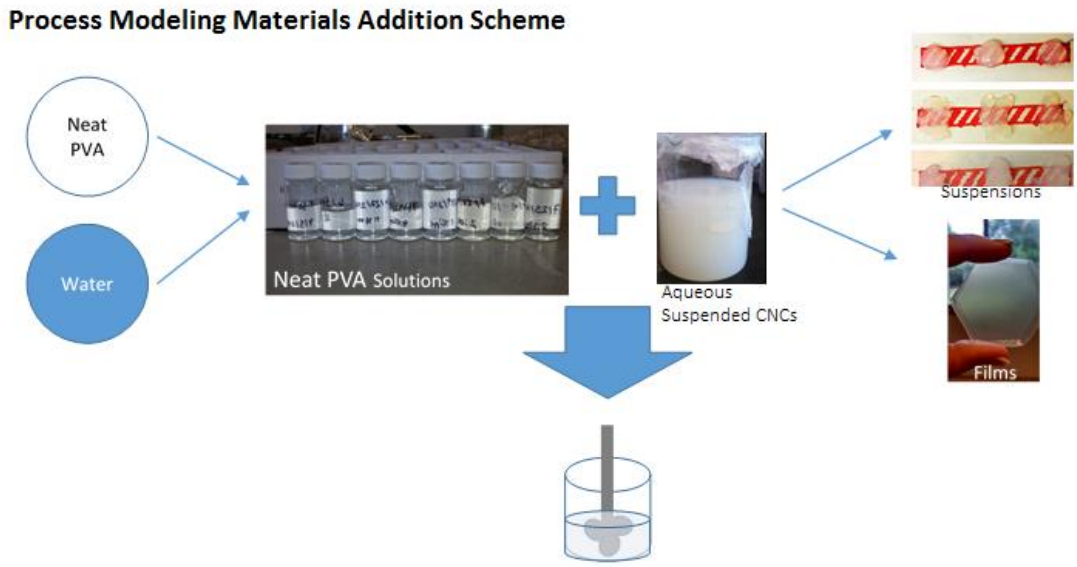

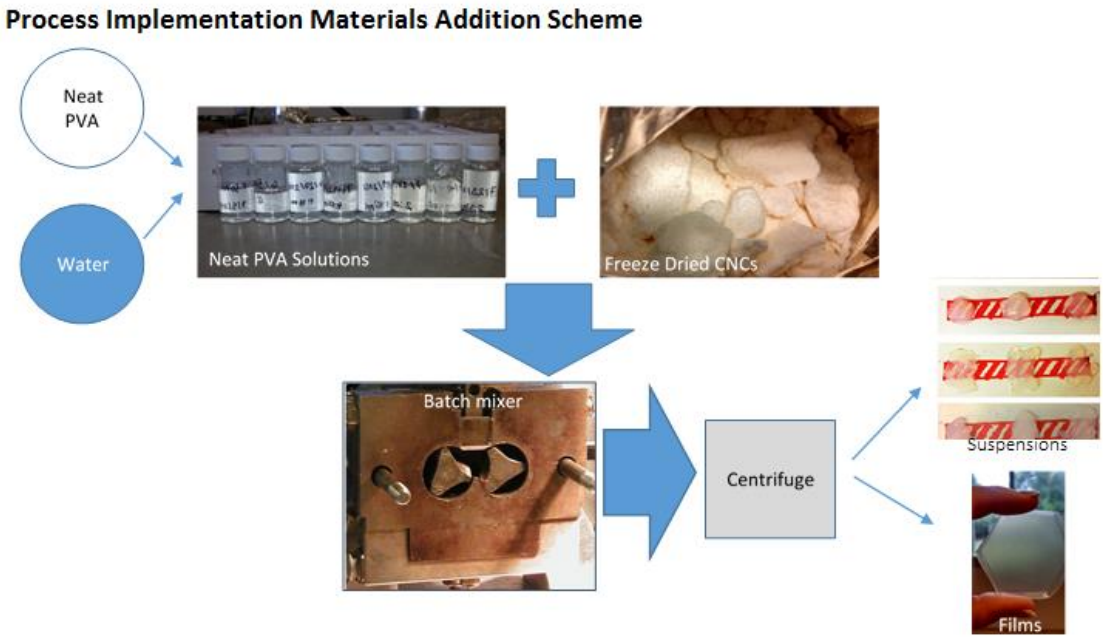

Figure 4.2. Process modeling and process implementation materials addition schemes

4.3 Solution Processing

Neat PVA solutions and some CNC/PVA suspensions were prepared using a solution processing protocol described in Chapter 3. Neat PVA solutions at 5 wt.%, 10 wt.%, and 15 wt.% solids and aging times of 1 day, 3 days and 5 days for each molecular weight were prepared for solution state characterization via steady shear rheology. The procedure used to characterize the steady shear rheological behavior can be found in Chapter 3. These data were used to determine what molecular weight and solids loading would best match the processing window for shear mixing. These aging and loading data for 31K, 85K and 146K are shown in Figure 4.3. From Figure 4.3, it was seen that viscosity increased with increasing solids loading. Aging also increased with increasing solids loadings as there was more PVA-PVA chain entanglement and interaction. The 1 day aging data were used as a metric for determining if the viscosity was large enough for shear mixing. Figure 4.4 shows the bounding viscosity values for shear mixing. Bounding values were determined based on the batch mixer capabilities, values of commonly melt processed polymers such as polyethylene,[161] and the viscosity of neat PVA solutions. Solid lines in this image indicate fixed boundaries set by mixer speed limitations while dashed lines indicate approximate boundaries for the viscosity. In order to be used with batch mixing, the solution had to have a viscosity high enough that it would not seep out of the mixer while also being process-able within the torque range available in the mixer. As a steady shear viscosity of 10 Pa·s or greater was needed for processing in the mixer, neat 85K 15 wt.% and neat 146K 15 wt.% possessed viscosities high enough to continue to the shear processing stage. Through the mechanical analysis conducted (Chapter 7), it was seen that 146K molecular weight samples had slightly higher mechanical properties,

and therefore 146K molecular weight was chosen as the molecular weight to continue onward in the presented research for all the process implementation steps or studies involving freeze-dried CNCs.

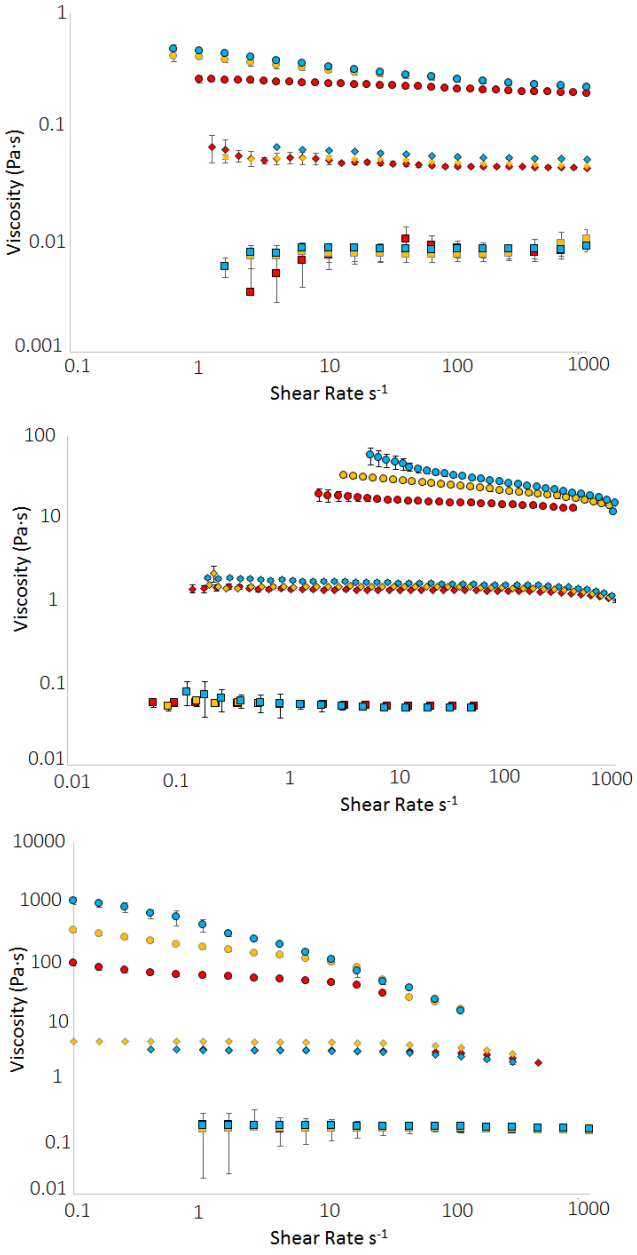

Figure 4.3: Steady shear viscosity for neat PVA. Top: 31K molecular weight. Middle: 85K molecular weight. Bottom: 146K molecular weight. Each molecular weight data set shows both aging and solids loading as a function of shear rate. Aging samples are shown at 1 day (red), 3 days (yellow), and 5 days (blue) of aging time. Solids loading are shown for each sample as 5 wt.% (square), 10 wt.% (diamond), and 15 wt.% (circle).

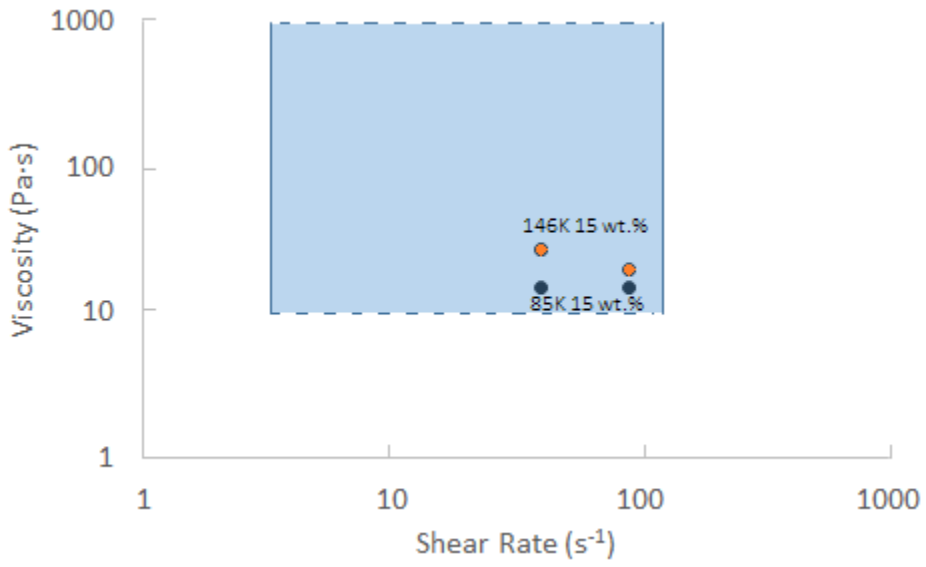

Figure 4.4 Viscosity necessary for shear mixing (blue box) and viscosity of neat PVA solutions after 1 day of aging (yellow and blue points).

Based on these bounding values and the rheological data, PVA solutions with a solids loading of 15 wt.% were chosen for shear processing. The same overall solids loading was used for the nanocomposite suspensions. Aqueous suspended CNC systems were characterized first to serve as a process modeling step. Once the microstructural, rheological and mechanical characterization were completed on the aqueous suspended CNC systems, nanocomposites containing freeze-dried CNCs were processed and characterized, in the process implementation step.

4.4 Shear Processing

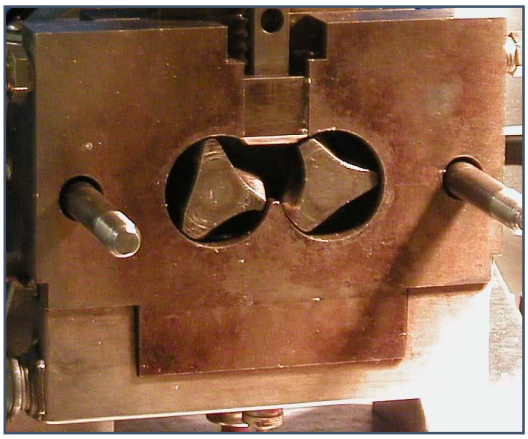

Figure 4.5: Internal mixer used to shear processes neat and nanocomposite systems.

Shear mixing was used as a processing method in order to evaluate the efficacy of an industrially-relevant processing method in dispersing the freeze-dried CNCs in PVA solutions. An image of the batch mixer used is shown in Figure 4.5. The shear mixing data were correlated to the rheology data through the use of equations 4.1 and 4.2, found below:

$$\dot{\gamma} = \frac{2\pi N}{\ln \beta} \qquad (4.1)$$

$$\eta = \frac{\Gamma}{N} \frac{\beta^2 - 1}{8\pi^2 L R_e^2 (1+g)} \qquad (4.2)$$

In equation 4.1, $\dot{\gamma}$ is the shear rate, N is the mixer speed in RPM, and β is the radius ratio of the mixing blades designated as $\frac{R_e}{R_i}$ where R_e is the external radius (39.3 mm) and R_i is the internal radius (36.5 mm). The shear rate was calculated from the mixing speed data using euation 4.1 and the viscosity of the solutions or suspensions during mixing was

calculated using equation 4.2. In this equation, Γ is the torque, L is the length of the mixing blades (47.0 mm), and g is the gear ratio (3/2).

Two PVA solutions, 15 wt.% 85K and 15 wt.% 146K, were shear processed, shown in the top plot of Figure 4.6. The increase in viscosity seen at the beginning of testing was due to start up shear, followed by a leveling out of the viscosities after 8 minutes. The viscosity values for 85K were lower than those for 146K due to the increased molecular weight of the 146K. As shown, the 146K molecular weight did not reach the rheologically tested viscosity value after 10 minutes indicating that it might take longer for 146K molecular weight to reach the steady state viscosity value.

The effect of shear mixing was then studied on aqueous suspended CNC/PVA systems. The data obtained for a composite suspension containing the 85K PVA polymer and CNCs at a loading of 33 wt.% CNC w.r.t. PVA in a 15 wt.% total solution shown in the bottom plot of Figure 4.6. From these data, comparable viscosities were seen with increasing mixing speed for both the mixer and rheologically measured viscosity within the error of the rheological measurements of ± 2.5 Pa·s. Although viscosity was comparable, an increase in mixing speed was accompanied by a change in the morphology, determined through observation. While the system processed at 40 RPM maintained a suspension morphology with the capacity to flow, the morphology of the material processed at 80 RPM changed a more grainy consistency, indicating phase separation during mixing. This shear induced phase separation has been seen in similarly concentrated physically crosslinked solutions and gel networks such as gelatin.[162] In these gels, physical crosslinks were broken apart due to shear forces and phase separation

occurred. PVA has also been seen to break and reform hydrogen bonds due to shear as the polymer chains oriented in the direction of flow.[14] This orientation, seen on the macro-scale, especially at high shear rates, could be causing phase separation of the system. The steady state value, or point where the viscosity plateaued, was reached at 6 minutes opposed to 8 minutes for the composite systems due to the incorporation of CNCs decreasing the overall PDI of the suspension and allowing for fewer available PVA chain entanglements due to decreased PVA content.

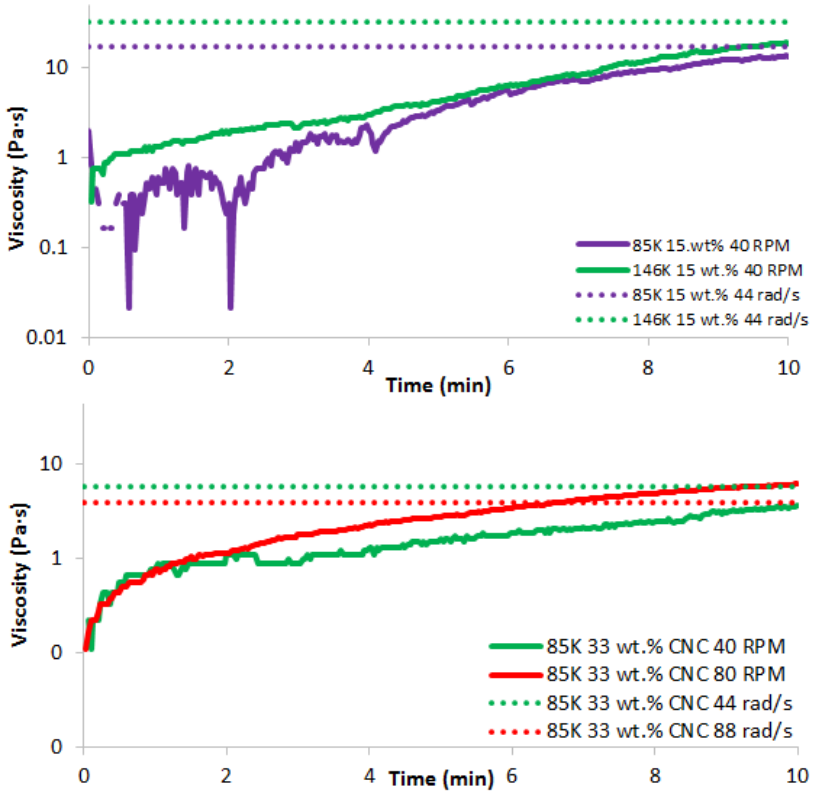

Figure 4.6: (Top) Viscosity values for 85K and 146K molecular weight PVA solutions obtained from rheological measurements (dashed lines) and mixer torque data (solid lines). (Bottom) Viscosity values for aqueous suspended CNC/PVA shear mixed systems at 85K and 40 and 80 RPM mixing speeds obtained from rheological measurements (dashed lines) and mixer torque data (solid lines).

Freeze-dried CNCs were then mixed into prepared 146K neat PVA solutions at concentrations of 20 wt.%, 33 wt.%, 50 wt.%, and 67 wt.% CNCs w.r.t. PVA at 40 RPM and 91 RPM. The viscosity data obtained from the processing torque are shown in Figure 4.7. For the 91 RPM shear mixed neat PVA, the data were not available to be shown as phase separation occurred causing the viscosity to raise to values that were no longer comparable to any rheological data collected. The morphology of the system was also discontinuous due to phase separation causing the PVA to aggregate into large bunches. From Figure 4.7 for the 40 RPM mixed samples, it was seen that increasing CNC content increased the shear mixing viscosity of the solution as one might expect during traditional shear processing up until the highest CNC loading of 67 wt.% CNC w.r.t. PVA. This drop in viscosity was seen as the CNCs became the predominant component in the system. A drop in G' was also seen in the dynamic rheological data with increased CNC loading at the corresponding frequencies, discussed in Chapter 5. In the start-up shear region, the 67 wt.% CNC composite reached steady state mixing more rapidly than the other loadings due to the increased amount of CNCs in the system, allowing for decreased time necessary to reach steady state due to the shorter lengths of the CNCs. The start-up shear needed to reach steady state mixing was also decreased with increasing CNC loading, indicating that PVA chains were the primary component contributing to the viscosity of the suspensions. The 67 wt.% CNC systems at 40 RPM showed a periodic drop in viscosity due to slightly less material present in the mixer. In comparison, the 91 RPM mixing data showed a different trend. While the 20 wt.% CNC suspension maintained the highest shear mixing viscosity, increasing CNC loading decreased the shear mixing viscosity. This behavior was attributed to the phase separation

of the PVA polymer. From the process modeling step, a distinct change in viscosity was not seen in the nanocomposite systems at 33 wt.% CNC with increasing shear rate due to previous incorporation of the aqueous suspended CNCs. As the 20 wt.% CNC w.r.t. PVA solution contained primarily PVA, the increased morphological change indicating phase separation was more dramatically seen, especially in the start-up mixing region as PVA chains phase separated and interacted with the freeze-dried CNCs. Also, with increasing CNC content, the larger fraction of short material in the system decreased the necessary start-up shear needed to reach steady state. This trend was seen for both 40 RPM and 91 RPM with increasing CNC loading.

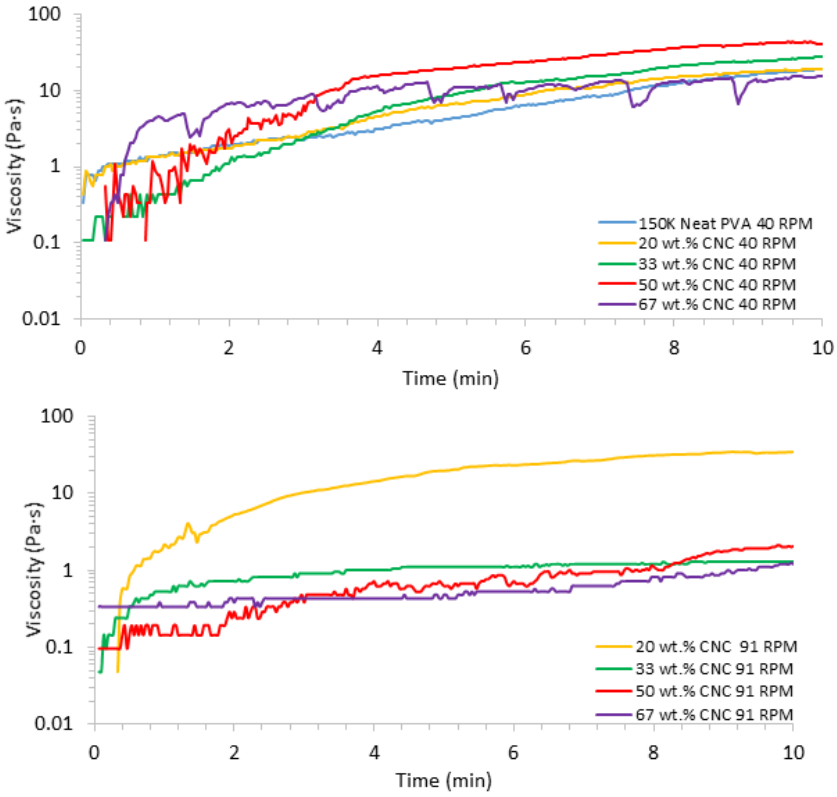

Figure 4.7: Shear mixing viscosity data for 146K neat and freeze-dried CNC nanocomposite systems mixed at 40 RPM and 91 RPM.

4.5 Optical Microscopy

Imaging with optical microscopy was conducted on aqueous suspended CNC/PVA systems and freeze-dried CNC/PVA systems produced by all of the processing methods used through the use of a 530 nm red waveplate. The images for the nanocomposite suspensions produced from aqueous suspensions of CNCs are shown in Figure 4.8. In these images, isotropic regions appeared as red or pink while anisotropic regions appeared as blue or yellow. As shown in Figure 4.8a and b, the neat CNC and neat PVA samples were mostly isotropic. Figure 4.8c and 4.8d showed that anisotropy increased with increasing CNC content and the CNCs appeared to be largely well distributed through the suspensions at this size scale due to the presence of a rainbow-like polarized color scheme opposed to CNC aggregates. In comparison, materials produced by the other processing strategies showed decreased levels of dispersion due to the presence of large CNC aggregates preventing analysis based on anisotropy due to the polarization of the CNC aggregates. The materials produced by solution processing with freeze-dried CNCs, shear mixing with CNCs at 40 RPM, and shear mixing with CNCs at 90 RPM are shown in Figures 4.9, 4.10, and 4.11 respectively. Overall, these methods were not as effective at dispersing CNCs in PVA solutions. In all images, bright whitish regions indicative of CNC clusters were observed. The results of solution processing with as-received freeze-dried CNCs and shear mixing at 40 RPM were qualitatively similar, and the higher mixing speed seemed to be less effective than the other two methods in dispersing CNCs. For comparison, another set of samples was made with solution processing, but a step was added to the processing method. The freeze-dried CNCs were first resuspended in water, and then this suspension was added to the PVA

solution. The images of materials produced by this processing method are shown in Figure 4.12. As seen from these images, distribution and homogeneity were improved. Anisotropy also increased with increasing CNC content, similar to what was seen in the solution processed aqueous suspended CNC system. By redispersing the freeze-dried CNCs in water before mixing them into the PVA solutions, aggregation of the CNCs decreased.

To further understand the effect of processing on morphology of the CNC/PVA freeze-dried nanocomposite systems, solution processed freeze-dried CNCs and 40 RPM and 91 RPM shear processed freeze-dried CNC/PVA suspension images were analyzed. Specifically, average particle size and fractal dimension were calculated and were used to analyze the morphology of the images. Average particle size was obtained by converting the images to binary color scale and outlining the aggregates through the use of the Analyze Particle function available in ImageJ to determine the size. Aggregates less than 16 μm were excluded as this was the size of one pixel at this magnification. The fractal dimension was analyzed using the box counting procedure in which grids of increasing size were applied to the image and the number of aggregates that passed through each box was counted. The number of boxes was plotted against the box size on a log-log plot and the slope of the line was calculated giving the fractal dimension (*d*). Average particle size and fractal dimension data can be found in Figure 4.13. The calculated fractal dimension increased with increasing CNC content indicating increased a change in aggregate shape from more triangular to more square. Likewise, CNC aggregate average area tends to increase with increasing CNC loading due to increased particle size. Fractal size between CNC loading did not change substantially with differing processing

methods indicating that the aggregate structure of freeze-dried CNCs through the direct addition to PVA solutions was not substantially altered through solution or shear processing.

While the solution processed, 40 RPM, and 91 RPM had similar size aggregates at CNC loading below 50 wt.%, 91 RPM had the largest average aggregates size at the highest loading of 67 wt.%. This larger aggregate size can be attributed to two features: phase separation and shear forces. From the 91 RPM mixing data, almost no start-up shear was necessary to reach steady state indicating almost immediate steady state mixing. The rapid onset of steady shear mixing indicated that the processing method most likely did not provide enough steady shear to disperse and distribute the components at such high CNC loadings. It also indicated that the PVA phase separation occurred very rapidly, preventing distribution of CNCs throughout the PVA and increasing CNC aggregate size. In other words, as the PVA aggregated, the CNCs aggregated as there was minimal PVA to disperse around the CNCs. Aggregate sizes seen in the shear processed samples corresponded to the aggregate size seen from dynamic light scattering, indicating that these processing methods did not break up native CNC aggregates.

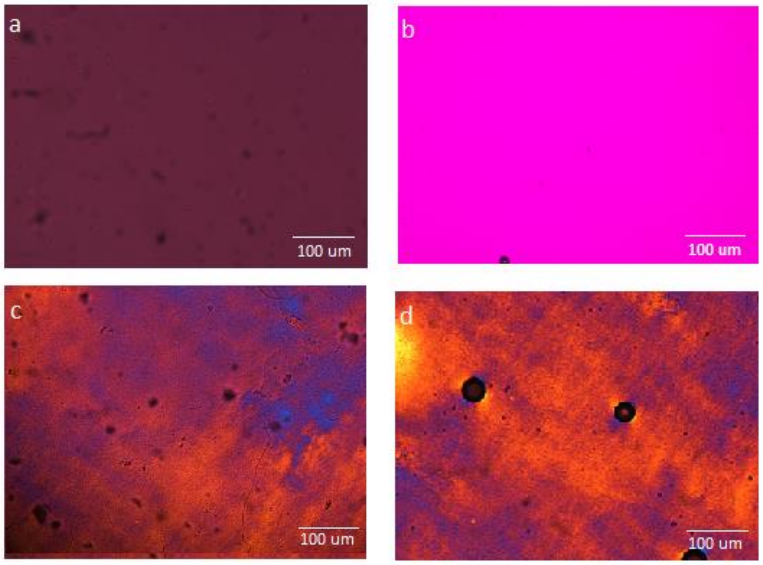

Figure 4.8: Solution processed images of aqueous suspended CNC/PVA nanocomposites systems. a) Neat CNC b) Neat PVA c) 85K 33 wt.% CNC w.r.t. PVA d) 85K 50 wt.% CNC w.r.t PVA.

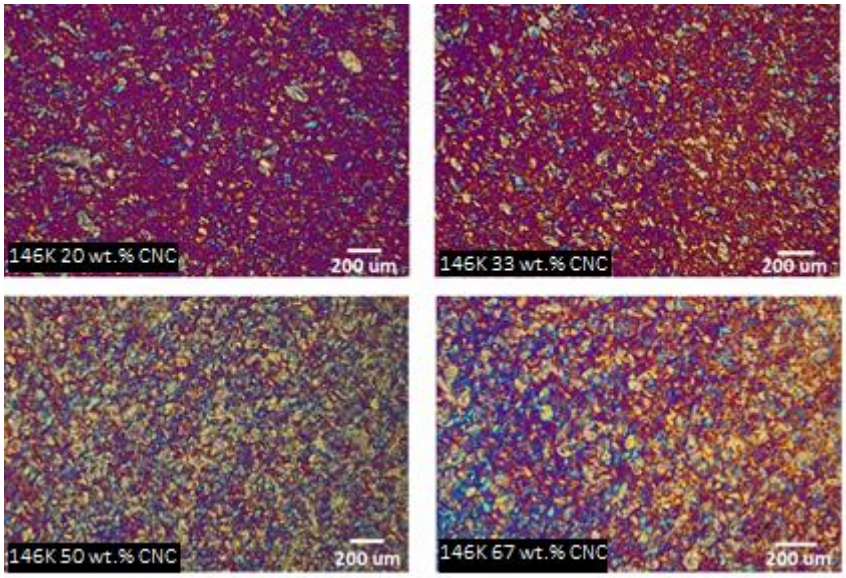

Figure 4.9: Solution processed freeze-dried CNC/PVA nanocomposites systems at 20 wt.%, 33 wt.%, 50 wt.%, and 67 wt.% CNCs w.r.t. PVA.

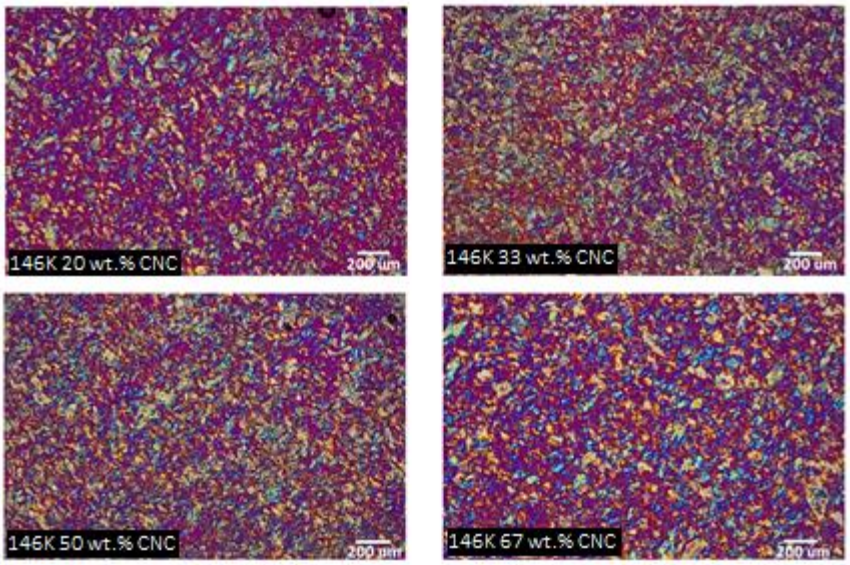

Figure 4.10: Shear processed solutions mixed at 40 RPM of freeze-dried CNC/PVA nanocomposite systems at 20 wt.%, 33 wt.%, 50 wt.% and 67 wt.% CNC w.r.t. PVA.

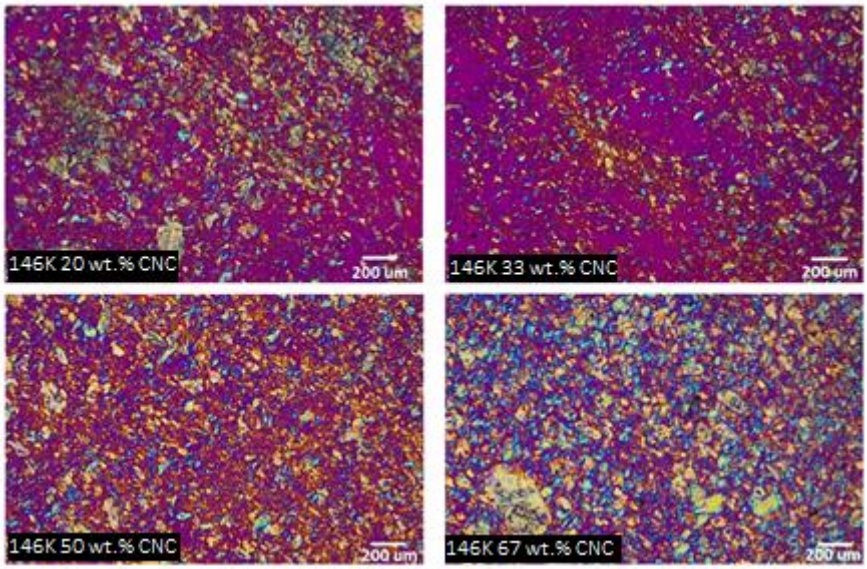

Figure 4.11: Shear processed solutions mixed at 91 RPM of freeze-dried CNC/PVA nanocomposite systems at 20 wt.%, 33 wt.%, 50 wt.% and 67 wt.% CNC w.r.t. PVA.

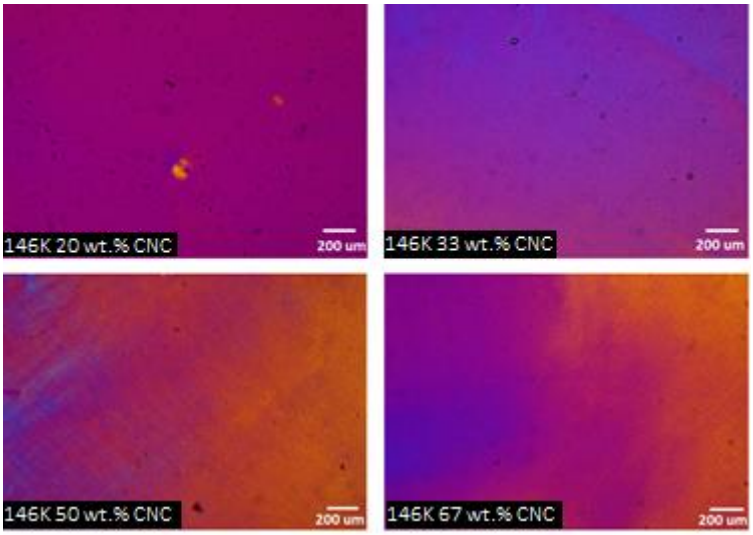

Figure 4.12: Redispersed freeze-dried CNC/PVA nanocomposite systems solution processed at 20 wt.%, 33 wt.%, 50 wt.% and 67 wt.% CNC w.r.t. PVA.

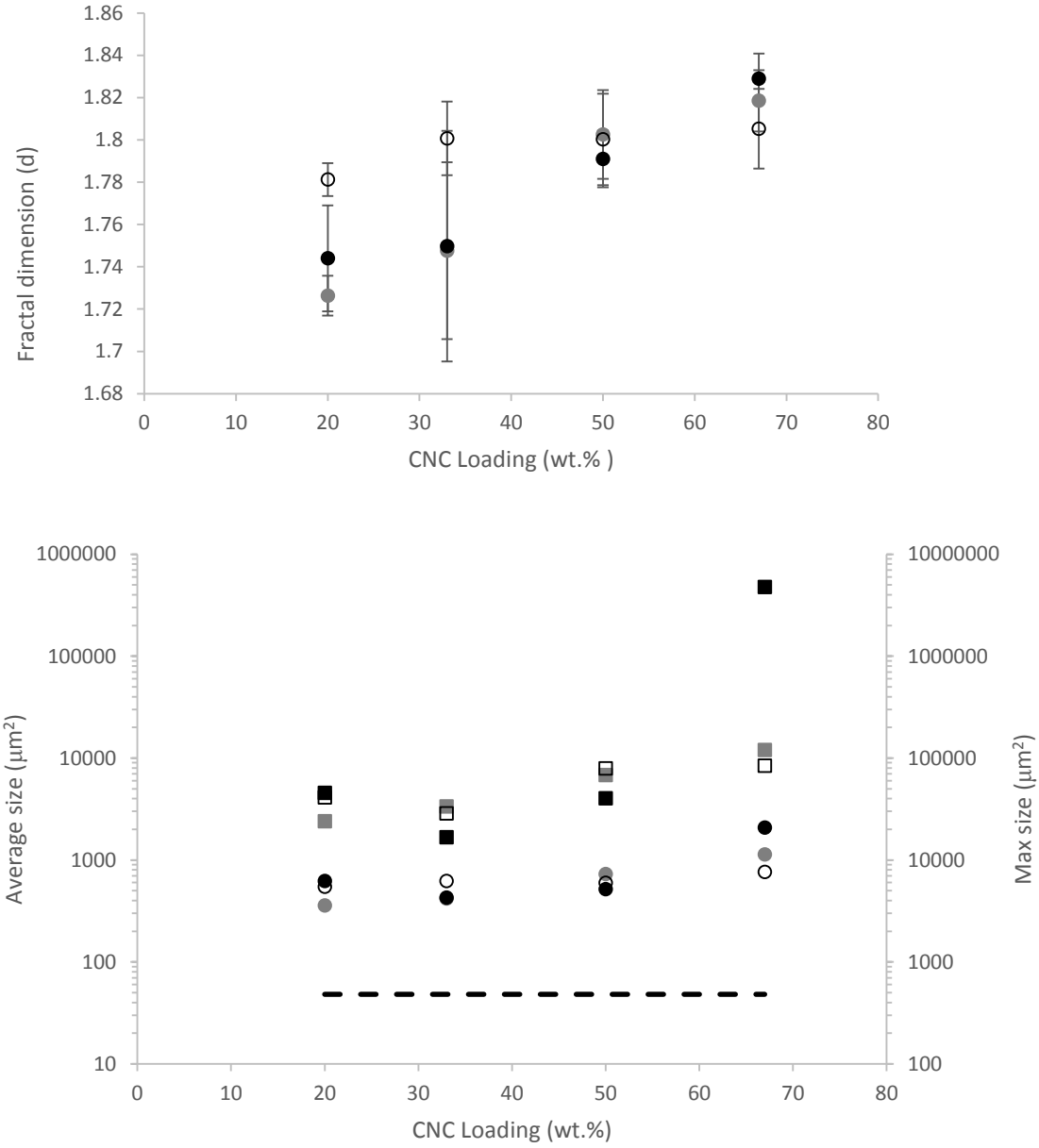

Figure 4.13: Fractal dimension (top) and average size (circles), maximum particle size (squares), and mode size (dashed line) (bottom) of particles analyzed though optical microscopy. Solution processed systems (grey), 40 RPM shear processed systems (open), and 91 RPM shear processed systems (black).

4.6. Conclusions

Aqueous suspended CNCs were mixed via solution processing in order to understand the morphological properties of CNCs in a PVA solution. To study the effect of processing on CNC/PVA nanocomposite systems, freeze-dried CNCs were processed using solution processing and shear mixing techniques. From this study, it was found that by adding as-received freeze-dried CNCs into PVA and solution or shear processing, CNC aggregation was increased compared to solution processing of aqueous CNC or RDFD CNC suspensions. Through adding freeze-dried CNCs into PVA and shear processing at 40 RPM and 91 RPM, the effect of shear processing on each of the nanocomposite components was seen through a decrease in the start-up shear time with increasing CNC content and a change in steady state mixing viscosity. Finally, it was seen that redispersing the freeze-dried CNCs in water and solution processing them in PVA provided more homogenous morphology compared to the solution processed and shear processed freeze-dried CNC systems. This behavior can be attributed to breaking up the freeze-dried aggregates prior to processing allowing for similar morphology to aqueous suspended, solution processed CNC/PVA systems. It was seen that shear processing of as-received freeze-dried CNCs were not able to break up native CNC aggregates. In the following Chapter, the processing-structure-property relationship will be discussed as a function of processing strategy and CNC media.

CHAPTER 5

RHEOLOGY

Rheological measurements were conducted in order to determine the steady shear and dynamic viscoelastic response of neat PVA and CNC/PVA nanocomposite suspensions. Neat PVA solutions of varying molecular weights and concentrations were tested under steady shear to determine the viscosity and to assess which samples were candidates for shear processing. Neat PVA solutions and CNC/PVA suspensions were tested using small angle oscillatory shear to better understand the viscoelasticity and the CNC contribution to the suspension viscoelastic response.

CNC/PVA suspensions made with aqueous dispersions of CNCs and freeze-dried CNCs were studied. For comparison, samples made with CNCs received in aqueous suspension, as-received freeze-dried CNCs, and aqueous suspensions of freeze-dried CNCs were characterized to understand the independent effects of CNCs and CNC production method on the viscoelastic response of the nanocomposite suspensions. These results were used for shear processing modeling and implementation in other aspects of this research. Rheological data were analyzed to determine the elastic contribution of the CNCs and to calculate the yield stress. The CNC percolation threshold was also calculated to better understand CNC contribution.

5.1 Introduction

Rheology is the science of the flow and deformation of matter. There are three main types of rheological deformation: reversible (elastic), irreversible (viscous), and a combination of reversible and irreversible (viscoelastic). Elastic, or solid-like, response is that behavior in which the fluid will give a reversible response while viscous, or liquid-like, response refers to behavior in which the energy is dissipated and an irreversible response is given through testing. Viscoelastic behavior is generally frequency dependent in which both solid and liquid-like characteristics are present. In this Chapter, the viscoelasticity of neat PVA and CNC/PVA suspension will be studied as a function of processing method.

The rheology of neat PVA systems has been extensively studied.[14,163–168] Gao *et al.*[163] found that by increasing the degree of polymerization, the shear thinning was increased due to the increased capability of orientation of the PVA chains under steady shear. They also found that increasing the degree of polymerization increased the complex viscosity and storage modulus (G') due to increased hydrogen bonding as hydroxyl group concentration increased. Gao *et al.*[14] also studied the effect of concentration on PVA/water solutions with a degree of polymerization of 1700 (60K molecular weight) using small angle oscillatory shear and concentrations of 10, 15, 20, and 25 wt.% solids. From this study, they found that PVA exhibited pure liquid-like (viscous) behavior at low loadings and viscoelastic behavior at high loadings. Yang *et al.*[169] studied the aging and microphase separation of 115K molecular weight PVA solutions via dynamic light scattering, video tracking, and micro-rheology and found that

PVA, like other polymer gelation, tends to undergo phase separation before gelation, and that the gelation of PVA is driven by phase separation. In the presented research, different molecular weights of PVA at varying concentration were studied as a function of time to gain further understanding of how PVA/water systems behave before adding CNCs.

The rheological properties of cellulose/PVA suspensions have been studied for their potential applications. Measurement of the dynamic viscoelastic properties of CMC/PVA composite suspensions showed G' and loss modulus (G'') values on the order of 10 kPa, appropriate for orthopedic applications.[170] The addition of CMF to a PVA matrix resulted in an increase in G' [42] as well as slightly increased thermal stability.[171] BC (bacterial cellulose) has also been added to PVA solutions to form nanocomposites with mechanical and morphological properties suitable for the replacement of cardiovascular tissue.[120] Specifically, mechanical tests indicated that BC/PVA suspensions could be formulated to closely mimic the anisotropic properties of the native tissue. Though these cellulose and nanocellulose fillers show property improvements when combined with PVA, CNCs are believed to be beneficial as structural fillers compared to other cellulosic particles due to their highly ordered and rigid nature opposed to the large disordered regions present in MFs and CMFs

Materials processing is an important enabling step to producing CNC/PVA composites. Since both components have an affinity for water, the processing may be accomplished through methods which use an aqueous medium. Thus, an understanding of the rheological properties of the nanocomposite suspension is needed to logically

process these materials and describe their interactions and structure; however, the rheological properties of CNC/PVA systems have been only briefly discussed in the literature and center around physically bonded cyrogels produced though multiple freeze and thaw cycles. Freeze/thaw cycles are of interest as they provide a mechanism for producing porous polymer matrices with a three-dimensional support system capable of optical and tissue engineering applications. Through the freeze/thaw method, stable sponges can be formulated though physical crosslinking.[71] Chang *et al.*[107] studied the linear viscoelastic response of fibrous cellulose powdered/PVA composites subjected to freeze and thaw cycles in weight per weight ratios of cellulose/PVA with loadings of 75/25, 50/50, and 25/75 and found that these systems displayed solid-like behavior due to the high loadings of cellulose. Additionally in work by Mihranyan,[170] physically crosslinked freeze/thaw gels were also seen to have rigid character with high elasticity after CNC loading.[170] Wang *et al.*[71] also observed significantly increased G' with CNC loading in PVA/starch freeze/thaw nanocomposite sponges, which was attributed to increased hydrogen bonding between the hydrophilic matrix and filler as well as compaction of the polymer chains and CNCs during freeze/thaw cycles. To compliment these studies, the aim of this research is to more fully understand the effect of CNCs on the rheological behavior of PVA in a physically crosslinked gel system without freeze and thaw cycles which may be more applicable to large scale processing of these materials with high CNC loadings and a wider range of applications.

Another goal of this research is to investigate a scalable processing method that could be implemented using traditional shear processing equipment. In this part of the research, CNCs obtained following freeze drying were used. These CNCs are in the form

of a powder. These freeze-dried powders allow for traditional shear processing methods to be used in conjunction with a water-based processing method as higher CNCs loadings can be achieved without the addition of 95 wt.% water. Transportation costs for freeze-dried CNCs are also lowered with respect to aqueous suspended CNCs as water is no longer a factor. Though freeze-dried CNCs offer exciting potential for industrial and environmentally beneficial processing, aggregation in polymer matrices presents a challenge. In a study by Jiang *et al.*,[160] freeze-dried CNCs and aqueous suspended CNCs were incorporated into a poly(3-hydroxybutyrate-co-3-hydroxyvalerate) (PHBV) matrix using PEG as a compatibilizer for the CNCs via solution processing followed by melt mixing. Due to the agglomeration of freeze-dried CNCs, solution casting of aqueous suspended CNCs gave better dispersion properties than those properties found when the freeze-dried CNCs were mixed in the twin screw extruder and injection molded. This increased dispersion in solution cast systems was due to aggregation during extrusion as the extruder stripped the PEG compatibilizer from the CNCs as well as aggregation of freeze-dried CNCs prior to extrusion. The goal of the presented research is to achieve freeze-dried CNC nanocomposites properties as close to aqueous suspended CNCs nanocomposites as possible.

5.2 Neat PVA

The neat PVA solutions were characterized using steady shear rheological measurements at aging times of 1 day, 3 days, and 5 days and loading of 5, 10, and 15 wt.% solids. These aging and loading data for 31K, 85K and 146K are shown in Figure

5.1. While the 31K PVA showed very little aging, there was a significant increase in aging as molecular weight was increased to 85K and 146K. There was also an increase in shear thinning with increasing molecular weight and solids loading. These trends were attributed to increased polymer chain entanglements with increasing molecular weight and solids loading.

As mentioned in Chapter 4, steady shear rheology was conducted in order to determine what molecular weight and concentration of PVA was necessary to continue to the process implementation stage. A steady shear viscosity of 10 Pa·s or greater was needed for processing in the mixer. From the neat data, only neat 85K 15 wt.% and neat 146K 15 wt.% possessed viscosities high enough to continue to the shear processing stage. Through the mechanical analysis conducted in Chapter 7, it was seen that 146K molecular weight samples had slightly higher mechanical properties, and therefore 146K molecular weight was chosen as the molecular weight to continue onward in the presented research for all the process implementation steps or studies involving freeze-dried CNCs.

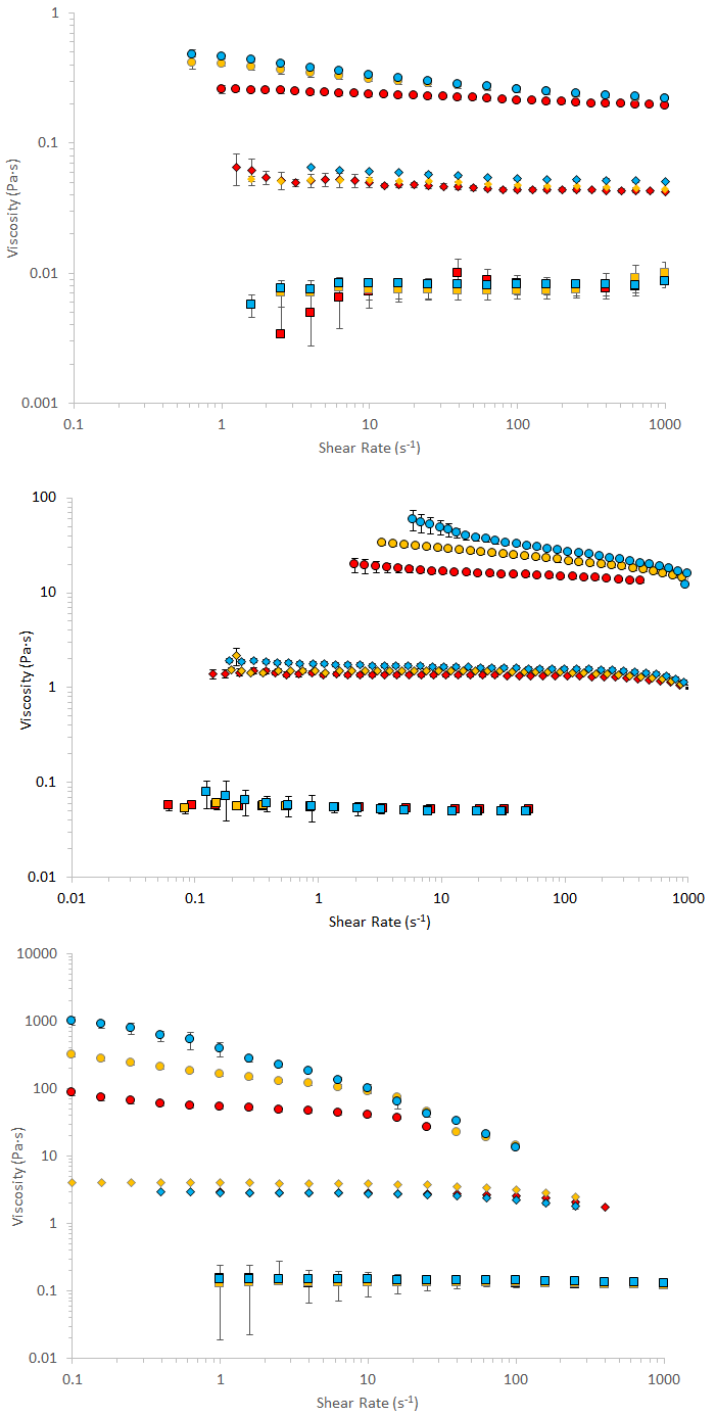

Figure 5.1: Steady shear viscosity for neat PVA. Top: 31K molecular weight. Middle: 85K molecular weight. Bottom: 146K molecular weight. Each molecular weight data set shows both aging and solids loading as a function of shear rate. Aging samples are shown at 1 day (red), 3 days (yellow), and 5 days (blue) of aging time. Solids loading are shown for each sample as 5 wt.% (square), 10 wt.% (diamond), and 15 wt.% (circle). Error bars represent the standard deviation of the average value.

To further understand the 15 wt.% neat PVA viscoelastic response, the 31K, 85K and 146K were compared, shown in Figure 5.2. Neat 31K showed Newtonian behavior over the majority of the shear rate range tested as well as limited change in the viscosity at aging times beyond 1 day. The neat 85K and neat 146K samples showed slight shear thinning as well as increased aging from 1 to 5 days indicated by the increase in the magnitude of the viscosity. This increase in viscosity with molecular weight can be attributed to the polymer chain entanglements forming a weak network of entanglements in PVA solutions. These structures are formed via two mechanisms: hydrogen bonding between hydroxyl groups of PVA and water and crystallite formation between PVA chains.[22] Crystallites were formed when at least two PVA chains were aligned over several PVA molecular segments. These segments were connected through hydrogen bonding and van der Waals forces.[22] As the molecular weight of the PVA was increased, there was an increase in crystallite formation shown through increased viscosity and elasticity as more crystallite segments were formed in the system.

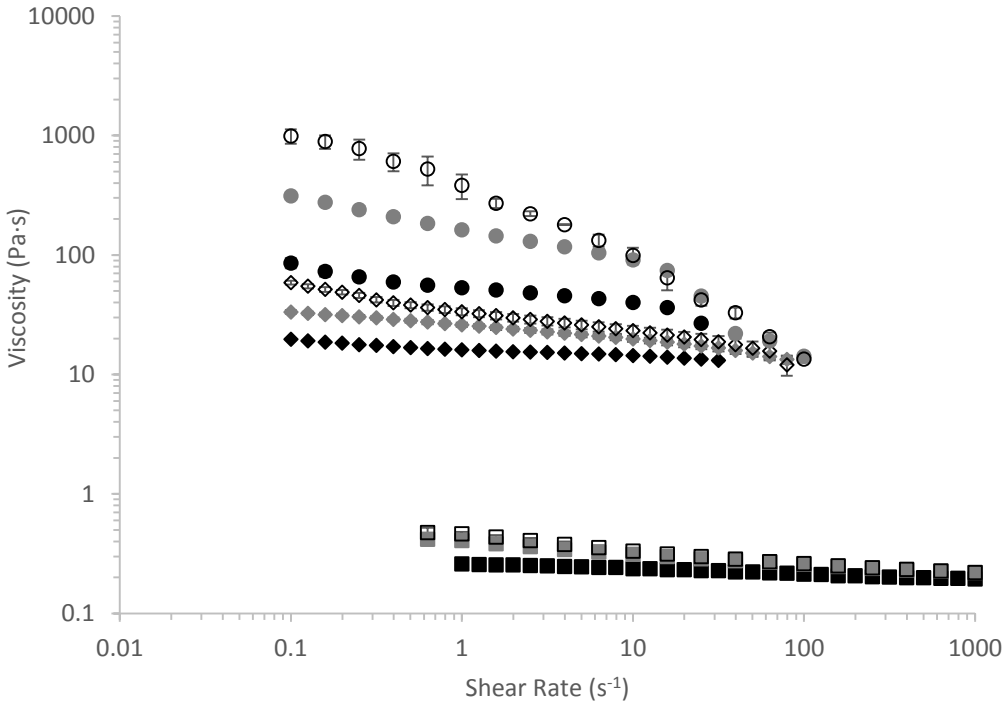

Figure 5.2: Shear viscosity data for neat 31K at 15 wt.% (□), neat 85K at 15 wt.%(◊), and neat 146K at 15 wt.% (○) at 1 day (black), 3 day (grey), and 5 day (open) aging points. Little aging was seen at the lowest molecular weight while more significant aging was seen at the higher molecular weights as well as slight shear thinning at high shear rates. Error bars represent the standard deviation of the average value.

The change in the viscosity with aging time for the neat 31K sample at a shear rate of 1 s^{-1} from 1 to 5 days was approximately an 80% increase while the change in the viscosity for the neat 146K sample was a 620% increase. These trends were expected due to increased molecular entanglements and attributed to differences in entanglement density and network formation for the different molecular weights studied here. The rate of aging also decreased as aging time increased. For example, in the neat 146K sample, viscosity increased 53% from 1 day to 3 days but only increased 13% from 3 days to 5 days at 1 s^{-1}. The decrease in aging rate in the latter portion of the aging cycle was

attributed to increased compaction of the chains during the first stage of aging as junction points between polymer chains were formed.

The shear thinning character of these solutions was described by fitting the viscosity data to a power law given by the equation below:

$$\eta(\dot{\gamma}) = m\dot{\gamma}^{n-1} \qquad (5.1)$$

where $\eta(\dot{\gamma})$ is the viscosity as a function of shear rate, m is the consistency index, $\dot{\gamma}$ is the shear rate, and n is the power law exponent. When n was equal to 1, the viscosity was constant with shear rate, indicating Newtonian behavior, and when n was less than 1, the viscosity decreased with increasing shear rate, indicating that the material was shear thinning. Smaller n values indicated a greater degree of shear thinning. The values for n for neat solutions as a function of aging time are given in Figure 5.3. Generally, the value of n decreased with aging, indicating increased shear thinning character with increased aging times for the neat PVA solutions.

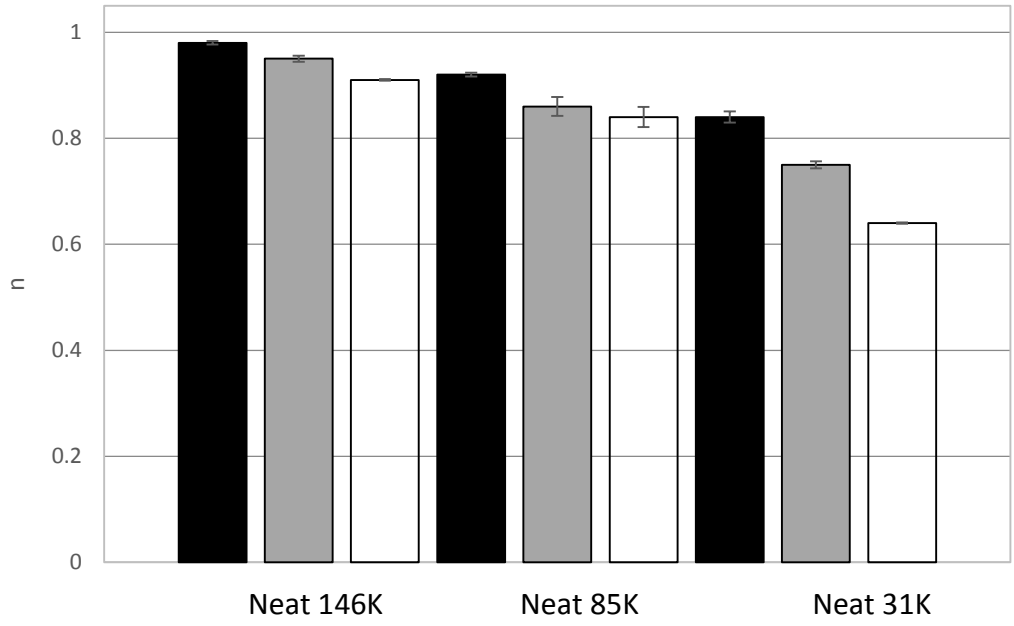

Figure 5.3: Values of *n* for neat PVA solutions at 15 wt.% solids. Black bars indicate 1 day of aging, grey bars indicate 3 days of aging, and white bars indicate 5 days of aging. Error bars represent the standard deviation of the average value.

5.3 Aqueous Suspended CNC Systems

Aqueous suspended CNCs were added into each of the three molecular weights at loadings of 20, 33, 50, and 67 wt.% w.r.t PVA. The total solids concentration was 15 wt.% in these nanocomposite suspensions. To further understand the effect of CNCs on polymer viscoelasticity, loadings of 1, 5, and 10 wt.% CNCs w.r.t PVA were added into 146K molecular weight solutions at the same solids loading. When aqueous suspended CNCs were added to the polymer solutions, the rheological behavior changed dramatically. As a result of increased elasticity in the nanocomposite suspensions, steady shear viscosity measurements could not be performed on these samples. Small angle oscillatory shear measurements of complex viscosity (η^*), G' and G'', were used instead

to characterize the viscoelastic behavior of the nanocomposite suspensions and the CNCs' contribution to these properties. For comparison, the rheological properties of the neat PVA solutions were measured again using small angle oscillatory shear testing. The trends in complex viscosity as a function of angular frequency were similar to the trends in viscosity as a function of shear rate for the neat PVA samples. Specifically, the value of the complex viscosity was found to vary more with angular frequency as the aging time and PVA molecular weight increased. Due to the almost negligible elasticity of the neat 31K 15 wt.% samples, small angle oscillatory shear data were not able to be collected for this sample.

As shown in Figure 5.4, the η^* data changed less with aging time as the concentration of CNCs increased. The first noticeable effect of CNC addition was seen in the mitigation of aging due to the increased rigidity of the system with respect to the neat polymer solutions. Interactions between CNCs and the PVA as well as interactions between CNCs were thought to restrict polymer chain mobility and hinder increased polymer chain entanglement. Conversely in the neat PVA systems, the chains were free to rotate, entangle and form crystalline network junction with one another over time due to physical bonding between the water molecules and the PVA chains.[14]

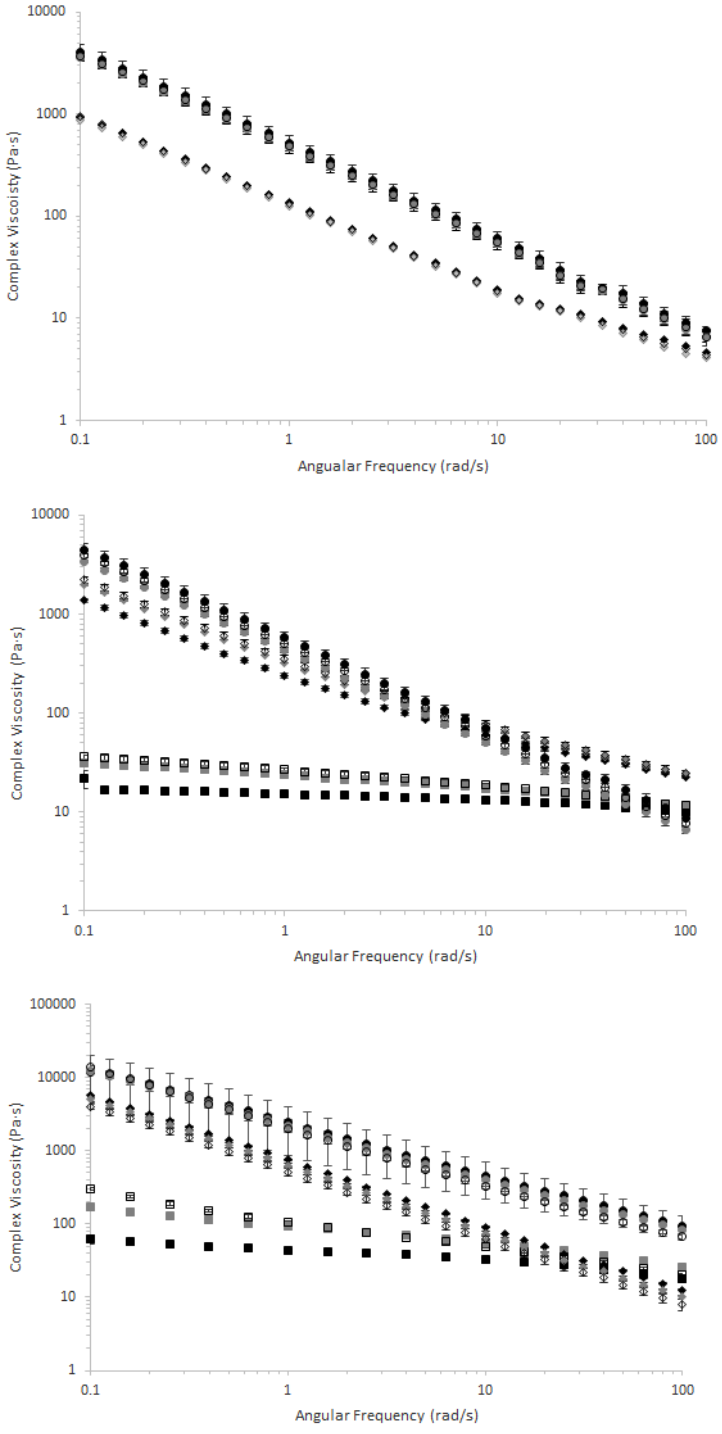

Figure 5.4: Aging of neat and nanocomposite suspensions at 1 day (black), 3 day (grey), and 5 day (open) for neat (■), 20 wt.% CNC (◆) and 67 wt.% CNC (●). Top(31K samples). Middle (85K samples). Bottom (146K samples). Error bars represent the standard deviation of the average value.

To understand this behavior more fully, a modified power law based on η^* was applied to the data:

$$\eta^*(\omega) = m^*\omega^{n^*-1} \qquad (5.2)$$

Where $\eta^*(\omega)$ is the complex viscosity as a function of angular frequency, m^* is the consistency index and n^* is the power law exponent for complex viscosity. Figure 5.5 shows the value of n^* as a function of aging time for all 146K samples. These results were representative of all PVA molecular weights studied here. While distinct aging was seen in neat polymer solution, the structure of the nanocomposite suspensions at high CNC loadings of 20 wt.% CNC and above changed less with increasing time, shown by smaller changes in the value of n^* as compared to the neat PVA solutions. As CNC loading increased in the suspension, the value of n^* from 1 day to 5 days of aging time became nearly constant, indicating limited aging.

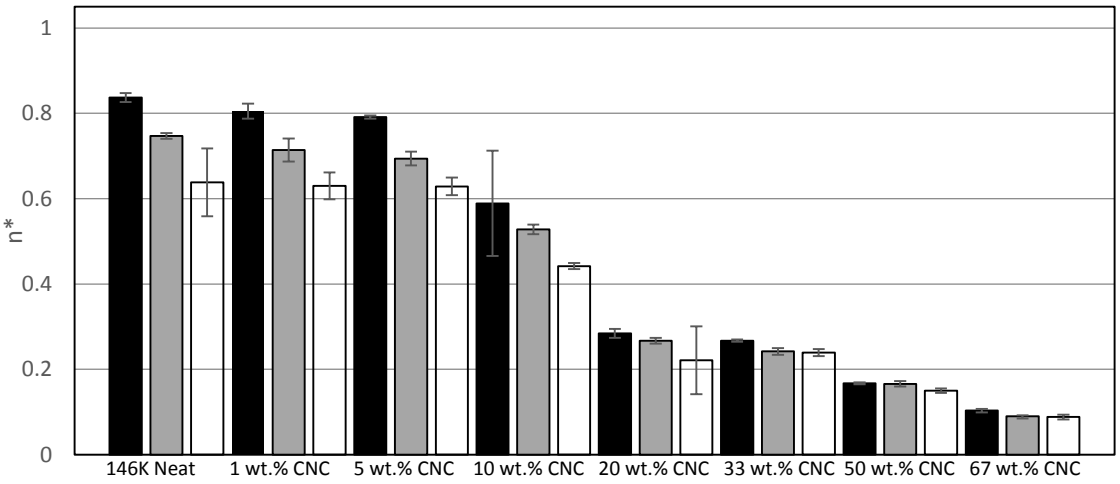

Figure 5.5: CNC contribution to sample aging shown with the *n**. Neat samples have distinct aging characteristic with time while CNC loaded samples, especially at high CNC loadings, show very little aging. Black bars indicate 1 day of aging, grey bars indicate 3 days of aging, and white bars indicate 5 days of aging. Error bars represent the standard deviation of the average value.

Analysis of the dynamic moduli data also led to insights into the effect of adding CNCs to the PVA suspensions. Figure 5.6 shows the dynamic moduli data, G' and G'', obtained for the 85K neat PVA solution at 15 wt.% and 85K 20 wt.% CNC w.r.t. PVA. An important difference was seen between these samples. For 85K neat PVA, the value of G'' was greater than the value of G' for the range of frequencies measured, indicating the sample was a concentrated solution and not a gel. For the nanocomposite suspension shown (85K 20 wt.% CNC w.r.t. PVA), the value of G' was greater than the value of G'' over the range of frequencies measured indicating gelation had occurred. Additionally, the frequency dependence of G' and G'' was weaker in the nanocomposite suspension, suggesting that an elastic network was formed in the suspension. All other nanocomposite suspensions showed similar trends in G' and G'' at loadings of 20 wt.% CNC w.r.t. PVA and above, and the frequency dependence of G' and G'' continued to weaken with increasing CNC loading, shown in Figure 5.7.

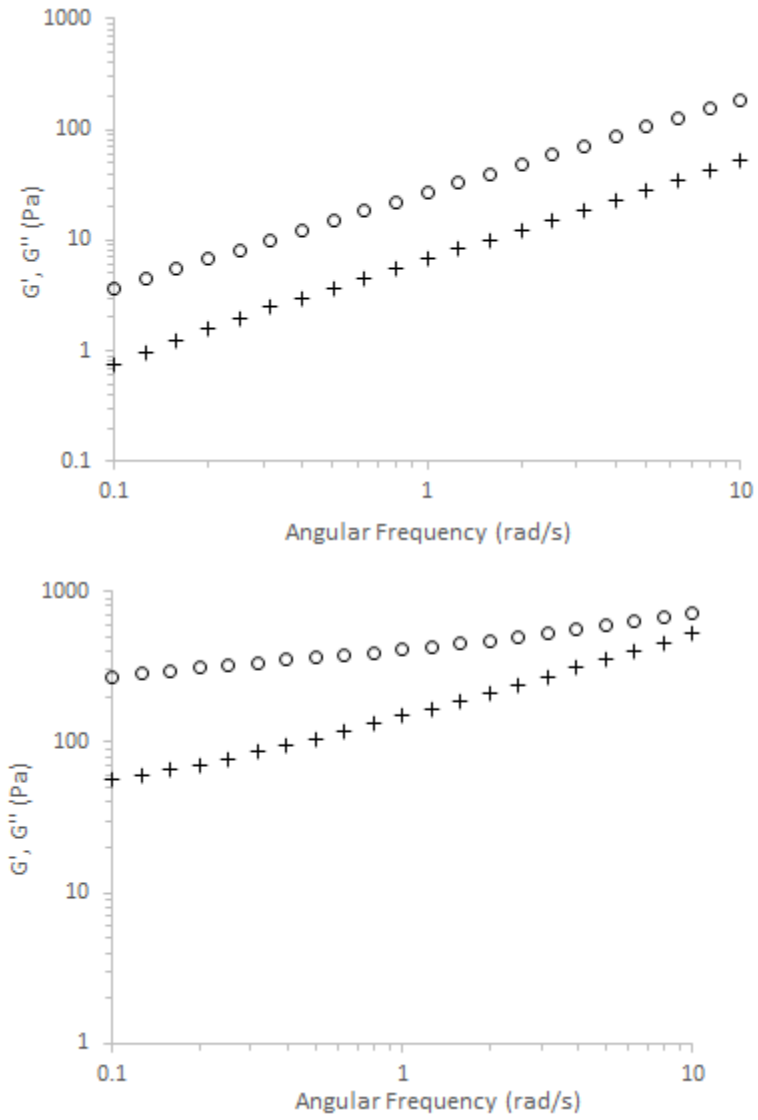

Figure 5.6: G' and G'' for neat and CNC suspension. The top plot shows the data for 85K neat PVA at 15 wt.% while the bottom plot shows the data for 85K 20 wt.% CNC w.r.t. PVA. G' is denoted with (+) while loss modulus is denoted with (○).

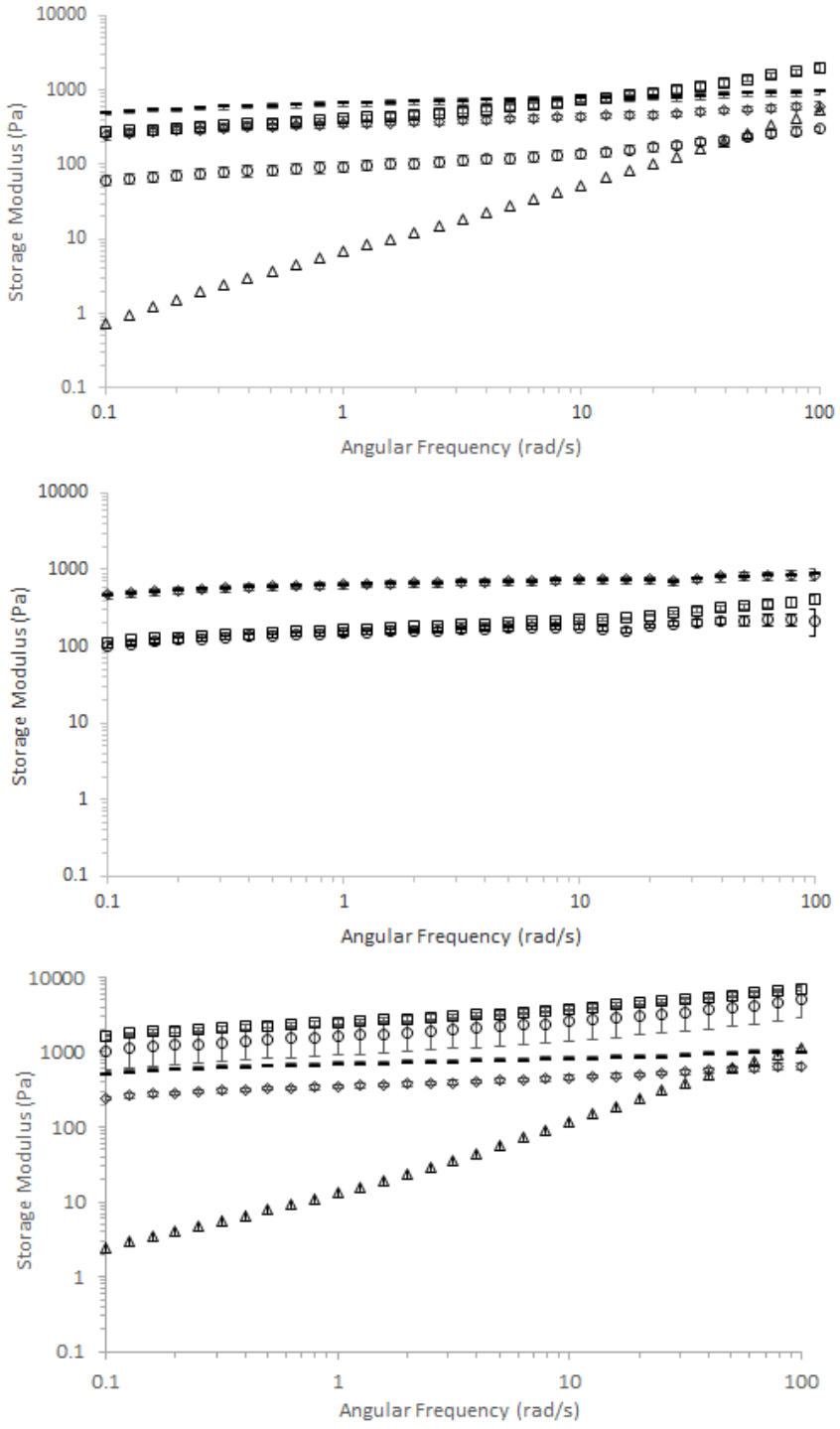

Figure 5.7: *G′* data for neat and nanocomposite suspensions at 5 days aging time. Top: 31K neat PVA and nanocomposite suspensions. Middle: 85K neat PVA and nanocomposite suspensions. Bottom: 146K neat PVA nanocomposite suspensions. Neat PVA (△), 20 wt.% CNC w.r.t. PVA (□), 33 wt.% CNC w.r.t. PVA (○), 50 wt.% CNC w.r.t. PVA (◊), and 67 wt.% CNC w.r.t. PVA (—).Error bars represent the standard deviation of the average value.

The same behavior was not observed for the 146K CNC/PVA nanocomposite suspensions at CNC loadings of 10 wt.%. In these samples, the value of $G' > G''$ was observed at lower frequencies and then the opposite relationship was observed at higher frequencies. The frequency associated with the transition from solid-like to liquid-like behavior was defined as the crossover frequency. These data for each concentration at 1 day, 3 days, and 5 days of aging is shown in Figure 5.6. The elastic character of the suspensions increased with both CNC loading and aging time. While solution behavior was seen at 1 day of aging, crossover behavior was seen at 3 and 5 days of aging. This increase in elastic behavior with time could be attributed to the increased PVA chain entanglements with time due to PVA crystallite formation and increased compaction of the PVA chains due to phase separation. During this phase separation, the CNCs were able to form a weak gel network. The increase in elastic behavior with increasing CNC loading was due to increased stiffness imparted by the CNCs as the CNCs and PVA began to form a gel network inside the suspensions.

Another trend seen in Figure 5.8 was the behavior of G' and G'' before and after the crossover frequency at loadings of 10 wt.% CNCs. At loadings below 10 wt.% CNCs, the system acted as a solution over the entire frequency range. At lower frequencies below the crossover point, the suspensions behave as a gel while above the crossover point, suspensions behave as a liquid. Similar behavior has been seen in gel systems containing methoxyl pectin near the gelation time.[172] In these weak gels, the pectin systems acted as a liquid shortly before the gel time in a similar fashion to the CNC/PVA suspension at 10 wt.% CNCs at 1 day of aging. Shortly after the gel time, the pectin system saw $G' > G''$ at low frequencies with G' and G'' superimposed at higher

frequencies. In the CNC/PVA systems at low loadings, gelation was driven by phase separation of the PVA and CNCs until a weak composite network was formed. Due to the weak gel network formed, the application of frequency caused the gel network to revert back to solution behavior in the linear viscoelastic region as it was very near the gel point.

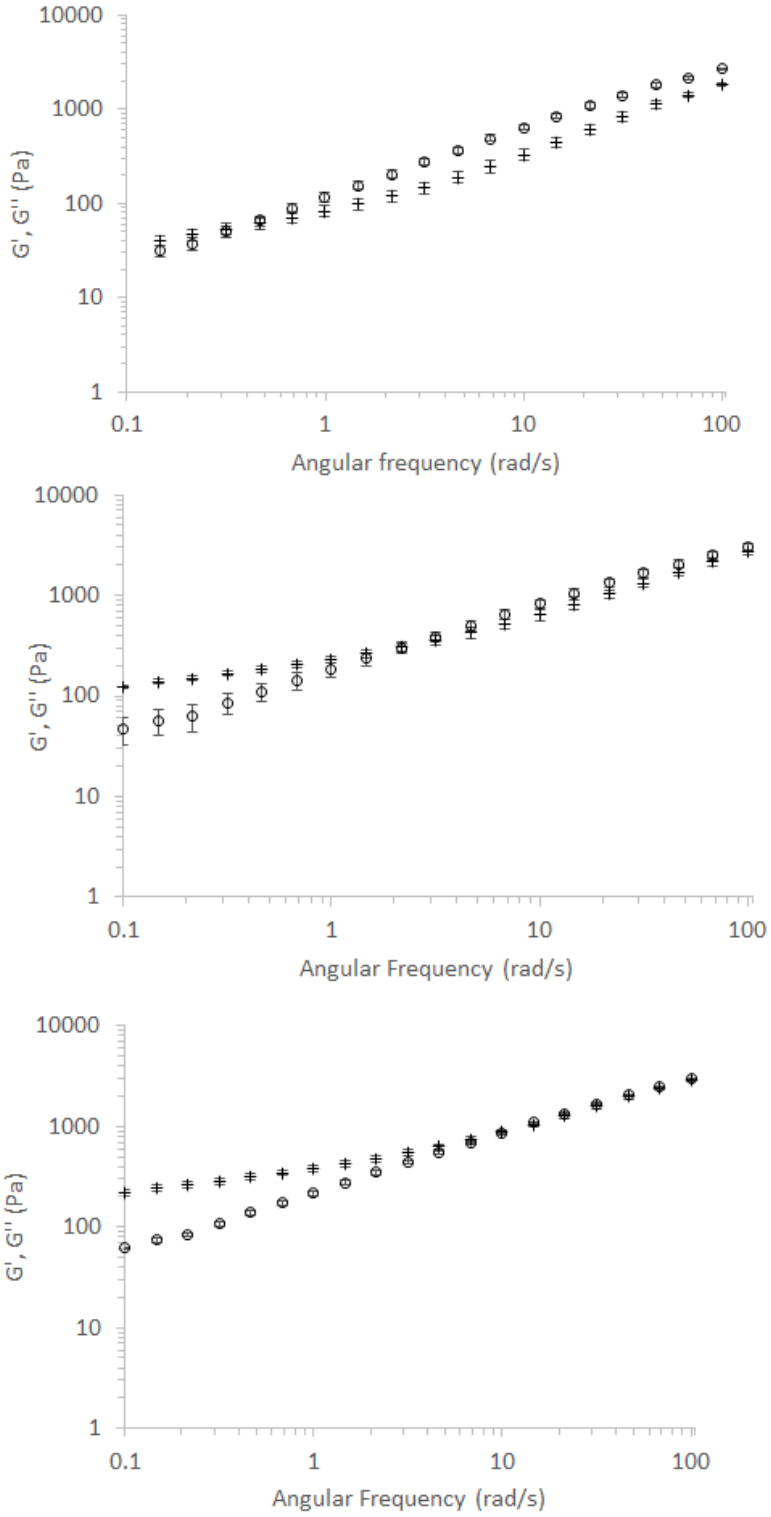

Figure 5.8:G' (+) and G'' (○) data for 146K 10 wt.% CNC loading w.r.t. PVA as a function of solids loading and time.

Next, the values of G' for neat solutions and nanocomposite suspensions were compared in order to better understand the contribution of both the PVA and the CNCs in the suspensions. From these data, two different trends were seen, and they were related to the polymer molecular weight and CNC loading. First, the trends observed for G' at lower CNC loadings were dependent on the polymer molecular weight. For the 31K molecular weight samples, G' increased with increasing CNC loading; however, the 146K molecular weight samples saw a decrease in G' with increasing CNC loading above 20 wt.% CNC. The 85K molecular weight samples showed trends intermediate to the 31K and 85K molecular weight samples. The trends observed for the three molecular weights were attributed to differences in the nature of the neat polymer solutions. For the neat 31K molecular weight solution, the rheological characterization indicated that this solution behaved similarly to a Newtonian fluid with little shear rate dependence of the viscosity. This description was further supported by the inability to perform a small angle oscillatory shear experiment on the sample. Conversely, the 85K and 146K neat PVA solutions showed more elastic character though their behavior was still more liquid-like than solid-like. Therefore, the addition of CNCs to these solutions affected the value of G' differently because the neat PVA solutions at these molecular weights were structured differently. Second, the value of G' at higher CNC loadings was similar for nanocomposite suspensions made with different polymer molecular weights. This observation suggested that the observed behavior was related more strongly to the structuring of CNCs in the suspensions.

In order to quantify the relative changes in the data with increasing CNC content and polymer molecular weight, the power law model presented earlier was adapted again for use with the G' data for the neat polymer solutions and the CNC nanocomposite suspensions from Figure 5.7. The results are shown in Figure 5.9. The modified expression is shown below:

$$G'(\omega) = m'\omega^{n'} \qquad (5.3)$$

Where $G'(\omega)$ is the storage modulus as a function of angular frequency, m' is the consistency index, and n' is the modified power law exponent for storage modulus. The value of n' gave an indication of the differences in network behavior with lower values of n' corresponding to a more rigid network in the sample. As shown in Figure 5.7, the value of n' decreased with increasing CNC content. At high CNC loadings, the value of n' was approximately 0.08 for nanocomposite suspensions made with all three molecular weights, suggesting that the suspensions were structured similarly at these loadings.

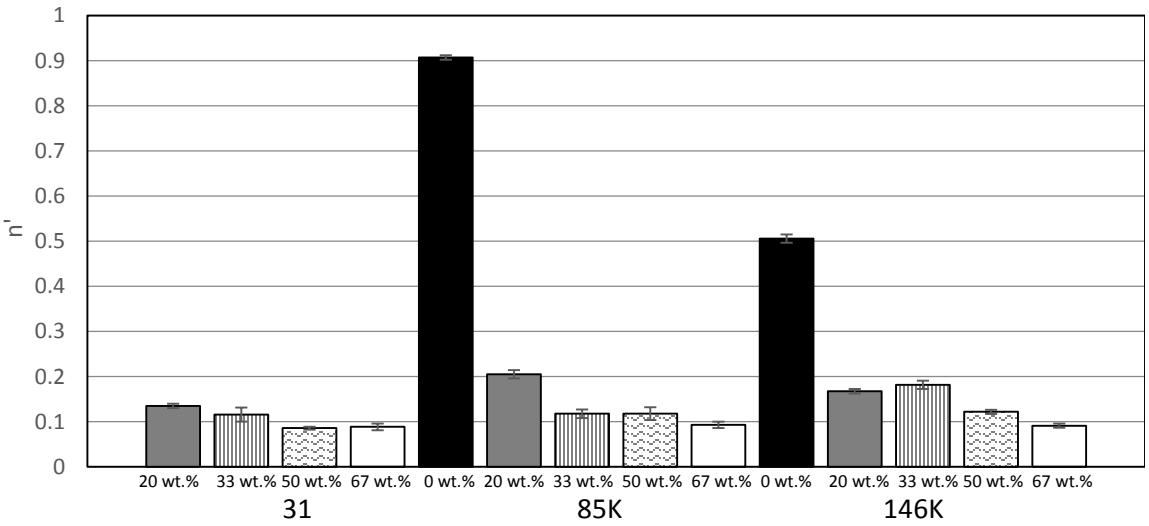

Figure 5.9. Power law exponent from fitting power law to G' at 5 days of aging.

Using the small angle oscillatory shear data, the yield stress was calculated for the CNC suspensions. The method used was based on Doraiswamy *et al*.[173] and Mas and Magnin [174]. The angular frequency was converted to shear rate using the equation below in

$$\dot{\gamma} = \gamma\omega \qquad (5.4)$$

Where $\dot{\gamma}$ is the shear rate, γ is the shear strain, and ω is the angular frequency. The yield stress primarily represented the minimum stress required to disrupt the networks formed from PVA and CNCs and the microdomains present in the system,[16] CNC or PVA. The yield stress was determined from the following equation:

$$\tau^{1/2} = \tau_0^{1/2} + \mathrm{K}\dot{\gamma}^{1/2} \qquad (5.5)$$

Where τ is the shear stress, $\dot{\gamma}$ is the shear rate, and τ_o is the yield stress. The yield stress was determined from a Casson plot in which the square root of the shear stress was plotted against the square root of shear rate. Figure 5.10 shows an example Casson plot for 85K 20 wt.% CNC w.r.t. PVA. The yield stress was related to the intercept of the line through the equation shown above. Figure 5.11 shows the results of this analysis. The trends in the yield stress values were similar to those seen for the G' data. A molecular weight dependence was observed at lower CNC loadings, and a common convergence point was seen at the highest CNC loading for all of the polymer molecular weights studied due to similarities in nanocomposite suspension structure.

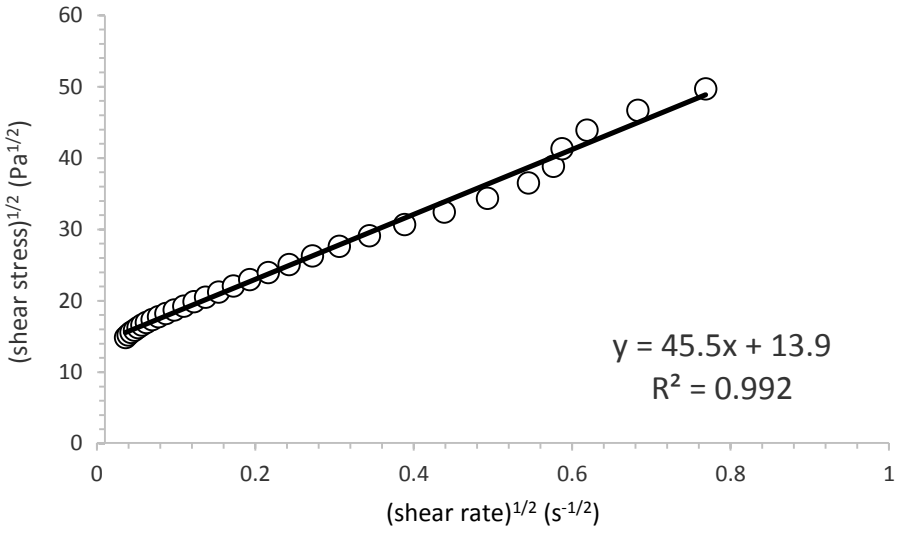

Figure 5.10: Example Casson plot construction for determining yield stress for sample 85K 20 wt.% CNC.

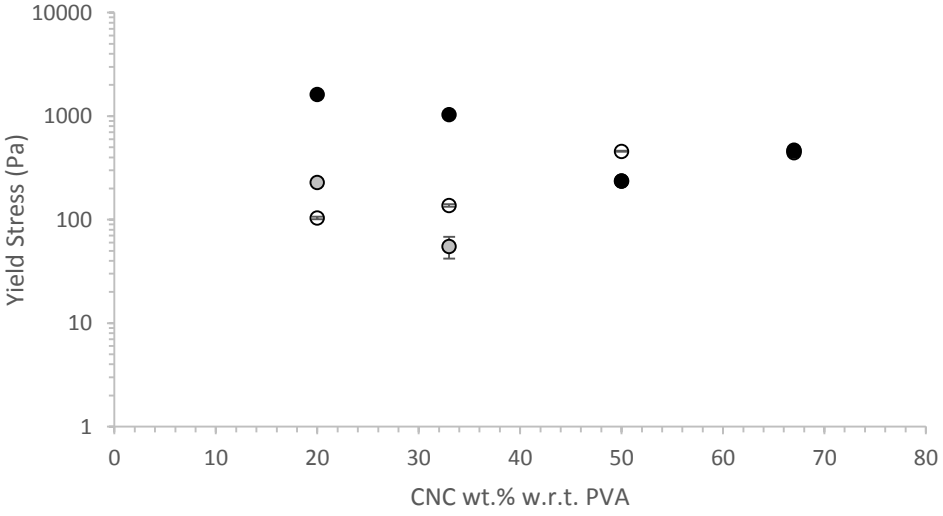

Figure 5.11: Yield stress calculations for each molecular weight. As shown, a common convergence occurred at CNC/PVA ratio equals 2. Suspensions are denoted as: 31K (open), 85K (grey), and 146K (black).

Rheological characterization of the neat PVA solutions and nanocomposite suspensions provided insight into the dynamics and structure of the materials. Aging

processes were impacted by the addition of CNCs. Specifically, the addition of CNCs reduced aging, suggesting that the driving forces for phase separation between the PVA and water were kinetically suppressed.[21] In the neat PVA solutions, aging occurred as junctions between individual polymer chains formed over time leading to microscale phase separation between the PVA and water. These connections, either in the form of polymer entanglements or microscale crystalline junctions, increased the viscosity of the solution and its elasticity.[21,22] CNCs appeared to impede the aging process by physically interacting with the PVA and reducing its ability to form polymer junctions. All of the CNC concentrations used here were high enough to suppress these processes over the time scale of observation, leading to the need to understand their structuring in the nanocomposite suspensions more fully.

With regard to structure, the data obtained suggested that for the CNC loadings studied, networks were present in some of the nanocomposite suspensions. Network formation was indicated by the solid-like behavior of the nanocomposite suspensions, i.e. G' was greater and G''. Complete network structure at all frequencies was seen at loadings of 20 wt.% CNC and above while crossover behavior was seen at l0 wt.% CNC. Conversely, the neat PVA solutions at each molecular weight appeared to be more liquid-like, though junctions between polymer chains in the form of entanglements or small crystallites would have been present.[21,22] Network formation dramatically increased the viscosity and elasticity of the suspensions with respect to the neat PVA solutions as would be expected. However, trends in the G' data indicated that the type of network present in the sample was dependent on the CNC loading. For nanocomposite suspensions with PVA-CNC compositions of 20 wt.% CNC w.r.t. PVA and 33 wt.%

CNC w.r.t., the network present in the material was suggested to be composed of CNC and PVA with the polymer chains or their entanglements connecting CNCs. The stiffness and strength of these polymer mediated junctions were directly related to the molecular weight of the polymer, as indicated by the values of G' and yield strength, respectively. As the polymer molecular weight increased, the polymer mediated CNC network became more robust. For nanocomposite suspensions with PVA-CNC compositions of 50 wt.% CNC w.r.t. PVA and 67 wt.% CNC w.r.t., the network present in the material was composed primarily of CNC with polymer mediated junctions playing a smaller role. This network structure was indicated by similar values of G' and yield strength in the samples made with all three polymer molecular weights. The strength and stiffness of this network were in some cases less than those of the polymer mediated CNC network, suggesting that entanglements and/or crystalline junctions present in the 146K neat PVA and 85K neat PVA samples were stiffer than CNC-CNC interactions. Overall, these trends indicated that more effective reinforcement was attained for lower molecular weight polymers; however at appropriate CNC concentrations, polymer mediated junctions can synergistically stiffen the nanocomposite gel.

This transition between network types approximately corresponded to the CNC percolation threshold. The percolation threshold, V_c, was estimated to be at a CNC volume fraction of 0.025, calculated by dividing 0.5 by the CNC aspect ratio (20),[175,176] and the volume fractions for PVA-CNC loadings of 1 wt.%, 5 wt.%, 10 wt.%, 20 wt.%, 33 wt.%, 50 wt.%, and 67 wt.% CNC w.r.t. PVA corresponded to 0.001, 0.005, 0.009, 0.019, 0.031, 0.048, and 0.064, respectively. Therefore, polymer mediated networks played a greater role in determining the rheological response at CNC loadings slightly

below or near the percolation threshold, and CNC networks were determined by the rheological response at CNC loadings well above the percolation threshold.

5.4 Freeze-dried CNC Systems

Freeze-dried CNC systems were studied during the process implementation phase of the presented research. While the freeze-dried CNCs were produced via acid hydrolysis with similar zeta potential to the aqueous suspended CNCs, they tended to have increased agglomeration in aqueous suspension since it was difficult to break apart agglomerates of CNCs that formed during the freeze drying process. This agglomeration lead to differences in solution behavior. To study these differences, freeze-dried CNCs were processed using solution processing and shear processing methods, and the results of rheological experiments were compared to those obtained for materials made with CNCs that were never dried from aqueous suspension. In the solution processing methods used, pristine freeze-dried CNCs were added directly to PVA solutions, or the CNCs were redispersed in deionized water and then added to PVA solutions in the same processing method used for the aqueous suspended CNCs. In the shear processing method used, pristine freeze-dried CNCs were added to neat PVA solutions and mixed in the batch mixer for 10 minutes as described in Chapter 3. All freeze-dried CNC analyses were conducted using 146K molecular weight polymer.

5.4.1 Solution Processing

Freeze-dried CNCs were processed in the solution state in two different ways: direct addition of freeze-dried CNCs to PVA solutions (solution processed CNC/PVA suspensions) or redispersion of freeze-dried CNCs in deionized water followed by addition to PVA solutions (RDFD CNC/PVA suspensions). First, the aging of the RDFD CNCs was studied to mimic the aqueous suspended CNC systems. This aging and complex viscosity behavior was used as an indirect assessment of the aggregation in the CNC/PVA suspensions. If increased aging was seen between similar nanocomposite suspensions, then it was likely that there was decreased dispersion and distribution of the CNCs due to the increased ability of the PVA chains to compact and phase separate. If a decrease in overall complex viscosity was seen, it can be correlated to increased aggregation of the freeze-dried CNCs, causing the fillers to act as micro-fillers instead of nanofillers and decreasing their ability to transfer stress. The aging of the RDFD CNC systems were studied at 1 wt.%, 5 wt.%, 10 wt.%, 20 wt.%, 33 wt.%, 50 wt.% and 67 wt.% CNCs w.r.t. PVA in 15 wt.% total solids solutions. The data for this analysis can be found in Figure 5.12 for 1 wt.%, 10 wt.%, 33 wt.% and 67 wt.% CNC w.r.t. PVA in 15 wt.% total solids solution. Similar to the aqueous suspended CNC systems, increasing CNC content decreased the aging as the CNCs restricted polymer phase separation. The slope of the complex viscosity also increased with increasing CNC content, a behavior that will be further discussed with respect to the G' and G'' data. At high shear rates, the complex viscosity data for the CNC/PVA nanocomposite suspensions at loadings of 33 wt.% CNC and greater dropped below the complex viscosity data of the neat PVA. This behavior was attributed to the decreased stiffness of the CNC network composed of

aggregated CNCs with respect to the PVA network and CNC-PVA network present in samples with lower CNC loadings.

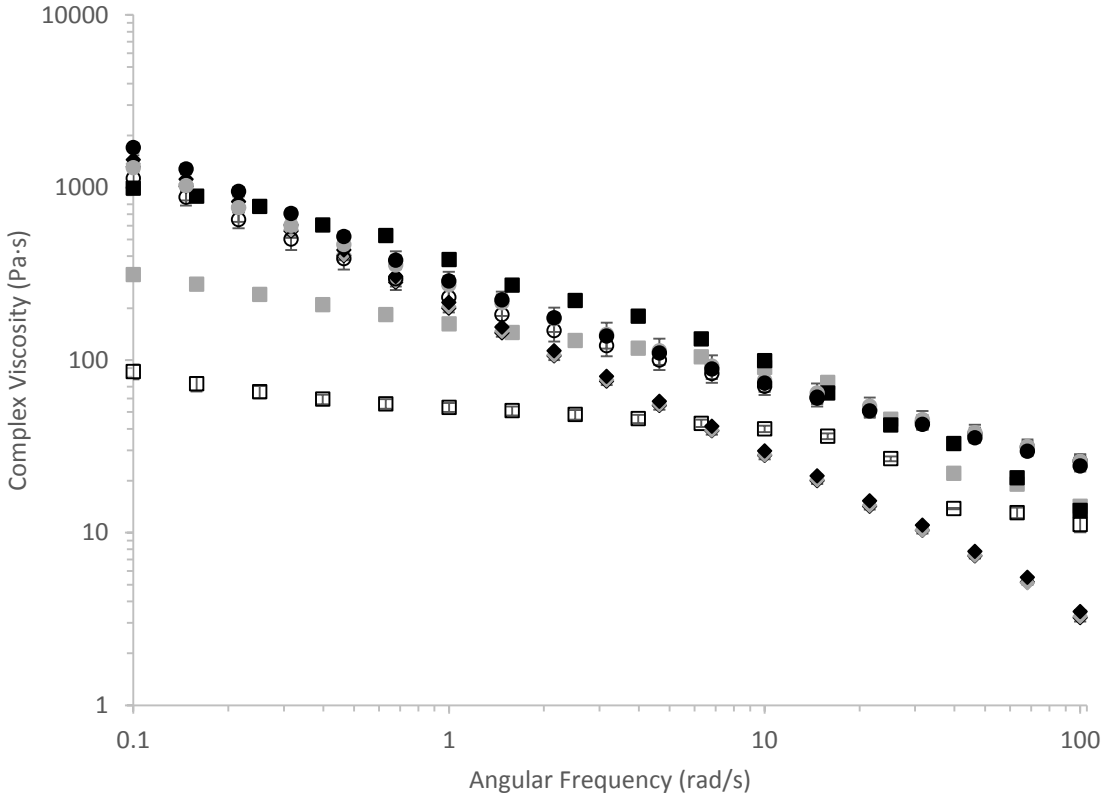

Figure 5.12: Complex viscosity and aging data for Neat 146K (□), 20 wt.% (○), and 67 wt.% (◇) RDFD CNCs w.r.t PVA in 15 wt.% solution. Data for 1 day shown as open markers, 3 day data shown as grey markers, and 5 day data shown as black markers. Error bars represent the standard deviation of the average value.

Aging of solution processed CNC/PVA suspensions can be found in Figure 5.13 for 146K neat PVA, solution processed freeze-dried 20 wt.% CNC w.r.t. PVA, and solution processed freeze-dried 67 wt.% CNC w.r.t PVA. From these data it was seen that very little aging occurred in either the solution processed freeze-dried 20 wt.% CNC or 67 wt.% CNC. A decrease in complex viscosity was also seen when comparing similar

samples produced from the RDFD and aqueous suspended CNCs. This decrease in complex viscosity can be attributed to the higher degree of CNCs aggregation present in these samples.

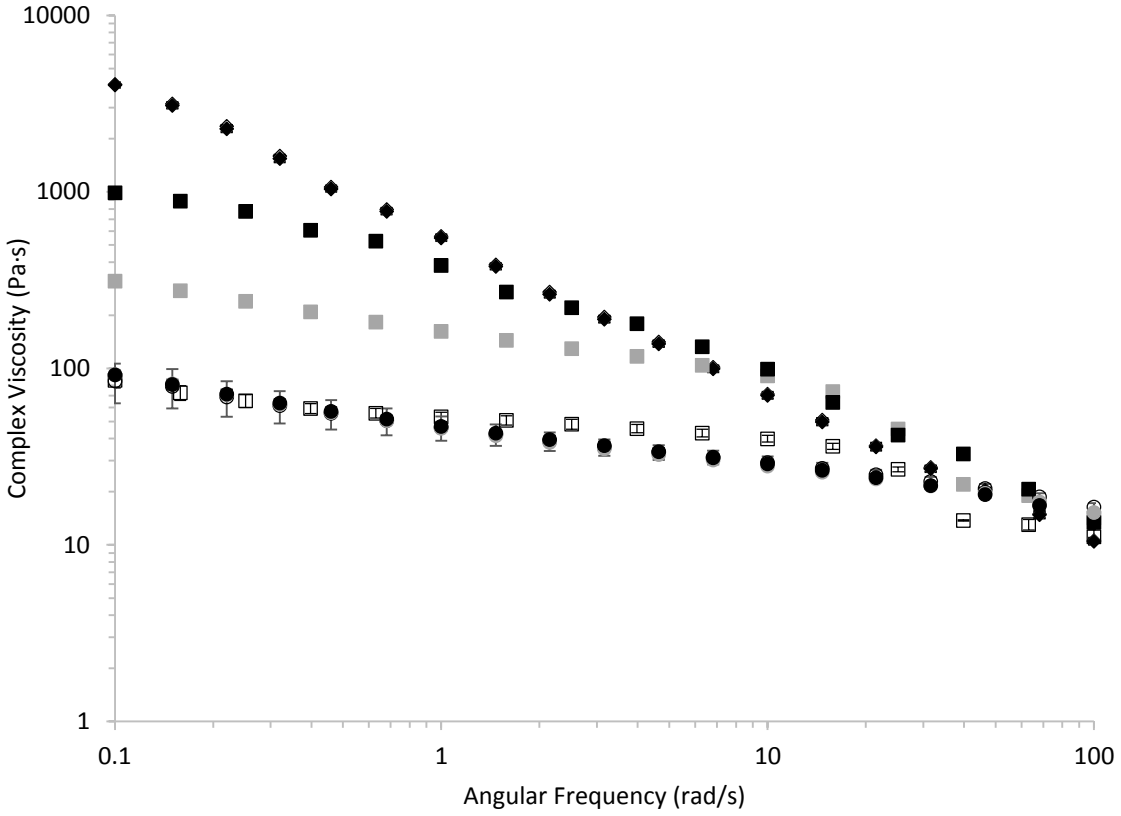

Figure 5.13: Complex viscosity and aging data for 146K Neat PVA (□), freeze-dried solution processed 20 wt.% CNC w.r.t PVA (○), and freeze-dried solutions processed 67 wt.% CNC w.r.t. PVA (◇) in 15 wt.% solution. Data for 1 day shown as open markers, 3 day data shown as grey markers, and 5 day data shown as black markers. Error bars represent the standard deviation of the average value.

To further understand the aging behavior, the modified power law equation 5.2 was used to fit the n^* to the RDFD complex viscosity data and is shown in Figure 5.14. Just as the

aqueous suspended CNC aging data showed, aging was decreased with increased CNC loading. The neat PVA experienced the largest change in complex viscosity from 1 to 3 to 5 days of aging with a 12% change in power law exponent from 1 to 3 days and a 17% change in power law exponent from 3 to 5 days while only adding 1 wt.% CNCs to the PVA solution caused no change from 1 to 3 days and a 9% change from 3 to 5 days. This was likely due to the increased rigidity of the CNCs on the PVA chains prohibiting chain compaction and phase separation even at low loadings of 1 wt.%. In comparison, 5 wt.% CNC w.r.t. PVA saw increased aging from the 1 wt.% CNC w.r.t. PVA solutions but decreased aging from 146K neat PVA in that the sample decreased in n^* from 1 day to 3 days by 8% and by 11% from 3 days to 5 days. This increase in aging could be attributed to decreased dispersion of the CNCs as the PVA chains were more able to compact, phase separate and age, especially since the CNC/PVA suspension was not in a stable gel state. Above the percolation threshold, little aging was seen for RDFD CNCs as the CNCs formed a rigid network, prohibiting the PVA from aging.

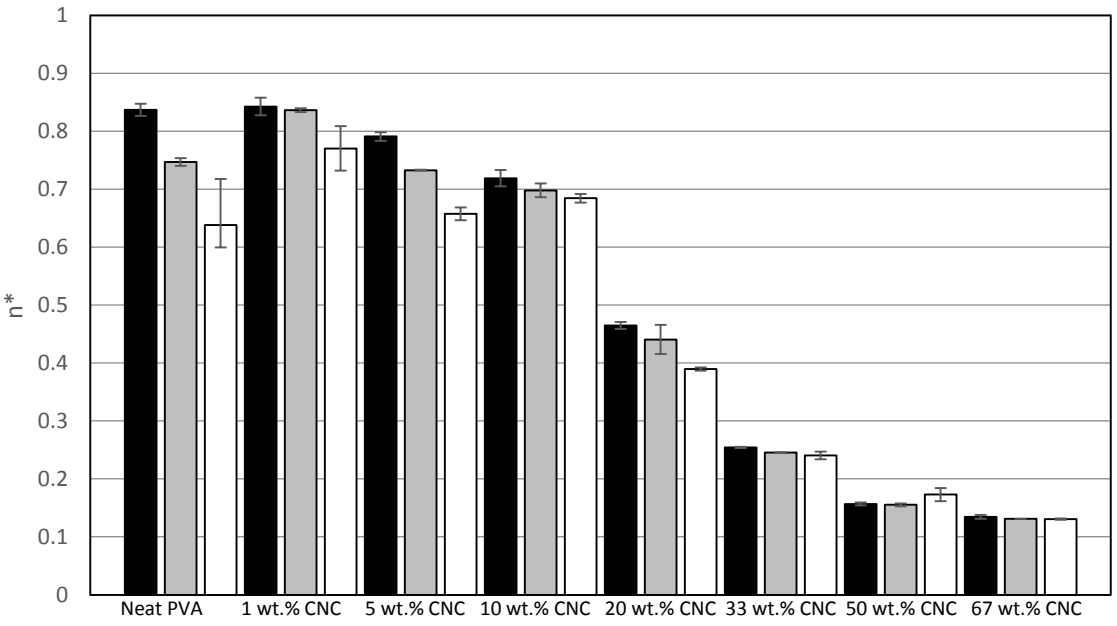

Figure 5.14: Aging modeled by the *n** from equation 5.2 of RDFD CNC/PVA nanocomposite suspensions solution processed. Data for 1 day shown as black, 3 day data shown as grey, and 5 day data shown at white. Error bars represent the standard deviation of the average value.

In addition, *n** was fit to the solution processed freeze-dried CNC data shown in Figure 5.15. From this analysis decreased aging was seen compared to the aqueous suspended CNC systems and similar to the RDFD CNC systems. The total percent change *n** from 1 day to 5 days was 10% for solution processed freeze-dried 20 wt.% CNC w.r.t PVA, most likely due to poor dispersion giving larger regions of CNCs, decreasing the total PVA-PVA aging in the system. The values of *n** were also larger for the solution processed freeze-dried CNC/PVA suspensions compared to RDFD, indicating a decreased frequency dependence on the suspension most likely due to the decreased network structure of the CNCs brought on by aggregation.

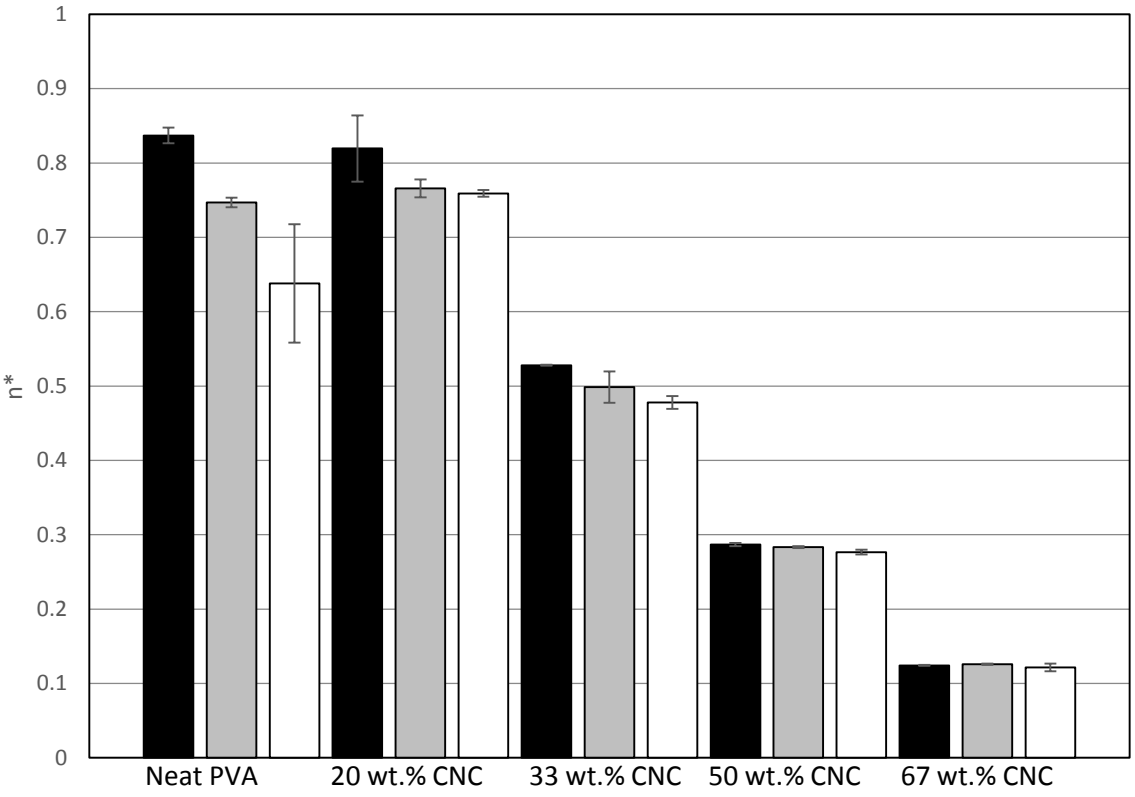

Figure 5.15: Aging modeled by the *n** from equation 5.2 of solution processed freeze-dried CNC/PVA nanocomposite suspensions. Data for 1 day shown as black, 3 day data shown as grey, and 5 day data shown at white. Error bars represent the standard deviation of the average value.

To more fully understand the differences in aging between the solution processed freeze-dried CNC, aqueous suspended CNC, and RDFD CNC systems, Table 5.1 was constructed to compare the changes in *n** as well as complex viscosity in order to get a better idea of the solution morphology. In general, Δ*n**, the change in *n** from 1 day to five days, trended towards lower values with increasing CNC content indicated decreased aging from 1 day to 5 days with the exception of the RDFD system. In this system, Δ*n** decreases overall but fluctuated from higher to lower values, especially in the low loading systems of CNCs and PVA. This fluctuation in Δ*n** could be attributed to some phase

separation instability in the RDFD systems especially at low loadings. The complex viscosity of the three solution processed systems also showed trends with increasing CNC content at 5 days of aging. All solution processed systems saw some decrease in complex viscosity with CNC loading, especially at loadings below the percolation threshold (20 wt.% CNC w.r.t. PVA and below). This decreased complex viscosity could be due to the CNCs competing with the PVA to form a network structure, a concept which will be discussed more thoroughly in this chapter when understanding the G' and G'' behavior. Complex viscosity maintained the largest values for the aqueous suspended system while these values decreased for the freeze-dried systems, most likely due to aggregation of the system. Complex viscosity also increased and then decreased with increasing CNC loading in the aqueous suspended CNC/PVA suspensions. A similar trend in viscosity was also seen in PEO systems and attributed to the increased bonding character of the oxygen bonds to the hydroxyl groups. Once this bonding was maximized, the viscosity decreased.[106] While distinct aggregation was seen in the solution processed freeze-dried CNC system and no distinct aggregation was seen in the RDFD CNC systems, it is still possible that very small aggregates of CNCs were present and could not be observed with polarized light microscopy.

Table 5.1: Total change in n^* with time for all solution processed CNC systems as well as complex viscosity at 5 days of aging.

Loading	Solution Processed					
	Aqueous Suspended CNCs		Freeze Dried		RDFD CNCs	
	Δn*	η* (Pa·s)	Δn*	η* (Pa·s)	Δn*	η* (Pa·s)
Neat 146K	0.199 ± 0.11	52 ± 3.4	0.199 ± 0.11	52 ± 3.4	0.199 ± 0.11	52 ± 3.4
1 wt.% CNC	0.175 ± 0.09	188 ± 46	0	0	0.072 ± 0.09	58 ± 0.39
5 wt.% CNC	0.162 ± 0.08	142 ± 15	0	0	0.134 ± 0.08	202 ± 40
10 wt.% CNC	0.147 ± 00.08	441 ± 26	0	0	0.035 ± 0.08	79 ± 0.91
20 wt.% CNC	0.063 ± 0.11	2020 ± 183	0.0605 ± 0.08	52 ± 2.4	0.075 ± 0.08	287 ± 21
33 wt.% CNC	0.028 ± 0.08	1337 ± 129	0.050 ± 0.08	126 ± 7.4	0.014 ± 0.08	192 ± 8.9
50 wt.% CNC	0.017 ± 0.08	275 ± 17	0.010 ± 0.08	178 ± 3.2	0.016 ± 0.08	354 ± 7.2
67 wt.% CNC	0.015 ± 0.08	516 ± 56	0.003 ± 0.08	581 ± 39	0.004 ± 0.08	216 ± 4.2

To further understand the effect of processing on aqueous suspended and freeze-dried CNC/PVA systems, G' and solution to gel (sol-gel) or gel to solution (gel-sol) transitions were examined. First, the G' behavior was studied for the RDFD CNC and solution processed freeze-dried CNC systems, shown in Figure 5.16. From these data, it was seen that the trends in G' behavior varied with processing method, especially at high frequencies. In the aqueous suspended and RDFD systems at high frequencies around 100 rad/s, G' decreases with increasing CNC content while the solution processed freeze-dried CNC system saw a convergence of the G' values at high frequency. This behavior can be attributed to the better dispersion of the CNCs inside the aqueous suspended and RDFD CNC systems, allowing for the CNC/PVA suspensions to go towards a more CNC predominant network. The G' trends at lower frequencies showed a different trend. The relative trend in G' behavior at 1 s^{-1} is shown in Figure 5.17 for comparison. At low frequencies, G' increases with increasing CNC loading for the solution processed freeze-

dried CNC/PVA systems while G' tended to increase up until 20 wt.% CNC and then decrease for the aqueous suspended CNC/PVA systems and plateau after 20 wt.% for the RDFD systems. This increase in G' for the solution processed freeze-dried CNC systems can be attributed to the larger agglomerates of the CNCs, minimizing the effect of the PVA contribution to the network below the percolation threshold (as shown by lower G' values below percolation). The plateau of G' behavior above the percolation threshold in the RDFD systems can be attributed to the formation of a CNC network structure. The values of G' were seen to be lower for the RDFD systems, most likely due to the slight aggregation of the CNCs decreasing CNC-PVA interaction. From the plots of each of the solution processed CNC systems in Figure 5.16, it can be seen that the slope of the G' curve varied with CNC loading. To better understand the change in elastic behavior with frequency and CNC loading, equation 5.3 was used in which the power law model was again modified to account for G' behavior and n' was calculated. The results from this model can be seen in Figure 5.18 for each of the solution processed CNC/PVA systems. From this analysis, it was seen that G' was generally largest for the aqueous suspended CNC systems and smallest for the solution processed freeze-dried systems with the RDFD CNC systems in between. This decrease in modulus through the incorporation of CNCs shows that during solution processing, the freeze-dried CNC systems were likely more aggregated than those made from an aqueous suspension of CNCs. The analysis of n' from equation 5.3 in Figure 5.18 gave increased insight. While the value of n' decreased with increasing CNC content for each system, the magnitude of n' for each system was quite different. While n' values close to 1 indicate strong G' dependence on frequency, n' values closer to 0 indicated G' frequency independence. Figure 5.18 shows

a decreasing frequency dependence with increasing CNC content as the CNCs form a more rigid network structure. In comparison, freeze-dried CNC systems showed increased n' values compared to aqueous suspended CNCs systems as the freeze-dried CNCs were not able to impart as much rigidity to the system as the aqueous suspended CNCs. Solution processed freeze-dried CNCs maintained consistently higher values than the RDFD CNCs, indicating that through redispersion of freeze-dried CNCs, the CNCs were most likely distributed and dispersed more homogeneously allowing for increased load transfer. There was a leveling out of the values of n' at the highest CNC loading of 67 wt.% CNC w.r.t. PVA again indicating some sort of common CNC network structure forming, independent of nanocomposite suspension processing.

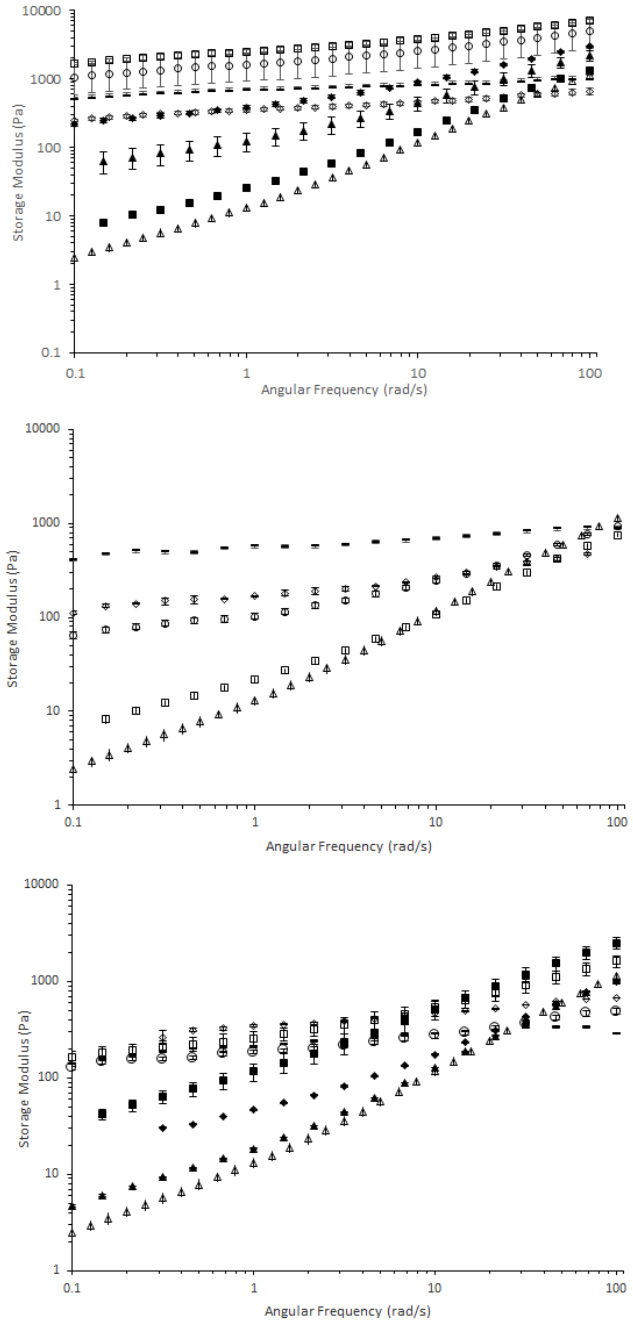

Figure 5.16: *G′* comparison for all solution processed CNC/PVA samples. Top: Aqueous suspended CNC/PVA systems. Middle: Solution processed Freeze-dried CNC/PVA systems. Bottom: RDFD solution processed CNC/PVA systems. Neat PVA(△), 1 wt.% CNC w.r.t. PVA (▲), 5 wt.% CNC w.r.t. PVA (■), 10 wt.% CNC w.r.t. PVA (◆), 20 wt.% CNC w.r.t. PVA (□), 33 wt.% CNC w.r.t PVA (○), 50 wt.% CNC w.r.t. PVA (◇), 67 wt.% CNC w.r.t. PVA (-).Error bars represent the standard deviation of the average value.

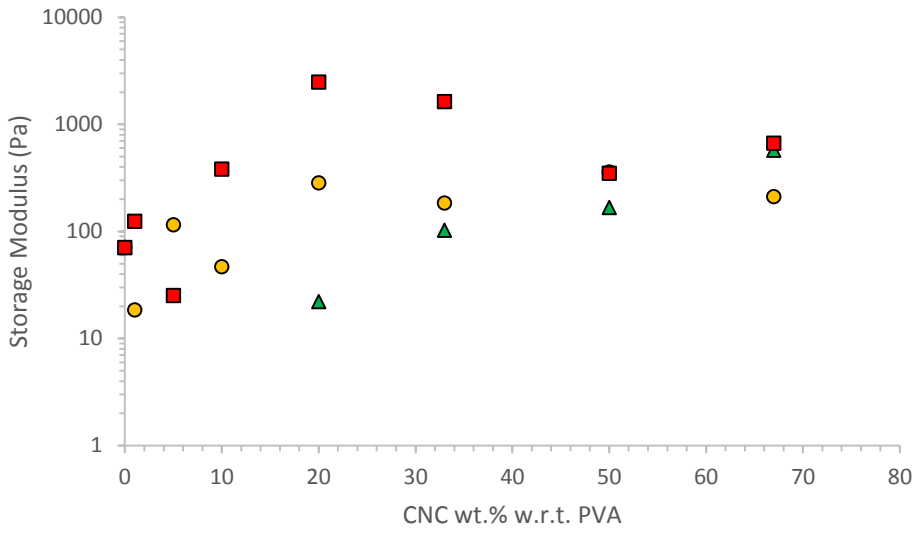

Figure 5.17: *G'* for solution processed CNC/PVA systems at 1 s^{-1}. Aqueous suspended CNC/PVA systems (■), solution processed freeze-dried CNC/PVA systems (▲), RDFD CNC/PVA systems (●).

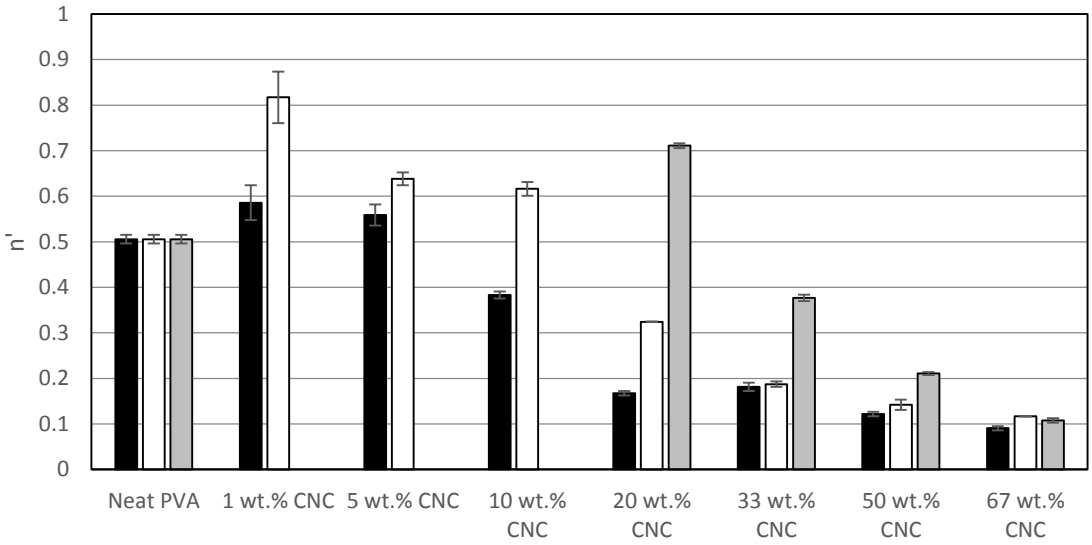

Figure 5.18: *n'* values fitted to *G'* data for each solution processed CNC/PVA system. Aqueous suspended CNC/PVA systems (black), solution processed freeze-dried CNC/PVA systems (grey), RDFD CNC/PVA systems (white). Error bars represent the standard deviation of the average value.

Another feature of the dynamic data collected was the gel-sol crossover behavior of the CNC/PVA nanocomposites. As previously discussed, the percolation threshold was estimated to be 0.025 vol.% (24 wt.% w.r.t. PVA) CNCs. The complete gel-sol transition occured for the aqueous suspended CNC systems between 10 wt.% and 20 wt.%, but differing behavior was seen for the solution processed freeze-dried CNC systems. For these systems, the crossover point occurred at 20 wt.% CNC for the RDFD systems and 33 wt.% CNC for the solution processed systems. The crossover behavior increased with increasing aging time from 1 day to 5 days in a similar manner to the 10 wt.% aqueous suspended system. The gelation behavior for the RDFD and solution processed freeze-dried CNC data can be found in Figure 5.19. In Figure 5.19, only CNC/PVA compositions experiencing weak gelation are shown. Those loadings below and above the CNC/PVA loadings presented behaved as either a solution or a gel, respectively. From these data, it was seen that the gel-sol transition occurred at higher CNC loadings for solution processed freeze-dried than for RDFD CNC/PVA system, i.e. gelation time increased with increasing aggregate size, allowing for some understanding of the morphological behavior. In the aqueous suspended CNC systems, the CNC dispersion was the most homogeneous, allowing for earlier gelation and network formation as the CNCs were better able to interact with one another. The RDFD systems also showed relatively good dispersion allowing for increased rigidity to be imparted on the system and gel behavior at lower CNC loadings compared to solution processed freeze-dried CNCs. The solution processed freeze-dried CNC systems had increased aggregation, decreasing the interaction of the individual CNC aggregates due to the increased CNC content needed to form a gel network.

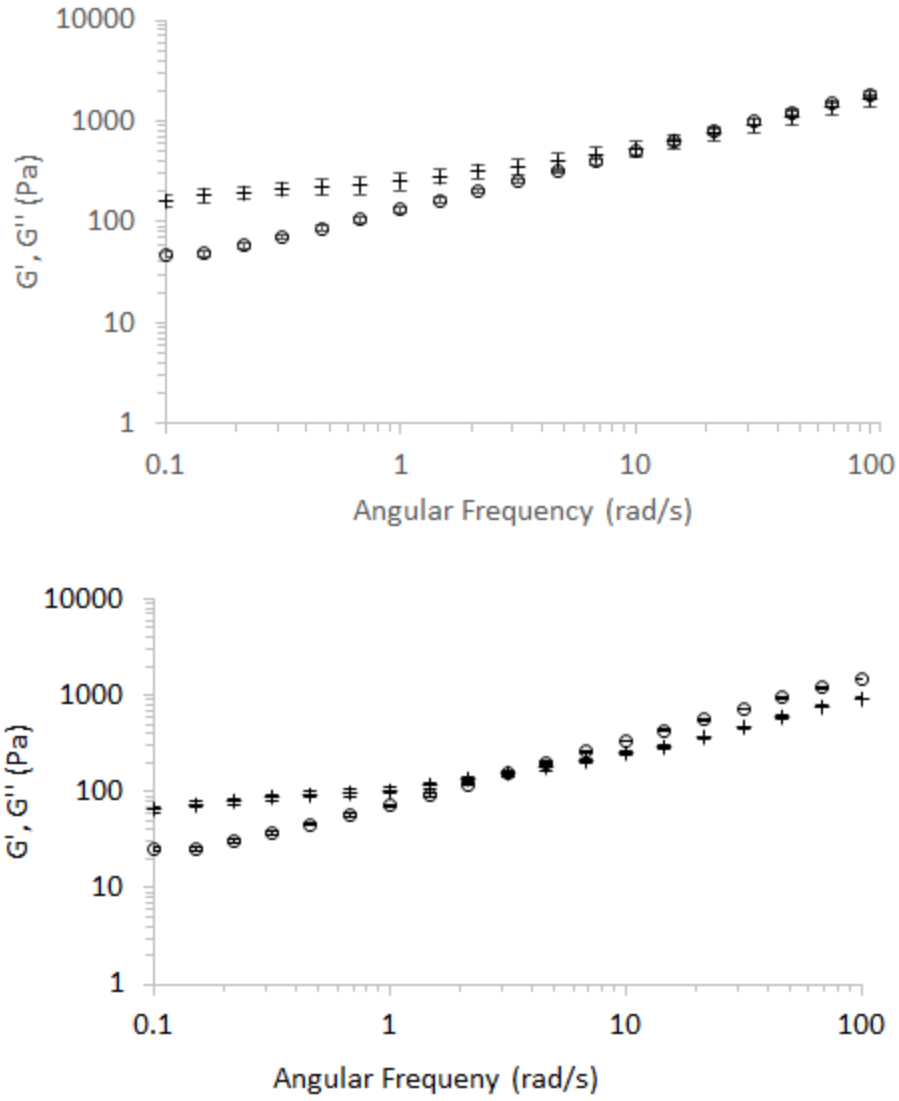

Figure 5.19: G' (+) and G'' (○) crossover behavior showing gelation of freeze-dried CNC systems formulated through solution processing techniques. RDFD 20 wt.% CNC (top) and solution processed freeze-dried 33 wt.% CNC (bottom). Error bars represent the standard deviation of the average value.

Finally, the network structure was studied using the same method as the aqueous suspended CNCs systems in whch the yield stress was calculated using a Casson type plot. Figure 5.20 shows the yield stress comparison of all the solution processed systems. While the yield stress tended to increase with increasing CNC content, the freeze-dried

CNC systems maintain a consistantly lower yield stress than the aqueous suspended CNC systems. This lower yield stress in the freeze-dried CNC systems could be attributed to the decreased rigidity imparted by the CNCs on the systems due to increased aggregation. The trend in yield stress seen in the freeze-dried systems could be used to gain increased understanding of component interactions. While the aqueous suspended CNC/PVA system showed a PVA predominant and CNC predominant region due to increased dispersion and interactions, the RDFD CNC/PVA system showed a plateau of yield stress around the percolation threshold. This plateau indicated that the CNC network formed was the predominant reinforcing mechanism in the suspension due to the independence of PVA loading, but as slight aggregation of the RDFD CNCs occured, the network formed was weaker than the aqeuous suspended CNC/PVA suspension network. In other words, the system behaved independent of PVA contribution near percolation, most likely due to the slightly increased aggregation in the RDFD system. The RDFD CNC/PVA suspension did not reach the CNC predominant yield stress at 67 wt.% CNC most likely due to decreased interaction between the CNCs. The yield stress of solution processed freeze-dried CNC systems increased with increased CNC loading. This increase in yield stress indicated that while the CNCs were acting as reinforcment to the suspension, there were both polymer and CNC contributions affecting the yield stress values, most likely due to the large CNC aggregates giving more PVA rich or CNC rich regions allowing for increased PVA contribution but decreasing the ability of the CNCs to form a network.

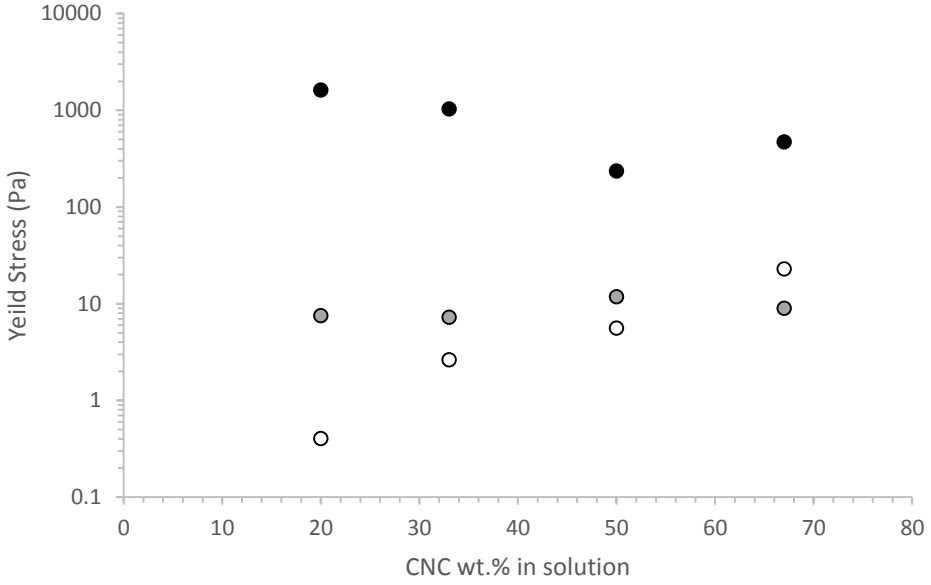

Figure 5.20. Yield stress behavior for all solution processed systems. Aqueous suspended CNCs (black), RDFD CNCs (grey), solution processed freeze-dried CNCs (open).

Through the incorporation of freeze-dried CNCs via direct addition and redispersion solution processing, aqueous suspended CNCs and freeze-dried CNCs were able to be compared and it was seen that aggregation increased with the incorporation of freeze-dried CNCs. This aggregation behavior was confirmed through increased aging, decreased complex viscosity, decreased gelation behavior, and decreased yield stress in both the RDFD and solution processed freeze-dried CNC systems. Redispersing the freeze-dried CNCs allowed for increased dispersion of the CNCs compared to directly adding CNCs to PVA and then solution processing. In the following section, shear processing of freeze-dried CNCs will be discussed.

5.4.2 Shear Processing

The effect of shear processing on the dispersion of the freeze-dried CNCs in PVA was studied. Shear mixing was also done to better understand the scalability of the presented research as a goal of this project was to determine a scalable method to produce CNC/PVA nanocomposite systems. First, neat 146K was mixed in the batch mixer under the same mixing conditions as the CNC/PVA nanocomposites at both 40 and 91 RPM, and rheological testing was conducted on the neat PVA to determine the effect of mixing on neat PVA. Data for 91 RPM is not available as the PVA phase separated during mixing making it unusable for further characterization. A mixing speed of 40 RPM (shear rate of 44 rad/s) was chosen as it was located in the center of the rheological data set studied. A mixing speed of 91 RPM (shear rate of 100 rad/s) was chosen as it was thought that increased shear might have more success in breaking up the aggregates. A comparison of the rheological data collected after solution processing followed by shear mixing vs. solution processing of 146K neat PVA at 15 wt.% is shown in Figure 5.21.

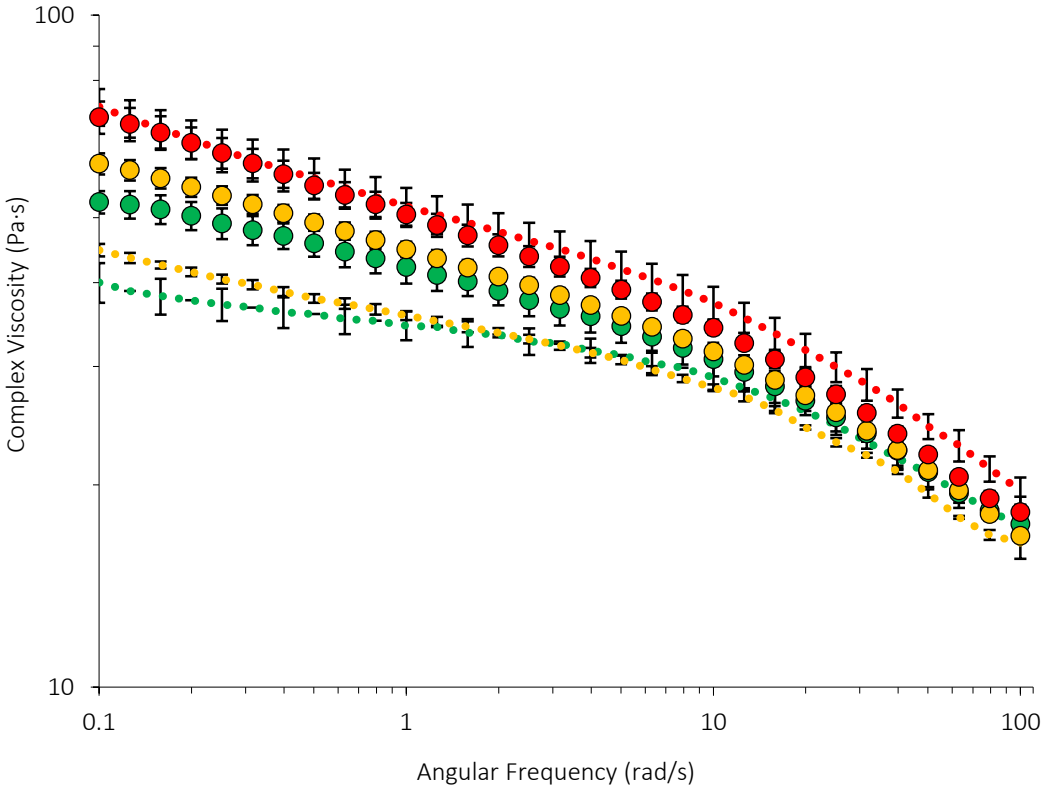

Figure 5.21: 146K neat PVA at 15 wt.% after solution processing (····) and solution processing followed by shear mixing (○) for aging points of 1 day (green), 3 day (yellow), and 5 day (red).

From Figure 5.21, it was seen that while the viscosity was very similar after 5 days of aging for shear processed and solution processed 146K neat PVA, the aging varied for 1 day and 3 days data points. This increase in aging was due to increased PVA network formation as the shear mixing increased the PVA-PVA interaction. During the processing of shear mixing, some phase separation occurred while the polymer chains were compacted together, leading to increased complex viscosity behavior at earlier time points. The yield stress calculated for the solution processed and shear processed neat PVA was 10 Pa.

After the neat PVA solution processing behavior was characterized, freeze-dried CNCs were added to solution processed 146K neat PVA in the mixer in concentrations of 20 wt.%, 33 wt.%, 50 wt.%, and 67 wt.% CNC w.r.t. PVA at mixing rates of 40 RPM and 91 RPM. The rheological behavior of these samples was then tested at 1 day, 3 days, and 5 days of aging. The aging data are shown in Figure 5.22. Decreased aging was seen in the 91 RPM samples compared to the 40 RPM samples and the relative complex viscosities were very similar. The modified power law was again fit to the 40 RPM and 91 RPM data as shown in Figure 5.23 to gain further understanding on the aging of the shear mixed samples. From these data, it can be quantitatively seen that increasing CNC content decreased aging behavior similar to other CNC nanocomposite suspensions studied here. It was also seen that in general, there was increased aging in the 40 RPM samples compared to the 91 RPM samples. This decrease in aging at 91 RPM can be attributed to the accelerated phase separation seen at high shear rates. When the PVA was mixed at a high shear rate, this aging was accelerated (as seen in the 40 RPM samples). As the 91 RPM 146K neat PVA was not able to be tested rheologically, it can be assumed that the 91 RPM shear mixed PVA experienced more accelerated aging due to the phase separation and compaction of the polymer chains at higher RPM.

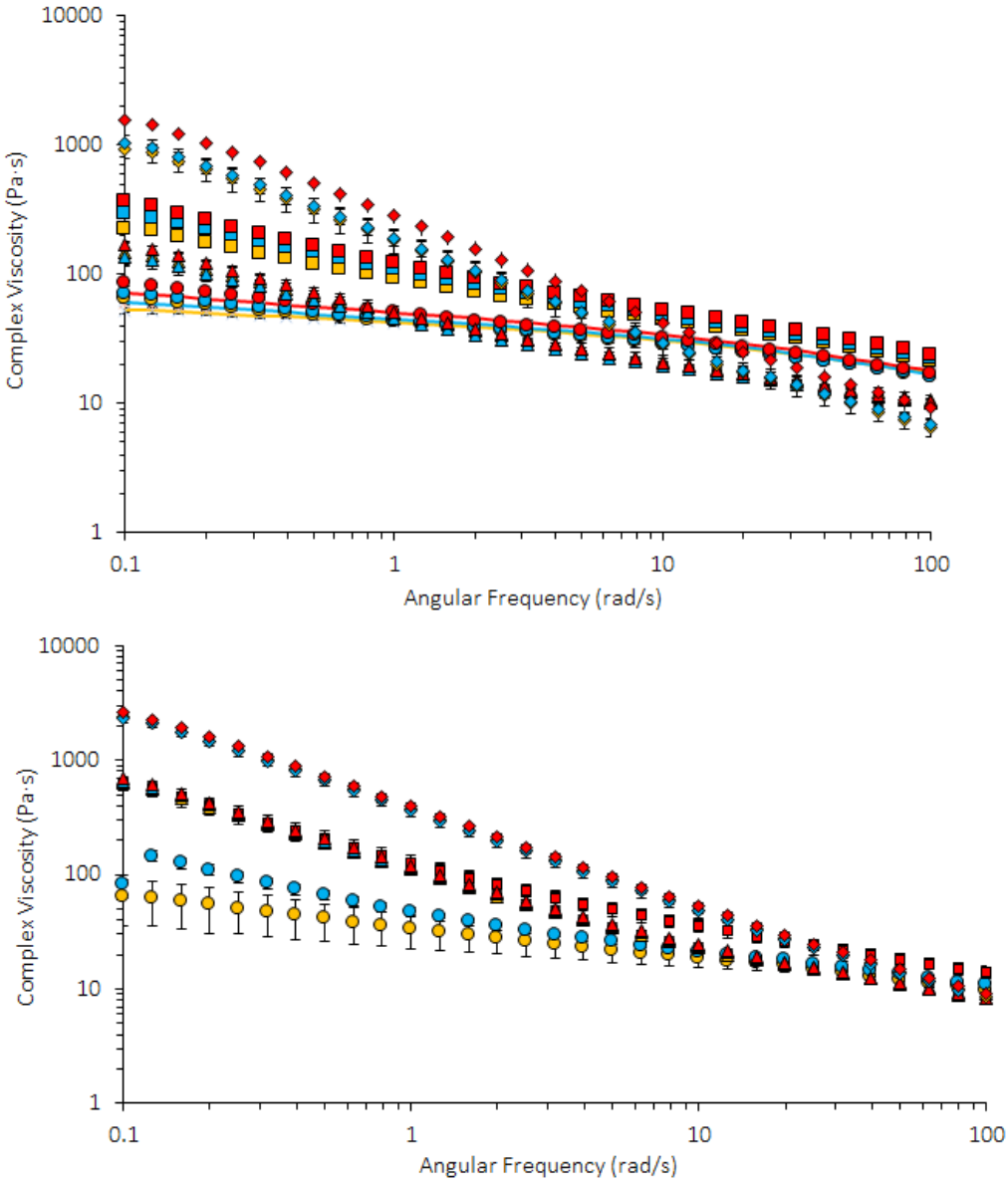

Figure 5.22: Freeze-dried shear processed CNC/PVA systems at 40 RPM (top) and 91 RPM (bottom). Samples shown are Neat PVA (lines), 20 wt.% CNC w.r.t. PVA (●), 33 wt.% CNC w.r.t. PVA (■), 50 wt.% CNC w.r.t PVA (▲), and 67 wt.% CNC w.r.t. PVA (◆) at aging times of 1 day (yellow), 3 day (blue), and 5 day (red). Error bars represent the standard deviation of the average value.

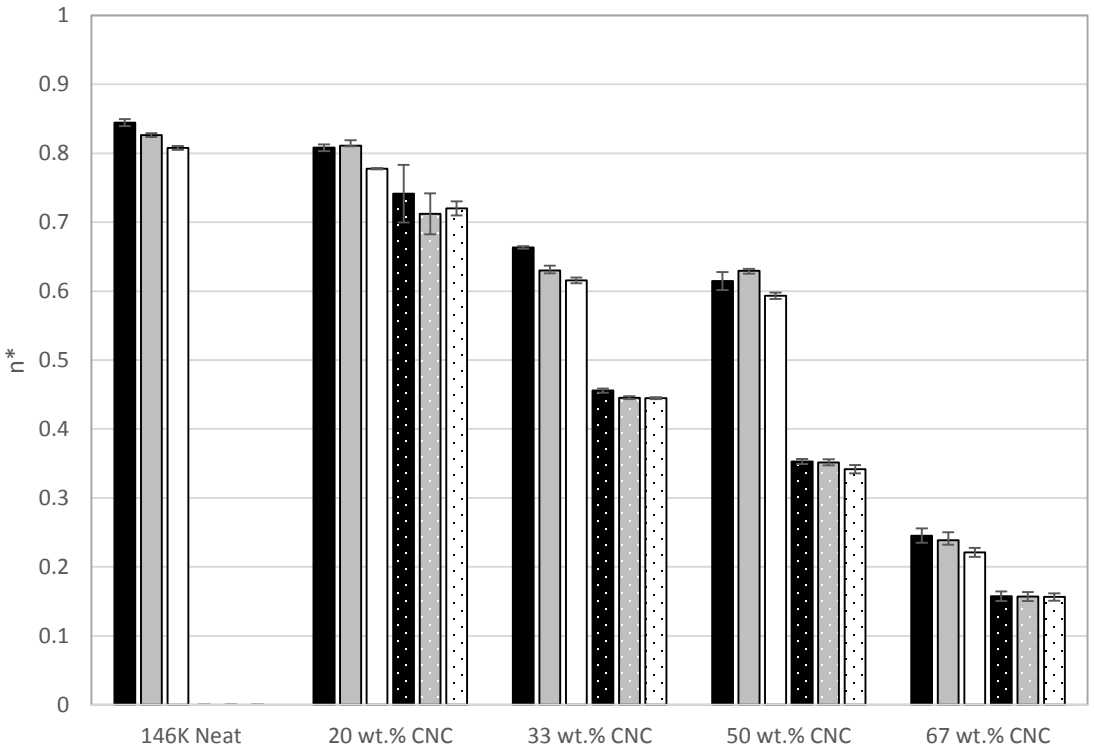

Figure 5.23: Modified power exponent values from 40 RPM (solid) and 91 RPM (dotted) neat and freeze-dried CNC/PVA systems at aging point of 1 day (black), 3 day (grey), and 5 day (white).

Table 5.2: Total change in *n** with time for all shear processed CNC systems as well as complex viscosity at 5 days of aging at 1 rad/s.

	40 RPM		91 RPM	
	Δn*	η* (Pa·s)	Δn*	η* (Pa·s)
Neat PVA	0.039 ± 0.003	50 ± 2	N/A	N/A
20 wt.% CNC	0.031 ± 0.001	50 ± 2	0.021 ± 0.000	47 ± 4
33 wt.% CNC	0.048 ± 0.004	121 ± 7	0.011 ± 0.001	126 ± 20
50 wt.% CNC	0.021 ± 0.004	52 ± 2	0.011 ± 0.006	119 ± 6
67 wt.% CNC	0.31 ± 0.006	283 ± 36	0.001 ± 0.005	394 ± 22

The trend in complex viscosity also gave insight into the morphology of the shear processed freeze-dried CNC systems. Table 5.2 shows the change in *n** from 1 day to 5 days of aging as well as the trend in complex viscosity at 5 days of aging and 1 s^{-1}. As

shown, there was less aging seen in the 91 RPM samples due to shear induced phase separation of the PVA. The complex viscosity of the 91 RPM system increased with increasing CNC loading, but the 40 RPM shear processed complex viscosity showed a different trend. In the 40 RPM sample, the complex viscosity increased from 20 wt.% CNC w.r.t. PVA to 33 w.t% CNC w.r.t. PVA, dropped at 50 wt.% CNC w.r.t. PVA, and increased again at 67 wt.% CNC w.r.t. PVA. The decrease in complex viscosity at 50 wt.% CNC w.r.t. PVA for the 40 RPM shear processed system could be attributed to the transition from PVA predominant to CNC predominant solids content and more CNC dominated network, leading to the increase in complex viscosity at 67 wt.% CNC. This network structure will be discussed further in this section in regards to the G' data.

The G' behavior was studied for the freeze-dried systems and is shown in Figure 5.24. The relative G' magnitude at 1 s^{-1} is shown in Figure 5.25. As seen in Figure 5.24, the G' data tended to converge at high shear rates around the neat PVA G' value, most likely due to the polymer chain motion controlling the shear flow as the chains have much longer length scales compared to the CNCs. It was also noticed from Figure 5.25 that the G' values tended to increase with increased CNC loading as the CNCs imparted more rigidity into the system. The G' values tended to be similar for each RPM with a slight increase in G' with increased shear rate, most likely due to the phase separation of the PVA and compaction of the polymer chain adding rigidity to the system.

The G' values were modeled using the modified power law equation 5.3 and these values are shown in Figure 5.26. From this modeling, it was seen that the shear processed 40 RPM freeze-dried CNC systems had larger n' values than the shear processed 91 RPM freeze-dried CNC systems, indicating the shear processed 40 RPM

CNC/PVA systems had increased frequency dependence compared to the shear processed 91 RPM systems and therefore less rigidity. This increase in frequency dependence indicated that the systems were not as strongly connected compared to the shear processed 91 RPM systems. This increase in rigidity from 40 RPM to 91 RPM shear processed CNC/PVA system was likely also caused by the increased rigidity imparted by the phase separated PVA.

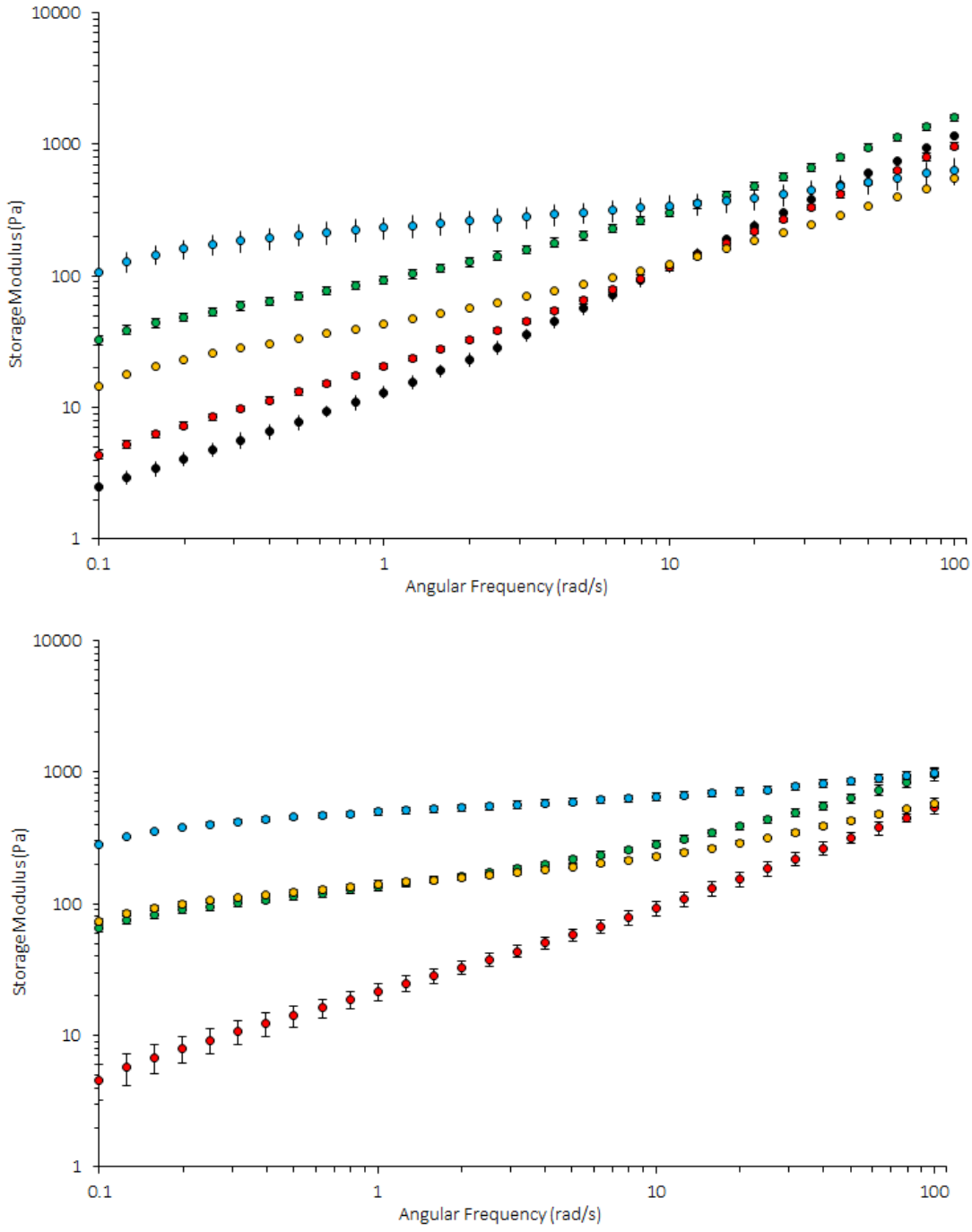

Figure 5.24: *G′* behavior of the shear processed neat PVA and freeze-dried CNC/PVA systems at 40 RPM (top) and 91 RPM (bottom) at 5 days of aging. Neat PVA (●), 20 wt.% CNC w.r.t. PVA (●), 33 wt.% CNC w.r.t. PVA (●), 50 wt.% CNC w.r.t. PVA (●), and 67 wt.% CNC w.r.t. PVA (●). Error bars represent the standard deviation of the average value.

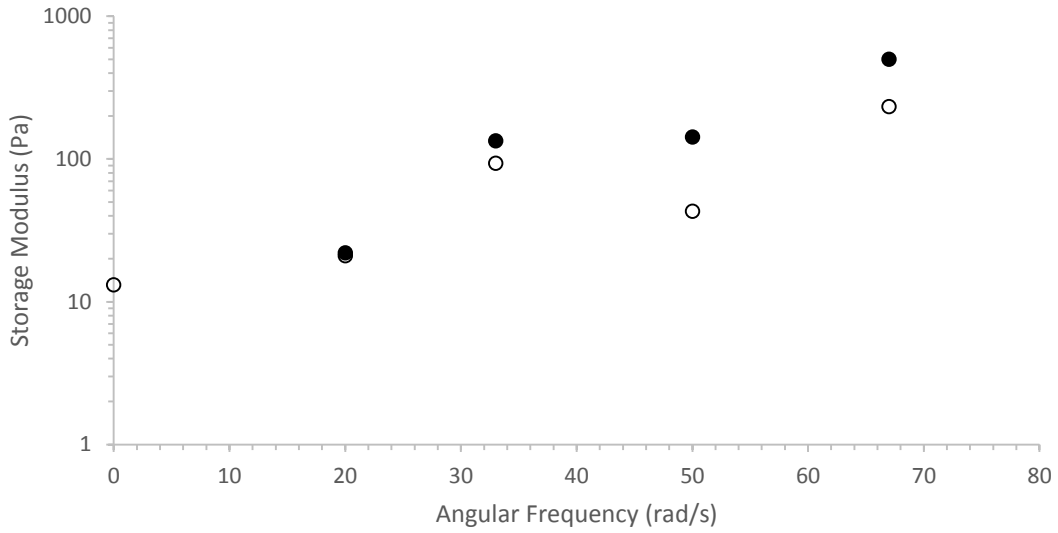

Figure 5.25: G' at 1 s^{-1} for both shear processed freeze-dried CNC/PVA systems. 40 RPM (open markers), 91 RPM (filled markers)

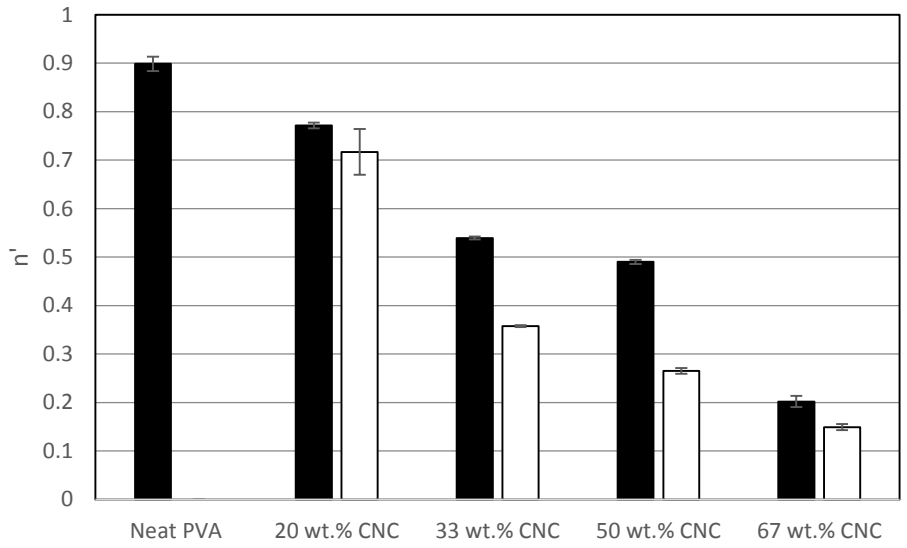

Figure 5.26: n' for shear processed 40 RPM (black) and 91 RPM (white) neat PVA and CNC/PVA systems at 5 days of aging. Error bars represent the standard deviation of the average value.

Figure 5.27 shows the gelation crossover behavior for 40 RPM and 91 RPM shear processed freeze-dried systems. In comparison to the solution processed CNC/PVA systems, there were a larger range of compositions near the gelation point for the shear processed systems, most likely due to increased aggregation of CNC causing weaker gel networks to be formed as the CNC aggregates were not able to form a network structure as easily. While the gel point occurred between 10 and 20 wt.% for the aqueous suspended systems, 20 and 33 wt.% for the RDFD systems, and 33 wt.% to 50 wt.% for the solution processed freeze-dried systems, weak gel systems near the gel point occurred over a range from 20 wt.% to 67 wt.% CNC for the shear processed systems. In other words, for shear processed freeze-dried CNC systems, solution behavior was seen over the entire frequency range for 20 wt.% CNC and gel behavior was seen over the entire frequency range for 67 wt.% CNCs, indicating that a weak gel structure was present for the intermediate loadings. This weaker gel structure can be attributed to increased aggregation of both PVA and CNCs leading to larger phase separation between each component and hindering the CNCs ability to form a stronger gel structure due to decreased CNC-CNC aggregate interaction.

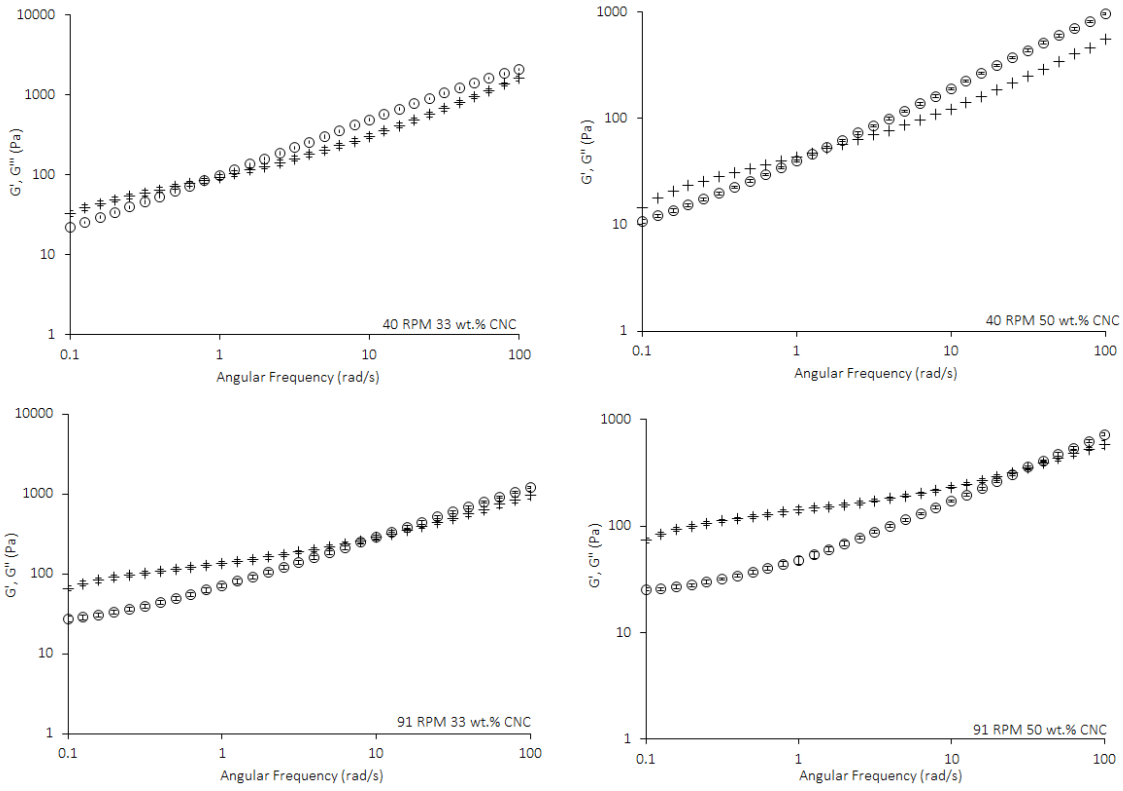

Figure 5.27: G' (+) and G'' (○) crossover behavior of shear processed freeze-dried CNC/PVA systems at 40 RPM (top) and 91 RPM (bottom).

To further understand this shear processed network behavior, the yield stress was calculated using the Casson type model from equations 5.5 and 5.6 in Figure 5.28. As seen, the yield stress increased with increasing CNC content and was slightly larger for the 91 RPM samples due to increased phase separation. The PVA appears to act as a stronger reinforcing agent in the 91 RPM shear processed systems, compensating for the increase in CNC aggregation. Processing methods will be compared in the following section based on the rheological behavior of each system.

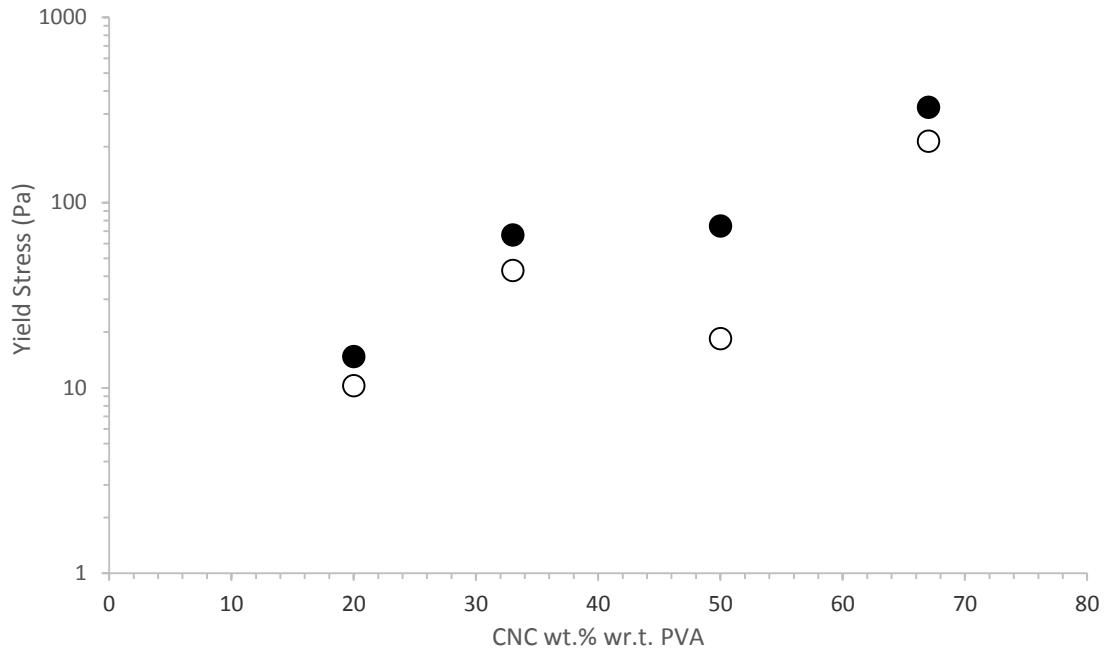

Figure 5.28: Yield stress behavior of freeze-dried CNC/PVA systems at 40 RPM (open) and 91 RPM (closed).

5.4.3 Solution Processing and Shear Processing Comparison

Finally, all five CNC/PVA systems were compared to gain increased understanding of the structural and morphological differences between solution processing, shear processing, aqueous suspended CNCs, and freeze-dried CNCs all at 146K molecular weight PVA. First, the aging and complex viscosity of each system was considered, shown in Figure 5.29 at 1 s^{-1}. The complex viscosity data is all shown at 5 days of aging. From these data, it was seen that solution processed neat PVA experienced significantly more aging compared to shear processed 40 RPM neat PVA as the shear processing expedited aging and phase separation. Aging decreased with CNC loading for

all the nanocomposite systems studied regardless of processing method, but the extent of aging, especially at CNC loading of 20 wt.% CNC w.r.t. PVA and above, varied greatly with processing strategy. The shear processed 40 RPM samples contained the largest amount of aging at high CNC loadings (33 wt.% CNC w.r.t. PVA and above) while the shear processed 91 RPM samples had the lowest aging values at these high CNC concentrations. This large difference in aging, especially when compared to the solution processed CNC systems, was attributed to the effect of shear processing specifically on the aggregation of PVA chains. It was seen in the neat PVA systems that shear processing accelerated aging due to the increased phase separation and aggregation caused during high shear. The 91 RPM samples experienced the largest amount of shear and showed the largest amount of aggregation of both PVA and CNCs, confirmed through rheology and optical microscopy, and therefore would experience lower amounts of aging as this aging of PVA was accelerated through processing. The 40 RPM, however, had similar morphology to the solution processed freeze-dried samples and while the aging behavior was similar at lower loadings of 20 wt.% and 33 wt.% CNC w.r.t. PVA, the aging was increased at higher loadings of 50 wt.% and 67 wt.% CNC w.r.t. PVA. It was known that the PVA had increased phase separation and therefore should show decreased aging with shear processing, therefore it was likely that this increase in aging compared to the other solution processed and shear mixed systems can be attributed to an accelerated aging rate of CNC aggregates and the resulting PVA aging. A schematic further illustrating this aging can be found in Figure 5.30. In this image, the effect of processing on CNC and PVA morphology and the resulting aging is shown. Blue rods represent the CNCs while red lines represent the PVA. As shown, in the aqueous suspended and RDFD systems,

well distributed CNCs are able to restrict the PVA from phase separating. The PVA was also well suspended in these systems due to solution processing. In the solution processed freeze-dried CNC systems, the PVA was well suspended but CNC aggregation allowed for increased aging to occur due to the less restrictive nature of the CNCs in their aggregated state. In the shear processed systems, aging was accelerated due to phase separation and compaction of the PVA chains during shear processing, decreasing the amount of aging behavior seen in the samples as phase separation primarily occurred during the mixing processes before rheological characterization was conducted.

In terms of complex viscosity, higher values were seen universally in the solution processed aqueous suspended CNC systems. This was attributed to the increased dispersion and distribution of the CNCs allowing for increased rigidity to be imparted on the system. While the solution processed RDFD complex viscosity values were generally higher than the solution processed freeze-dried samples and shear processed samples, they were lower than the aqueous suspended CNC samples due to small aggregates present but not visible with the optical microscope. The solution processed freeze-dried samples and shear processed 40 RPM and 91 RPM freeze-dried samples all had similar complex viscosities due to the aggregation of the CNCs.

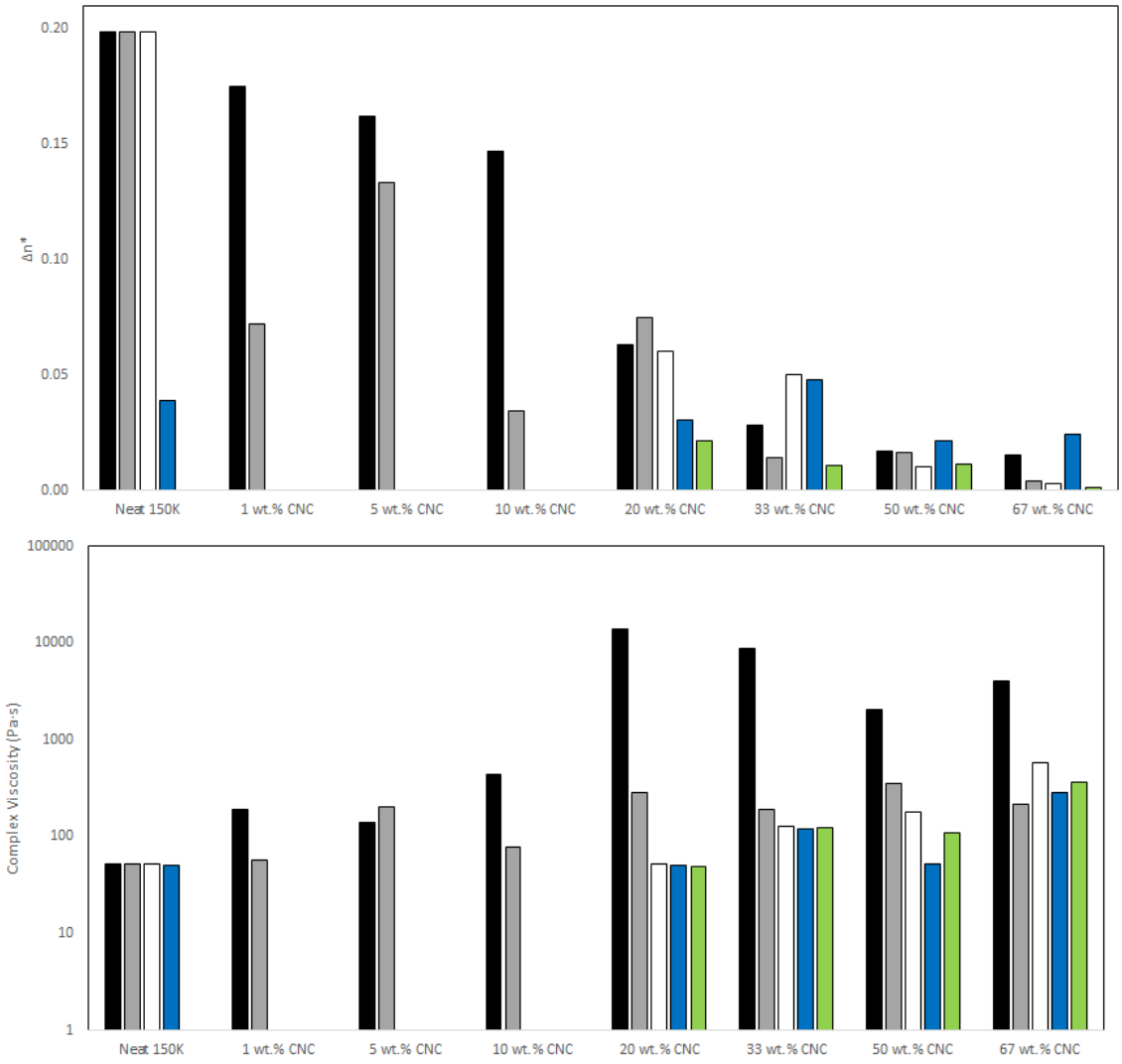

Figure 5.29: CNC loading w.r.t. PVA and the systems representative *n** values from 1 to 5 days of aging for all solution and shear processed CNC/PVA systems (top) and complex viscosity values for all solution and shear processed systems at 5 days of aging at 1 s^{-1}. Solution processed aqueous suspended CNC/PVA nanocomposites (black), solution processed RDFD CNC/PVA nanocomposites (grey), solution processed freeze-dried CNC/PVA nanocomposites (white), shear processed 40 RPM freeze-dried CNC nanocomposites (blue), shear processed 91 RPM freeze-dried CNC nanocomposites (green).

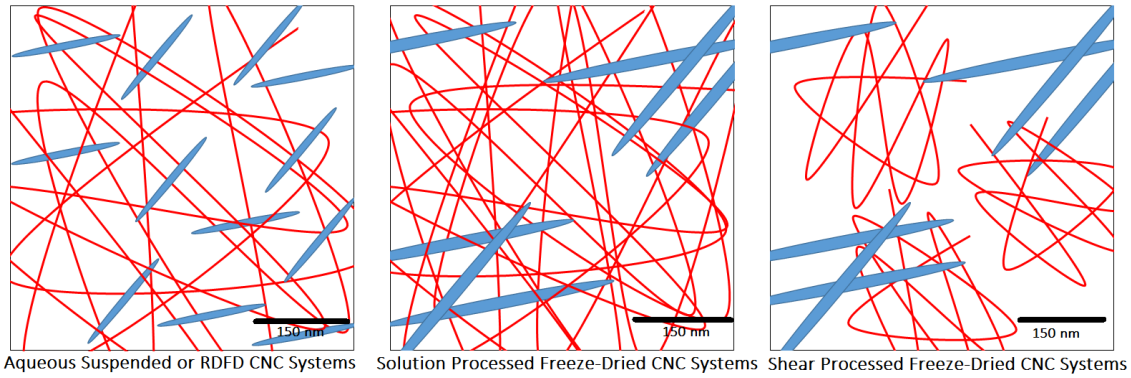

Figure 5.30: Aging schematic for aqueous suspended and freeze-dried CNC systems where CNCs are shown by blue rods and red lines represent PVA chains.

The G' behavior for each solution processed and shear processed system was compared based on relative value at 1 s^{-1} and 5 days of aging, shown in Figure 5.31. While the solution processed aqueous suspended CNC/PVA systems had noticeably larger G' values at lower CNC loadings below 33 wt.% w.r.t. PVA, the G' values of each CNC/PVA system regardless of processing technique tended to trend towards a common value at 67 wt.% CNC w.r.t. PVA. The samples with CNC loading of 50 wt.% and 67 wt.% CNC w.r.t. PVA were of particular interest as the CNCs should be the predominant contributors to suspension behavior, while the lower loading samples of 20 wt.% and 33 wt.% CNC w.r.t. PVA should show behavior indicative of the state of the PVA in the suspension and the dispersion of the CNCs.

Figure 5.31 further elaborated on the G' behavior using n'. As samples trended to go to the same n' value with increasing CNC content, the 40 RPM samples generally maintained higher n'. This increased n' value indicated decreased rigidity and most likely weaker component interactions as previously discussed. Aqueous suspended CNC and RDFD CNC systems tended to have the lowest n' values due their increased dispersion

and distribution leading to increased stress transfer and rigidity. The n' values for freeze-dried CNC systems at 20 wt.%, 33 wt.% and 50 wt.% CNC w.r.t. PVA were generally higher due to the increased aggregation seen from the optical images.

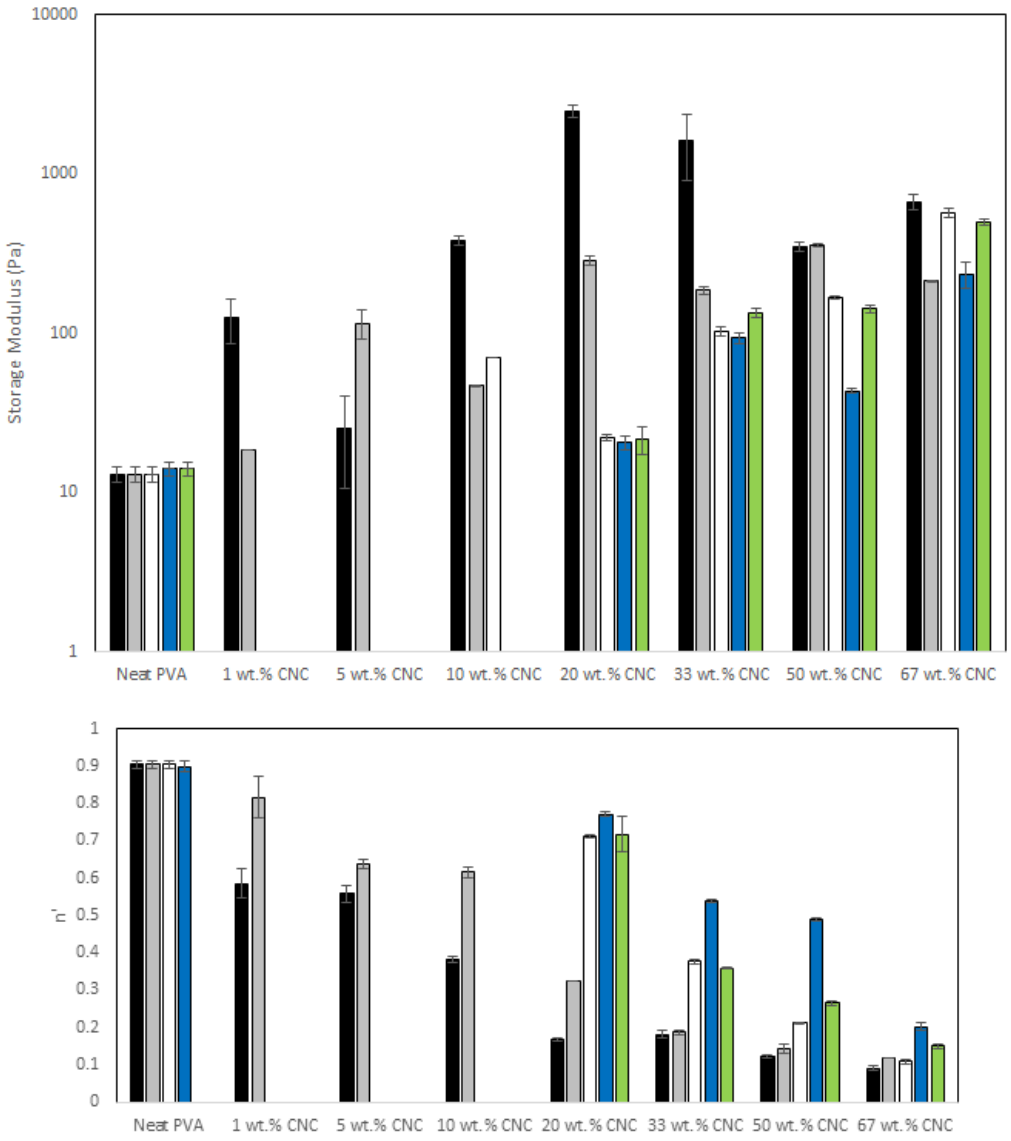

Figure 5.31: G' at 1 s^{-1} for all solution and shear processed CNC/PVA systems (top) and n' values for solution processed and shear processed CNC/PVA systems (bottom) at 5 days of aging. Solution processed aqueous suspended CNCs (black), solution processed RDFD CNCs (grey), solution processed freeze-dried CNCs (white), shear processed 40 RPM freeze-dried CNCs (blue), and shear processed 91 RPM freeze-dried CNCs (green). Error bars represent the standard deviation of the average value.

Finally, the network structure of the solution processed and freeze-dried CNC systems was compared through the yield stress shown in Figure 5.32. From this yield stress analysis, it can be seen that the solution processed aqueous suspended CNC/PVA system and the shear processed 40 RPM and 91 RPM freeze-dried CNC systems had the most similar yield stress behavior while the solution processed freeze-dried and RDFD systems had lower yield stress. This increase in yield stress for freeze-dried CNCs allowed for increased understanding of the participation of the CNCs and PVA in the suspension through shear mixing. While it was understood that shear mixing increased compaction of the PVA chains, this compaction may help increase the network structure of the overall system even if rigidity was not as large as seen in the G' analysis. Through the yield stress, it would appear that shear processing increased the network structure most likely through increasing the polymer molecular entanglements with the CNCs. Aggregation in the freeze-dried solution processed and shear processed samples allowed for PVA and CNC participation throughout all the loadings studied, as shown by the increasing yield stress with CNC content. In comparison, aqueous suspended CNC/PVA and RDFD CNC/PVA systems showed polymer dependent and independent regions around and above the percolation threshold.

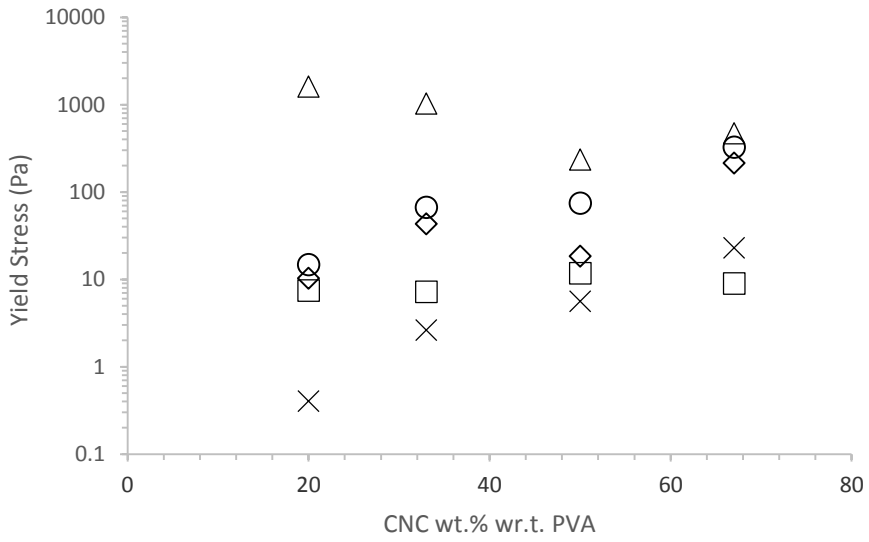

Figure 5.32: Yield stress behavior for all solution and shear processed CNC/PVA systems. Solution processed aqueous suspended CNCs (△), solution processed freeze-dried CNCs (X), solution processed RDFD CNCs (□), shear processed 40 RPM freeze-dried CNCs (◇), and shear processed 91 RPM freeze-dried CNCs (○).

Figure 5.33 shows a schematic of the postulated network formed determined through the yield stress. CNCs are shown in blue while the PVA radius of gyration is shown as yellow circles. Due to the rheological and mechanical properties achieved, the aspect ratio of the RDFD CNCs was assumed to be similar to the aspect ratio of the aqueous suspended CNCs. As seen from Figure 5.33, the effect of aggregation on the CNCs, even small amounts as seen in the RDFD samples, play a role in the network formation of the suspensions. While aqueous suspended CNC/PVA systems form a more compact network structure due to their dispersion, RDFD systems at the same volume fraction form a weaker network structure as the size of the CNC contribution was increased due to aggregation. The shear processed and solution processed freeze-dried CNC/PVA suspensions showed the largest amount of aggregation, on the micrometer scale, decreasing the benefits provided by nanofillers such as increased surface area for

hydrogen bonding. This increased aggregation also gave PVA dominant and CNC dominant regions, increasing component phase separation.

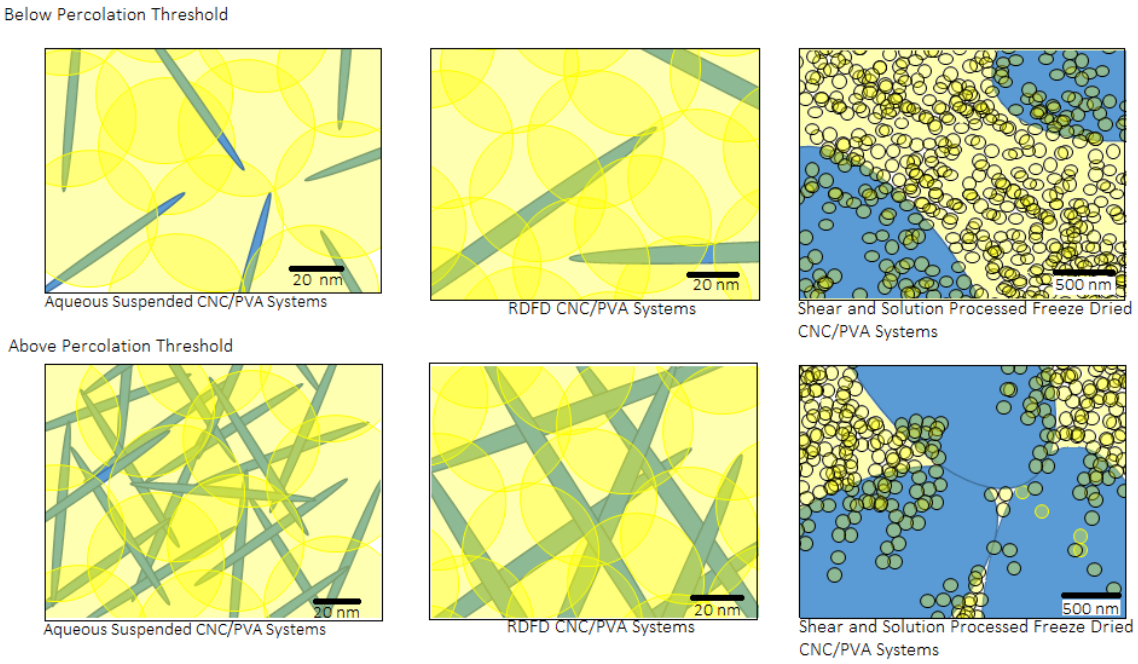

Figure 5.33: Schematic for the behavior of CNCs and PVA below and above the percolation threshold for all the CNC processed systems.

5.5 Conclusion

In conclusion, the steady shear viscosity of neat PVA at various solids loadings was studied to determine the most feasible molecular weight and concentration for shear processing. From this analysis, 146K PVA at 15 wt.% total solids was determined to have the best viscosity for processing. Next, aqueous suspended CNC/PVA systems were studied at each molecular weight to see the effect of CNC loading and molecular weight. It was seen that 146K had the largest amount of viscoelastic behavior due to the increased

molecular weight entanglements. It was also seen that the addition of CNCs increases viscoelastic behavior as the CNCs impart more rigidity on the system. Five different CNC/PVA systems were studied and the effects of adding solution processed or freeze-dried CNCs or processing via solution or shear were addressed. From this analysis, it was seen that CNC aggregation was increased as CNCs have an affinity for one another when highly concentrated in the dry state. Shear processing was seen to produce aggregates of CNC as well, but increase the overall network structure compared to solution processing of freeze-dried CNCs, even RDFD CNCs, as shown by the yield stress. From this rheological study, it was determined that solution processed aqueous suspended CNCs will yield the highest viscoelastic properties due to their increased dispersion and distribution. From a process implementation standpoint, taking scalability into account, shear processed 91 RPM samples maintained the highest viscoelastic properties due to increased rigidity incorporated by both phase separation of PVA leading to increased compaction of the chains and CNC addition. In the following Chapter, the structure of CNC/PVA nanocomposite systems in the dry state will be discussed.

CHAPTER 6

STRUCTURE

Neat PVA and CNC/PVA nanocomposite structure was studied by conducting XRD, FT-IR, and DSC on dried films. From this structural study, the crystallinity, chemical structure, and chain mobility and dynamics were compared. This structural understanding will be compared to the mechanical characterization discussed in Chapter 7.

6.1 Introduction

PVA is a synthetically derived polar polymer containing multiple hydroxyl groups and a monoclinic crystal structure.[177] These hydroxyl groups allow for the polymer to be water soluble and biodegradable. As the number of hydroxyl groups is increased on the PVA main polymer chain, there is an increased ability to form hydrogen bonds on both inter and intra molecular scale.[27] The strong hydrogen bonds formed allow for PVA polymer films to have high tensile strength, good adhesive properties, be resistant to abrasion and alkali solvents, and maintain good gas barrier properties.[36,158] While the hydrogen bonds contribute to good application properties, they also cause the melting point and degradation point of PVA to be very close to one another, making traditional melt processing a challenge.[158]

CNCs are formed from the acid hydrolysis of the cellulose in which the amorphous regions are removed leaving small crystalline rod-like structure, schematically shown in Figure 6.1. CNC are d-anhydro glucose bonded molecules with

1-4 linkages on either side of the molecule. The CNCs used in this research are a combination of the cellulose type I and type II allomorph, produced from plants, trees, tunicates and algae with a monoclinic crystal structure.[58,178,179] The allomorph of the CNCs used in this research is a combination of Iα (triclinic) and Iβ (monoclinic) allomorphs with Iβ as the dominant allomorph and arranged in a "parallel up" configuration, shown in Figure 6.1.[45,179,180] Specifically, the 1-4 linkages on the cellulose main chain, shown in Figure 6.1, have the ability to be structured on either side of the molecule. A parallel up configuration refers to all of the cellulose 1-4 linkages structured in the same direction. Altering the direction of these linkages will change the properties of the CNC.[45,178,181] As both CNCs and PVA contain hydroxyl groups and have a monoclinic crystalline form, intermolecular complexation should occur. CNC/PVA nanocomposite systems can take advantage of intermolecular complexation as the increase in secondary binding forces such as hydrogen bonding and charge transfer should allow for the confinement of the PVA chains, decreasing mobility and giving novel properties to these CNC/PVA nanocomposite systems such as increased mechanical properties.[182]

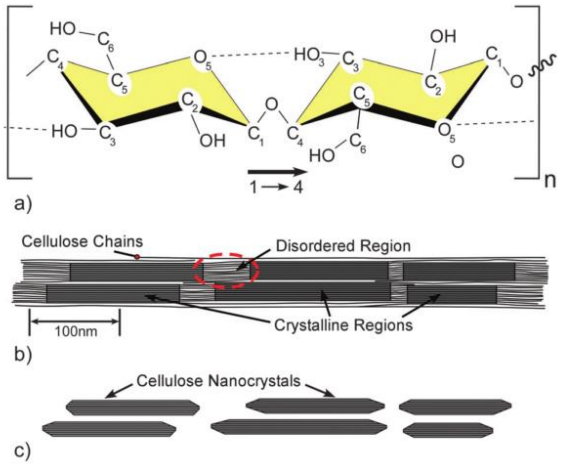

Figure 6.1: a) Molecular structure of cellulose showing the directionality of the 1-4 chain linkage. b) CMF with crystalline and amorphous regions before acid hydrolysis. c) CNCs after the disordered regions are removed from the cellulose microfibril.[45]

The crystal structures of PVA and CNCs have been studied extensively through XRD measurements as the physical and mechanical properties of nanocomposites can be directly related to the crystallinity of the system.[42,158,183–185] PVA has a monoclinic crystal structure and a primary XRD crystal peak around $2\theta = 19.5°$ with a d spacing of 4.5 Å from CuKα.[42,75] Neat PVA tends to have a crystallinity of about 35%.[158] The CNCs are a combination of cellulose type I and type II and a combination of the Iα and Iβ allomorphs with an emphasis on Iβ as previously stated from cellulose type I. There are five crystalline peaks for CNCs with three predominant peaks at $2\theta = 15.5°$, 16.5°, and 22.6° corresponding to the Iα and Iβ peak 100 and $1\bar{1}0$, Iα and Iβ peak 010 and 110, and Iβ and Iα peak at 110 and 200 respectively.[186]

Crystallinity has been studied with respect to CNC/PVA composites. In their neat, aqueous solution form, PVA solutions are almost completely amorphous with crystallites nucleating at the last stages of drying. A level of ambient humidity is necessary during

the drying stages or the PVA will become glassy, stopping crystallization and freezing the crystallites in the glassy state. Initially, plasticization occurs due to ambient humidity present at room temperature and allows for slow, cold crystallization of PVA forming row nucleated crystals at the onset of crystallization. Dendritic crystals then form in the intermediate stages of aqueous PVA crystallization while spherulites form in the final stages of crystallization as the crystals impinge upon one another. In the final stages of PVA crystallization from an aqueous solution, all three crystal morphologies are present: row nucleated, dendritic, and spherulite. The combination of these morphologies can be described as PVA dendrites or hedrites.[187] The degree of crystallinity has been shown to increase with increasing CNC loading for composites produced by hot drawing (CNC loading up to 9 wt.%) and electrospinning processes (CNC loading up to 15 wt.%) as a result of diminishing voids in the polymer matrix and inherent CNC alignment.[69,95] Neat PVA fibers were seen to have a crystallinity of 48%.[177] PVA crystallinity with 1 wt.% single walled carbon nanotube addition in PVA fibers was seen to be 63%.[188]

FT-IR is an additional method for determining the interactions and structure of the CNCs and PVA. FT-IR gives increased understanding of the interactions of the hydroxyl groups, surface interactions, and can be related to the crystallinity of the structure.[46,75,189,190] For example, the shifting of the C-O bond peaks for CNCs and PVA toward one another can indicate increased hydroxyl group interaction due to an increase in the contact of hydrophilic surfaces.[190] The C-C intensity of the C-C stretch in PVA at about 1143 cm^{-1} can also be related to the crystallinity of the overall system.[75]

Finally, DSC was conducted to better understand the confinement and mobility of the CNC on the polymer chains through the study of the T_g. Experiments have been

conducted on CNC/PVA nanocomposites systems in which the T_g was recorded as a function of the second heating scan opposed to the first and found to be in the vicinity of 70-85°C.[42,70,185,191] Increasing the degree of hydrolysis increases the thermal degradation of the polymer. The PVA nanocomposite systems tested during this research degraded after the first heating cycle in the DSC; therefore, the T_g of the first heating cycle will be used to discuss the thermal behavior of the DSC samples.

6.2 XRD

6.2.1 Neat PVA XRD

The percent crystallinity of neat PVA at 31K, 85K, and 146K, neat CNC and CNC/PVA nanocomposite systems at 31K, 85K, and 146K molecular weight and 20 wt.%, 33 wt.%, 50 wt.% and 67 wt.% aqueous suspended CNCs w.r.t. PVA was studied through XRD. 146K RDFD CNC/PVA systems at 20 wt.%, 33 wt.%, 50 wt.% and 67 wt.% were also examined. Each scan was performed from 2θ values of 11° to 45°. The crystallinity (χ) of PVA in each system was calculated using the following equation:[192]

$$\chi = \frac{A_c}{A_c + A_m} \qquad (6.1)$$

where A_c is the area under the crystalline peak of the PVA (101) and A_m is the area under the amorphous peak. The crystallinity was then converted to a percent. To simplify the calculation, specifically for the nanocomposite samples, the 2θ region was restricted to the range of 15° to 30°. The XRD spectra for each neat PVA sample is shown in Figure 6.2 where the red highlighted curve is the PVA crystal peak (101) and the green highlighted curve is the amorphous peak. The error calculated for each sample was about

10%. Table 6.1 displays the percent crystallinity of each of the neat PVA samples. As shown in Table 6.1, the percent crystallinity remained constant with PVA molecular weight when considering experimental error.

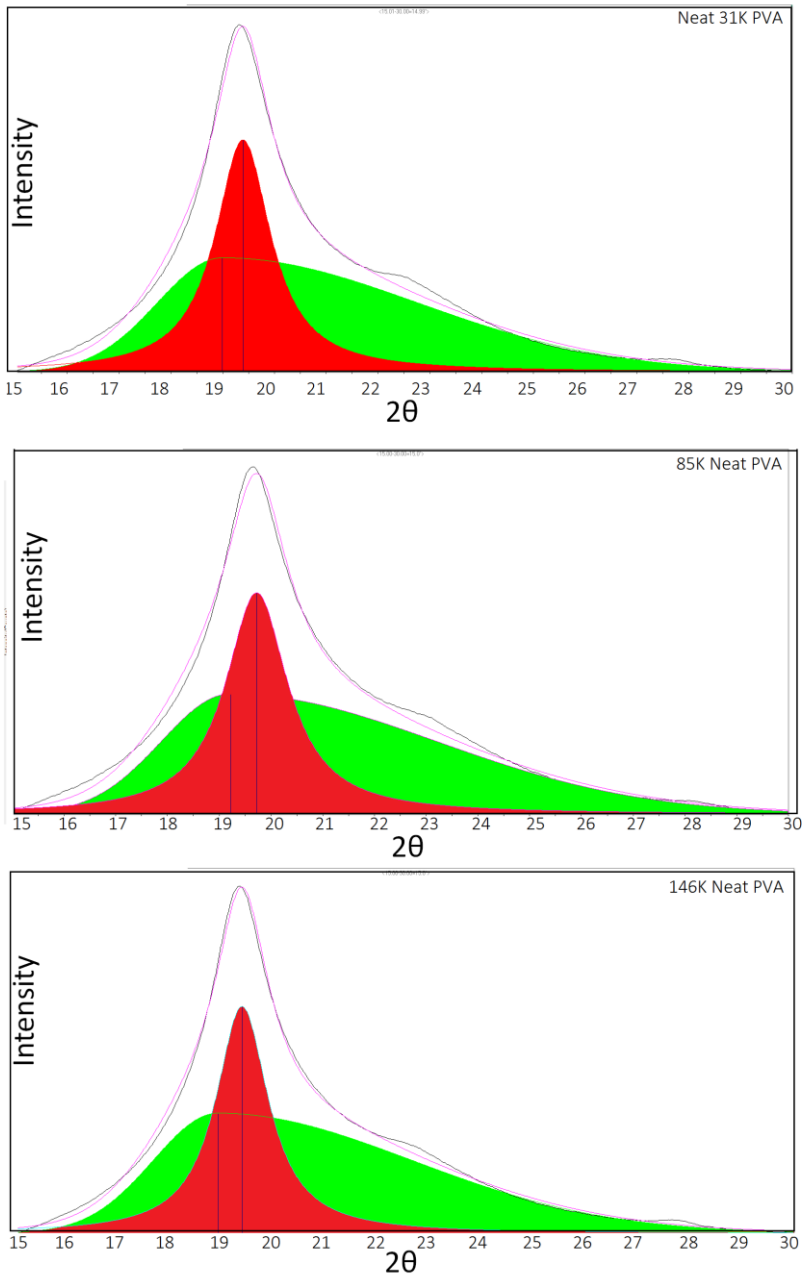

Figure 6.2: XRD data for each of the neat PVA films at 31K (top), 85K (middle) and 146K (bottom). The yellow highlighted peak is the crystal peak while the green highlighted peak is the amorphous peak used in calculating the percent crystallinity.

Table 6.1: χ% calculated for each of the neat PVA systems using equation 6.1.

Sample	χ %
31K Neat PVA	38%
85K Neat PVA	37%
146K Neat PVA	35%

6.2.2 Neat CNC XRD

Neat CNC XRD spectra for aqueous suspended CNCs and freeze-dried CNCs were taken and are shown in Figure 6.3. The XRD data showed that the aqueous suspended CNCs used were a combination on cellulose I and II, giving the neat CNC structure a monoclinic unit cell. The crystal peak indices can be found in Table 6.2.[45,184,186,193] As shown by Figure 6.3, there was a small amorphous peak present for each of the CNC samples. Aqueous suspended CNC crystallinity was calculated to be 92% while freeze-dried CNC crystallinity was calculated to be 96%. In order to calculate the percent crystallinity of the PVA in the CNC/PVA nanocomposite systems, the percent amorphous content contributed by the CNCs to the nanocomposite systems was taken out of the area of the amorphous peak, shown by the following equation:

$$A_{m_{PVA}} = A_m - A_m V_{f_{CNC}} A_{m_{CNC}} \qquad (6.2)$$

where $A_{m_{PVA}}$ is the amorphous contribution of the PVA, A_m is the amorphous contribution of the nanocomposite, $V_{f_{CNC}}$ is the volume fraction of the CNCs, and $A_{m_{CNC}}$ is the amorphous fraction contribution of the CNCs (0.08 for the aqueous suspended CNCs and 0.04 for the freeze-dried CNCs).

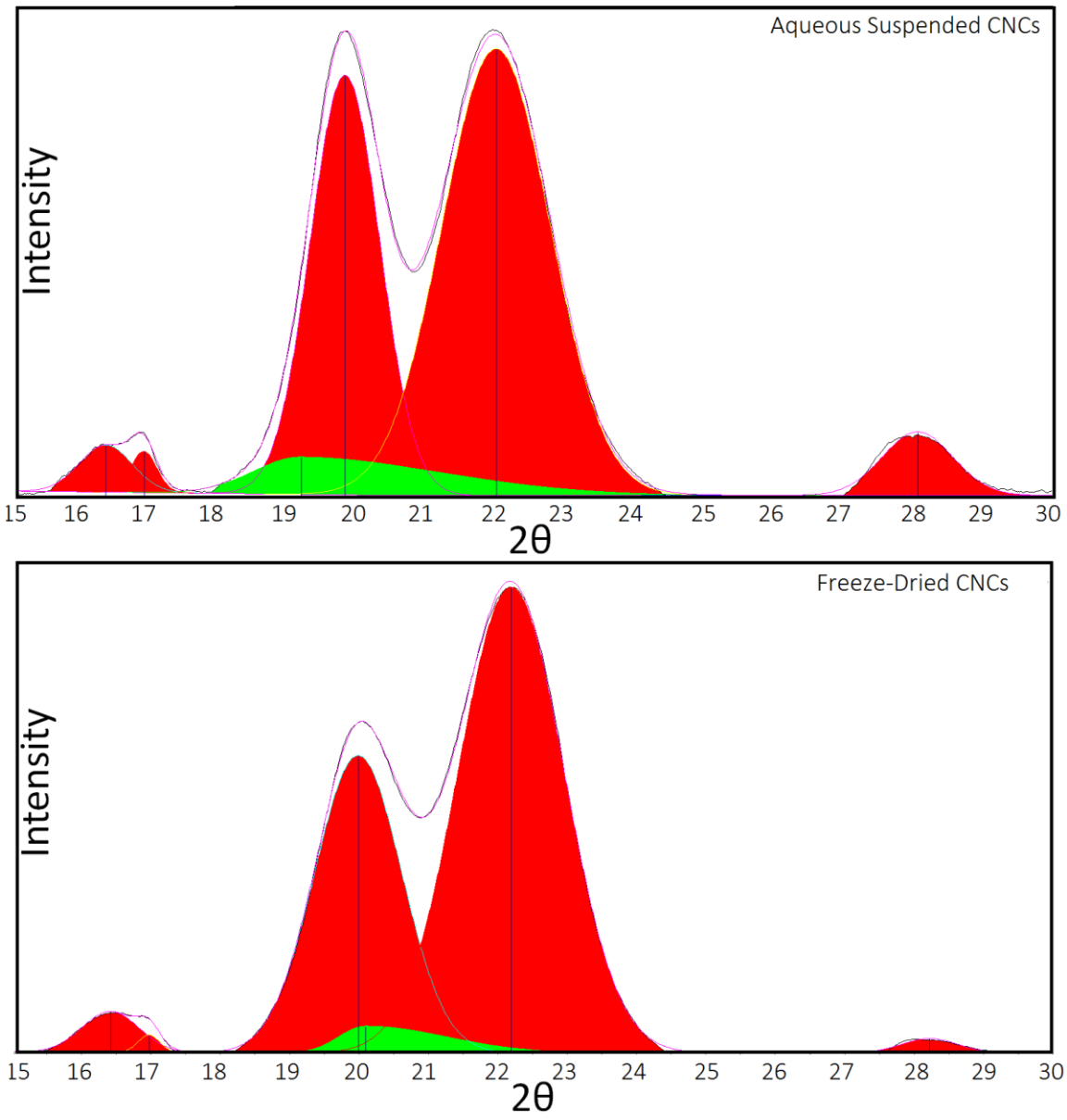

Figure 6.3: XRD structure of neat aqueous suspended CNCs.

Table 6.2: Peak indices for the neat CNC crystal structure.

2θ Position	Cellulose I	Cellulose II
16.5°	220	
19.8°		100
22°	200	
28°		210

6.2.3 CNC/PVA Nanocomposite XRD

The XRD spectra for each of the aqueous suspended CNC/PVA nanocomposite systems studied are shown in Figure 6.4. The XRD spectra for the freeze-dried CNC/PVA nanocomposite systems are shown in Figure 6.5. The percent crystallinity of the PVA in the system was calculated and is shown in Table 6.3. As seen in the table, PVA percent crystallinity increased with increasing CNC content for each molecular weight. This was due to the confinement of the PVA chains by the CNCs. As the CNC content was increased and PVA chains were further confined in the system, crystallite formation between the PVA chains increased, increasing the PVA crystallinity. Crystallinity also increased with increasing molecular weight, attributed to increased crystallite formation. Given the error of 10 %, the change in crystallinity between the freeze-dried and aqueous suspended CNCs was minimal. A schematic illustrating PVA crystallite and CNC morphology inside the nanocomposite system is shown in Figure 6.5. The CNCs shown are aqueous suspended CNCs drawn to scale with lengths of 160 nm and widths of 8 nm. The crystallite size of the neat PVA was calculated and found to be 6 nm, in agreement with studies conducted by Minus *et al.*[194] As shown by Figure 6.6, as CNC content was increased, the spacing available for the PVA was decreased increasing the formation of crystallites due to PVA chain compaction.

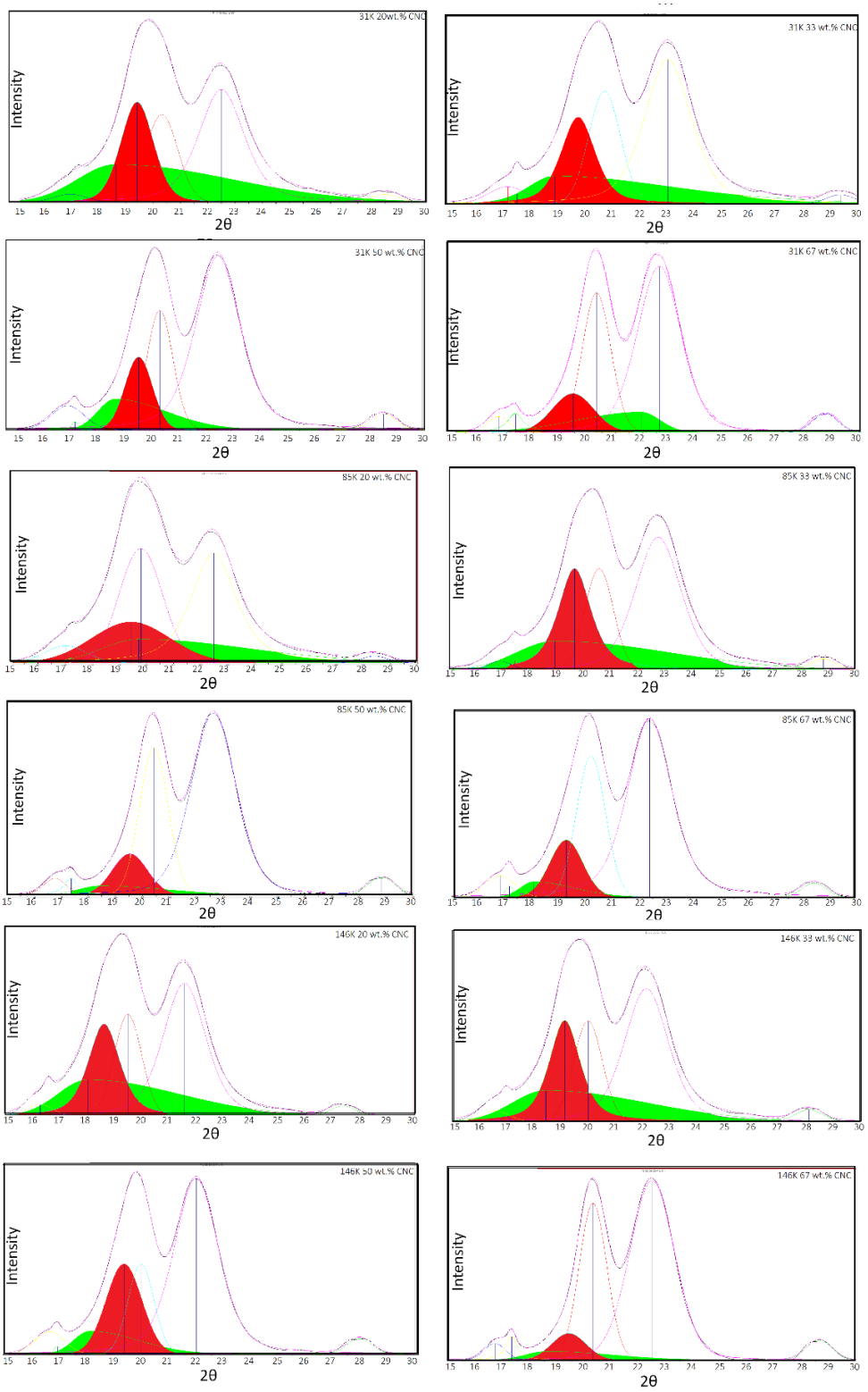

Figure 6.4: XRD spectra for aqueous suspended CNC/PVA nanocomposite films.

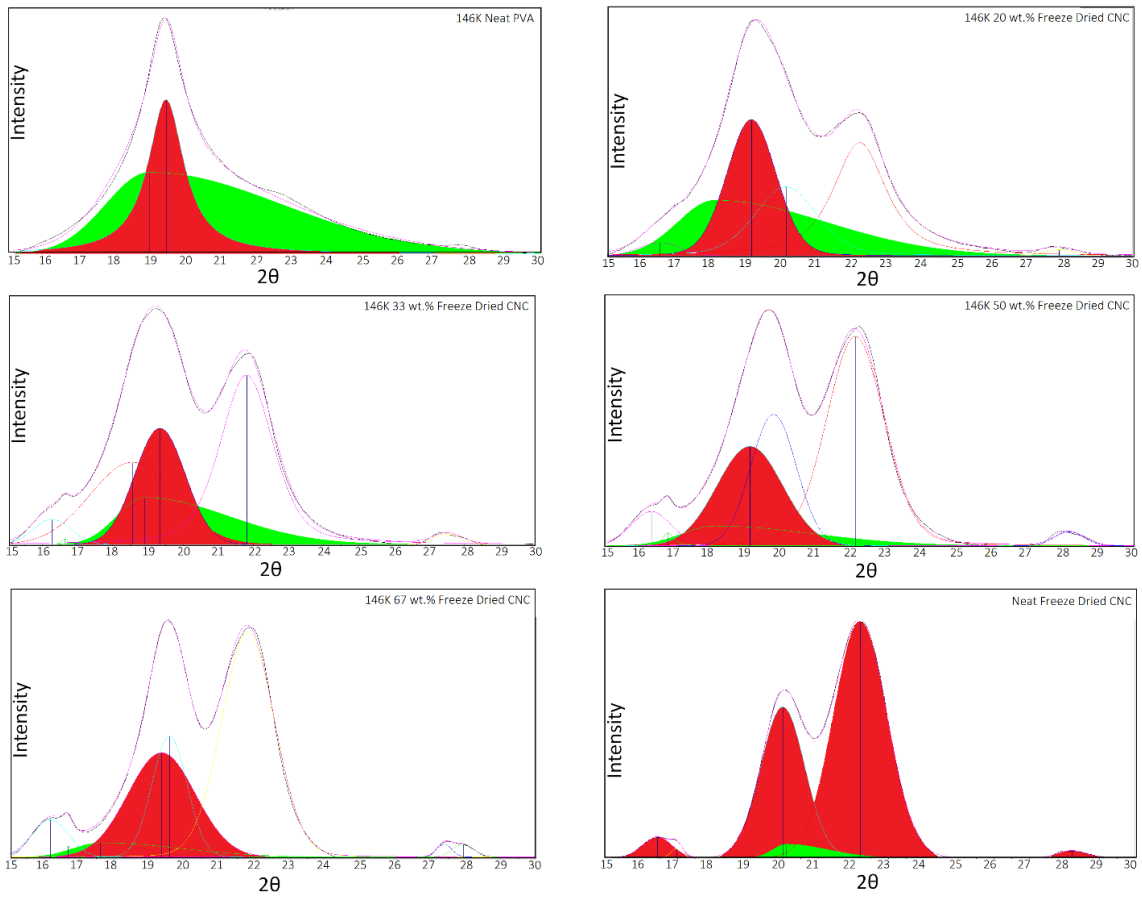

Figure 6.5: XRD spectra for freeze-dried CNC/PVA nanocomposite films.

Table 6.3: Percent crystallinity calculated for each of the CNC/PVA films using equation 6.1 and 6.2

Sample	Crystallinity (%)			
	31K Aqu. Susp.	85K Aqu. Susp.	146K Aqu. Susp.	146K RDFD
Neat PVA	38	37	35	35
20 wt.% CNC w.r.t. PVA	38	38	39	46
33 wt.% CNC w.r.t. PVA	46	49	48	50
50 wt.% CNC w.r.t. PVA	50	65	69	72
67 wt.% CNC w.r.t. PVA	50	70	74	82
Neat CNC	92	92	92	96

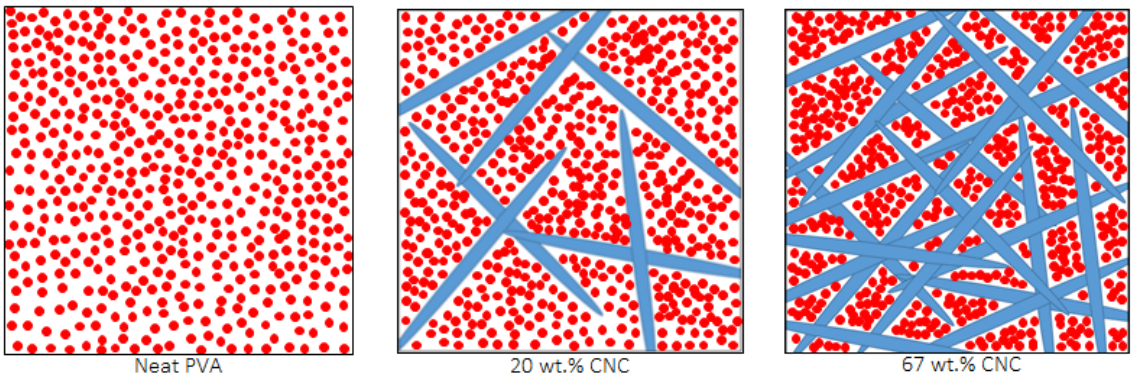

Figure 6.6: Schematic of the morphology of neat PVA and CNC/PVA systems. PVA crystallites are shown by red dots while CNCs are shown by blue rods. The CNCs represented are aqueous suspended CNCs. As CNC concentration is increased, PVA crystallinity is increased shown by the red dots.

6.3 FT-IR

6.3.1 Neat PVA and CNC FT-IR

To further understand the chemical structure and molecular interactions of the CNC/PVA nanocomposite systems, FT-IR spectroscopy experiments were conducted. First, the neat PVA was studied in comparison to each of the molecular weights used in this research. A few characteristic peaks were seen in the neat PVA systems shown in Figure 6.7. Area I was attributed to the –OH stretching from the inter- and intra-molecular hydrogen bonding present shown by a broad peak from 3600 to 3000 cm^{-1}. The peaks in area II (3000 to 2340 cm^{-1}) were due to the C-H stretch of the alkyl groups. Area III peaks at 1600 and 1750 cm^{-1} were caused by the residual acetyl group present from the PVAc and were seen to be weak due to the high degree of hydrolysis used for each molecular weight.[27,46,189] Area IV, the C-C stretch at 1143 cm^{-1} was attributed to the C-C stretch and can be related to the crystallinity of the system. Finally, the peaks at 1088, 919, and 838 cm^{-1} from area V were attributed to the C-O stretch, -CH_2 bend, and the –

CH rocking respectively.[75,195] The spectra for each of the molecular weights used was similar to one another with the exception of area I and area II. In area I, there was a slightly more intense and broad peak for the 31K and 146K samples corresponding to the slightly larger increase in hydrolysis (99 +% vs. 98 -99% for 85K). There was also an increased presence of the C-H stretch in area II for the 85K and 146K molecular weights due to slightly increase –OH groups.

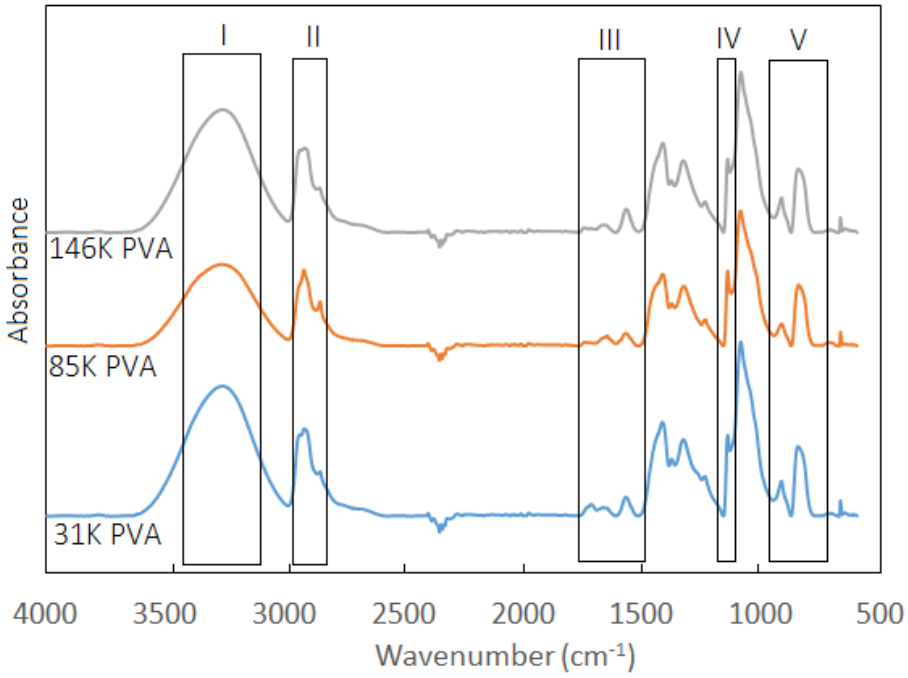

Figure 6.7: FT-IR spectra for each of the neat PVA polymers studied.

The CNC system also had unique characteristic peaks in the FT-IR spectra, shown in Figure 6.8. Area I highlighted refers to the –OH groups from 3000 to 3600 cm^{-1}. A few distinct peaks inside this –OH band refer to the different types of inter and intra molecular hydrogen bonds formed between the cellulose and the different structure of the –OH groups due to the anhydroglucose rings. Area 2 referred to the CH_2 vibration around 2900 cm^{-1}. The large peak seen in area 3 was due to the aromatic C-H plane of

deformation for the anhydroglucose rings while small peaks at 1050 cm^{-1} and 1027 cm^{-1} referred to the C-O and O-C-O stretching. The small peaks at 1375, 1325, and 1252 cm^{-1} were attributed to the CH, CH_2 and –OH stretch typical of polysaccharides. As shown in Figure 6.8, no structural difference was seen between the freeze-dried CNCs and the aqueous suspended CNC films.[46,70,196]

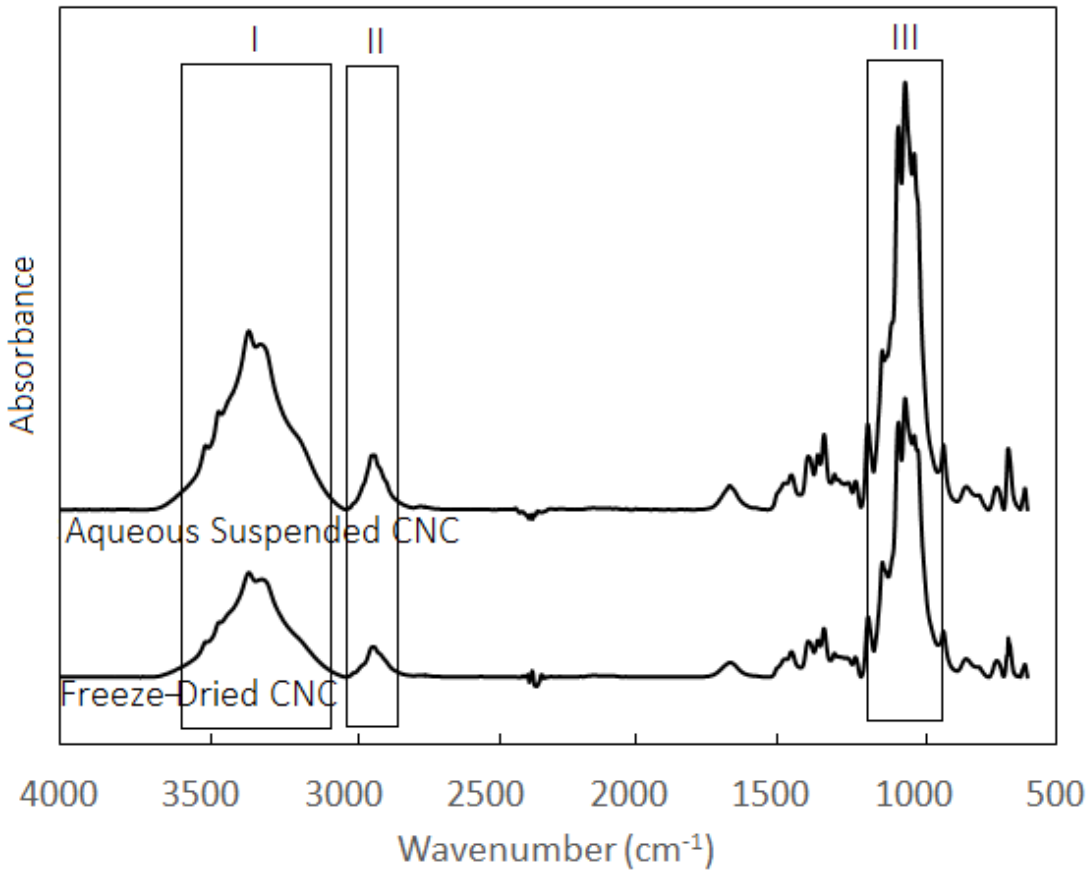

Figure 6.8: FT-IR spectra of the aqueous suspended and freeze-dried neat CNC films.

6.3.2 FT-IR Spectroscopy of CNC/PVA Nanocomposites

The CNC/PVA nanocomposite FT-IR spectra for both aqueous suspended CNC/PVA films and freeze-dried CNC/PVA films are shown in Figure 6.9. From this

figure, a direct comparison can be made between the neat PVA, neat CNC, and CNC/PVA nanocomposite systems on the structural changes that occur when adding CNCs into PVA. First, it was seen that the peak from 3000 to 3600 cm-1 shifted to higher wave numbers with increased CNC loading due to an increase in hydrogen bonding. This shift of the –OH peak also indicated that hydrogen bonding was increasing at the surfaces of the CNCs and PVA.[70] With increasing CNC content, there was also a sharpening of the CNC characteristic peaks at 1375, 1325, 1252, and 1050 cm^{-1} as the CNC contribution became predominant in the system. The increased splitting of the peak at 1050 cm^{-1} was attributed to the increased acetyl linkages with increased CNC loading. In addition, there was a decrease in the peak at 1431 cm^{-1} and an increase in the peak at 1325 cm^{-1} with CNC addition due to the increased C-O stretch contributed from the CNCs. Finally, the peak at 1145 cm^{-1} for PVA which was correlated to the crystallinity of the PVA shifted to wave numbers with CNC addition, indicating a change in the PVA crystallinity as was verified by XRD in the previous section.[155]

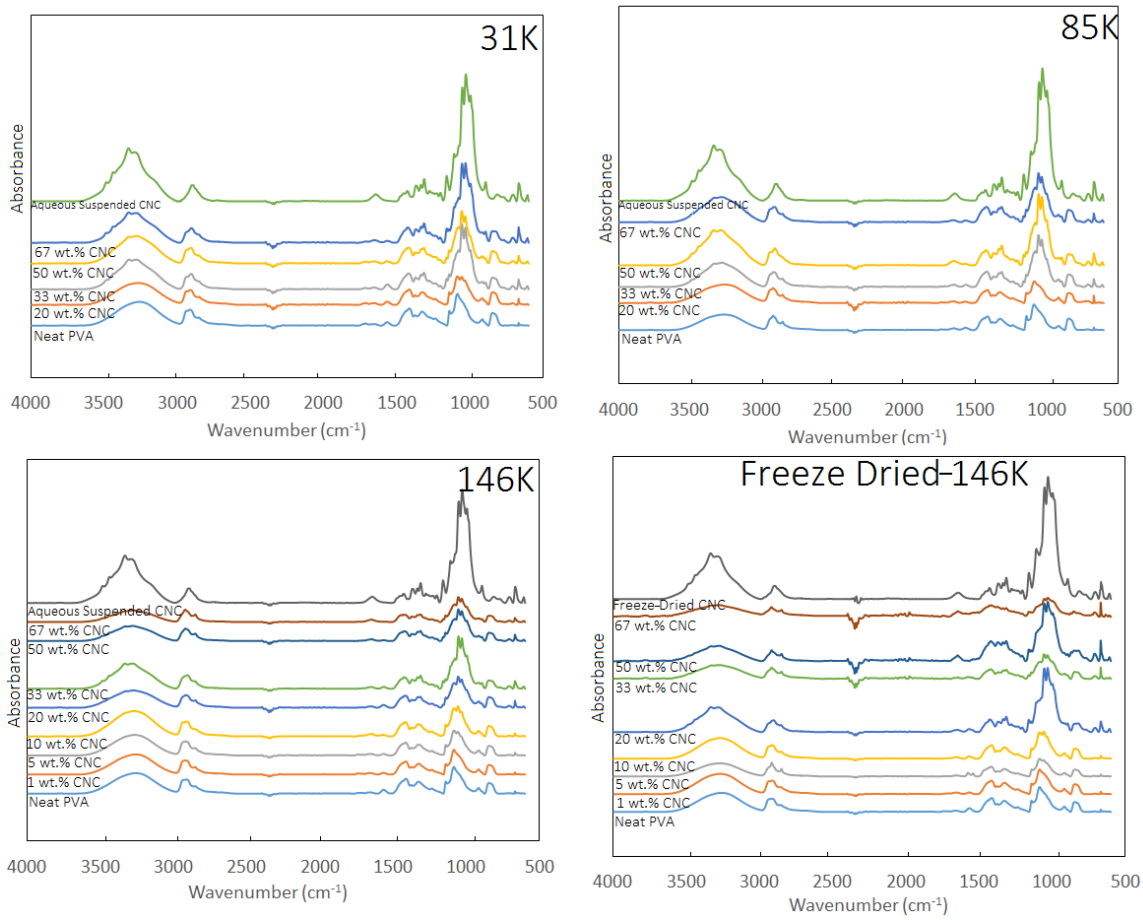

Figure 6.9: FT-IR spectra for aqueous suspended and freeze-dried CNC/PVA systems.

6.4 DSC

6.4.1 Neat PVA DSC

DSC was conducted to increase understanding on the molecular dynamics of the system as a function of temperature in order to further elucidate the structure. Neat PVA systems were tested at each of the molecular weights studied. The T_g was calculated using the onset temperature. Figure 6.10 shows representative data for these neat systems for the 146K neat PVA systems, with the T_g highlighted. The T_g data for 31K, 85K, and 146K can be found in Figure 6.9 as well as the change in heat flow from the onset to the

offset of T_g (ΔH_f). The T_g values presented were comparable to the data from similar molecular weight and percent hydrolyzed PVA presented by Roohoni *et. al.*[17] but lower than the generally accepted T_g value of 85 °C.[191] Two temperature sweeps were initially conducted on PVA and CNC/PVA samples in the DSC. From these sweeps, it was found that degradation of the samples was occurring during testing due to distinct sample color change from clear to brown after opening the DSC pans. The T_g found from the second data sweep was about 85 °C but this T_g was also reflective of the degradation of the samples, decreasing chain mobility. From Figure 6.11, it was seen that both the T_g and ΔH_f changed very little with increasing molecular weight.

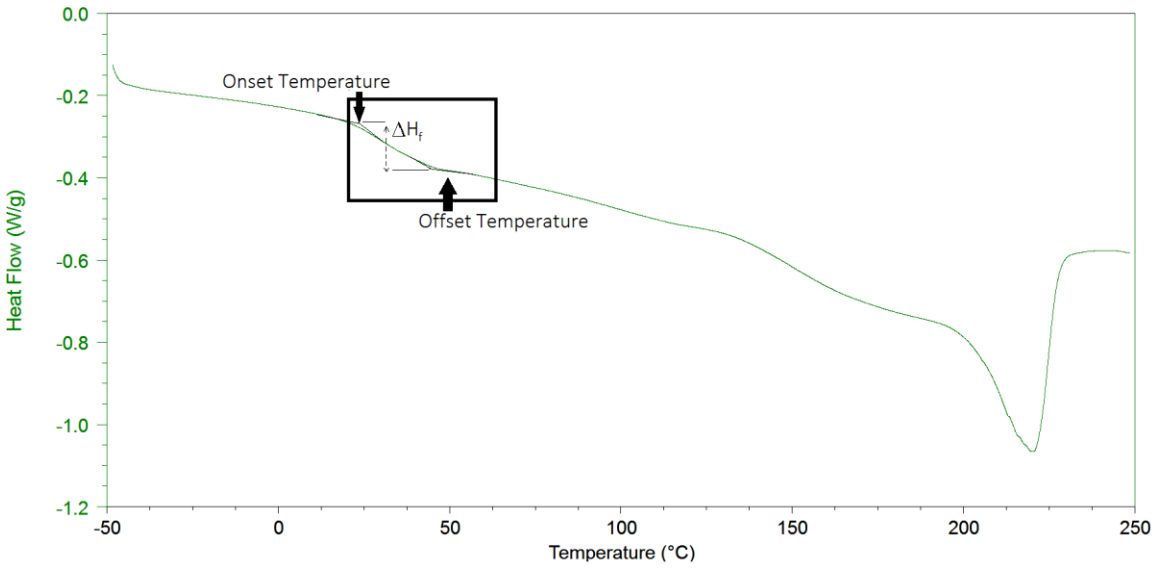

Figure 6.10: T_g behavior representative of all neat PVA systems shown for 146K neat PVA with onset and offset temperature and ΔH_f shown.

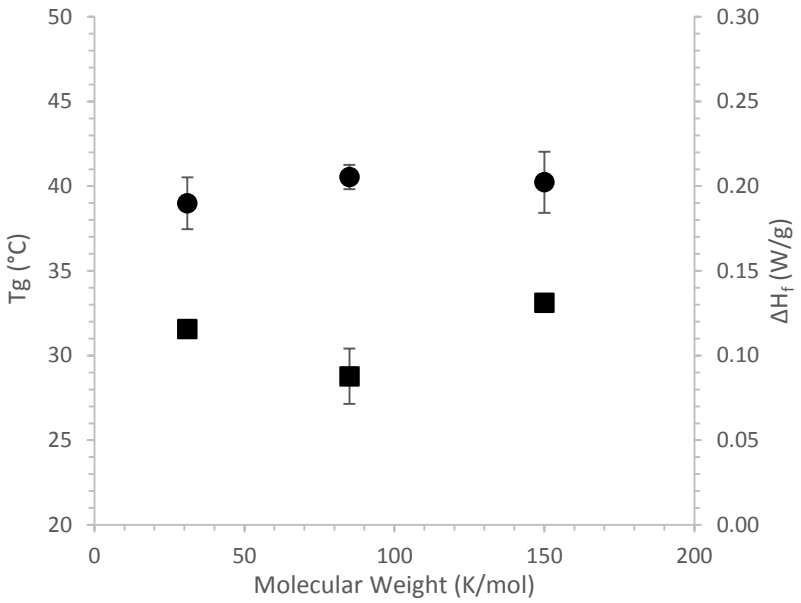

Figure 6.11: T_g and ΔH_f behavior for neat PVA system at 31K, 85K, and 146K. T_g (●) and ΔH_f (■).

6.4.2 CNC/PVA Nanocomposite DSC

The CNC/PVA nanocomposite systems were also tested to better understand the effect of incorporating CNCs into the structure of PVA using DSC. Both aqueous suspended CNC/PVA films at 31K, 85K, and 146K and RDFD CNC/PVA films at 146K were prepared. It was seen that even a small amount of CNCs (1 wt.%) into the PVA had a dramatic effect on the T_g of the nanocomposite. Figure 6.12 shows the effect of adding 1 wt.% aqueous suspended CNC and 1 wt.% freeze-dried CNC into 146K PVA. The aqueous suspended CNC system at 1 wt.% visually increased the ΔH_f while the incorporation of 1 wt.% freeze-dried CNCs into the system showed very little change in ΔH_f . This increase in ΔH_f could be due to the increased dispersion of the aqueous suspended 1 wt.% CNC/PVA film compared to the RDFD 1 wt.%.

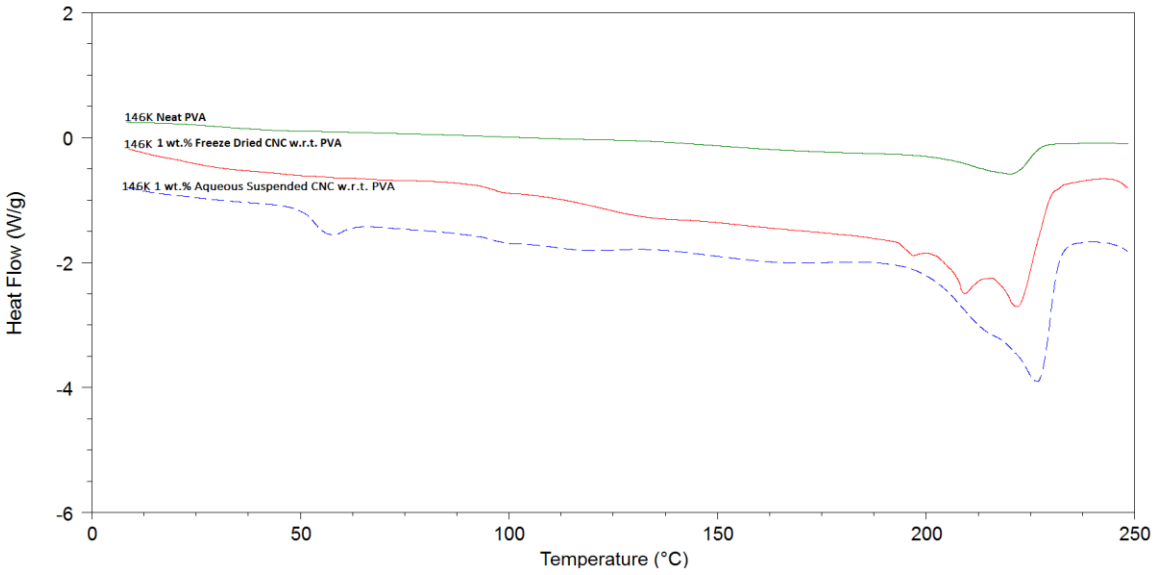

Figure 6.12: DSC thermogram for 146K neat, 1 wt.% aqueous suspended CNC/PVA nanocomposites, and 1 wt.% freeze-dried CNC/PVA nanocomposites.

Figure 6.13 shows the T_g for aqueous suspended and freeze-dried CNC/PVA systems at 146K molecular weight. As seen from the image, T_g was not as pronounced with increasing CNC content as the crystallinity of the system increased as shown by the XRD data. As the CNCs loading was increased, more crystals were formed as the CNCs confined the PVA leading to decreased molecular mobility of the system and a less pronounced T_g. Figure 6.14 shows the T_g and ΔH_f data for 31K, 85K, and 146K molecular weight. As shown, the T_g decreased with increasing CNC content and ΔH_f decreased with increasing CNC content. This disappearance of T_g with increasing CNC content can be attributed to the CNCs as no T_g for CNCs was observed as CNCs simply degrade due to the strong hydrogen bonding interactions present.[4] There was a difference seen in T_g when comparing molecular weight. The 31K samples had a higher T_g, especially in the primarily PVA regime, with decreasing T_g as molecular weight was increased. This could be due to the effect of molecular weight and bound water. While

the samples were dried before testing, a very small amount of bound water may still be present. Due to the increased entanglement of the higher molecular weight systems of 85K and 146K, more bound water could be trapped, decreasing the T_g. In the CNC predominant regime, there was a convergence of T_g as CNC loading went from 50 wt.% to 67 wt.% in the film for all molecular weights. ΔH_f also decreased with increasing CNC content for each molecular weight. This convergence of T_g and disappearance of ΔH_f was attributed to the predominant presence of the CNCs controlling the molecular relaxations of the nanocomposite systems.

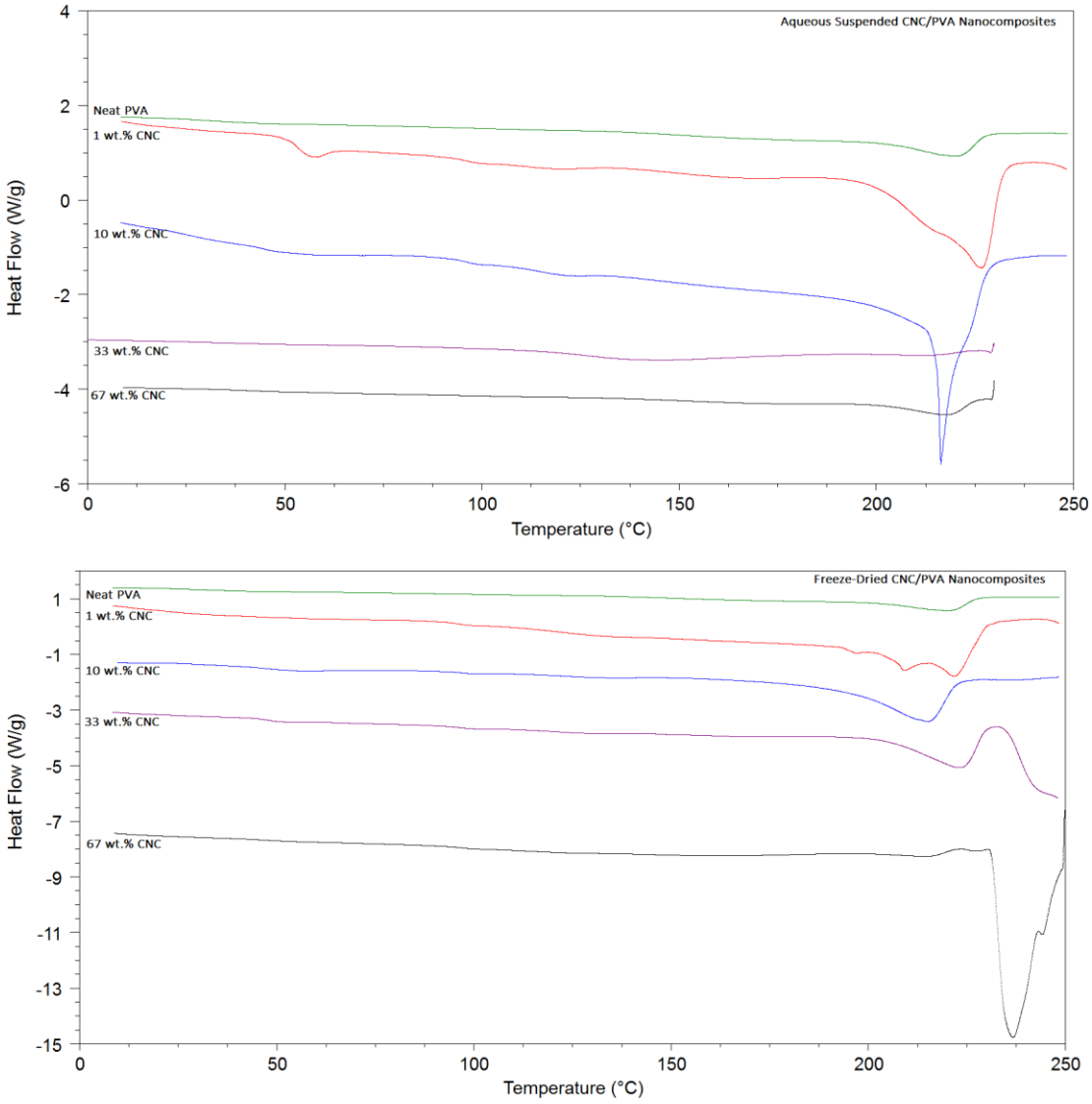

Figure 6.13: Thermal behavior of aqueous suspended and freeze-dried CNC/PVA nanocomposite systems.

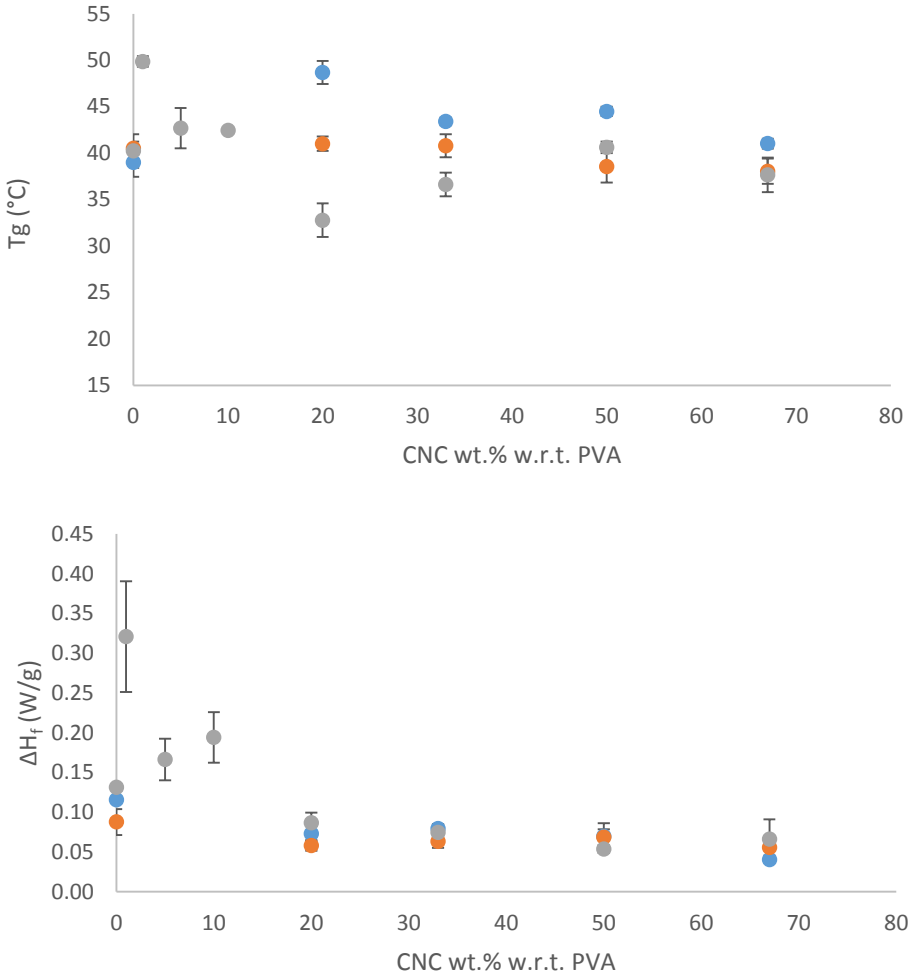

Figure 6.14: T_g (top) and ΔH_f (bottom) behavior of aqueous suspended CNC/PVA nanocomposite systems at 31K (●), 85K (●), and 146K (●) molecular weights.

The freeze-dried and aqueous suspended CNC/PVA systems were then compared to see if there was a difference in interaction between the different particles, shown in Figure 6.15. The freeze-dried CNC/PVA systems showed increased T_g and ΔH_f behavior most likely due to the increased size and aggregation of the CNCs in the freeze-dried state. While the aggregates of the CNCs were not optically visible as discussed in Chapter 4, the dynamic light scattering measurements showed increased size and aggregation of the freeze-dried systems. This increase in CNC size will allow for

increased CNC-CNC interaction, increasing the CNC character of the system and therefore increasing the T_g. The increased aggregation could impart more CNC character on the freeze-dried CNC/PVA systems, also increasing the T_g as polymer chains were confined but CNCs were also confined within one another, decreasing chain mobility even further.

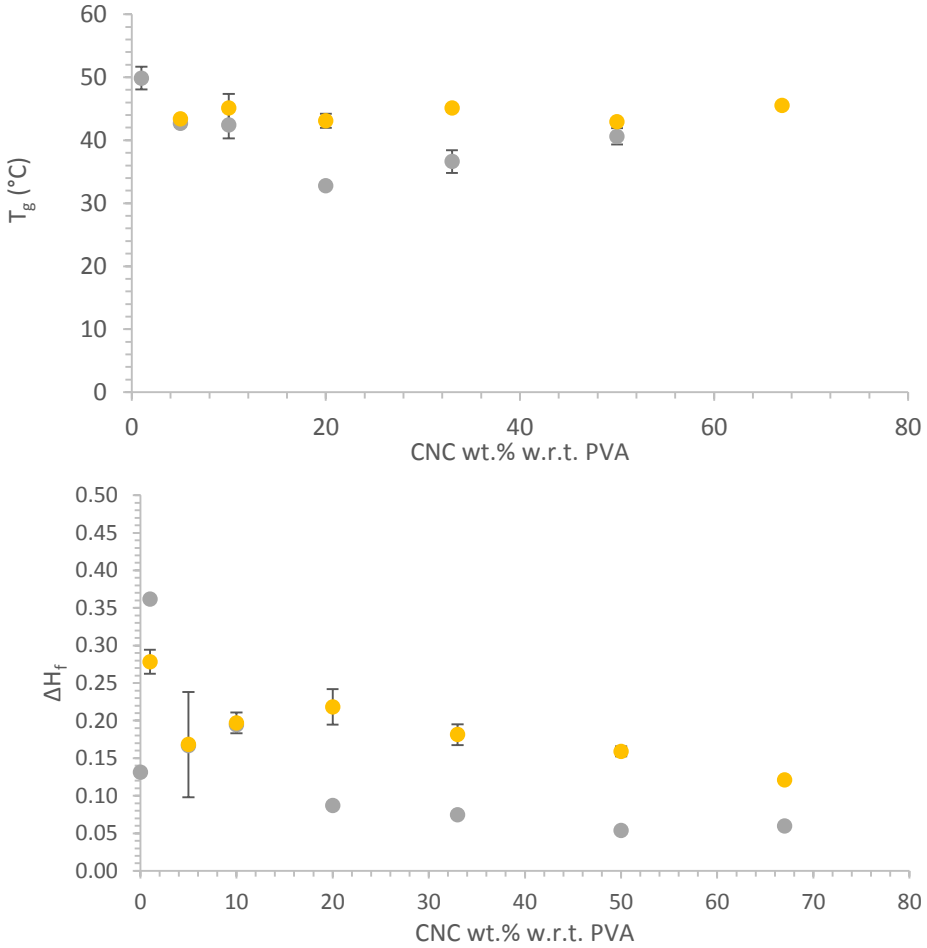

Figure 6.15: T_g (top) and ΔH_f (bottom) behavior of aqueous suspended CNC/PVA nanocomposite systems (●) and freeze-dried CNC/PVA nanocomposite systems (●) at 146K molecular weight.

6.5 Conclusions

In conclusion, the structure of the CNC/PVA nanocomposite systems was studied through XRD, FT-IR, and DSC. Through this analysis, it was seen that percent crystallinity increased with increasing CNC content due to compaction of the PVA chains increasing PVA crystallite formation. Little difference in crystallinity was seen between the individual molecular weights in neat PVA. FT-IR showed that the freeze-dried CNCs and aqueous suspended CNCs were very similar chemically. The neat PVA systems were also similar chemically with increased hydroxyl groups on the 31K and 146K neat systems due to a slightly larger percent hydrolysis. Finally, the molecular mobility was examined using DSC. It was seen that increasing CNC content decreased the molecular mobility due to increased system rigidity imparted by the CNCs. The molecular weight of the neat polymer systems may play a role in trapping bound water due to increased molecular entanglements present. Freeze-dried CNCs showed increased T_g due to increased CNC-CNC interaction due to aggregation. In the next Chapter, the mechanical properties of the CNC/PVA systems will be discussed and related back to the structure.

CHAPTER 7

MECHANICAL PROPERTIES

The mechanical properties of neat PVA and CNC/PVA nanocomposite films were studied using DMA and MTT techniques. DMA was used to determine the dynamic moduli behavior as a function of temperature to increase understanding of the molecular structure of PVA. The T_g was determined via the loss modulus (E'') data and compared to the T_g found via DSC. MTT were conducted on "wet" CNC/PVA films containing 3 wt.% water and "dry" CNC/PVA dried in an oven at 110 °C for 1 hour. These data were used to better understand the effect of water as a plasticizing agent on the CNC/PVA nanocomposite systems.

7.1 Introduction

CNC/PVA nanocomposite films are of interest because of their biodegradability, biocompatibility, sustainability, and mechanical properties and have been extensively studied to increase the understanding of their mechanical response.[17,41,64–66,70,95,121,151,153,197,198] Due to their increased reinforcing potential, mechanical characterization using DMA has been conducted on a variety of CNC/PVA nanocomposites at low CNC loadings (below 20 wt.% CNC). In a study conducted by Peresin *et al.*,[95] CNC/PVA nanocomposites with CNCs derived from ramie fibers were electrospun and the thermo-mechanical properties were examined through dynamic mechanical analysis. Peresin *et al.*[95] found the storage modulus (E') to be three times that of the neat PVA matrix with the addition of CNCs due to strong hydrogen bonding

interactions of fully hydrolyzed PVA with the CNCs as well as increased filler alignment above the T_g . Roohani *et al.*[17] saw E' increase above the T_g with the addition of cotton derived CNCs to a PVA matrix at 3, 6, 9 and 12 wt.%. Tensile strength was also increased to up to almost 3 GPa with CNC loading at 12 wt.%, and it was noted that the stress transfer characteristics were directly proportional to the degree of hydrolysis of PVA in the CNC/PVA nanocomposites in that stress transfer increased with increasing hydrolysis. In a study conducted by Fortunati *et al.*,[70] thin film tensile tests were conducted on CNC/PVA nanocomposites with CNCs derived from okra. In this study, neat and nanocomposite films were made at 1 wt.%, 2 wt.%, 5 wt.%, and 10 wt.% CNC loading. Elongation at break initially decreased from neat PVA to 1 wt.% CNC loaded PVA and then increased with a maximum elongation at break seen at 5 wt.% loading. Young's modulus was also seen to decrease from neat PVA to 1 wt.% CNC loaded PVA and then increase with increasing CNC loading. This behavior was attributed to the formation of stress concentrators at low loadings below 5 wt.%. At 5 wt.%, the mechanical properties were increased as the interaction of the cellulose and PVA was increased due to increased CNC surface area throughout the composite with increased CNC loading. At 5 wt.% CNC, the available surface area of cellulose was at its optimal dimension giving better mechanical properties. The crystallinity also increased with the addition of 1 wt.% CNC and then decreased slightly, determined through DSC measurements.

The mechanical behavior of wood based CNC/PVA nanocomposite systems has been studied less.[41,65,66] Frone *et al.*[66] and Cho and Park[41] utilized wood based CNC/PVA systems similar to those presented in this research. In the study conducted by Frone *et*

al.,[66] the tensile properties of CNC/PVA nanocomposite systems at loading up to 4 wt.% CNC were examined. From this study, an increase in tensile strength and decrease in elongation was seen with increasing CNC loading. The increase in tensile strength was attributed to increased hydrogen bonding and filler matrix interaction through the incorporation of CNCs. CNCs of different fiber diameters were also studied by Frone *et al*.[66] and from this analysis, it was seen that smaller diameter CNCs gave better tensile modulus and strength due to increased interface area leading to a larger probability of hydrogen bonding. This understanding can be applied to the freeze-dried CNC systems presented as they have larger lengths and increased affinity for aggregation, indicating that their mechanical properties should be decreased compared to aqueous suspended systems as there is less surface area leading to decreased probability of hydrogen bonding. Cho and Park[41] conducted a study on wood based isotropic CNC/PVA nanocomposite systems utilizing DMA and tensile testing at CNC loadings of 1, 3, 5, and 7 wt.%. From this study, they saw very little change in tensile strength and modulus at 1 wt.% CNC and attributed this behavior to the failure strain of the PVA matrix being much larger than the failure strain of the CNC. With respect to the CNC/PVA mechanical behavior in the DMA, E' was seen to increase with increasing CNC content from 3 wt.% to 5 wt.% compared to the neat PVA by 74% and 69% respectively at 25 °C. This increase in E' was attributed to improved nanocomposite stiffness as imparted by the CNCs and increased hydrogen bonding as the CNCs were able to form a network above their percolation threshold. While tensile and thermo-mechanical characterization has been conducted on CNC/PVA nanocomposite systems at lower loadings (less than 20 wt.% CNC), little work has been done on similar systems at high CNC loadings (above

20 wt.% CNC). In the presented work, CNC/PVA nanocomposite systems at high CNC loadings up to 67 wt.% will be characterized to gain increased understanding of the reinforcing potential of CNCs at very high loadings.

7.2 DMA Neat PVA

The neat PVA data was studied using DMA to compare the difference in mechanical behavior with molecular weight. These data can be found in Figure 7.1 for E' and E''. For further clarity, the average of the E' data were taken at 30 °C and 110 °C and compared in Figure 7.2 as a function of molecular weight. These temperatures were chosen for comparison because they are well below and well above T_g of neat PVA. As shown, in Figure 7.1, the values of E' for the neat PVA films were very similar below T_g at 30 °C but increased with decreasing molecular weight above at 110 °C. This difference in E' was indicative of the upper and lower bounds of the mechanical response of the material below and above T_g. Below T_g, the polymer was rigid while above the T_g, the polymer mobility increased, increasing the contribution of the CNCs. The T_g for neat PVA polymers was calculated by finding the peak of the E''. As shown in Figure 7.1, the E'' peak shifts to lower values with increasing molecular weight, evidence of increased chain mobility. This shift further indicated the presence of a small amount of bound water trapped inside the neat PVA acting as a plasticizer and increasing chain mobility.

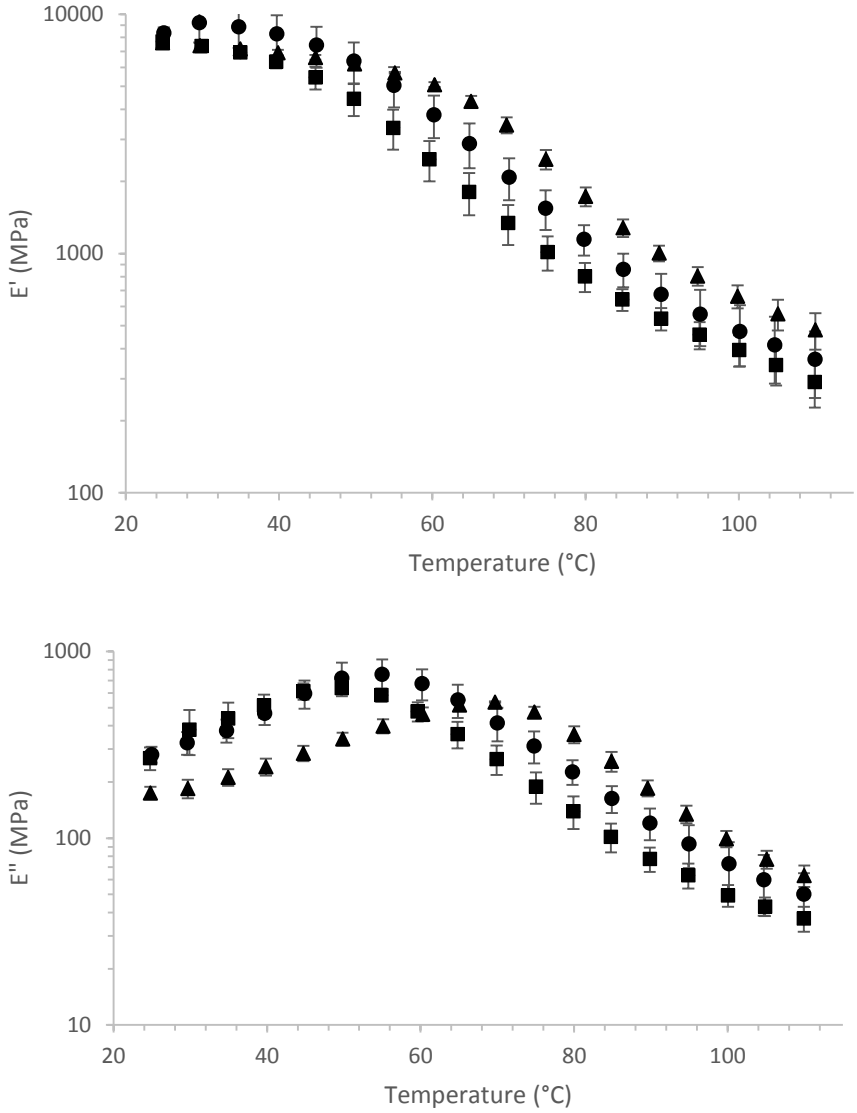

Figure 7.1: *E′* (top) and *E″* (bottom) average data for 31K (▲), 85K (●), and 146K (■) molecular weight neat PVA.

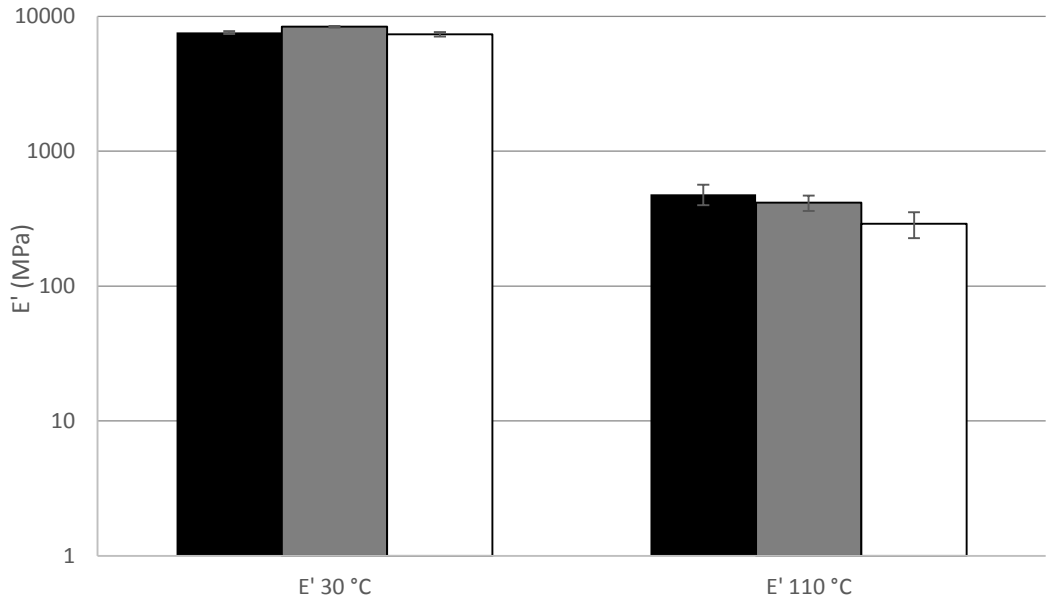

Figure 7.2: *E'* behavior below and above the T_g of the neat PVA. 31K (black), 85K (grey), 146K (white).

T_g values found in the DMA and the DSC were compared in Figure 7.3. The T_g in the DMA was found to be higher than the T_g[199] from the DSC as well as possess a larger dependence on molecular weight. The T_g values found from the DSC were lower than the expected T_g for neat PVA systems (about 80 °C). This decrease in T_g was attributed to small fraction of bound water left in the samples after drying for one hour, increasing the mobility of the PVA chain backbone.[200] DMA is a more sensitive measurement technique for semi-crystalline polymer systems and can lead to increased understanding of the molecular interactions.[201] The T_g values found from the DMA, especially for 31K neat PVA, can lead to increased understanding of the drying behavior of neat PVA systems and the effect of bound water. The increase in T_g for 31K and subsequent decrease in T_g for 85K and 146K were attributed to increased bound water inside of the system due to increased entanglements of the PVA, increasing the difficulty in the release of the bound

water during drying. This increased release of bound water will be further examined in the CNC/PVA nanocomposite systems.

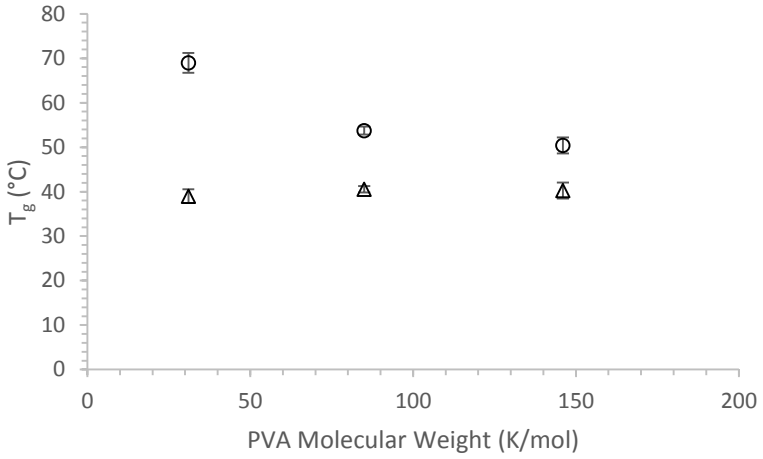

Figure 7.3: T_g determined by DMA (○) and DSC (△) for neat PVA samples.

7.3 DMA of Composites Containing Aqueous Suspended CNCs

DMA was conducted to determine the thermo-mechanical behavior of the aqueous suspended nanocomposite films CNC/PVA films. The E' behavior for 31K, 85K, and 146K molecular weight CNC/PVA samples can be found in Figure 7.4. From these data, it was seen that the change in E' at T_g decreased with increasing CNC content. It was also seen that increasing CNC content had a larger effect on E' with increasing molecular weight. This behavior can be seen more clearly in Figure 7.5 in which the E' values at 30 °C and 110 °C for each molecular weight and CNC loading were compared. From Figure 7.5, it was seen that E' increased with increasing CNC content both below and above the T_g due to the increased stiffness and rigidity imparted by the CNCs as nanocomposite crystallinity increased and increased hydrogen bonding imparted by the

CNC network, especially above the percolation threshold.[41,42,51,131,202] Below the T_g, CNCs had the most significant reinforcing effect on the 146K molecular weight most likely due to the increased crystallinity of the sample. The deviation in E' was seen to a lesser extent above the T_g due to increased chain mobility in the rubbery region decreasing the impact of molecular weight on E' behavior.

E'' was plotted for each molecular weight and CNC loading shown in Figure 7.6. From Figure 7.6., it was seen that the T_g was less pronounced with CNC addition as the crystallinity of the system increased with increasing molecular weight. The T_g was found by fitting the E'' curve with a polynomial function and finding the maximum of the peak. Figure 7.7 shows the T_g values for the E'' data. From these data, it was seen that upon initial CNC loading below 20 wt.% CNCs for the 146K molecular weight data, the T_g decreased in comparison to the 146K neat PVA with increasing CNC loading. This decrease in T_g can be attributed to the incomplete formation of a CNC network allowing for the PVA backbone to have increased mobility as the CNCs break up PVA chain entanglements but do not form a network structure. An increase in T_g was seen from 20 wt.% to 33 wt.% CNC for all the PVA samples indicating decreased PVA chain mobility as a CNC network was formed restricting the PVA chains. This increase in T_g also indicated increased component interactions between both the PVA and the CNCs. Finally, for the 50 wt.% and 67 wt.% CNC samples for 31K and 146K PVA, a decrease in T_g was seen again indicating increased chain mobility. This decrease in T_g could be attributed to the decreased contribution of the PVA as CNCs were the primary component in the nanocomposite system. As fewer PVA chains were present in the system, the entanglement of the PVA chains was decreased allowing for increase PVA

chain mobility as the network structure shifted from a polymer component controlled to CNC component controlled system.

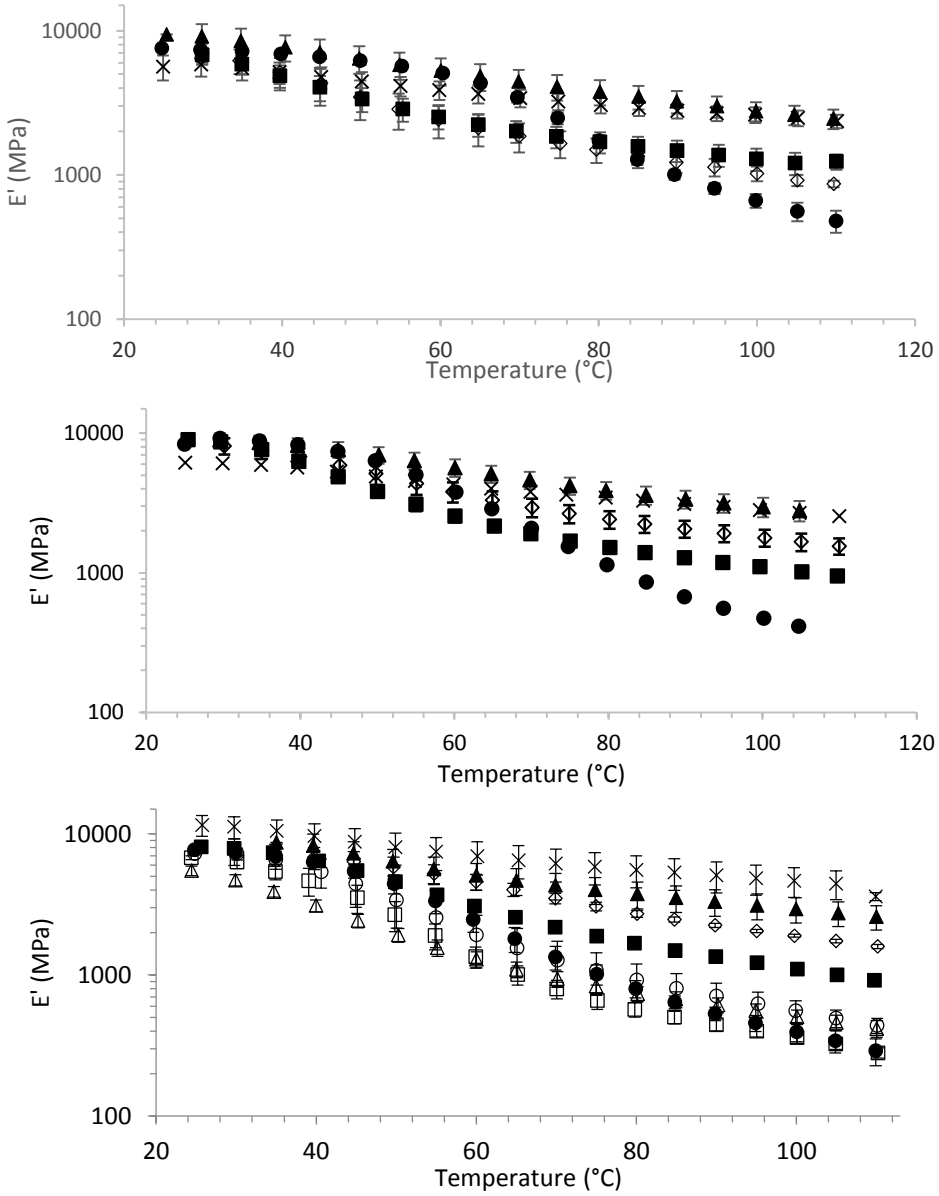

Figure 7.4: *E'* behavior for 31K (top), 85K (middle), and 146K (bottom). Loadings are shown for neat PVA (●), 1 wt.% CNC (□), 5 wt.% CNC (○), 10 wt.% CNC (△), 20 wt.% CNC (■), 33 wt.% CNC (◇), 50 wt.% CNC (▲), and 67 wt.% CNC (X).

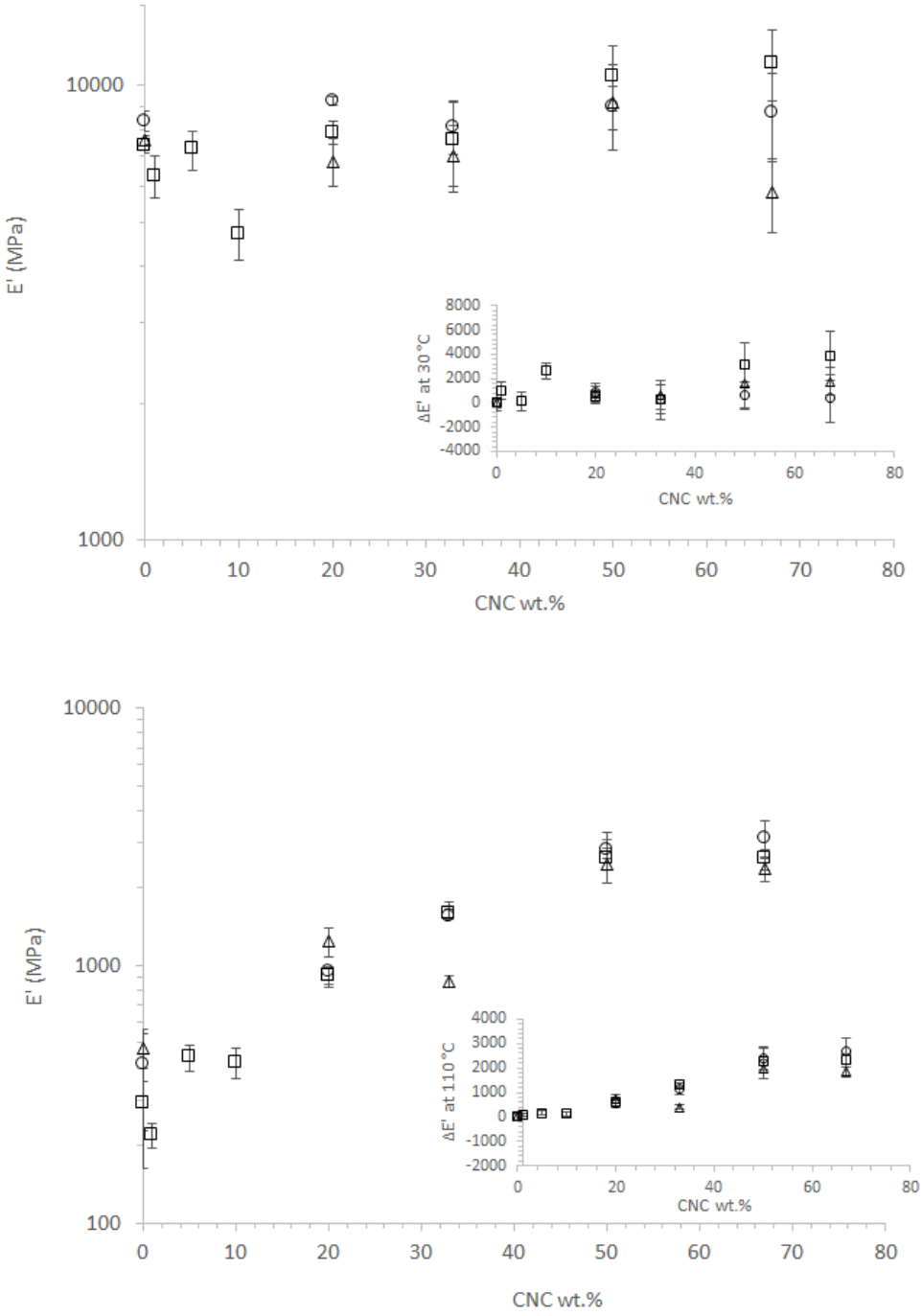

Figure 7.5: *E′* comparison of 31K (△), 85K (○), and 146K (□) as a function of CNC loading for temperatures below the T_g (30 °C) (top) and above the T_g (110 °C) (bottom). The inset shows $\Delta E'$ at each CNC loading for each molecular weight: 31K (△), 85K (○), and 146K (□).

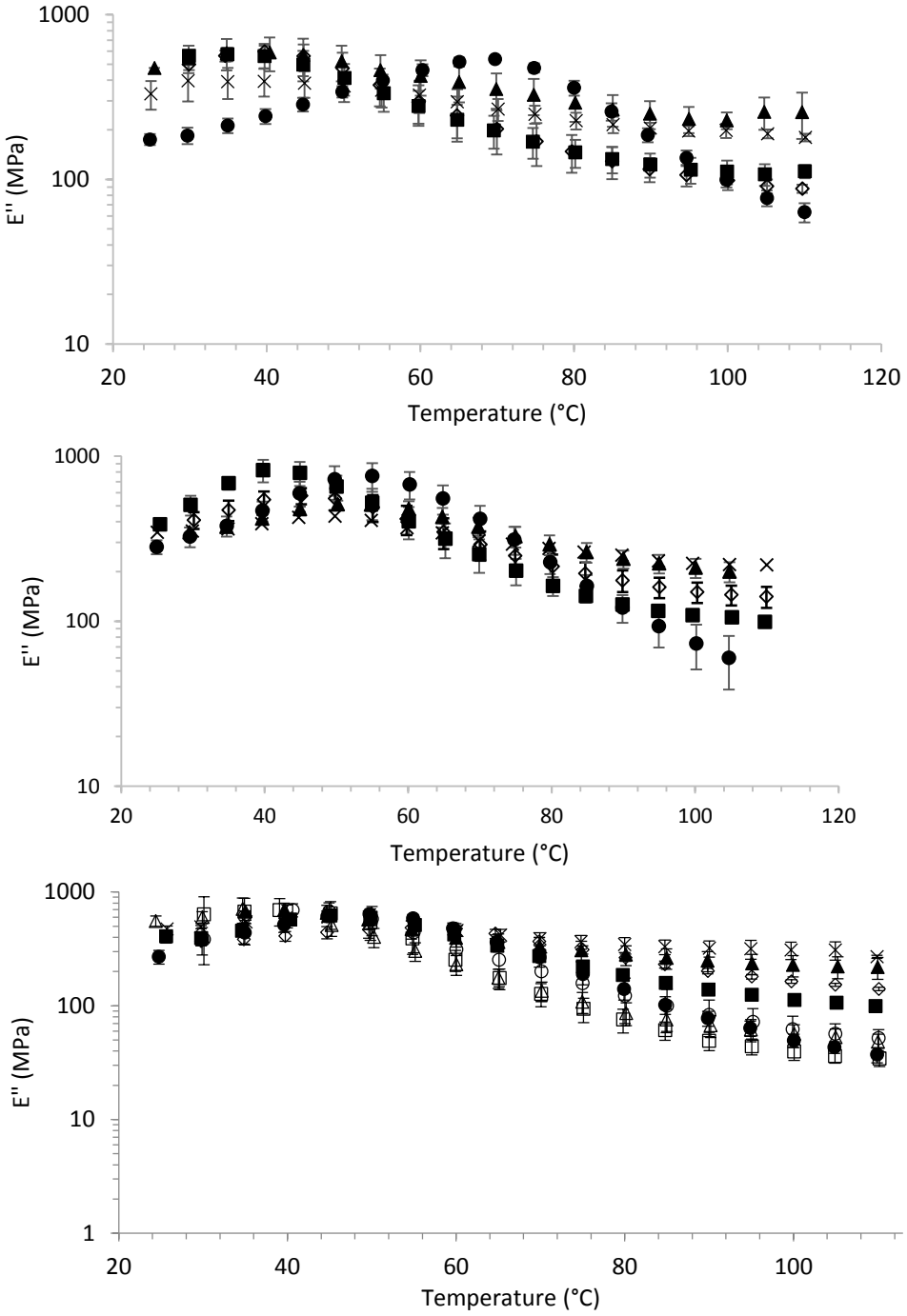

Figure 7.6: *E''* behavior of 31K (top), 85K (middle), and 146K (bottom) CNC/PVA nanocomposite systems as a function of CNC loading. Neat PVA (●), 1 wt.% CNC (□), 5 wt.% CNC (○), 10 wt.% CNC (△), 20 wt.% CNC (■), 33 wt.% CNC (◇), 50 wt.% CNC (▲), and 67 wt.% CNC (X).

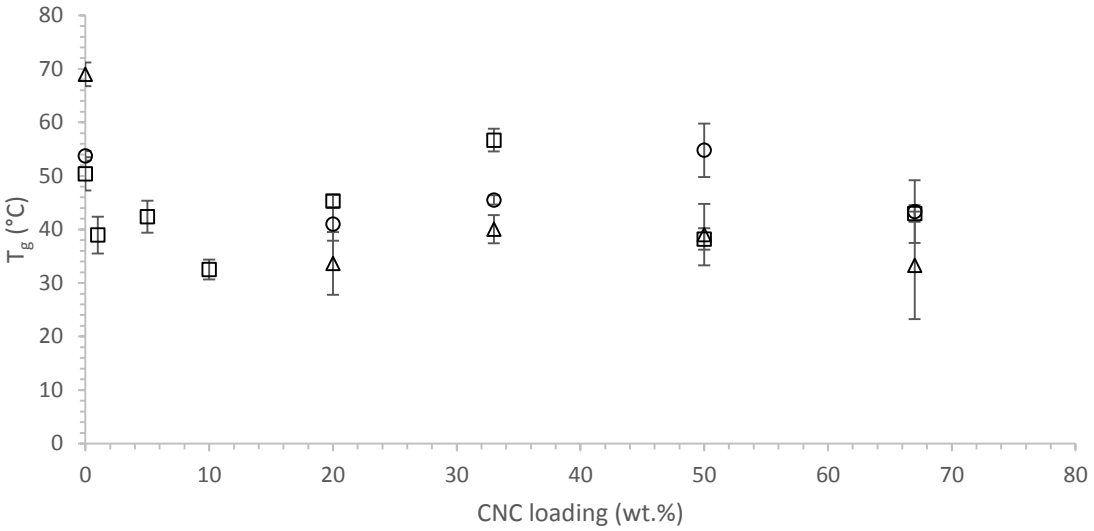

Figure 7.7: T_g values found from the *E"* peak for each molecular weight: 31K (△), 85K (○), 146K (□).

The DMA and the DSC data for each molecular weight in the aqueous suspended CNC systems were compared in Figure 7.8. In general, the DSC T_g values were less affected by CNC content than the DMA T_g values. T_g showed larger changes with CNC content at higher molecular weights compared to lower molecular weights for the DMA measured T_g. These differences were most likely due to the sensitivity of the measurement technique. DMA collects T_g data based on energy lost and mechanical response while DSC collects data based on changes in heat capacity.[201] This difference in measurement technique could lead to the DMA being more responsive to the mobility of the components of the system.

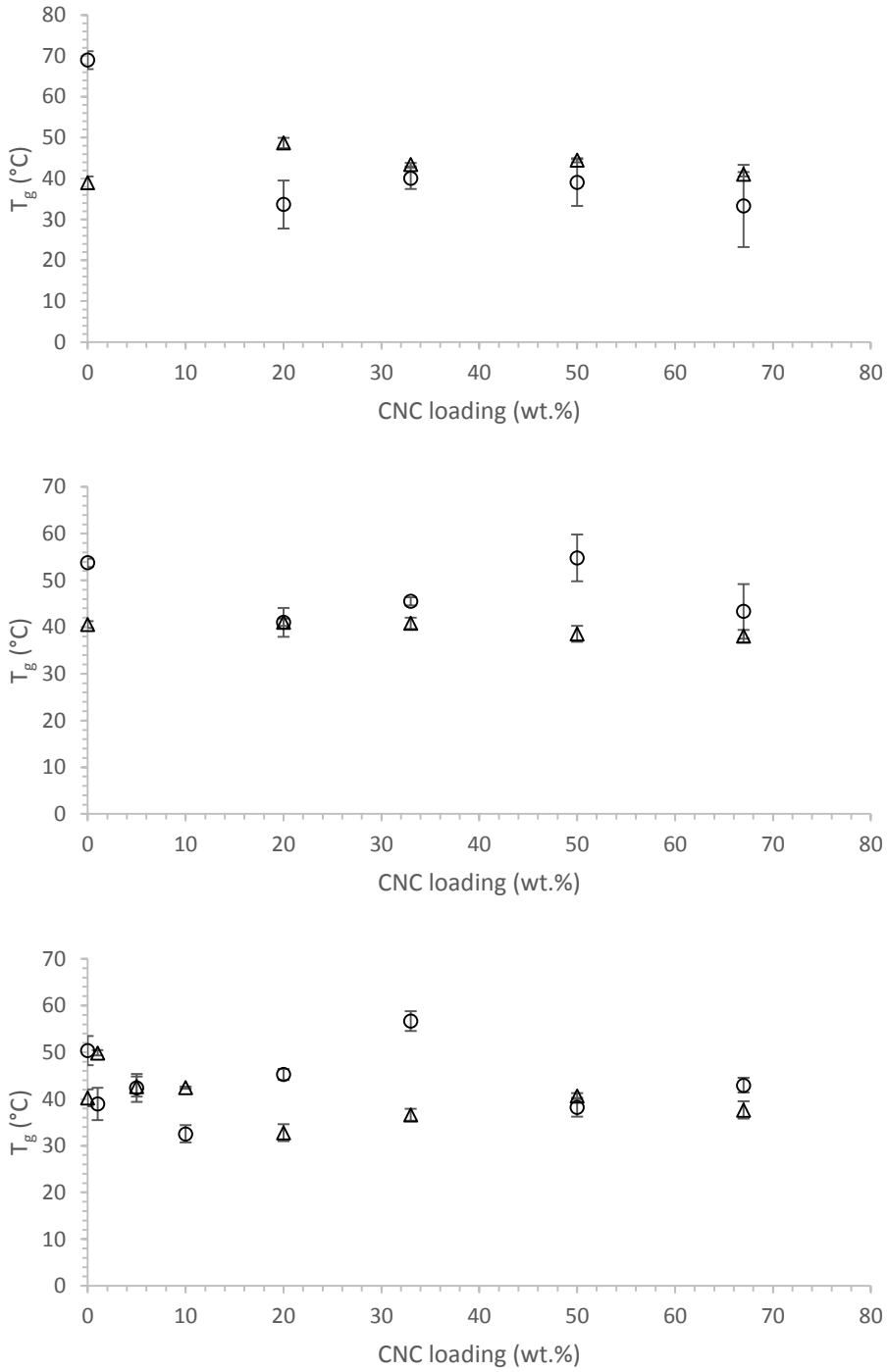

Figure 7.8: DMA (○) and DSC (△) comparison for 31K (top), 85K (middle), and 146K (bottom) molecular weight as a function of CNC loading.

To further understand the interactions of the CNCs in the PVA matrix, mechanical percolation was modeled using a method described by Loos and Manas-

Zloczower modifying the Takayanagi series-parallel model, known as Model II.[130,203] In this model, three component phases where considered: the polymer matrix, the dispersed CNCs, and the aggregated CNCs. All these phases were assumed to exhibit linear elastic response and be isotropic. The well dispersed CNCs were represented by the aspect ratio while the aggregated CNCs were represented by the percolated network. This model does not account for CNC/PVA debonding, CNC slippage from the PVA matrix, or any other voids or defects present in the system. Percolation modeling consisted of first calculating the percolation threshold for CNCs using the equation below

$$V_c = \frac{0.5}{l/d} \qquad (7.1)$$

where V_c is the percolation threshold and l/d is the aspect ratio of the CNC. This value can be lower in actuality if a large range of aspect ratios is present.[175,176] With an aspect ratio of 20, V_c was found to be 0.025. For loadings where $V_c < V_f$ and V_f is the volume fraction of the CNCs in the nanocomposite film, Model II was used to approximate the nanocomposite mechanical behavior below and above T_g for these mechanically percolating systems.

$$E_c = \frac{(1-\lambda)(1-V_f)E_f^{disp}E_f^{agg} + (1-\lambda)(V_f+\lambda-1)E_m E_f^{agg} + \lambda^2 E_m E_f^{disp}}{(1-V_f)E_f^{disp} + (V_f+\lambda-1)E_m} \qquad (7.2)$$

In Model II percolation, E_c is the composite modulus, E_f^{disp} is the moduli of the dispersed filler network or CNC moduli, E_f^{agg} is the moduli of the aggregated network or pure

CNC film moduli, and E_m is the moduli of the pure PVA matrix. E_f^{disp} was taken to be 50 GPa,[204] and E_f^{agg} was determined by fitting E_c to the experimental data to see the reinforcing potential for each system.[52,145] λ was calculated using the following expression

$$1 - \lambda = V_f \left(\frac{V_f - V_c}{1 - V_c}\right)^b \qquad (7.3)$$

where b is 0.4 for a three dimensional network.[205,206] Figure 7.9 shows the percolation model fits for 31K, 85K, and 146K films.

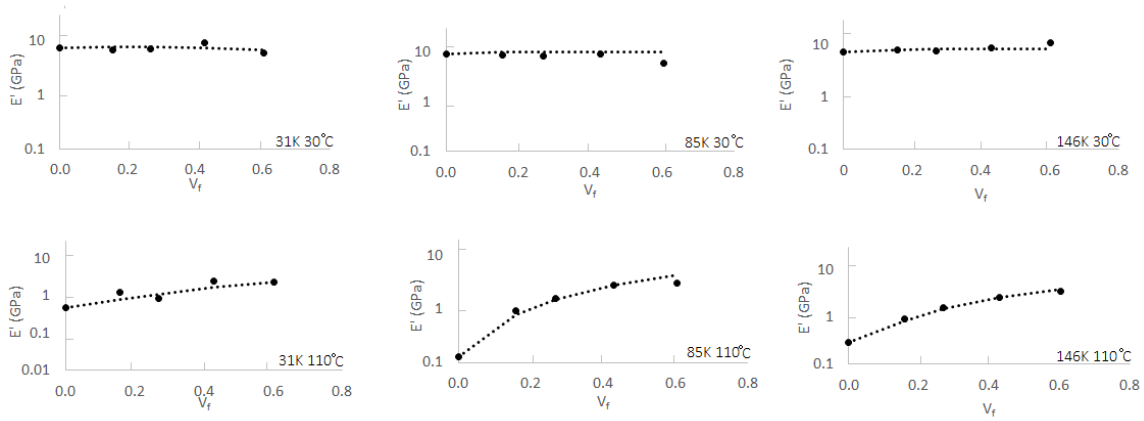

Figure 7.9: Model II percolation models fitted using equation 7.2 for E' values below and above the T_g for CNC/PVA nanocomposites.

From these models, E_f^{agg} was used as an adjustable parameter and used to understand the relative network strength in each system. The values for E_f^{agg} are shown in Table 7.1 with deviation on the E_f^{agg} values calculated by modeling the lowest and highest modulus behavior found for the three DMA tests conducted on each sample.

Percolation type behavior was seen to be more pronounced for the high temperature data as polymer mobility was increased and the relative contribution of the CNCs was increased due to larger differences in the component moduli at higher temperatures. A better model fit was also seen for the 85K and 146K compared to the 31K nanocomposite data due to the larger effect of T_g at lower molecular weights as the 85K and 146K nanocomposites were closer to T_g than the 31K, altering the polymer modulus values to be outside the model assumptions. Comparable E_f^{agg} values were seen for the high temperature 85K and 146K data indicating increased nanocomposite reinforcement of the CNCs, most likely due to increased network contribution of PVA with increasing molecular weight allowing for higher potential modulus compared to 31K data. The values of E_f^{agg} calculated for the high temperature systems was used for the low temperature fit due to the increased percolation behavior seen at high temperatures. At high temperatures, the reinforcing contribution of the CNCs was more predominant as the polymer mobility was increased. A good fit was seen for all low temperature values using this method besides the 67 wt.% CNC systems for each molecular weight. For the 31K and 85K systems, experimental values were lower than predicted while for the 146K systems, experimental values were higher than predicted. This was most likely due to the increased crystallinity seen from XRD with increasing nanocomposite molecular weight.

Table 7.1: E_f^{agg} data calculated from Model II percolation modeling for CNC/PVA systems at 31K, 85K, and 146K samples

Sample	E_f^{agg}
31K 30 °C	4.2 ± 0.9
31K 110 °C	4.2 ± 0.5
85K 30 °C	8.9 ± 4.1
85K 110 °C	8.9± 0.2
146K 30 °C	7.8 ± 0.5
146 110 °C	7.8 ± 1.6

The behavior of the loadings below V_c were modeled using the Halpin-Tsai equation[207] shown below. The Halpin-Tsai model assumed uniform distribution of the CNCs inside the PVA matrix as well as good adhesion between the CNCs and PVA.

$$E = \frac{3}{8}E_t + \frac{5}{8}E_l \qquad (7.4)$$

$$E_l = \left[\frac{1+2\frac{l}{d}\eta_l V_f}{1-\eta_l V_f}\right]E_m \qquad (7.5)$$

$$E_t = \left[\frac{1+2\eta_t V_f}{1-\eta_t V_f}\right]E_m \qquad (7.6)$$

$$\eta_l = \frac{\frac{E_f}{E_m}-1}{\frac{E_f}{E_m}+2\frac{l}{d}} \qquad (7.7)$$

$$\eta_t = \frac{\frac{E_f}{E_m}-1}{\frac{E_f}{E_m}+2} \qquad (7.8)$$

where E is the composite modulus determined by the Halpin-Tsai Model, E_t is the transverse elastic modulus of the composite, E_l is the longitudinal elastic modulus of the composite, $^l/_d$ is the aspect ratio of the CNC, η_l helps to correlates the stiffness of the

composite in the longitudinal direction and η_t correlates the stiffness of the composite is the transverse direction. E_f is the fiber elastic modulus and E_m is the matrix elastic modulus. Figure 7.10 shows the fit of the Halpin-Tsai model for the 146K films below V_c at 30 °C and 110 °C. As shown by the model in Figure 7.10, the Halpin-Tsai model showed a good fit for those films at very low loadings below or around V_c of 0.8 vol.% and 4.0 vol.% CNC with increasing deviation as the CNC loading was increased. These data showed that at low CNC loadings, there if uniform distribution of CNCs as well as good adhesion with the PVA matrix. In comparison, the fit for the data at temperatures below T_g shown in Figure 7.10 was not as good. These differences in fit can be thought of as upper and lower bounds for the CNC/PVA systems. While the model at high temperatures gave a good understanding of a more CNC controlled system, the model at low temperatures varied due to the increased effect of PVA in the glassy state.

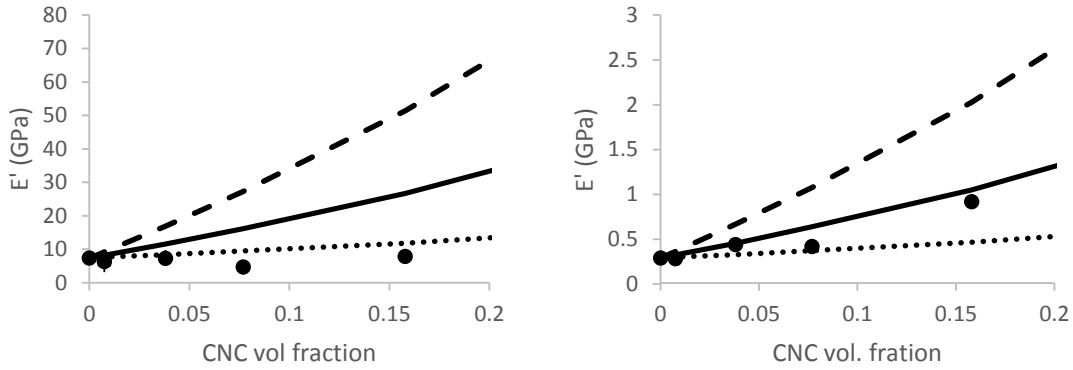

Figure 7.10: Halpin-Tsai model fit to 146K data at loadings below V_c. 30 °C data shown on the left while 110 °C data shown on the right. E_l (long dashed line), E_t (dotted line), E (solid line), and experimental data shown by markers.

To increase understanding of the morphology of the CNCs inside the polymer matrix, a representative volume element model was constructed to determine CNC

spacing within the matrix. In this model, the aspect ratio of the CNCs was taken into account to determine the approximate spacing between each CNC if individually dispersed, shown in Figure 7.11. The distance (*2d*) between each CNC are given in Table 7.2. The diameters of the CNCs were between 6 and 10 nm while the length of the CNCs were 163 nm as determined through the dynamic light scattering size test. From this representative volume element analysis, it can be seen that the percolation threshold found to be about 2.5 vol.% (3.2 wt.%) was a reasonable assumption. At 5 wt.% CNC, it can be seen that the distance between each CNC was about three to four times the diameter of the CNC and less than a fourth of the length, giving good probability for the formation of a percolated system.

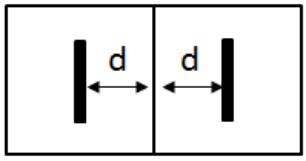

Figure 7.11: Representative volume element shown to calculate the *d* spacing between CNCs.

Table 7.2: Calculated values from the representative volume element model.

CNC wt.%	CNC vol.%	$2d_x$ (nm)
1	0.8	82
5	4.0	32
10	8.1	20
20	16.5	12
33	28.0	7
50	44.1	4
67	61.5	2

7.4 DMA Freeze-dried CNCs

Freeze-dried CNCs were added into the 146K PVA systems using solution processing and shear processing methods. CNCs were solution processed by either adding freeze-dried CNC powder directly to the PVA solutions or by redispersing the freeze-dried CNC powder and adding it to PVA solutions followed by film casting. CNCs were shear processed in a batch mixer at either 40 RPM or 91 RPM by directly adding freeze-dried CNC powder into a PVA solution, stirring the solution by hand to wet the fibers, and then adding the suspension into the mixing bowl. DMA was conducted on each of these films and the E' data below and above T_g is shown in Figure 7.12. As shown in Figure 7.12, E' did not increase systematically with increasing CNC content for all processing methods. This scatter of data was attributed to aggregation of the CNCs. Aqueous suspended CNC/PVA nanocomposites saw continuously increasing E' with increasing CNC loading due to good dispersion and distribution of the CNCs inside of the matrix allowing for adhesion of the components through hydrogen bonding and CNC network formation as previously discussed. Through the incorporation of freeze-dried CNCs, aggregation was increased, most likely decreasing the level of potential hydrogen bonding inside the matrix as well as the ability for CNCs to form a continuous network at higher CNC loadings.

To better understand the morphology of each processing method of freeze-dried CNCs, the individual values were examined. The first, the solution processed freeze-dried CNCs experienced an increase in E' with CNC loading from neat PVA to 20 wt.% to 33 wt.% CNCs in the film, indicating increased hydrogen bonding and interaction of the components at these loading levels followed by a decrease in E' at loadings of 50 wt.%

and 67 wt.%, most likely due to increased aggregation of the CNCs leading to decreased stress transfer capabilities. The RDFD CNC/PVA nanocomposite system at high CNC loadings of 20 wt.% to 50 wt.% experienced a similar trend with increased E' from neat PVA to 50 wt.% CNCs followed by a decrease in E' at 67 wt.% CNCs. This increase in E' compared to solution processed freeze-dried CNC/PVA systems indicated better stress transfer characteristics and therefore increased dispersion and distribution of the CNCs inside the PVA. The shear processed CNC/PVA systems at 40 RPM and 91 RPM both saw increasing E' with CNC content from 20 wt.% to 67 wt.% CNC but also experienced a decrease in E' with CNC addition. This decrease in E' from neat PVA to 20 wt.% CNC indicated that the CNCs reinforcing potential was not as great due to aggregation. At low loadings (1 wt.% to 10 wt.% CNC) in the RDFD CNC/PVA system, a similar trend was seen as in the aqueous suspended CNC system. The E' at low loadings of 10 wt.% and below remained fairly constant within the calculated error both below and above T_g due to the proximity to the percolation threshold.

The E' trend above the T_g at 110 °C was significantly more systematic due to increased component mobility decreasing the effect of bound water acting as a plasticizing agent as well as increased contrast in the component moduli. Aqueous suspended CNC/PVA systems increased with increasing CNC content as previously discussed. The shear processed samples at 40 RPM and 91 RPM also increased with increasing CNC content due to the confinement of the PVA chains and increased stiffness of the CNCs but had lower values than the solution processed freeze-dried, RDFD, and aqueous suspended CNC/PVA systems due to increased aggregation of CNCs. RDFD and aqueous suspended CNC/PVA systems tended to have similar mechanical behavior

due to increased dispersion and distribution. A trend was seen in the solution processed freeze-dried CNC/PVA system in which the 20 wt.%, 33 wt.%, and 50 wt.% CNC films experienced increased E' compared to any other nanocomposite system tested. From the images taken of the solution processed freeze-dried system seen in Chapter 4, it was known that aggregation of CNCs was present. This aggregation should have caused decreased E' behavior due to the aggregates breaking up the PVA network and acting as stress condensers in the system. This increase in E' could be contributed to the CNC aggregates acting as a network of aggregates increasing hydrogen bonding between CNCs as shear induced phase separation was not seen in the solution processed systems. Future research on these systems could include the development of a methodology for imaging such dried systems to further understand the morphology.

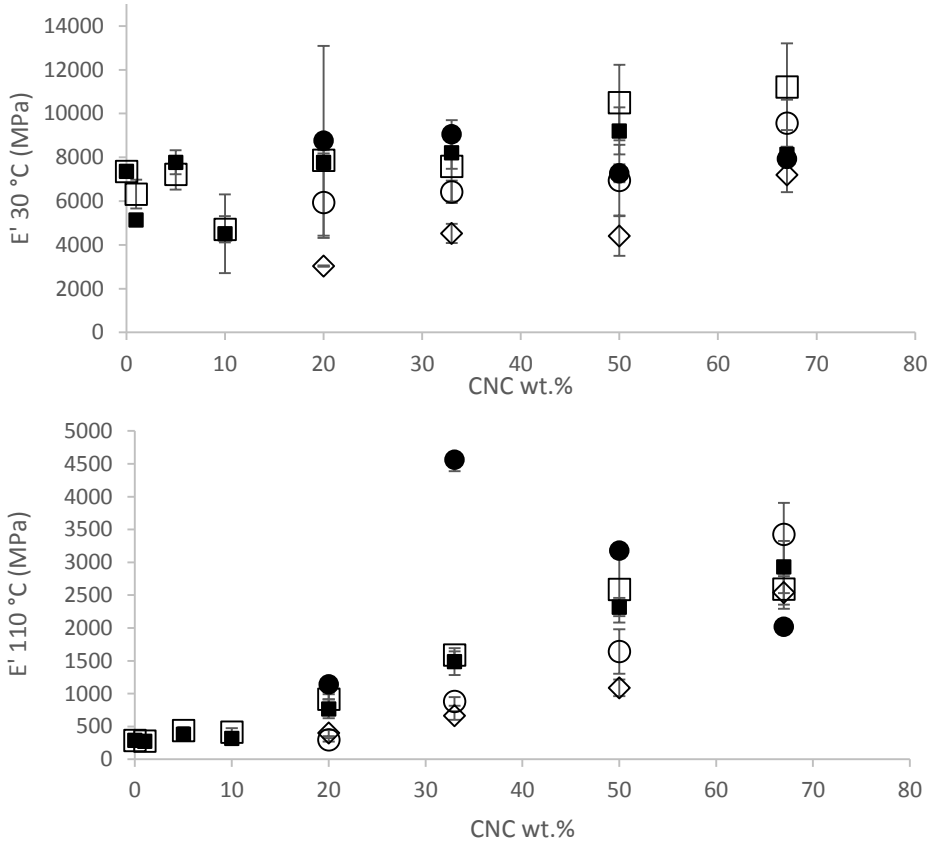

Figure 7.12: *E'* behavior at below the T_g (30 °C) (top) and above the T_g (110 °C) (bottom) of aqueous suspended and freeze-dried CNC/PVA systems from various processing methods: aqueous suspended solution processed CNC/PVA systems (□), freeze-dried solution processed CNC/PVA systems (●), RDFD CNC/PVA systems (■), freeze-dried shear processed 40 RPM systems (○), and freeze-dried shear processed 91 RPM systems (◇).

The T_g of each of the CNC/PVA film was compared as shown in Figure 7.13 with respect to CNC addition method. For example, the aqueous suspended solution processed CNC/PVA films were compared to the RDFD systems in the top plot of Figure 7.13, the systems in which freeze-dried CNC powder was directly mixed into PVA solutions are shown in the middle plot of Figure 7.13, and all the freeze-dried CNC systems are shown in the bottom plot of Figure 7.13. Aqueous suspended CNC/PVA systems and RDFD CNC/PVA systems showed similar T_g behavior with the exception of

the 20 wt.% and 33 wt.% CNC systems. In these systems, the aqueous suspended CNC/PVA nanocomposites showed high T_g indicating decreased molecular mobilty leading to increased interactions. The increase in T_g for these two nanocomposite loading is most likely due to RDFD CNC aggregation. In comparison, in the systems in which direct addition of CNCs were examined, it was seen that the 40 RPM has the highest T_g values. This increase in T_g could be attributed to the effect of shear mixing on PVA compared to solution processing. For example, shear induced phase separation of PVA was seen rheologicially in the neat PVA system mixed at 40 RPM while extensive shear induced polymer phase separation was seen in the system mixed at 91 RPM. The increase in T_g at 40 RPM could be attributed to this increased polymer phase separation leading to increased polymer only and cellulose only regions and therefore PVA crystallite formation, decreasing the overall mobility of the chains, especially with the addition of CNCs. While the 91 RPM system still contained crystallites from the shear induced phase separation of the PVA during mixing, aggregation of CNCs was increased, increasing the phase separation in the system and the regions of pure PVA and pure CNC in the nanocomposite, thus increasing the available mobility due to larger phase separated regions. In the solution processed system, crystallite formation was not as prevelant and shear induced phase separation of the PVA was not as severe leading to lower interaction of the CNCs and PVA and a lower T_g. While all three systems showed similar aggregation of CNCs through optical microscopy, the 40 RPM systems had the highest T_g while the solution processed freeze-dried and the 91 RPM systems had similar T_g values with the exception of 20 wt.% CNC where the effect of PVA would be more prevalent. Finally, the bottom plot of Figure 7.13 shows the comparison of all the freeze-dried CNC

systems. From this comparison, the effect of shear processing on the 40 RPM CNC/PVA system can be most effectively seen as this system possessed the highest T_g values most likely due to increased PVA crystallite formation with minimized aggregation compared to the 91 RPM system. It was also seen that there appeared to be two regions in T_g behavior: a PVA dominant region and a CNC dominant regions. At loadings below 50 wt.%, the effects of processing and dispersion were more clearly seen in the variation of T_g with CNC type and processing method while at loadings of 50 wt.% and 67 wt.% especially, there appeared to be a convergence of T_g as the CNCs were the predominant component in the system, similar to the yield stress seen through the rheological characterization in Chapter 5.

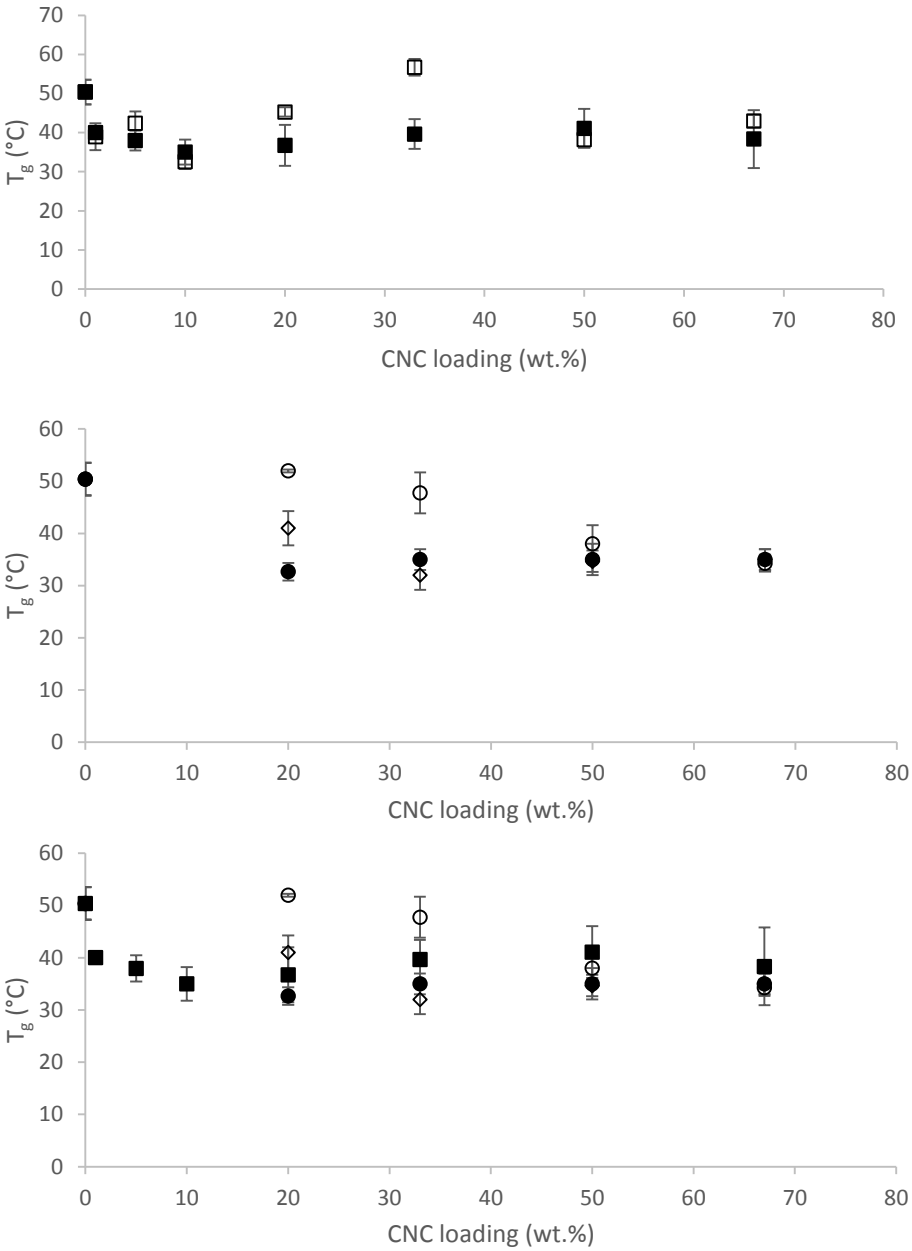

Figure 7.13: T_g values for each CNC/PVA nanocomposite processing method studied: CNC/PVA films made from suspension of CNCs (top), CNC/PVA films made through direct addition of freeze-dried CNC powder (middle), all freeze-dried CNC/PVA solutions (bottom). Aqueous suspended solution processed CNC/PVA systems (□), freeze-dried solution processed CNC/PVA systems (●), RDFD CNC/PVA systems (■), freeze-dried shear processed 40 RPM systems (○), and freeze-dried shear processed 91 RPM systems (◇).

Finally, the T_g of RDFD CNC/PVA nanocomposite systems found from DSC and DMA was compared in Figure 7.14. The RDFD CNC/PVA systems showed comparable T_g values for both the DSC and DMA at high loadings of 20 wt.% CNC and above, most likely due to increased aggregation of the CNCs decreasing the variability of T_g measured through energy lost vs. heat capacity. There was some variation at the low RDFD CNC loadings of 1 wt.%, 5 wt.%, and 10 wt.% CNC, specifically, the DSC showed a higher T_g value than the DMA. This higher T_g value was most likely attributed to the increased agglomeration of the CNCs. The T_g values determined through DMA showed a decrease in T_g from 1 wt.% to 10 wt.% CNC followed by an increase in T_g at 20 wt.% CNCs. This was most likely due to CNC network formation.

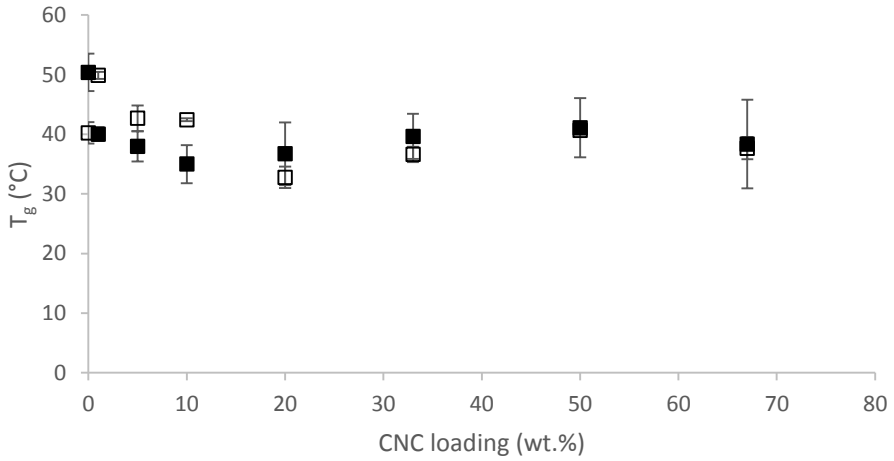

Figure 7.14: T_g values from the DMA (■) and DSC (□) for RDFD CNC/PVA nanocomposite systems.

The percolation model used for the aqueous suspended CNC systems was also used to study the freeze-dried CNC systems. Increased percolation was seen above T_g compared to below T_g due to the increased reinforcing effect of the CNCs as PVA

mobility increased above T_g. Model II, shown in section 7.3 equation 7.2, was used to fit the data using E_f^{agg} from the 146K aqueous suspended CNC films (8 GPa) due to their increased dispersion, shown in Figure 7.15. As shown in Figure 7.15, below T_g, the deviation from the experimental data to the modeled data was very large in general due to the rigid state of the PVA, decreasing the effect of the CNCs reinforcement as E' represented an upper bound for the mechanical data. The percolation model had the best fit for the aqueous suspended and RDFD CNC systems due to the increased dispersion of the CNCs inside the PVA, giving these systems higher E_f^{agg} values. All freeze-dried films without redispersion of CNCs saw large deviations from experimental to modeled data. The shear processed systems at 40 RPM and 91 RPM saw similar data trends in that the model predicted higher E' than was experimentally collected due to large amounts of aggregation of the CNCs weakening the CNC network. Finally, the solution processed freeze-dried systems showed very different E' behavior than any of the other CNC systems, aqueous suspended or freeze-dried. In this system, a maximum E' values was seen at 33 wt.% CNC followed by decreasing E' values. This increase at 33 wt.% could be due to polymer mediated and CNC mediated networks formed in the solid state as mobility of the PVA is decreased due to decreased phase separation of PVA during solution processing, allowing for the CNCs to be more distributed within the PVA, decreasing the PVA only domains and their ability to become rubbery above T_g.

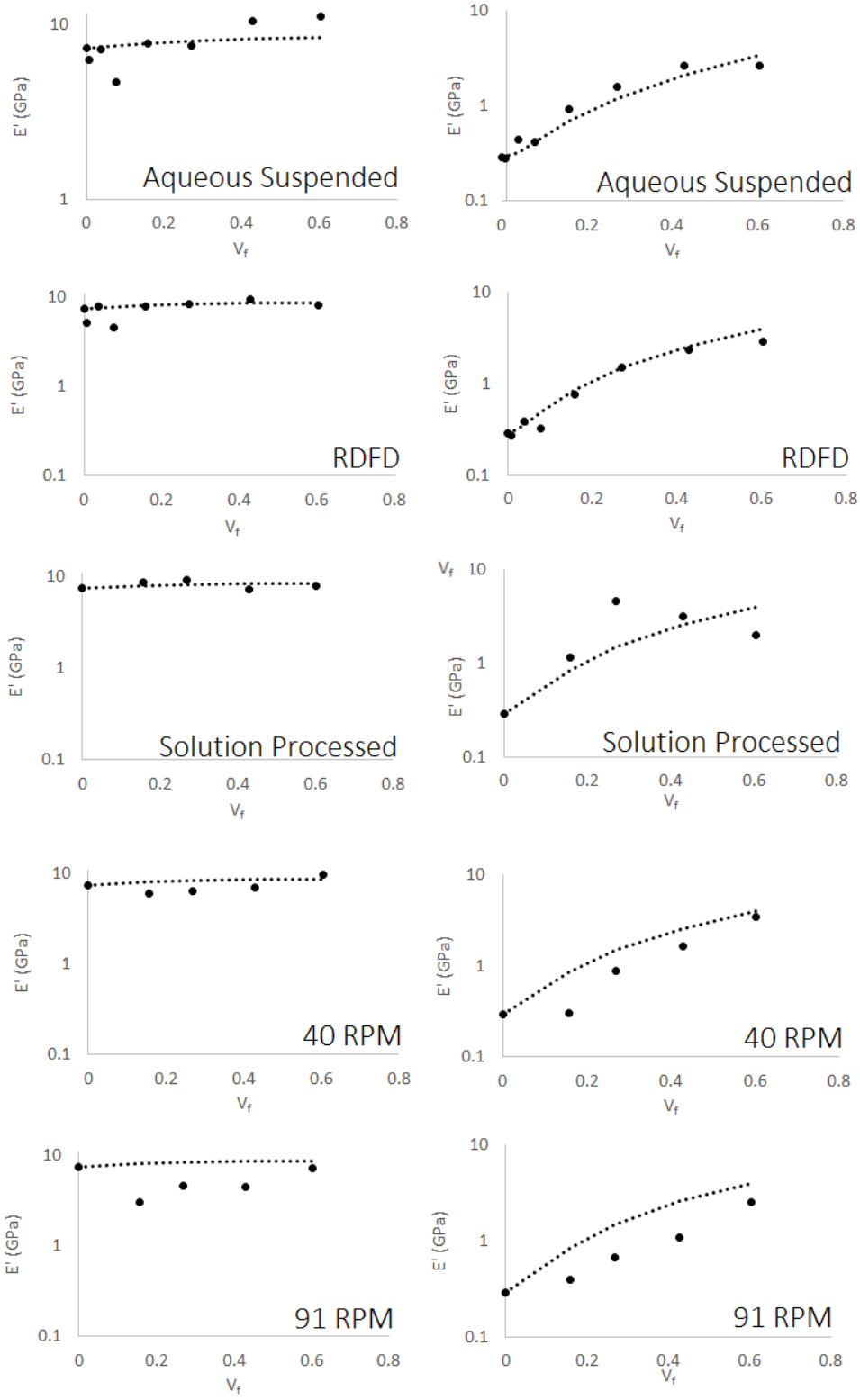

Figure 7.15: Model II percolation fit to freeze-dried CNC/PVA systems with the aqueous suspended CNC/PVA systems shown for comparison at 30 °C (left) and 110 °C (right). All samples are at 146K molecular weight.

The Halpin-Tsai model was also applied to the RDFD systems and compared to the aqueous suspended CNC systems shown in Figure 7.16. The RDFD CNC data were very similar to the aqueous suspended CNC data at temperatures above T_g in that below and very near percolation the Halpin-Tsai model showed a good fit while this fit deviated with increasing CNC loading due to aggregation of CNC. At temperatures below T_g, the experimental data deviated from the Halpin-Tsai predicted data toward E_t for all loadings of the RDFD CNC samples, most likely due to the increased size seen from the dynamic light scattering measurements lowering V_c for these systems and potentially adding increased orientation defects which were corrected above T_g as previously discussed.

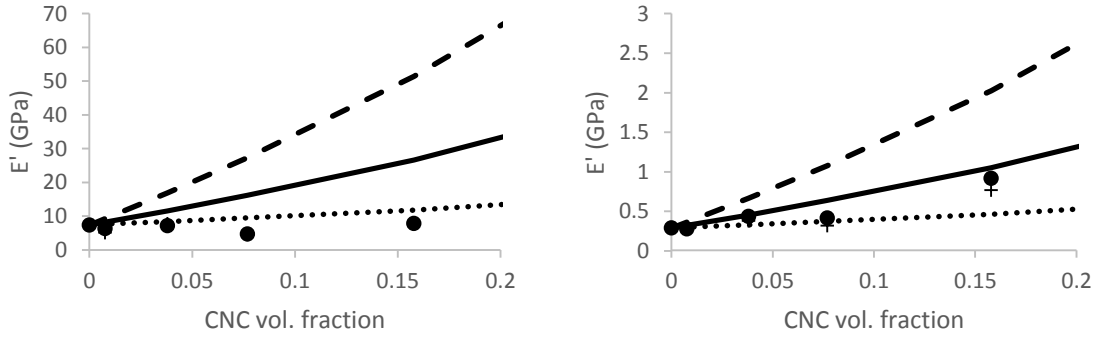

Figure 7.16:Halpin-Tsai model fit to 146K RDFD data at CNC/PVA loadings below V_c. 30 °C data shown on the left while 110 °C data shown on the right. E_l (long dashed line), E_t (dotted line), E (solid line), aqueous suspended CNC systems (●), and RDFD CNC systems (+).

7.5 Tensile Testing of Solution Processed and Freeze-dried CNC/PVA Systems

MTT was conducted on both aqueous suspended CNC/PVA and RDFD CNC/PVA systems at 146K molecular weight to determine the tensile stress and strain at failure. Tensile stress and strain at failure occurred either at the onset of crack propagation in more elastic samples (those that contained a yield stress) or at sample break (in the brittle samples without yield stress). Both wet and dry samples were tested. Representative tensile data from these wet and dry specimens are shown in Figure 7.17 for both systems. As expected, the wet tensile data showed a higher percent strain at failure while the dry tensile data showed higher stress at failure as the water acts as a plasticizing agent in the wet CNC system. Strain at failure was seen to decrease with CNC loading due to the increased crystallinity of the samples for both wet and dry specimens. Yield stress was also seen to increase with CNC loading due to the increased reinforcing effect of the CNCs.

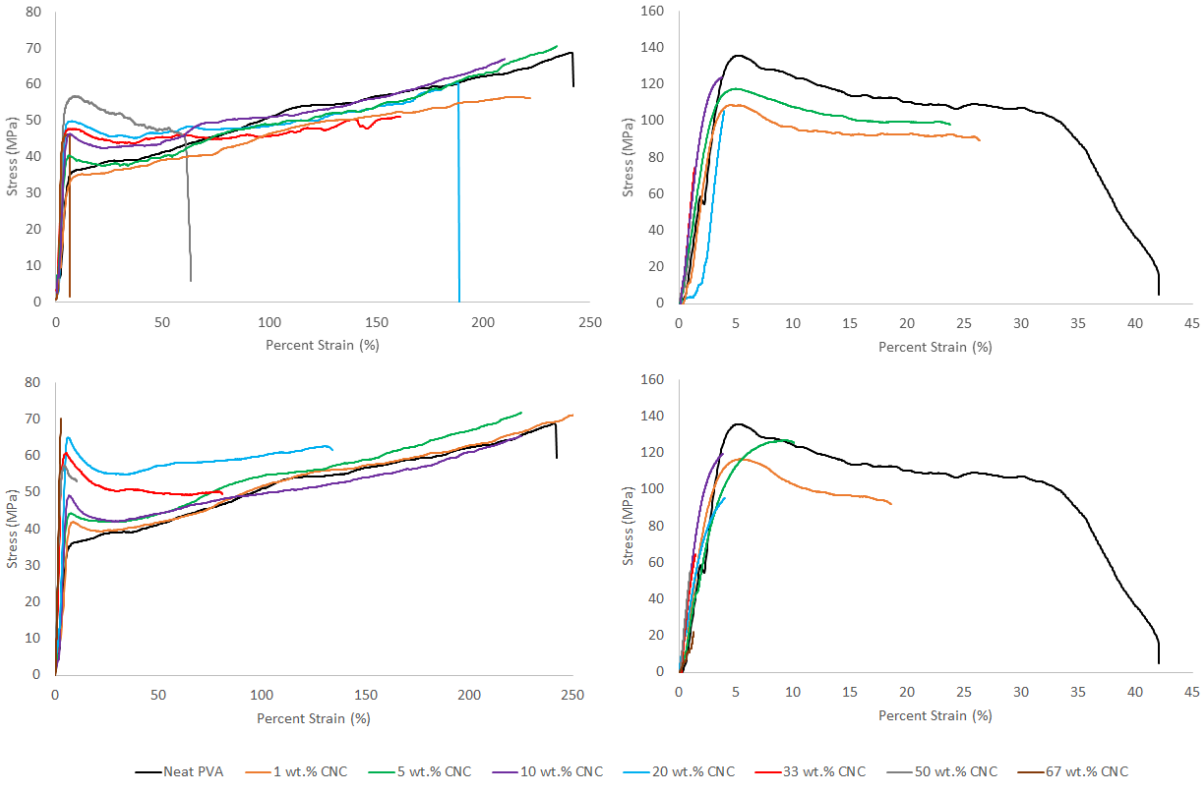

Figure 7.17: Representative stress and strain data for wet and dry aqueous suspended and RDFD CNC/PVA systems. Wet aqueous suspended CNC/ PVA systems (top left), dry aqueous suspended CNC/PVA systems (top right), wet RDFD CNC/PVA systems (bottom left), and dry DRFD CN/PVA systems (bottom right).

Tensile stress at yield and break and percent strain at yield and break are shown in Figure 7.18. Tensile stress at yield was seen for all the aqueous suspended CNC wet samples and almost all the RDFD CNC wet samples but for only the very low loaded dry samples for both aqueous suspended and RDFD CNC/PVA systems due the increased brittleness. The absence of a yield behavior for the dry samples above 5 wt.% CNC was due to the increased crystallinity of the system and the absence of water acting as a plasticizer. For the aqueous suspended and RDFD CNC systems, yield stress increased slightly in the wet samples and remained relatively constant in the dry samples exhibiting yield. The slight increase seen in yield stress in the wet CNC samples was attributed to

the increased strength imparted on the system by the CNCs as the films were less brittle. Percent strain at yield decreased for both CNC systems in the wet and the dry state due to increased crystallinity with the exception of 1 wt.% CNC in the aqueous suspended systems. This increase in percent strain at yield was due to the increased dispersion of the aqueous suspended CNCs compared to the RDFD CNCs as well as CNC loading below the percolation threshold, allowing for the PVA to impart increased elasticity. While the tensile stress at break was 30 to 70% larger for dry samples compared to wet samples, the percent strain at break was on the order of 7000% larger for wet samples compared to dry samples for both aqueous suspended and freeze-dried CNC/PVA systems when PVA was the predominant component. This behavior was attributed to increased mobility of polymer chains with the addition of water. Tensile stress at break decreased in both wet and dry samples with increasing CNCs presumably due to the increased crystallinity of system. The difference in wet and dry percent strain at break also decreased with increasing CNC loading, and converged at similar values for the highest CNC loading of 67 wt.% due to the very high crystallinity of the PVA at these loadings.

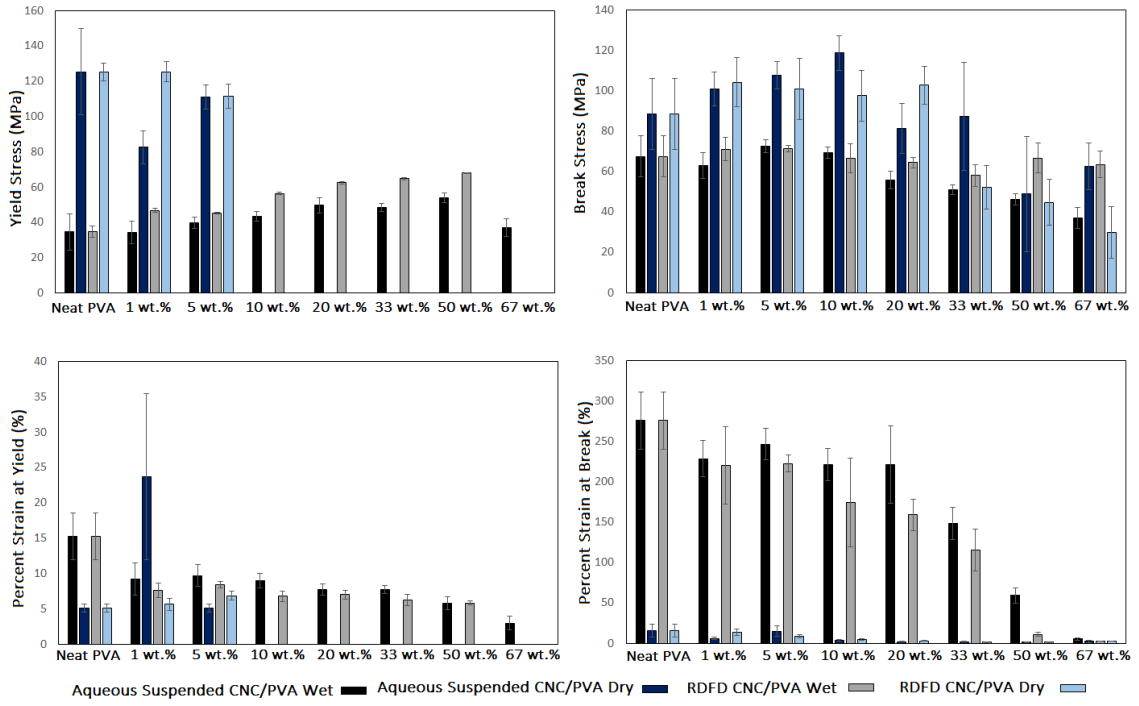

Figure 7.18: Tensile yield stress and strain and break stress and strain for aqueous suspended and RDFD nanocomposite systems.

7.6 Conclusions

In conclusion, E' for neat PVA decreased with increasing molecular weight above T_g due to increased bound water. T_g found from E'' was compared to T_g found from the DSC and was seen to have increased sensitivity to molecular weight as T_g decreased with increasing molecular weight due to increased polymer mobility with bound water. Aqueous suspended CNC system E' increased with increasing molecular weight and CNC content above and below T_g due to the increased rigidity imparted on the system by the CNCs. For the aqueous suspended CNC systems, T_g found from E'' was seen to be less pronounced with increased CNC content due to increased crystallinity. Three regions

of mobility were seen below, at, and above the percolation threshold. First, T_g decreased with increasing CNC content below the percolation threshold due to incomplete CNC network formation allowing increased mobility of the PVA. Next, T_g increased around the percolation threshold due to decreased chains mobility as the CNC network restricted the PVA. Thirdly, T_g decreased at loadings far above the percolation threshold due to the increased contribution of the CNCs as the predominant component decreasing polymer chain – polymer chain entanglements. Below T_g, trends in the elastic rheological data corresponded to the DMA data. Here, aqueous suspended CNC systems had the highest E' due to increased dispersion of the CNCs allowing for increased mechanical behavior. Increasing aggregation decreased E' below T_g as aggregates broke up the PVA chain entanglement creating stress condensers. Above T_g, E' increased with increasing CNC content for all samples processed. Here, the reinforcing effect of the CNCs in the rheological data was not directly related to the solid-state data in that increased aggregation did not directly correlate to decreased mechanical properties.

Solution processed freeze-dried CNCs were seen to have the largest E', attributed to increased aggregate-aggregate interaction as phase separation was not as pronounced in solution processing compared to shear processing. The T_g data collected from E'' correlated to the rheological data in that increasing aggregation increased PVA chain mobility due to larger PVA regions and CNC regions. While aqueous suspended CNC systems had three regions of T_g, freeze-dried CNC systems had either two (RDFD CNC and 40 RPM): polymer controlled and CNC controlled, or one (solution processed and 91 RPM): CNC controlled, due to the effects of aggregation on the system limiting polymer mobility and polymer phase separation. Percolation was modeled and found to be in good

agreement with the experimental data. A percolation threshold of 0.025 was calculated. The Halpin-Tsai model was used to understand the dispersion of aqueous suspended and RDFD CNCs below the percolation threshold. The aqueous suspended CNC systems and the RDFD CNC systems were seen to have good dispersion below percolation.

MTT showed water acted as a plasticizer increasing CNC/PVA percent strain and decreasing stress. In general, aqueous suspended CNC systems had higher percent strain and stress due to increased dispersion. Stress decreased with increased CNC content due to increased crystallinity. Yield stress was present in systems at low CNC loading but not present at systems above 10 wt.% CNC due to increased crystallinity of the system causing increased brittleness in the nanocomposite.

CHAPTER 8

SUSTAINABILITY AND SCALABILITY

In Chapter 8, the biodegradation, water recoverability, and scalability potential of CNC/PVA nanocomposite systems will be discussed. Only aqueous suspended CNC/PVA systems were studied for their ability to biodegrade and for water to be recovered. The potential for industrial scalability will also be assessed through the examination of current batch mixing processes.

8.1 Introduction

Although PVA is a biodegradable polymer system in the presence of certain microorganisms such as *Fusarium lini*, a phytopathogenic fungus, limited biodegradation is seen in composting environments with neat PVA systems, especially those with a higher degree of hydrolysis. Chiellini *et al.*[10] proposed that the primary reason for this limited biodegradation is due to adsorption by inorganic and organic particles in the soil. This adsorption was seen to only increase with hydrolysis due to the presence of hydroxyl groups further decreasing the biodegradability in soil of neat PVA. As CNCs are a naturally biodegradable material, it is assumed the addition of CNCs will increase biodegradation of PVA based films in soil burial tests. Though significant work has not be conducted on the biodegradation of CNC/PVA composites, PVA with lignocellulosic fibers of sugar cane bagasse (SCB) studied through respirometric procedure and saw up to 35% mineralization after 150 days with pure SCB and 24% mineralization at 50/50

PVA/SCB ratios.[208] A similar increase in biodegradation is anticipated after the addition of CNCs to PVA films.

8.2 Biodegradation

Biodegradation studies were conducted to determine the environmental sustainability of the nanocomposite films. Both 85K and 146K molecular weight samples were examined via soil burial tests. Swell, degradation, and FTIR tests were conducted to analyze the biodegradation characteristics of the CNC/PVA films. Figure 8.1 show the swell testing results for 85K and 146K samples respectively. From the normalized percent swell data, for both 85K and 146K samples, a large decrease in percent swell was seen between the first 13 days followed by a plateau region in which the normalized percent swell did not change drastically between day 13 and 101, shown in the inset of Figure 8.2. While the normalized percent swell decreased more quickly in the predominantly PVA 85K samples with a biodegradation rate, or the change in normalized percent swell with time shown below,

$$biodegradation\ rate = \frac{S^n}{time\ in\ days} \qquad (8.1)$$

of 0.24 compared to 0.14 for the 85K 67 wt.% CNC samples, there was a larger decrease in normalized percent swell after 101 days in the 85K 67 wt.% CNC samples. These 85K 67 wt.% CNC films decreased to 62% normalized percent swell while the 85K neat PVA and 85K 67 wt.% CNC samples showed 74% and 72% normalized percent swell. This

larger decrease in swell indicated increased biodegradation behavior. In the 146K samples, percent swell increased only slightly with biodegradation rate of 0.19, 0.20, and 0.22 for 146K neat PVA, 146K 33 wt.% CNC, and 146K 67 wt.% CNC respectively showing little difference in swell or network behavior due to increased crystallinity.

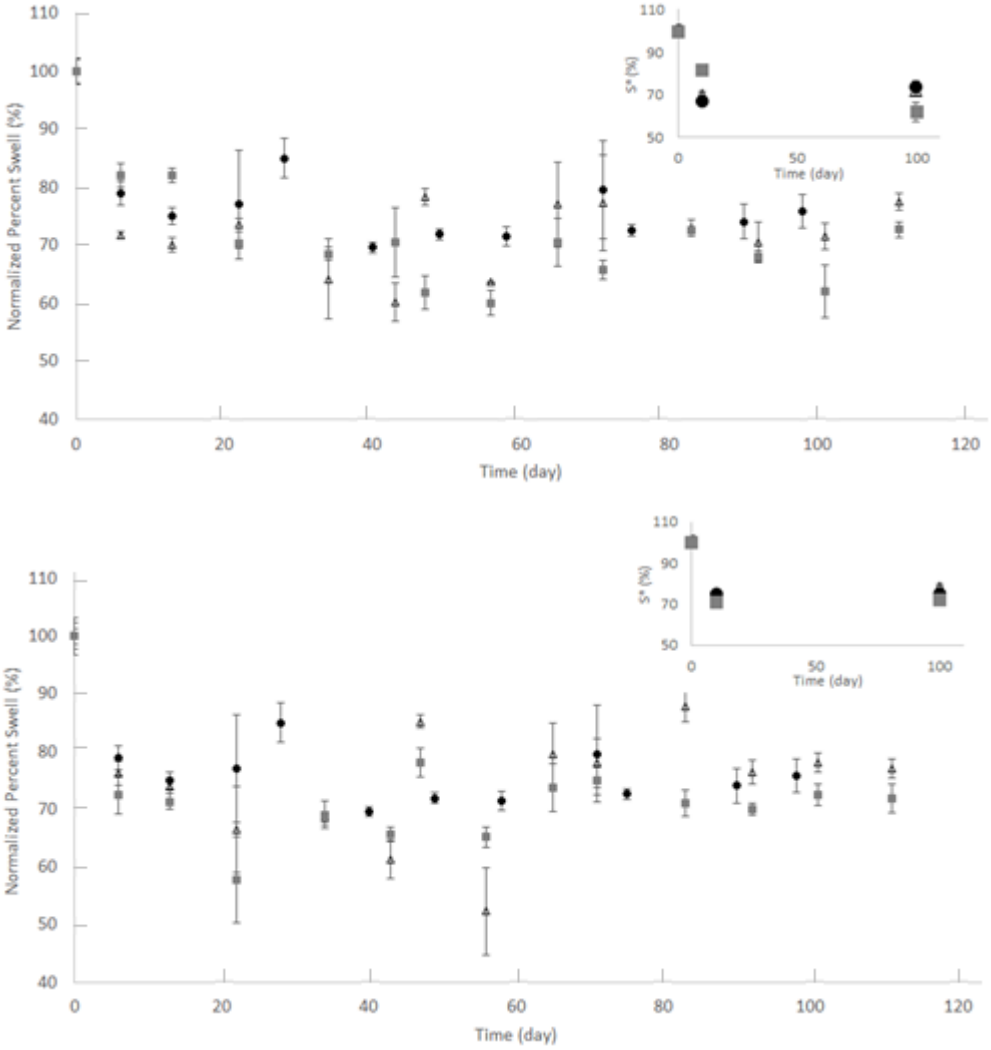

Figure 8.1: Normalized percent swell for 85K (top) and 146K (bottom) biodegradation samples. Neat PVA (●), 33 wt.% CNC (△), and 67 wt.% CNC (■).

To further understand the mechanisms of biodegradation in the CNC/PVA films, degradation analysis of the onset temperature was studied through TGA experiments. The

results of these experiments can be found in Figure 8.3. While the neat films onset temperature increased universally with biodegradation, the 67 wt.% CNC sample onset temperature decreased with increasing biodegradation. Fully hydrolyzed PVA is only slightly biodegradable in soil.[10] The increase in swell behavior for the neat PVA samples could be attributed to an increase in C-H bonding during biodegradation as confirmed by FTIR, increasing the degradation onset temperature. The addition of CNCs shows a steadily decreasing degradation onset temperature indicating increased biodegradation characteristics as the bonds are cleaved and the samples become less thermally stable.

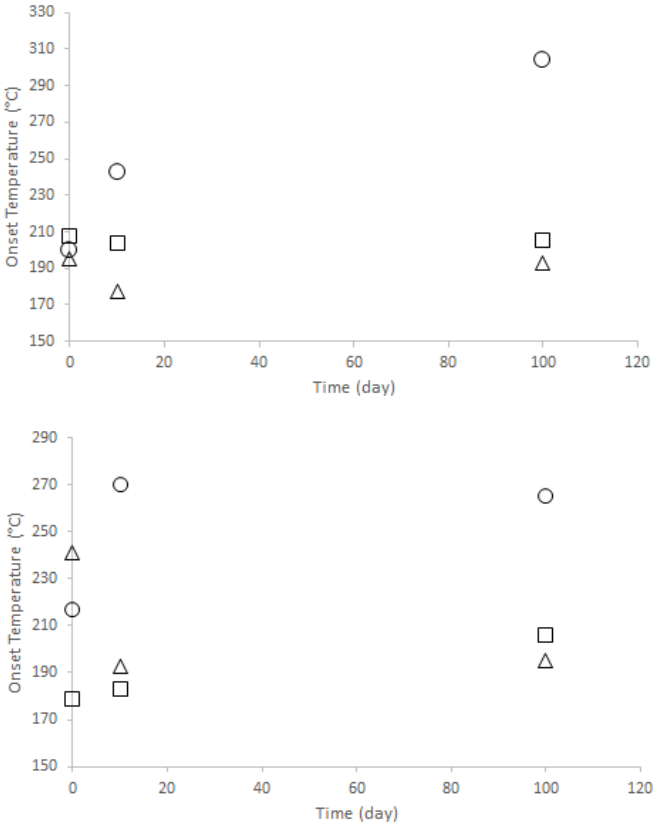

Figure 8.2: TGA onset temperature at biodegradation time points of 0, 13, and 100 times. Top 85K and bottom 146K. Neat PVA samples (○), 33 wt.% CNC samples (□), and 67 wt.% CNC samples (△).

Finally, FTIR was used to determine the structural changes occurring during biodegradation. Figure 8.3 displays 146K neat PVA and 146K 67 wt.% CNC for comparison. There is a reduction in the asymmetric C-H stretching absorbencies at 2908-2911 cm^{-1} due to sample degradation for the 146K 67 wt.% CNC films. An opposite trend was seen for the neat PVA, in which there was a sharpening of the C-H stretching absorbencies at 2908-2911 cm^{-1}. This sharpening of the asymmetric peak could be due to increased C-H bonds in the 146K neat PVA samples, indicating increased sample crystallinity as the amorphous regions were degraded preferentially. Sharp peaks appeared at 1649 cm^{-1} and small peaks appeared at 1558 cm^{-1} to 1560 cm^{-1} indicating amide I and II group formation pointing toward microbial growth in the 146K neat PVA and 146K 67 wt.% CNC films.[11,209] There was also an increase in the band at 1649 cm^{-1} for the 146K 67 wt.% CNC samples indicating microorganism growth on the films. Microbial growth was also visually seen on neat and nanocomposite samples during the biodegradation process.

Through the FTIR analysis, it can be seen that the addition of CNCs increased the biodegradation process while only minimally affecting the biodegradation rate. Through the swelling behavior, onset temperature, and FTIR analysis, it was seen that PVA was minimally biodegradable – most notably seen through the onset temperature increase. While increasing CNC content increased the biodegradation characteristics of the films (decreased bonding ability and microbial growth) over the full time period tested, the biodegradation during the initial 13 days was only minimally increased with CNC loading. The effect of molecular weight showed little change on the biodegradation of the films through the analysis conducted.

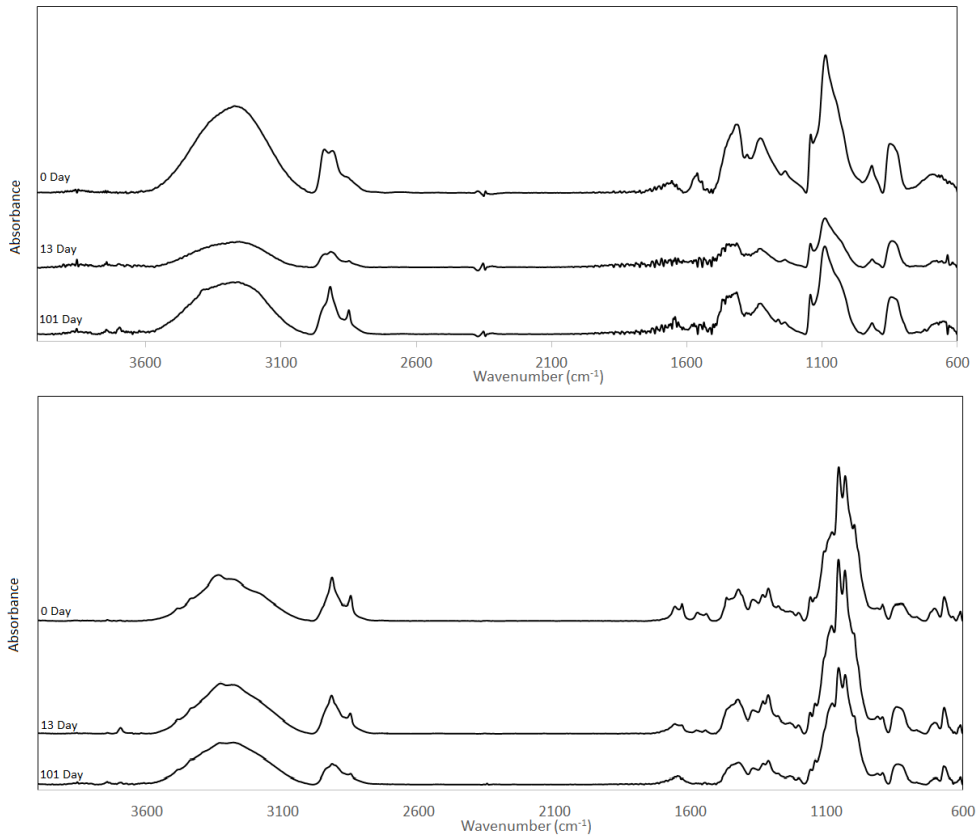

Figure 8.3: FTIR biodegradation data for 146K neat PVA (top) and 146K 67 wt.% CNC (bottom).

8.3 Water Recovery and Scalability

One of the goals of the presented research was to develop a method for recovering the water used during processing of the polymer nanocomposite systems. In order to achieve this goal, CNC/PVA samples at 7 wt.%, the loading used to process the tensile specimens, were placed in a vacuum oven for one hour at either 30 °C or 70 °C and the amount of water recovered during this time period was measured by weighing the samples before and after testing. The results of this study are shown in Table 8.1. From

these tests, it was seen that while most of the water could be recovered within a one hour time period at 30°C, all of the water could be recovered after one hour of testing at 70 °C. The water from these tests was recovered into a solvent trap attached to the vacuum oven. The amount of water recovered was not dependent on CNC loading.

Table 8.1: Water recovery measurements for CNC/PVA nanocomposite systems at 30 °C and 70 °C after 60 minutes.

Sample	Temperature (°C)	Percent water recovery
146K Neat PVA	30	59
146K 20 wt.% CNC	30	54
146K 33 wt.% CNC	30	53
146K 50 wt.% CNC	30	71
146K 67 wt.% CNC	30	64
146K Neat PVA	70	100
146K 20 wt.% CNC	70	100
146K 33 wt.% CNC	70	98
146K 50 wt.% CNC	70	100
146K 67 wt.% CNC	70	100

Due to the rheological and mechanical properties discussed, the presented research could be scaled to an industrial batch mixing process with a water reclamation line attached to the drying cycle to recycle the recovered water. The system could be implemented in a plant with solution processing capability to suspend or plasticize the PVA in water followed by batch mixing capability to disperse freeze-dried CNCs inside the PVA. Samples could be dried under vacuum after film casting and the water could be recycled and reused. As the viscosity was optimized for batch mixing during the rheological and processing characterization, the suspension viscosities formulated would be ideal for industrial batch mixing. Through the use of freeze-dried CNCs, the process

would also be more scalable than through the use of aqueous suspended CNCs as transportation costs would be lowered. Processing of these CNC/PVA systems would also take place at lower temperatures (110 °C and below), requiring decreased energy consumption.

8.4 Conclusions

In conclusion, CNC/PVA systems present a scalable, biodegradable, and sustainable option for polymer processing. While neat PVA is mildly biodegradable in soil, the addition of CNCs to the system increased biodegradation significantly. Due processing optimization during rheological testing, CNC/PVA suspensions with adequate viscosities for batch mixing were produced. These suspensions could be mixed in industrial plants with batch mixers and the water could be recovered with vacuum oven drying. This water could be recycled to the solution processing step of the process and continuously reused, increasing the sustainability of the processing. Processing temperatures would also be lowered decreasing energy consumption during processing.

CHAPTER 9

CONCLUSIONS AND FUTURE WORK

In this chapter, a summary of the conclusions for the CNC/PVA systems studied will be presented and the efficacy of the development of a scalable water-based processing strategy will be discussed. Potential future work will also be outlined.

9.1 Conclusions

9.1.1 Chapter 4 Conclusions

- Solution processing with aqueous suspended or RDFD CNCs into PVA solution followed by dehydration of the system to an appropriate solids loading produced the least amount of CNC aggregation and most homogeneous suspension morphology.
- Dispersing freeze-dried CNCs without suspending them in aqueous solution prior to processing in PVA via either solution processing or batch mixing increased the total aggregation of the CNC/PVA suspension due to the microscale CNC aggregation.
- Increasing mixing speed increased the amount of phase separation seen in the neat PVA systems. Increasing mixing speed decreased the amount of start-up shear time necessary due to the overall decreased length scale of the system with increasing CNC incorporation.

- CNC aggregate size in freeze dried shear processed and solution processed CNC/PVA suspensions increased with increasing CNC loading. CNC aggregate size was seen to be largest in 91 RPM shear processed 67 wt.% CNC systems due phase separation of PVA.
- Comparison between dynamic light scattering and optical microscopy analysis revealed that by adding as-received freeze-dried CNCs into PVA and solution processing and shear processing at 40 RPM and 91 RPM did not break up native CNC aggregates.

9.2.2: Chapter 5 Conclusions

- Viscosity and aging behavior of neat PVA solutions increased with increasing molecular weight and time due to increased PVA chain entanglement and phase separation, respectively.
- Shear mixing increased the rate of aging in neat PVA systems due to increased phase separation of PVA during mixing.
- Solution processed aqueous suspended and freeze-dried CNC/PVA suspensions showed decreased aging with increased CNC content due to the increased restriction of the PVA chains. Aging behavior was decreased in the aqueous suspended and RDFD systems due to improved CNC distribution compared to the as-received solution processed and shear processed freeze dried samples as PVA chains had more freedom to phase separate. Increasing shear rate in shear processed freeze dried CNC systems accelerated phase separation of PVA,

decreasing the amount of aging seen from 40 RPM to 91 RPM shear mixed samples.

- Gelation was seen to occur as a function of CNC concentration and aging w.r.t. phase separation. Gelation occurred more rapidly and at lower concentration in CNC systems with better dispersion while in systems with increased aggregation, gelation occurred at high CNC loadings. This decrease in gelation behavior with increasing CNC aggregation was due to the decreased ability of the CNCs to form a percolated network.
- For aqueous suspended CNC/PVA systems, more effective reinforcement of CNCs was attained for lower molecular weight polymers, however, at high CNC loadings of 50 wt.% and above, polymer mediated junctions synergistically stiffened the nanocomposite gel leading composite elasticity to be independent of molecular weight.
- Yield stress was used as a metric to understand CNC network structure. Aqueous suspended CNC/PVA systems saw polymer mediated and CNC mediated regions while freeze-dried CNC/PVA systems experienced mainly CNC mediated regions due to increased aggregation. Shear processing was seen to increase the yield stress in freeze-dried CNC systems compared to solution processing due to increased PVA-PVA interaction.
- The percolation threshold was calculated to be 24 wt.% CNC. Polymer mediated networks played a greater role in determining the rheological response at CNC loadings slightly below or near the percolation threshold, and CNC networks were

determined by the rheological response at CNC loadings well above the percolation threshold for aqueous suspended CNC systems.

9.2.3: Chapter 6 Conclusions

- Percent crystallinity of neat PVA films did not change with molecular weight and percent crystallinity of aqueous suspended CNC and freeze-dried CNC films were similar, however, percent crystallinity increased with increasing CNC content and molecular weight due to the confinement of the PVA by the CNCs.
- Neat PVA at all molecular weights showed similar FTIR chemical structure with the exception of increased hydroxyl groups present in the 31K and 146K molecular weights due to slightly increased hydrolysis. Freeze-dried CNCs and aqueous suspended CNCs had similar chemical structure.
- Increasing CNC content increased hydrogen bonding as the 3000 to 3600 cm^{-1} peak shifted to higher wave number. PVA crystallinity was seen to change with increasing CNC loading due to the shift in the peak at 1145 cm^{-1}.
- Increasing the CNC content decreased the T_g and the ΔH_f due to the restriction of the CNCs on the polymer chains and increased crystallinity.
- Freeze-dried CNCs showed increased T_g and the ΔH_f compared to aqueous suspended CNCs due to increased CNC-CNC confinement due to increased aggregation.

9.2.4: Chapter 7 Conclusions

- E' for neat PVA decreased with increasing molecular weight above T_g due to increased bound water due to increased molecular weight trapping the bound water after drying.
- T_g found from E'' was compared to T_g found from the DSC and was seen to have increased sensitivity to molecular weight as T_g decreased with increasing molecular weight due to increased polymer mobility with bound water.
- Aqueous suspended CNC system E' increased with increasing molecular weight and CNC content above and below T_g due to the increased rigidity imparted on the system by the CNCs.
- For the aqueous suspended CNC systems, T_g found from E'' was seen to be less pronounced with increased CNC content due to increased crystallinity. Three regions of mobility were seen below, at, and above the percolation threshold. First, T_g decreased with increasing CNC content below the percolation threshold due to incomplete CNC network formation allowing increased mobility of the PVA. Next, T_g increased around the percolation threshold due to decreased chains mobility as the CNC network restricted the PVA. Thirdly, T_g decreased at loadings far above the percolation threshold due to the increased contribution of the CNCs as the predominant component decreasing polymer chains –polymer chain entanglements.
- Percolation was modeled and found to be in good agreement with the experimental data. A percolation threshold of 0.025 was calculated. The Halpin-Tsai model was used to understand the dispersion of aqueous suspended and

RDFD CNCs below the percolation threshold. The aqueous suspended CNC systems and the RDFD CNC systems were seen to have good dispersion below percolation.

- Below T_g, the elastic rheological data corresponded to the DMA data. Here, aqueous suspended CNC systems had the highest E' due to increased dispersion of the CNCs allowing for the PVA and CNC mediated mechanical behavior. Increasing aggregation decreased E' below T_g as aggregates broke up the PVA chain entanglement creating stress condensers.
- Above T_g, E' increased with increasing CNC content for all samples processed. Here, the reinforcing effect of the CNCs in the rheological data was not directly related to the solid-state data in that increased aggregation did not directly correlate to decreased mechanical properties. Solution processed freeze-dried CNCs were seen to have the largest E', attributed to increased aggregate-aggregate interaction as phase separation was not as pronounced in solution processing compared to shear processing.
- The T_g data collected from E'' correlated to the rheological data in that increasing aggregation increased PVA chain mobility due to larger PVA regions and CNC regions. While aqueous suspended CNC systems had three regions of T_g, freeze-dried CNC systems had either two (RDFD CNC and 40 RPM): polymer controlled and CNC controlled, or one (solution processed and 91 RPM): CNC controlled, due to the effects of aggregation on the system limiting polymer mobility and polymer phase separation.

- MTT showed water acted as a plasticizer increasing CNC/PVA percent strain and decreasing stress. In general, aqueous suspended CNC systems had higher percent strain and stress due to increased dispersion. Stress decreased with increased CNC content due to increased crystallinity.

9.2.5: Chapter 8 Conclusions

- Neat PVA was seen to be mildly affected by biodegradation in soil with no change in biodegradation with increasing molecular weight. The incorporation of CNCs increased biodegradation confirmed through swell testing, TGA, and FT-IR.
- A scalable processing method for CNC/PVA nanocomposite formulation was constructed through optimizing the rheological properties. Water can be recovered through vacuum oven drying and energy requirements reduced through the use of room temperature processing.

In conclusion, the processing-structure-property relationship of CNC/PVA nanocomposite systems produced via aqueous suspended and freeze-dried CNCs was assessed and a scalable water-based processing method traditional shear processing equipment was developed. From this analysis, it was seen that the rheological properties could be related to the solid state mechanical properties above T_g when molecular mobility was a larger contributor to sample performance. This rheological characterization allowed for the development of a method to understand sample morphology when electron microscopy is not a feasible option due to sample

degradation. CNCs were seen to increase the mechanical properties of the PVA to produce biodegradable nanocomposites applicable for membranes, biomedical applications, or packaging.

9.2 Future Work

Future work to be conducted on CNC/PVA nanocomposite systems can be divided into the following categories:

1. Scalability optimization
2. Advancement to other renewable or biodegradable systems
3. Dispersion characterization
4. Applications development
5. Fiber spinning

Future research on further developing the scalability of the CNC/PVA systems is needed. For example, the current research focused on developing a method with the potential to be scaled, but research on the actual processing implementation of CNC/PVA nanocomposite systems would be a good study to follow this research. Determination of the equipment and processes necessary in an industrial plant and studies on the implementation of the CNC/PVA nanocomposites into the plant are necessary.

Another future study could consist of advancing the processing method developed for the CNC/PVA system to another renewable or biodegradable system. Other candidate

systems with gelation properties include clay/PVA or silk/CNC systems. These systems are biodegradable and renewable with good mechanical properties as well as biocompatible. The scalable processing of these materials could be useful in biomedical applications, films, and packaging.

As the CNC/PVA systems studied were not able to be imaged using electron microscopy during this research due to their lack of contrast with the polymer matrix, a method for taking images on the nanoscale of these systems would be instrumental for furthering the understanding of renewable and biodegradable nanocomposite systems. Through the ability to assess the actual orientation and dispersion of renewable fillers inside biodegradable or renewable matrices, increased understanding of how to formulate high performance composites could be achieved.

Studies on the design space and application development of highly loaded CNC/PVA systems could be conducted to determine their applicability in a consumer space. CNC/PVA fibers and films have been tested for biomedical implants, membranes, and fuel cells at low CNC loadings below 20 wt.%, but it would be interesting to see the design and application space for highly loaded CNC/PVA nanocomposite systems.

Finally, fiber spinning and characterization of highly loaded CNC/PVA fibers could also be conducted on these films. As PVA acts as a binder at high loadings, the 67 wt.% CNC/PVA gels could be gel spun, the PVA dissolved using methanol, and characterized to achieve highly oriented CNC fibers.

REFERENCES

1. Yu, L., Dean, K. & Li, L. Polymer blends and composites from renewable resources. *Prog. Polym. Sci.* **31,** 576–602 (2006).

2. Wang, N., Ding, E. & Cheng, R. Thermal degradation behaviors of spherical cellulose nanocrystals with sulfate groups. *Polymer (Guildf).* **48,** 3486–3493 (2007).

3. Roman, M. & Winter, W. T. Effect of sulfate groups from sulfuric acid hydrolysis on the thermal degradation behavior of bacterial cellulose. *Biomacromolecules* **5,** 1671–7 (2004).

4. Dufresne, A. *Nano-Cellulose: From nature to high performance tailored materials*. (Water de Gruyter GmbH, 2012).

5. Malinconico, M., Avella, M. & Immirzi, B. in *Biocomposites Mark. Evol.* 638–654 (2009).

6. Renner, M. in *Sustain. Prosper.* 3–21 (2012).

7. Fernandes, S. C., Freire, C. S., Silvestre, A. J., Pascoal Neto, C. & Gandini, A. Novel materials based on chitosan and cellulose. *Polym. Int.* **60,** 875–882 (2011).

8. Mohanty, A. K., Misra, M. & Hinrichsen, G. Biofibers, biodegradable polymers and biocomposites: An overview. *Macromol. Mater. Eng.* **276,** 1–24 (2000).

9. Pu, Y., Zhang, D., Singh, P. M. & Ragauskas, A. J. The new forestry biofuels sector. *Biofuels, Bioprod. Biorefining* **2,** 58–73 (2008).

10. Chiellini, E., Corti, A., D'Antone, S. & Solaro, R. Biodegradation of poly(vinyl alcohol) based materials. *Prog. Polym. Sci.* **28,** 963–1014 (2003).

11. Kibédi-Szabó, C. Z. *et al.* Biodegradation behavior of composite films with poly(vinyl alcohol) matrix. *J. Polym. Environ.* **20,** 422–430 (2011).

12. Alexy, P. *et al.* Effect of melt processing on thermo-mechanical degradation of poly(vinyl alcohol)s. *Polym. Degrad. Stab.* **85,** 823–830 (2004).

13. Lyoo, W. S. *et al.* Rheological properties of high molecular weight (HMW) syndiotactic poly(vinyl alcohol) (PVA)/HMW atactic PVA blend solutions. *Polymer.* **102,** 3934–3939 (2006).

14. Gao, H., Yang, R., He, J. & Yang, L. Rheological behaviors of PVA/H2O solutions of high-polymer concentration. *Jounral Appl. Polym. Sci.* **116,** 1459–1466 (2010).

15. Song, S. I. & Kim, B. C. Characteristic rheological features of PVA solutions in water-containing solvents with different hydration states. *Polymer.* **45,** 2381–2386 (2004).

16. Kim, S. S. *et al.* Rheological properties of water solutions of syndiotactic poly(vinyl alcohol) of different molecular weights. *J. Appl. Polym. Sci.* **92,** 1426–1431 (2004).

17. Roohani, M. *et al.* Cellulose whiskers reinforced polyvinyl alcohol copolymers nanocomposites. *Eur. Polym. J.* **44,** 2489–2498 (2008).

18. Ram, S. & Mandal, T. K. Photoluminescence in small isotactic, atactic and syndiotactic PVA polymer molecules in water. *Chem. Phys.* **303,** 121–128 (2004).

19. Jiang, S., Liu, S. & Feng, W. PVA hydrogel properties for biomedical application. *J. Mech. Behav. Biomed. Mater.* **4,** 1228–1233 (2011).

20. Pakzad, A., Simonsen, J. & Yassar, R. S. Gradient of nanomechanical properties in the interphase of cellulose nanocrystal composites. *Compos. Sci. Technol.* **72,** 314–319 (2012).

21. Nijenhuis, K. te. in *Thermoreversible Networks* 37–66 (1997).

22. Pritchard, J. . *Poly(vinyl alcohol) basic properties and uses*. (Gordon and Breach Science Publishers, 1969).

23. Hackel, E. in *Prop. Appl. Polyvinyl Alcohol* (Society of Chemical Industry, 1968).

24. Assendert, H. E. & Windle, A. H. Crystallinity in poly(vinyl alcohol) 2. Computer modeling of crystal structure of a range of tacticities. *Polymer.* **39,** 4303–4312 (1998).

25. Rozenburg, M. E. & Sorokin, A. Y. *Poly(vinyl alcohol): Developments*. (John Wiley & Sons, Inc., 1992).

26. Li, L., Chen, N. & Wang, Q. Effect of poly(ethylene oxide) on the structure and properties of poly(vinyl alcohol). *J. Polym. Sci. Part B Polym. Phys.* **48,** 1946–1954 (2010).

27. Mansur, H. S., Sadahira, C. M., Souza, A. N. & Mansur, A. A. P. FTIR spectroscopy characterization of poly(vinyl alcohol) hydrogel with different

hydrolysis degree and chemically crosslinked with glutaraldehyde. *Mater. Sci. Eng. C* **28,** 539–548 (2008).

28. Finch, C. A. in *Polyvinyl Alcohol - Dev.* 277 –278 (1992).

29. Wu, W. L. *et al.* Physical gels of aqueous poly(vinyl alcohol) solutions: a small-angle neutron-scattering study. *Macromolecules* **23,** 2245–2251 (1990).

30. Benoit, H., Benmouna, M. & Wu, W. L. Static scattering from multicomponent polymer and copolymer systems. *Macromolecules* **23,** 1511–1517 (1990).

31. Kokabi, M., Sirousazar, M. & Hassan, Z. M. PVA–clay nanocomposite hydrogels for wound dressing. *Eur. Polym. J.* **43,** 773–781 (2007).

32. Huang, C. C. *et al.* Evaluation of the preparation and biocompatibility of poly(vinyl alcohol)(PVA)/chitosan composite electrospun membranes. *Adv. Mater. Res.* **123-125,** 975–978 (2010).

33. Leitão, A., Silva, J., Dourado, F. & Gama, M. Production and characterization of a new bacterial cellulose/poly(vinyl alcohol) nanocomposite. *Materials.* **6,** 1956–1966 (2013).

34. Guo, G. Z., Sun, Y. Y., Yang, B. H. & Liu, Y. Q. Controlled preparation of microporous polymer membrane by simple biodegradation method. *Appl. Mech. Mater.* **109,** 110–113 (2011).

35. Watase, M. & Nishinari, K. Rheological and DSC changes in poly(viny alcohol) gels induced by immersion in water. *J. Polym. Sci. Polym. Phys. Ediition* **23,** 1803–1811 (1985).

36. Sakurada, I. *Polyvinyl Alcohol Fibers*. (Marcel Dekker, Inc., 1985).

37. Wu, W., Tian, H. & Xiang, A. Influence of polyol plasticizers on the properties of polyvinyl alcohol films fabricated by melt processing. *J. Polym. Environ.* **20,** 63–69 (2012).

38. Li, L., Chen, N., Wang, Q. & Coates, P. D. Small scale injection moulding of modified poly(vinyl alcohol). *Plast. Rubber Compos.* **39,** 411–419 (2010).

39. Nishino, T., Sugihashi, T. & Nakamae, K. Studies on the temperature dependence of the elastic modulus of crystalline regions of polymers. IX. Temperature dependence of the elastic modulus of crystalline regions of polytetrahydrofuran. *Kobunshi Ronbunshu* **45,** 979–984 (1988).

40. Duncalf, B. *et al. Polyvinyl Alcohol: Properties and Applications*. (John Wiley and Sons, 1973).

41. Cho, M.-J. & Park, B.-D. Tensile and thermal properties of nanocellulose-reinforced poly(vinyl alcohol) nanocomposites. *J. Ind. Eng. Chem.* **17,** 36–40 (2011).

42. Lu, J., Wang, T. & Drzal, L. T. Preparation and properties of microfibrillated cellulose polyvinyl alcohol composite materials. *Compos. Part A* **39,** 738–746 (2008).

43. Postek, M. T. *et al.* Development of the metrology and imaging of cellulose nanocrystals. *Meas. Sci. Technol.* **22,** 1–10 (2011).

44. Lahiji, R. R. *et al.* Atomic force microscopy characterization of cellulose nanocrystals. *Langmuir* **26,** 4480–4488 (2010).

45. Moon, R. J., Martini, A., Nairn, J., Simonsen, J. & Youngblood, J. Cellulose nanomaterials review: structure, properties and nanocomposites. *Chem. Soc. Rev.* **40,** 3941–94 (2011).

46. Abitbol, T., Johnstone, T., Quinn, T. M. & Gray, D. G. Reinforcement with cellulose nanocrystals of poly(vinyl alcohol) hydrogels prepared by cyclic freezing and thawing. *Soft Matter* **7,** 2373 (2011).

47. Cai, J. & Zhang, L. Unique gelation behavior of cellulose in NaOH/urea aqueous solution. *Biomacromolecules* **7,** 183–9 (2006).

48. Dorris, A. & Gray, D. G. Gelation of cellulose nanocrystal suspensions in glycerol. *Cellulose* **19,** 687–694 (2012).

49. Kumar, P., Sandeep, K. P., Alavi, S. & Truong, V. D. A review of experimental and modeling techniques to determine properties of biopolymer-based nanocomposites. *J. Food Sci.* **76,** E2–14 (2011).

50. Favier, V., Chanzy, H. & Cavaille, J. Y. Polymer nanocomposites reinforced by cellulose whiskers. *Macromolecules* **28,** 6365–6367 (1995).

51. Dubief, D., Samain, E. & Dufresne, a. Polysaccharide microcrystals keinforced amorphous poly(/3-hydroxyoctanoate) nanocomposite materials. *Macromolecules* **32,** 5765–5771 (1999).

52. Helbert, W., Cavaille, J. Y., Dufresne, A. & Fourier, U. J. Thermoplastic nanocomposites filled with wheat straw cellulose whisker. Part 1: Processing and mechancial mehavior. *Polym. Compos.* **17,** 604–611 (1996).

53. Dufresne, A., Cavaille, J.-Y. & Helbert, W. Thermoplastic nanocomposites filled with wheat straw cellulose whisker. Part 2: Effect of processing and modeling. *Polym. Compos.* **18,** 198–210 (1997).

54. Bossard, F. *et al.* Influence of dispersion procedure on rheological properties of aqueous solutions of high molecular weight PEO. *Rheol. Acta* **49,** 529–540 (2010).

55. Lu, Y., Weng, L. & Cao, X. Morphological, thermal and mechanical properties of ramie crystallite - reinforced plasticized starch biocomposites. *Carbohydr. Polym.* **63,** 198–204 (2006).

56. Dufresne, A. & Vignon, M. R. Improvement of starch film performances using cellulose microfibrils. *Macromolecules* **31,** 2693–2696 (1998).

57. Cao, X., Chen, Y., Chang, P. R., Muir, a. D. & Falk, G. Starch-based nanocomposites reinforced with flax cellulose nanocrystals. *Express Polym. Lett.* **2,** 502–510 (2008).

58. Azizi Samir, M. A. S., Alloin, F. & Dufresne, A. Review of recent research into cellulosic whiskers, their properties and their application in nanocomposite field. *Biomacromolecules* **6,** 612–26 (2005).

59. Samir, M. A. S. A., Alloin, F., Sanchez, J. Y. & Dufresne, A. Cross-linked nanocomposite polymer electrolytes reinforced with cellulose whiskers. *Macromolecules* **37,** 4839–4844 (2004).

60. Azizi Samir, M. A. S., Alloin, F., Sanchez, J. Y. & Dufresne, A. Cellulose nanocrystals reinforced poly(oxyethylene). *Polymer.* **45,** 4149–4157 (2004).

61. Samir, M. A. S. A., Alloin, F., Paillet, M. & Dufresne, A. Tangling effect in fibrillated cellulose reinforced nanocomposites. *Macromolecules* **37,** 4313–4316 (2004).

62. Zimmermann, T., Pöhler, E. & Geiger, T. Cellulose fibrils for polymer reinforcement. *Adv. Eng. Mater.* **6,** 754–761 (2004).

63. Leitner, J., Hinterstoisser, B., Wastyn, M., Keckes, J. & Gindl, W. Sugar beet cellulose nanofibril-reinforced composites. *Cellulose* **14,** 419–425 (2007).

64. Paralikar, S. a., Simonsen, J. & Lombardi, J. Poly(vinyl alcohol)/cellulose nanocrystal barrier membranes. *J. Memb. Sci.* **320,** 248–258 (2008).

65. Lee, S. Y. *et al.* Nanocellulose reinforced PVA composite films: Effects of acid treatment and filler loading. *Fibers Polym.* **10,** 77–82 (2009).

66. Frone, A. N. *et al.* Preparation and characterization of PVA composites with cellulose nanofibers obtained by ultrasonication. *Bioresources* **6,** 487–512 (2011).

67. Zimmermann, T., Bordeanu, N. & Strub, E. Properties of nanofibrillated cellulose from different raw materials and its reinforcement potential. *Carbohydr. Polym.* **79,** 1086–1093 (2010).

68. Sehaqui, H., Zhou, Q. & Berglund, L. a. Nanostructured biocomposites of high toughness—a wood cellulose nanofiber network in ductile hydroxyethylcellulose matrix. *Soft Matter* **7,** 7342 (2011).

69. Uddin, A., Araki, J. & Gotoh, Y. Toward 'strong' green nanocomposites: polyvinyl alcohol reinforced with extremely oriented cellulose whiskers. *Biomacromolecules* **12,** 617–624 (2011).

70. Fortunati, E. *et al.* Cellulose nanocrystals extracted from okra fibers in PVA nanocomposites. *J. Appl. Polym. Sci.* **128,** 3220–3230 (2013).

71. Wang, Y., Chang, C. & Zhang, L. Effects of freezing/thawing cycles and cellulose nanowhiskers on structure and properties of biocompatible starch/PVA sponges. *Macromol. Mater. Eng.* **295,** 137–145 (2010).

72. Chakraborty, A., Sain, M. & Kortschot, M. Reinforcing potential of wood pulp-derived microfibres in a PVA matrix. *Holzforschung* **60,** 53–58 (2006).

73. Ago, M., Jakes, J. E., Johansson, L.-S., Park, S. & Rojas, O. J. Interfacial properties of lignin-based electrospun nanofibers and films reinforced with cellulose nanocrystals. *ACS Appl. Mater. Interfaces* **4,** 6849–56 (2012).

74. Millon, L. E., Guhados, G. & Wan, W. Anisotropic polyvinyl alcohol-bacterial cellulose nanocomposite for biomedical applications. *J. Biomed. Mater. Res. B. Appl. Biomater.* **86,** 444–52 (2008).

75. Liu, D., Sun, X., Tian, H., Maiti, S. & Ma, Z. Effects of cellulose nanofibrils on the structure and properties on PVA nanocomposites. *Cellulose* **20,** 2981–2989 (2013).

76. Azizi Samir, M. A. S., Mateaos, A. M., Alloin, F., Sanchex, J.-Y. & Dufresne, A. Nanocomposite polymer electrolytes based on poly(oxyethylene) and cellulose whiskers. *Electrochim. Acta* **49,** 4667–4677 (2004).

77. Van der Berg, O., Capadona, J. R. & Weder, C. Preparation of homogeneous dispersions of tunicate cellulose whiskers in organic solvents. *Biomacromolecules* **8,** 1353–1357 (2007).

78. Schroers, M., Kokil, A. & Weder, C. Solid polymer electrolytes based on nanocomposites of ethylene oxide-epichlorohydrin copolymers and cellulose whiskers. *J. Appl. Polym. Sci.* **93,** 2883–2888 (2004).

79. Qi, H., Cai, J., Zhang, L. & Kuga, S. Properties of films composed of cellulose nanowhiskers and a cellulose matrix regenerated from alkali/urea solution. *Biomacromolecules* **10,** 1597–1602 (2009).

80. Noorani, S., Simonsen, J. & Atre, S. Nano-enabled microtechnology: Polysulfone nanocomposites incorporating cellulose nanocrystals. *Cellulose* **14,** 577–584 (2007).

81. Tang, L. & Weder, C. Cellulose whisker/epoxy resin nanocomposites. *Appl. Mater. Interfaces* **2,** 100954 (2010).

82. Heux, L., Chauve, G. & Bonini, C. Nonflocculating and chiral-nematic self-ordering of cellulose microcrystals suspensions in nonpolar solvents. *Langmuir* **16,** 8210–8212 (2000).

83. Kvien, I., Sugiyama, J., Votrubec, M. & Oksman, K. Characterization of starch based nanocomposites. *J. Mater. Sci.* **42,** 8163–8171 (2007).

84. Peng, Y., Gardner, D. J. & Han, Y. Drying cellulose nanofibrils: In search of a suitable method. *Cellulose* **19,** 91–102 (2012).

85. Rämänen, P., Penttilä, P. a., Svedström, K., Maunu, S. L. & Serimaa, R. The effect of drying method on the properties and nanoscale structure of cellulose whiskers. *Cellulose* **19,** 901–912 (2012).

86. Orts, W. J. *et al.* Application of cellulose microfibrils in polymer nanocomposites. *J. Polym. Environ.* **13,** 301–306 (2005).

87. Alloin, F., D'Aprea, A., Dufresne, A., Kissi, N. El & Bossard, F. Poly(oxyethylene) and ramie whiskers based nanocomposites: Influence of processing: Extrusion and casting/evaporation. *Cellulose* **18,** 957–973 (2011).

88. Suryanegara, L., Nakagaito, A. N. & Yano, H. The effect of crystallization of PLA on the thermal and mechanical properties of microfibrillated cellulose-reinforced PLA composites. *Compos. Sci. Technol.* **69,** 1187–1192 (2009).

89. Suryanegara, L., Okumura, H., Nakagaito, A. N. & Yano, H. The synergetic effect of phenylphosphonic acid zinc and microfibrillated cellulose on the injection molding cycle time of PLA composites. *Cellulose* **18,** 689–698 (2011).

90. Bondeson, D. & Oksman, K. Polylactic acid/cellulose whisker nanocomposites modified by polyvinyl alcohol. *Compos. Part A Appl. Sci. Manuf.* **38,** 2486–2492 (2007).

91. Nakagaito, A. N. & Yano, H. The effect of morphological changes from pulp fiber towards nano-scale fibrillated cellulose on the mechanical properties of high-

strength plant fiber based composites. *Appl. Phys. A Mater. Sci. Process.* **78,** 547–552 (2004).

92. Nogi, M., Handa, K., Nakagaito, A. N. & Yano, H. Optically transparent bionanofiber composites with low sensitivity to refractive index of the polymer matrix. *Appl. Phys. Lett.* **87,** 1–3 (2005).

93. Shimazaki, Y. *et al.* Excellent thermal conductivity of transparent cellulose nanofiber/epoxy resin nanocomposites. *Biomacromolecules* **8,** 2976–2978 (2007).

94. Park, W. I., Kang, M., Kim, H. S. & Jin, H. J. Electrospinning of poly(ethylene oxide) with bacterial cellulose whiskers. *Macromol. Symp.* **249-250,** 289–294 (2007).

95. Peresin, M. S., Habibi, Y., Zoppe, J. O., Pawlak, J. J. & Rojas, O. J. Nanofiber composites of polyvinyl alcohol and cellulose nanocrystals: manufacture and characterization. *Biomacromolecules* **11,** 674–681 (2010).

96. Podsiadlo, P. *et al.* Molecularly engineered nanocomposites: Layer-by-layer assembly of cellulose nanocrystals. *Biomacromolecules* **6,** 2914–2918 (2005).

97. Herrick, F. W., Casebier, R. ., Hamlton, J. K. & Sandberg, K. R. Microfibrillated cellulose: Morphology and accessiblity. *J. Appl. Polym. Sci. Symp.* **37,** 797–813 (1983).

98. Turbak, A. F., Snyder, F. W. & Sandberg, K. R. Microfibrilated cellulose: A new cellulose product: Properties, uses and commercial potential. *J. Appl. Polym. Sci. Polym. Symp.* **37,** 815–827 (1983).

99. Lowys, M. P., Desbrières, J. & Rinaudo, M. Rheological characterization of cellulosic microfibril suspensions. Role of polymeric additives. *Food Hydrocoll.* **15,** 25–32 (2001).

100. Agoda-Tandjawa, G. *et al.* Rheological characterization of microfibrillated cellulose suspensions after freezing. *Carbohydr. Polym.* **80,** 677–686 (2010).

101. Araki, J., Wada, M., Kuga, S. & Okano, T. Flow properties of microcrystalline cellulose suspension prepared by acid treatment of native cellulose. *Colloids Surfaces A Physicochem. Eng. Asp.* **142,** 75–82 (1998).

102. Marchessault, R. H., Morehead, F. F. & Walter, N. M. Liquid Crystal Systems from Fibrillar Polysaccharides. *Nature* **184,** 632– 633 (1959).

103. Chandrasekhar, S. *Liquid Crystals*. (Cambridge University Press, 1992).

104. Radel, S. R. & Navidi, M. H. *Chemistry*. (West Publishing Company, 1994).

105. Orts, W. J., Godbout, L., Marchessault, R. H. & Revol, J.-F. Enhanced Ordering of Liquid Crystalline Suspensions of Cellulose Microfibrils: A Small Angle Neutron Scattering Study. *Macromolecules* **31,** 5717–5725 (1998).

106. Azouz, K. Ben, Ramires, E. C., Van Den Fonteyne, W., El Kissi, N. & Dufresne, A. Simple method for the melt extrusion of a cellulose nanocrystal reinforced hydrophobic polymer. *ACS Macro Lett.* **1,** 236–240 (2012).

107. Chang, C., Lue, A. & Zhang, L. Effects of crosslinking methods on structure and properties of cellulose/PVA hydrogels. *Macromol. Chem. Phys.* **209,** 1266–1273 (2008).

108. Fengel, D. & Wegener, G. *Wood chemistry, ultrastructure, reactions*. (Walter de Gruyter, 1984).

109. Habibi, Y. & Dufresne, A. Highly filled bionanocomposites from functionalized polysaccharide nanocrystals. *Biomacromolecules* **9,** 1974–1980 (2008).

110. Fortunati, E. *et al.* Multifunctional bionanocomposite films of poly(lactic acid), cellulose nanocrystals and silver nanoparticles. *Carbohydr. Polym.* **87,** 1596–1605 (2012).

111. Zoppe, J. O., Peresin, M. S., Habibi, Y., Venditti, R. a. & Rojas, O. J. Reinforcing poly(ε-caprolactone) nanofibers with cellulose nanocrystals. *ACS Appl. Mater. Interfaces* **1,** 1996–2004 (2009).

112. Anglès, M. N. & Dufresne, A. Plasticized starch/tunicin whiskers nanocomposites. 1. Structural analysis. *Macromolecules* **33,** 8344–8353 (2000).

113. Garcia de Rodriguez, N. L., Thielemans, W. & Dufresne, A. Sisal cellulose whiskers reinforced polyvinyl acetate nanocomposites. *Cellulose* **13,** 261–270 (2006).

114. Azizi Samir, M. A. S., Alloin, F., Gorecki, W., Sanchez, J. & Dufresne, A. Nanocomposite polymer electrolytes based on poly(oxyethylene) and cellulose whiskers. *J. Phys. Chem. B* **108,** 10845–10852 (2004).

115. Brown, E. E. & Laborie, M. P. G. Bioengineering bacterial cellulose/poly(ethylene oxide) nanocomposites. *Biomacromolecules* **8,** 3074–3081 (2007).

116. Chakraborty, A. & Sain, M. Reinforcing potential of wood pulp-derived microfibres in a PVA matrix. *Holzforschung* **60,** 53–58 (2006).

117. Bruce, D. M., Hobson, R. N., Farrent, J. W. & Hepworth, D. G. High-performance composites from low-cost plant primary cell walls. *Compos. Part A Appl. Sci. Manuf.* **36,** 1486–1493 (2005).

118. Tang, C. & Liu, H. Cellulose nanofiber reinforced poly(vinyl alcohol) composite film with high visible light transmittance. *Compos. Part A* **39,** 1638–1643 (2008).

119. Chang, C. & Zhang, L. Cellulose-based hydrogels: Present status and application prospects. *Carbohydr. Polym.* **84,** 40–53 (2011).

120. Millon, L. E. & Wan, W. K. The polyvinyl alcohol – bacterial cellulose system as a new nanocomposite for biomedical applications. *J. Biomed. Mater. Res. Part B Appl. Biomater.* 245–253 (2006).

121. Silvério, H. A., Flauzino Neto, W. P. & Pasquini, D. Effect of incorporating cellulose nanocrystals from corncob on the tensile, thermal and barrier properties of poly(vinyl Alcohol) nanocomposites. *J. Nanomater.* **2013,** 1–9 (2013).

122. Iwatake, A., Nogi, M. & Yano, H. Cellulose nanofiber-reinforced polylactic acid. *Compos. Sci. Technol.* **68,** 2103–2106 (2008).

123. Dufresne, A., Dupeyre, D. & Vignon, M. Cellulose microfibrils from potato tuber cells : Processing and characterization of starch – cellulose microfibril composites. *Polymer.* **76,** 2080–2092 (1999).

124. Halpin, J. C. & Kardos, J. L. Moduli of crystalline polymers employing composite theory. *J. Appl. Phys.* **43,** 2235–2241 (1972).

125. Hajji, P., Cavaille, J. Y., Favier, V., Gauthier, C. & Vigier, G. Tensile behavior of nanocomposites from latex and cellulose whiskers. *Polym. Compos.* **17,** 161–164 (1996).

126. Chazeau, L., Cavaille, J. Y., Canova, G., Dendievel, R. & Boutherin, B. Viscoelastic properties of plasticized PVC reinforced with cellulose whiskers. *J. Appl. Polym. Sci.* **71,** 1797–1808 (1999).

127. Hammersley, J. M. Percolation processes: Lower bounds for the critical probability. *Ann. Math. Stat.* **28,** 790–795 (1957).

128. Balberg, I., Binenbaum, N. & Wagner, N. Percolation thresholds in the three-dimensional sticks system. *Phys. Rev. Lett.* **52,** 1465–1468 (1984).

129. De Gennes, P. G. On a relation between percolation theory and the elasticity of gels. *J. Phys. Lettres* **37,** 1–2 (1976).

130. Loos, M. R. & Manas-Zloczower, I. Micromechanical models for carbon nanotube and cellulose nanowhisker reinforced composites. *Polym. Eng. Sci.* 882–887 (2013).

131. Favier, V., Dendievel, R., Canova, G., Cavaille, J. Y. & Gilormini, P. Simulation and modeling of three-dimensional percolating structures: Case of a latex matrix reinforced by a network of cellulose fibers. *Acta Metall.* **45,** 1557–1565 (1997).

132. Favier, V., Canova, G. R., Shrivastava, S. C. & Cavaille, J. Y. Mechanical percolation in cellulose whisker nanocomposites. *Polym. Eng. Sci.* **37,** 1732 – 1739 (1997).

133. Bras, J., Viet, D., Bruzzese, C. & Dufresne, A. Correlation between stiffness of sheets prepared from cellulose whiskers and nanoparticles dimensions. *Carbohydr. Polym.* **84,** 211–215 (2011).

134. Yamanaka, S. *et al.* The structure and mechanical properties of sheets prepared from bacterial cellulose. *J. Mater. Sci.* **24,** 3141–3145 (1989).

135. Marchessault, R. H., Dube, M., St Pierre, J. & Revol, J. F. *New insight into fiber swelling, interfibre bonding and wet strength. In: fiber-water interactions in paper making*. (Oxford Technical Division, The British Paper and Board Industy Federation, 1978).

136. Abdul Khalil, H. P. S., Bhat, A. H. & Ireana Yusra, A. F. Green composites from sustainable cellulose nanofibrils: A review. *Carbohydr. Polym.* **87,** 963–979 (2012).

137. Jiang, L. & Hinrichsen, G. Flax and cotton fiber reinforced biodegradable polyester amide composites, 1. *Die Angew. Makromol. Chemie* **268,** 13–17 (1999).

138. Sorrentino, A., Gorrasi, G. & Vittoria, V. Potential perspectives of bio-nanocomposites for food packaging applications. *Trends Food Sci. Technol.* **18,** 84–95 (2007).

139. Luzier, W. D. Materials derived from biomass/biodegradable materials. *Proc. Natl. Acad. Sci. U. S. A.* **89,** 839–842 (1992).

140. Nord, F. F. Dehydrogenation activity of Fusarium lini B. *Naturwiss* **24,** 763 (1936).

141. Chiellini, E., Corti, A., Solaro, R. & Ceccanti, A. Environmentally degradable plastics: poly(vinyl alcohol) a case study. in *Interact. Work. Environ. Degrad. Polym. Polym. Mater. Environ.* (Said, Z. F. & Chiellini, E.) 103–118 (1999).

142. Chen, L., Imam, S. H., Gordon, S. H. & Greene, R. V. Starch- polyvinyl alcohol crosslinked film— performance and biodegradation. *J. Environ. Polym. Degrad.* **5,** 111–117 (1997).

143. Krupp, L. & Jewell, W. Biodegradability of modified plastic films in controlled biological environments. *Environ. Sci. Technol.* **26,** 193–198 (1992).

144. Xu, S., Girouard, N., Schueneman, G., Shofner, M. L. & Meredith, J. C. Mechanical and thermal properties of waterborne epoxy composites containing cellulose nanocrystals. *Polymer.* **54,** 6589–6598 (2013).

145. Reising, A. B., Moon, R. J. & Youngblood, J. P. Effet of particle alignment on mechanical properties of neat cellulose nanocrystals films. *J. Sci. Technol. For. Prod. Process.* **2,** 32–41 (2012).

146. Wang, R., Wang, Q. & Li, L. Evaporation behaviour of water and its plasticizing effect in modified poly(vinyl alcohol) systems. *Polym. Int.* **52,** 1820–1826 (2003).

147. Rousseaux, D. D. J. *et al.* Water-assisted extrusion of polypropylene/clay nanocomposites: A comprehensive study. *Polymer.* **52,** 443–451 (2011).

148. Stoclet, G., Sclavons, M. & Devaux, J. Relations between structure and property of polyamide 11 nanocomposites based on raw clays elaborated by water-assisted extrusion. *J. Appl. Polym. Sci.* **127,** 4809–4824 (2013).

149. Touchaleaume, F. *et al.* One-step water-assisted melt-compounding of polyamide 6/pristine clay nanocomposites: An efficient way to prevent matrix degradation. *Polym. Degrad. Stab.* **96,** 1890–1900 (2011).

150. Lebeau, J. M. & Boonyongmaneerat, Y. Comparison study of aqueous binder systems for slurry-based processing. *Mater. Sci. Eng. A* **458,** 17–24 (2007).

151. Fortunati, E. *et al.* Binary PVA bio-nanocomposites containing cellulose nanocrystals extracted from different natural sources: Part I. *Carbohydr. Polym.* **97,** 825–36 (2013).

152. Verbeek, C. J. R. & Berg, L. E. Van Den. Extrusion Processing and Properties of Protein-Based Thermoplastics. *Macromol. Mater. Eng.* **295,** 10–21 (2010).

153. Zhang, W. *et al.* High performance poly(vinyl alcohol)/cellulose nanocrystals nanocomposites manufactured by injection molding. *Cellulose* **21,** 485–494 (2013).

154. Raquez, J.-M., Narayan, R. & Dubois, P. Recent advances in reactive extrusion processing of biodegradable polymer-based compositions. *Macromol. Mater. Eng.* **293,** 447–470 (2008).

155. Sun, X., Lu, C., Liu, Y., Zhang, W. & Zhang, X. Melt-processed poly(vinyl alcohol) composites filled with microcrystalline cellulose from waste cotton fabrics. *Carbohydr. Polym.* **101,** 642–9 (2014).

156. Yu, Z.-Z., Hu, G.-H., Varlet, J., Dasari, A. & Mai, Y.-W. Water-assisted melt compounding of nylon-6/pristine montmorillonite nanocomposites. *J. Polym. Sci. Part B Polym. Phys.* **43,** 1100–1112 (2005).

157. Wu, W., Tian, H. & Xiang, A. Influence of polyol plasticizers on the properties of polyvinyl alcohol films fabricated by melt processing. *J. Polym. Environ.* **20,** 63–69 (2011).

158. Chen, N., Li, L. & Wang, Q. New technology for thermal processing of poly(vinyl alcohol). *Composites* **36,** 283–291 (2007).

159. Khoshkava, V. & Kamal, M. R. Effect of drying conditions on cellulose nanocrystal (CNC) agglomerate porosity and dispersibility in polymer nanocomposites. *Powder Technol.* **261,** 288–298 (2014).

160. Jiang, L., Morelius, E., Zhang, J., Wolcott, M. & Holbery, J. Study of the poly(3-hydroxybutyrate-co-3-hydroxyvalerate)/cellulose nanowhisker composites prepared by solution casting and melt processing. *J. Compos. Mater.* **42,** 2629–2645 (2008).

161. Franck, A. J. Understanding rheology of thermoplastic polymers. *TA Instruments Rheol. Thermoplast.* (2004).

162. Carvalho, W. de & Djabourov, M. Physical gelation under shear for gelatin gels. *Rheol. Acta* **36,** 591–609 (1997).

163. Gao, H., He, J., Yang, R. & Yang, L. Characteristic rheological features of high concentration PVA solutions in water with different degrees of polymerization. *J. Appl. Polym. Sci.* **116,** 2734–2741 (2010).

164. Liu, Y. *et al.* Thermal behavior and mechanical properties of physically crosslinked PVA/Gelatin hydrogels. *J. Mech. Behav. Biomed. Mater.* **3,** 203–9 (2010).

165. Murphy, D. J. *et al.* Physical characterisation and component release of poly(vinyl alcohol)-tetrahydroxyborate hydrogels and their applicability as potential topical drug delivery systems. *Int. J. Pharm.* **423,** 326–34 (2012).

166. Choi, J. H., Seok, W., Sohk, L. & Ko, W. Rheological properties of syndiotacticity-rich ultrahigh molecular weight poly(vinyl alcohol) dilute solution. *Polymer.* **82,** 569–576 (2001).

167. Tan, Y., Song, Y. & Zheng, Q. Hydrogen bonding-driven rheological modulation of chemically reduced graphene oxide/poly(vinyl alcohol) suspensions and its application in electrospinning. *Nanoscale* **4,** 6997 (2012).

168. Yang, X., Tong, Y.-Y., Li, Z.-C. & Liang, D. Aggregation-induced microgelation: a new approach to prepare gels in solution. *Soft Matter* **7,** 978 (2011).

169. Yang, N., Hutter, J. L. & de Bruyn, J. R. Microrheology, microstructure, and aging of physically cross-linked poly(vinyl alcohol)/poly(ethylene glycol) blends. *J. Rheol.* **56,** 797 (2012).

170. Mihranyan, A. Viscoelastic properties of cross-linked polyvinyl alcohol and surface-oxidized cellulose whisker hydrogels. *Cellulose* **20,** 1369–1376 (2013).

171. Qiu, K. & Netravali, A. N. Fabrication and characterization of biodegradable composites based on microfibrillated cellulose and polyvinyl alcohol. *Compos. Sci. Technol.* **72,** 1588–1594 (2012).

172. Silva, J. A. L. de & Goncalves, M. P. in *Cellul. Cellul. Deriv. Physico-chemical Asp. Ind. Appl.* (Kennedy, J. F., Phillips, G. O., Williams, P. O. & Piculell, L.) 279–285 (Woodhead Publishing Ltd, 1995).

173. Doraiswamy, D. The Cox–Merz rule extended: A rheological model for concentrated suspensions and other materials with a yield stress. *J. Rheol.* **35,** 647 (1991).

174. Mas, R. & Magnin, A. Experimental validation of steady shear and dynamic viscosity relation for yield stress fluids. *Rheol. Acta* **55,** 49–55 (1997).

175. Balberg, I., Anderson, C. H., Alexander, S. & Wagner, N. Excluded volume and its relation to the onset of percolation. *Phys. Rev. B* **30,** 3933–3943 (1984).

176. Celzard, A. *et al.* Critical concentration in percolating systems containing a high-aspect-ratio filler. *Phys. Rev. B* **53,** 6209–6214 (1996).

177. Minus, M. L. The study of crystallization and interfacial morphology in polymer/carbon nanotube composites. (2008).

178. Sullivan, A. C. O. Cellulose : the structure slowly unravels. *Cellulose* **4,** 173–207 (1997).

179. Nishiyama, Y. Structure and properties of the cellulose microfibril. *J. Wood Sci.* **55,** 241–249 (2009).

180. Tanner, S. F., Cartier, N. & Chanzy, H. High-resolution solid-state C nuclear magnetic resonance spectroscopy of tunicin, an animal cellulose. *Macromolecules* **22,** 1615–1617 (1989).

181. Gardivert, K. H. & Blackwell, J. The structure of native cellulose. *Biopolymers* **13,** 1975–2001 (2001).

182. Wang, Q., Gao, J., Dan, Y. & Chen, Z. Preparation of novel polymer materials through intermacromolecular complexation. *Mater. Sci. Eng. C* **10,** 135–140 (1999).

183. Chen, D., Lawton, D., Thompson, M. R. & Liu, Q. Biocomposites reinforced with cellulose nanocrystals derived from potato peel waste. *Carbohydr. Polym.* **90,** 709–716 (2012).

184. Peng, Y. *et al.* Influence of drying method on the material properties of nanocellulose I: thermostability and crystallinity. *Cellulose* **20,** 2379–2392 (2013).

185. Patel, A. K., Bajpai, R. & Keller, J. M. On the crystallinity of PVA/palm leaf biocomposite using DSC and XRD techniques. *Microsyst. Technol.* **20,** 41–49 (2013).

186. Hult, E., Iversen, T. & Sugiyama, J. Characterization of the supermolecular structure of cellulose in wood pulp fibres. *Cellulose* **10,** 103–110 (2003).

187. Strawhecker, K. E. & Manias, E. AFM of poly(vinyl alcohol) crystals next to an inorganic surface. *Macromolecules* **34,** 8475–8482 (2001).

188. Minus, M. L., Chae, H. G. & Kumar, S. Interfacial crystallization in gel-spun poly(vinyl alcohol)/single-wall carbon nanotube composite fibers. *Macromol. Chem. Phys.* **210,** 1799–1808 (2009).

189. Peresin, M. S. *et al.* Crosslinked PVA nanofibers reinforced with cellulose nanocrystals: Water interactions and thermomechanical properties. *J. Appl. Polym. Sci.* **131,** n/a–n/a (2014).

190. Fonseca, E., Fábia, S. & Sander, H. Synthesis and characterization of poly(vinyl alcohol) hydrogels and hybrids for rMPB70 protein adsorption. *Mater. Res.* **9,** 185–191 (2006).

191. Peppas, N. a. & Merrill, E. W. Differential scanning calorimetry of crystallized PVA hydrogels. *J. Appl. Polym. Sci.* **20,** 1457–1465 (1976).

192. Alexander, L. E. *X-ray diffraction methods in polymer science*. (Wileyinterscience, 1969).

193. Yang, D. *et al.* Effects of pretreatments on crystalline properties and morphology of cellulose nanocrystals. *Cellulose* **20,** 2427–2437 (2013).

194. Minus, M. L., Chae, H. G. & Kumar, S. Single wall carbon nanotube templated oriented crystallization of poly(vinyl alcohol). *Polymer.* **47,** 3705–3710 (2006).

195. Tadokoro, H., Seki, S. & Nitta, I. Some information on the infrared absorption spectrum of poly(vinyl alcohol) from deuteration and pleochroism. *J. Polym. Sci.* **669,** 563–566 (1956).

196. Schwanninger, M., Rodrigues, J. C., Pereira, H. & Hinterstoisser, B. Effects of short-time vibratory ball milling on the shape of FT-IR spectra of wood and cellulose. *Vib. Spectrosc.* **36,** 23–40 (2004).

197. Bai, L., Gao, Y., Li, S. & Zhang, L. P. Preparation and characterization of poly(vinyl alcohol/cellulose nanocomposites. *Adv. Mater. Res.* **233-235,** 2383–2386 (2011).

198. Uddin, A. J., Araki, J. & Gotoh, Y. Characterization of the poly(vinyl alcohol)/cellulose whisker gel spun fibers. *Compos. Part A* **42,** 741–747 (2011).

199. Menard, K. P. in *Dyn. Mech. Anal. A Pract. Introd.* (Taylor and Francis Group, 2008).

200. Park, J.-S., Park, J.-W. & Ruckenstein, E. On the viscoelastic properties of poly(vinyl alcohol) and chemically crosslinked poly(vinyl alcohol). *J. Appl. Polym. Sci.* **82,** 1816–1823 (2001).

201. Foreman, J., Sauerbrunn, S. R. & Marcozzi, C. L. *Exploring the sensitivity of thermal analysis techniques to the glass transition*. *TA Instruments. Therm. Anal. Rheol.* **TA082,** (2015).

202. Kamphunthong, W., Hornsby, P. & Sirisinha, K. Isolation of cellulose nanofibers from para rubberwood and their reinforcing effect in poly(vinyl alcohol) composites. *J. Appl. Polym. Sci.* (2012).

203. Loos, M. R. & Manas-Zloczower, I. Reinforcement efficiency of carbon nanotubes: Myth and reality. *Macromol. Theory Simulations* **21,** 130–137 (2012).

204. Eichhorn, S. J. Cellulose nanowhiskers: promising materials for advanced applications. *Soft Matter* **7,** 303 (2011).

205. Stauffer, D. *Introduction to Percolation Theory*. (Taylor and Francis, 1985).

206. De Gennes, P. G. *Scaling Concepts in Polymer Physics*. (Cornell Universtiy Press, 1979).

207. Halpin, J. C. & Kardos, J. L. The Halpin-Tsai equations: A review. *Polym. Eng. Sci.* **16,** 344–352 (1976).

208. Chiellini, Emo *et al.* Environmentally sound blends and composites based on water-soluble polymer matrices. *Macromol. Symp.* **154,** 83–94 (2000).

209. Klemenčič, D., Simončič, B., Tomšič, B. & Orel, B. Biodegradation of silver functionalised cellulose fibres. *Carbohydr. Polym.* **80,** 426–435 (2010).

VITA

CAITLIN E. MEREE

Caitlin Meree was born in Bethesda, Maryland She attended public school in Poquoson, Virginia. She received a B.S. in Polymer and Fiber Engineering from the Georgia Institute of Technology in, Atlanta, Georgia in 2011 before continuing at Georgia Tech to complete her Doctorate in Materials Science and Engineering. When Cait is not working on her research and love of materials engineering, she enjoys dancing, biking, rock climbing, horseback riding, and hiking.